UNIVERSITY OF LONDON

IMPERIAL COLLEGE OF SCIENCE AND TECHNOLOGY

Department of Electrical Engineering

A GENERAL STUDY OF THE TRANSIENT STABILITY OF SYNCHRONOUS MACHINES

by

Ronald Gordon HARLEY, M.Sc.(Eng.)(Elec)(Dist.)

Thesis submitted for the degree of
Doctor of Philosophy in the
Faculty of Engineering

LONDON, October 1969.

ABSTRACT

An investigation has been carried out into methods of representing synchronous machines in stability studies. Methods of improving the steady-state stability have also been studied.

Different types of large transient disturbances are analysed and the methods of analyses are classified according to the assumptions made. Mathematical models are developed to include some of the phenomena commonly neglected in digital computer studies. Damping is allowed for more accurately than by the simple method using a torque proportional to slip. An even more accurate solution also includes terms which depend on the rate of change of the flux linkages and it is used to assess in detail the "back-swing" after a three-phase fault. A comparative study is made of various numerical integration techniques suitable for a digital computer.

Steady-state stability studies of a machine with two field windings are carried out by linearising the system equations for small disturbances and using Nyquist's criterion. The excitation of the one winding is regulated by a rotor angle feedback signal and that of the other winding by a voltage feedback signal. Various regulators are considered with different transfer functions.

Transient and steady-state stability calculations are compared with test results of a 30 MW turbo-alternator incorporating voltage regulators and a governor, as well as with test results obtained from micro-machine experiments. All the experimental and theoretical results show reasonable agreement.

ACKNOWLEDGEMENTS

The work presented in this thesis was carried out under the supervision of Dr. B. Adkins, M.A., D.Sc.(Eng.), F.I.E.E., of the Electrical Engineering Department, Imperial College of Science and Technology, London. I wish to thank Dr. Adkins for his helpful guidance and constant encouragement.

I also wich to thank Messrs. B. Standley and J. Soper from the Central Electricity Generating Board, South Eastern Region, Cockfosters, for valuable discussions.

Financial assistance from the Central Electricity Generating Board (London), the Metal Box Co. Ltd. (S.A.), The Council for Scientific and Industrial Research of South Africa and The Electricity Supply Commission of South Africa, and temporary study leave from the University of Pretoria., Republic of South Africa, are gratefully acknowledged, I am also very grateful for the use of the micro-machine equipment and the IBM-computers at Imperial College and the CDC-computer at the University of London.

Finally, I would like to thank my wife June for her most loyal support, as well as all those individuals who have contributed, directly or indirectly, to the success of this venture.

INDEX

Abstract

Acknowledgements

List of symbols

PART ONE: GENERAL ASPECTS OF TRANSIENT STABILITY

CHAPTER 1 INTRODUCTION 13

1.1 General 13

1.2 Verification of Theories 16

1.3 New Formulations and Conclusions 17

1.4 Previously Published Material 18

CHAPTER 2 CLASSIFICATION OF TRANSIENT DISTURBANCES 19

2.1 Various Types of Disturbances 19

2.2 Basic System, Assumptions and Equations 22

2.3 Analyses of Disturbances 27

2.3.1 Switching in additional tie-line reactance 27

2.3.2 A change in the excitation voltage 36

2.3.3 Change in prime mover output 40

2.3.4 A symmetrical short-circuit 43

2.3.4.1 The single transmission line 43

2.3.4.2 The twin transmission line 43

2.4 Comparison of Various Disturbances 50

CHAPTER 3 CLASSIFICATION OF METHODS OF SOLUTION 53

3.1 Methods using Torque-angle Characteristics 53

3.2 Methods using a Step-by-step Computation 53

3.3 Lyapunov's Method 56

3.4 Choice of Method of Representation 56

PART TWO: MORE ACCURATE METHODS OF SOLUTION AND COMPARISONS WITH TEST RESULTS OF A THREE-PHASE FAULT

CHAPTER 4 THEORY OF MORE ACCURATE METHODS 59

4.1 General 59

4.2 Alternator Equations and Methods of Solution 63

4.2.1 Standard method 64

4.2.2 Approximate method 65

4.2.3 Accurate method 68

CHAPTER 5 EQUIPMENT USED FOR TESTS 71

5.1 General 71

5.2 A Large Practical System 71

5.2.1 The alternator 71

5.2.2 The voltage regulator 73

5.2.3 The governor and turbine 78

5.2.4 The tie-line impedance 80

5.3 A Micro-machine System 81

5.3.1 The alternator 81

5.3.2 The time constant regulator 86

5.3.3 The prime mover torque-speed characteristic 86

5.3.4 The tie-line impedance 88

CHAPTER 6 COMPARISON OF CALCULATED AND TEST RESULTS 90

6.1 General 90

6.2 Results of a Large System (Goldington) 90

6.2.1 Three-phase short-circuit at rated load 91

6.2.2 Three-phase short-circuit at various system conditions 93

6.2.3 Detailed assessment of the back swing 95

6.3 Results for a Micro-machine System 96

CHAPTER 7 NUMERICAL INTEGRATION TECHNIQUES 112

7.1 General 112

7.2 Methods of solution for the Goldington System 113

7.2.1 The approximate method 113

7.2.2 The accurate method 114

7.3 The Micro-machine System 117

7.3.1 The approximate method 117

7.3.2 The accurate method 118

7.4 Resume of integration methods and arrangements 123

PART THREE: STABILITY PROBLEMS OF A SYNCHRONOUS MACHINE WITH A DIVIDED WINDING ROTOR

CHAPTER 8 CALCULATIONS OF TRANSIENT STABILITY 126

8.1 Introduction 126

8.2 Transformations for the Field Windings 128

8.2.1 The current transformations 132

8.2.2 The voltage transformations 133

8.3 General Equations for the D.W.R. Machine 134

8.3.1 Basic equations 134

8.3.2 Equivalent circuits and operational impedances 135

8.3.3 Fundamental machine constants 137

8.4 Parameters of the Fictitious Field Windings 138

8.5 Equations for a Transient Disturbance 140

8.5.1 The approximate method 140

8.5.2 The accurate method 144

8.6 Calculated Results of a Fault on a Large System 145

8.6.1 System details 146

8.6.2 Results for a three-phase short-circuit 152

CHAPTER 9 STEADY-STATE STABILITY THEORY OF D.W.R. REGULATION

9.1 General 159

9.2 System Equations 160

9.2.1 The machine equations 161

9.2.2 Expressions for the feedback quantities 166

9.2.3 The open-loop transfer function 170

9.3 Equilibrium Diagrams. 171

9.4 Steady-state Stability of a D.W.R. Micro-machine 175

9.4.1 Proportionate bus angle regulator only 177

9.4.1.1 Bus angle δ held at 33.75^{o} 179

9.4.1.2 Bus angle δ held at 0^{o} 180

9.4.1.3 Bus angle δ held at 66.25^{o} 184

9.4.1.4 Bus angle δ held at 90^{o} 185

9.4.2 Proportionate terminal angle regulator only. 185

9.4.2.1 The effect of different values of δ_t 190

9.4.2.2 The effect of additional tie-line reactance 192

9.4.3 Comparison of d.w.r.- and q.a.r.-system results 192

9.4.4 Proportionate voltage regulator only. 192

9.4.5 Proportionate angle regulator and proportionate voltage regulator 197

9.4.6 Derivative angle regulator and proportionate voltage regulator 201

CHAPTER 10 THE D.W.R. MICRO-MACHINE EQUIPMENT 204

10.1 The Micro-alternator 204

10.1.1 Connection of field windings 205

10.1.2 Determination of parameters 209

10.1.3 Comparison with large machines 213

10.2 The Prime Mover 214

10.3 Feedback Signals 214

10.3.1 The angle feedback signal 214

10.3.1.1 The angle device 215

10.3.1.2 The filter units 223

10.3.2 The voltage feedback signal 227

10.4 The Regulators and Associated Circuitry 228

10.4.1 The angle regulator 228

10.4.2 The voltage regulator 232

CHAPTER 11 COMPARISON OF MEASUREMENTS AND COMPUTATIONS 234

11.1 General 234

11.2 The Stability Code 234

11.3 The Regulator Constants 236

11.3.1 The angle regulator gain K_t 236

11.3.2 The voltage regulator gain K_r 236

11.4 Starting of the System 237

11.5 Steady-state Stability Limit Curves for Proportionate Bus Angle Regulator 238

11.6 Steady-state Stability Limit Curves for Proportionate Terminal Angle Regulator 239

11.7 Steady-state Stability Limit Curves for Proportionate Terminal Angle Regulator and Proportionate Voltage Regulator 239

11.8 Steady-state Stability Limit Curves for Derivative Terminal Angle Regulator and Proportionate Voltage Regulator 240

CHAPTER 12 CONCLUSIONS 247

APPENDICES 253

REFERENCES 265

LIST OF SYMBOLS

Unless otherwise stated, the axis quantities are represented by small letters, whereas their corresponding R.M.S. values are represented by capital letters. The symbols represent the per unit values in accordance with reference 22.

v_d, v_q	: d- and q-axis components of voltage
i_d, i_q	: d- and q-axis components of current
v_t, v_r	: t- and r-winding voltages
v_{fd}, v_{fq}	: d- and q-axis field voltages
$v_{mt}(V_{mt})$	: machine terminal voltage
$v_b(V_b)$	: infinite bus voltage
r_a	: armature resistance
r_{fd}, r_{fq}	: d- and q-axis field resistances
T_e	: electromagnetic torque
T_L	: loss torque
T_{acc}	: accellerating torque
T_{in}, T_m	: turbine output torque
P_s	: steam input power to turbine
P_{in}	: turbine output power
P, Q	: active- and reactive power at the generator
P_o, Q_o	: active- and reactive power at the infinite bus
J	: polar moment of inertia
H	: inertia constant
X_2	: transmission line reactance
X_c, X_T	: total tie-line reactance
p	: operator $\frac{d}{dt}$
S	: slip

s	: Laplace operator
$\mathcal{L}$	: Laplace sign
K_t, K_r	: angle- and voltage regulator gains
$H_t(p)$, $H_r(p)$	: angle- and voltage regulator transfer functions
$K_{t\ min}$, $K_{t\ max}$	: minimum and maximum angle regulator gains
X_a	: armature leakage reactance
X_{md}, X_{mq}	: d- and q-axis magnetising reactance
X_d, X_q	: d- and q-axis synchronous reactance
X_{fd}, X_{fq}	: d- and q-axis field leakage reactance
L_{fd}, L_{fq}	: d- and q-axis field leakage inductance
L_{ffd}, L_{ffq}	: complete self-inductance of d- and q-axis field winding
X_{kq}, X_{kq}	: d- and q-axis damper leakage reactance
L_{kd} , L_{kq}	: d- and q-axis damper leakage inductance
L_{kkd}, L_{kkq}	: complete self-inductance of d- and q-axis damper winding
L_{dd}, L_{qq}	: complete self-inductance of d- and q-axis armature winding
$X_d(p)$, $X_q(p)$	: d- and q-axis operational reactances
Ψ_f, Ψ_{fd}	: d-axis field flux linkage
Ψ_{fq}	: q-axis field flux linkage
Ψ_{kd}, Ψ_{kq}	: d- and q-axis damper flux linkage
Ψ_d, Ψ_q	: d- and q-axis armature flux linkage

Δt	: time step of integration
δ	: rotor angle with reference to the infinite bus
δ_f	: value of δ at the instant of fault removal
δ_t	: rotor angle with reference to the terminal voltage
ϕ_t	: angle between t-winding and the d-axis
ϕ_r	: angle between r-winding and the d-axis
Ψ	: flux linkage
ω	: synchronous speed in rad/sec.
ν	: rotor speed in rad/sec.
τ_t	: time delay of the angle regulator
τ_r	: time delay of the voltage regulator
w_n	: natural frequency of the closed loop system
w	: frequency of small oscillations
CR	: ratio of computer time to real time
DE	: differential equation
IV's	: integrable variables
NIV's	: non-integrable variables
IR	: integration routine
c.w.r.(C.W.R)	: conventionally wound rotor
d.w.r.(D.W.R.)	: divided winding rotor
q.a.r.	: quadrature-axis regulated
t.c.r.	: time constant regulator
a.v.r.	: automatic voltage regulator
o	: subscript to denote steady-state value

PART ONE

GENERAL ASPECTS OF TRANSIENT STABILITY

CHAPTER 1

1. INTRODUCTION

1.1 General

The operation of a synchronous generator in a power system is severely limited by considerations of stability, particularly at leading power factors. The problem has been more acute in recent years because of the charging current taken by high voltage transmission lines and because modern generators have higher reactances and lower inertia constants. On the other hand the range of stable operation can be extended by the use of continuously acting excitation regulators. All these factors make it necessary to have more accurate methods than hitherto for calculating where the limit of stability lies and how to improve it where possible.

A power system containing machines is an inherently non-linear system. Its stability may be endangered by two types of distubances viz. a small disturbance or a large one. Studies concerned with the first type deal with steady-state stability while the larger disturbances are studied as transient stability problems. This thesis is concerned with the transient stability of a synchronous machine with one field winding on the rotor d-axis, referred to as a "conventionally wound rotor" (c.w.r.) machine. The steady-state and transient stability of a synchronous machine with two displaced field windings, referred to as a "divided winding rotor" (d.w.r.) machine, is also considered.

For steady-state stability the differential equations can be linearised for small disturbances and tested for stability by established criteria. However, a system is regarded as transiently stable if after a large disturbance synchronism is not lost. This definition has been used by most authors although the limit of transient stability may differ for each type of disturbance. Conditions of pole slipping and asynchronous operation are excluded from this definition The differential equations are solved by using step-by-step integration methods involving laborious and repetitive calculations which are ideally suited for a digital computer. In addition more complicated and accurate machine representations are possible on modern computers and the number of machines that can be included in a system study is limited only by the capacity of the computer. Comparative results about the speed and accuracy of different numerical integration methods are presented.

Methods of representing a c.w.r. machine and solving the equations, are classified according to the assumptions made, and some views are presented about their application. In Ref. 1 Heaviside's theory is applied to a "simplified representation" and one type of disturbance is studied. In this thesis the Laplace transforms are applied to the same representation in order to investigate the same type of disturbance as well as others. Expressions are found and compared for the transient electrical torques after different disturbances.

Two methods which are more accurate than the simplified representation are developed for a c.w.r. - as well as a d.w.r. machine. The "approximate method" makes full allowance for damping and system resistance and subtransient saliency and variations in the speed, but neglects the changes in flux linkages represented by $p\Psi_d$ and $p\Psi_q$. The "accurate method", however, accounts for

$p\Psi_d$ and $p\Psi_q$ as well. The accurate method is used to study in detail the angular back swing or retardation which can be caused by a three-phase short-circuit. Although not considered here, the accurate method is also essential to investigate the behaviour of a rectifier excitation system during any transient condition when the field current falls to zero.

The steady-state stability limits of c.w.r. machines with different types of regulators, have been tested and calculated extensively[2,3] and it has been shown[4] that under light load conditions there are stability limitations which cannot be overcome by any regulator on a c.w.r. machine. However, the limitation can be overcome by using a second rotor winding whose M.M.F. is controlled in a suitable manner[4,5]. Hence the divided winding rotor machine has a feedback control to each field winding. Permitting certain assumptions, it is proved that a suitable choice of the d.w.r. feedback signals will enable the current in one field winding (the "torque winding") to control the machine's electrical torque, independant of the current in the other field winding (the "reactive winding") which can be used to control the reactive power only. The d.w.r. system improves the steady-state stability over the whole range from no-load to full-load by an amount which depends on the transfer functions of the feedback regulators.

A "transformation matrix" is derived and used to replace, mathematically, torque- and reactive windings (t and r- windings) which are not on the main magnetic axes, by fictitious field windings fd and fq on the d and q- axes. Stability studies are made as-if the machine has two input field voltages v_{fd} and v_{fq} while the transformation matrix is regarded as part of the feedback regulators. The steady-state stability limit is found for different regulator- and system parameters to establish the influence of one feedback loop upon the other.

PARTS ONE and TWO of the thesis describe the different transient disturbances and methods of representing the c.w.r machine with particular interest in the three-phase fault. PART THREE investigates the steady-state and transient stability of a d.w.r. machine with particular reference to the regulator feedback loops.

1.2 Verification of Theories

In the development of any machine theory it is necessary to verify the validity of the theory for practical use, by comparison with practical tests carried out on a number of machines of different size. It is difficult and expensive to carry out tests on full size machines to prove the accuracy of the theory and it is therefore necessary to resort to model machines. Micro-machines have been designed specifically for this purpose and although not perfect, behave in a similar manner to large machines. With the exception of a few parameters, the per unit values are similar to those of full size commerical machines. The field resistance can be reduced as required by means of suitable control equipment.

The steady-state and transient stability theories were verified by measurements on a c.w.r. and a d.w.r. micro-machine. Transient stability calculations were also compared with test results and analoque computations[6] for a 30 MW c.w.r. turbo-alternator as well as with analoque computations[5] for a hypothetical 30 MW d.w.r. turbo-alternator.

1.3 New Formulations and Conclusions

Some important new formulations and conclusions, most of which have been confirmed experimentally, are summarized as follows.

(a) The expressions for the transient electrical torque show three familiar torque components which are common to the large disturbances analysed.

(b) The development of more general machine equations which allow for damping as well as for the $p\Psi_d$ and $p\Psi_q$ terms. The error due to neglect of the $p\Psi$ terms in the analysis of a three-phase fault is shown with particular reference to the braking torque and "back swing" of the rotor.

(c) A novel arrangement is shown of the system equations when they are solved by a fifth order integration routine on a digital computer.

(d) The theory of a d.w.r. machine is developed and a transformation matrix is found so that the d.w.r. may mathematically be treated as a machine with a field winding on each axis.

(e) A complete transfer function for a d.w.r. machine with a control loop to each field winding is developed and rearranged for ease of use of the Nyquist criterion.

(f) The control signals of a d.w.r. machine are studied in order to find a maximum steady-state operating region and to determine the effect of gains and time delays of the individual control loops.

(g) Results from a digital computer calculation are presented for a three-phase short-circuit when the $p\Psi_d$ and $p\Psi_q$ terms are retained in the equations of a d.w.r. turbo-alternator with a composite representation of the turbine and governor, the angle regulator feedback and the voltage regulator feedback.

1.4 Previously Published Material

During the last five years the author of this thesis has published several papers[7,8,9] on the subject of synchronous machine stability. Reference 9 was based on the earlier part of the thesis.

---o0o---

CHAPTER 2

2. CLASSIFICATION OF TRANSIENT DISTURBANCES

Different types of large disturbances have been considered by various authors who studied the transient stability of synchronous machines and used various methods of analysis. This Chapter presents a survey of various disturbances, and it analyses and compares the effects of some disturbances on the electrical torque of the machine.

2.1 Various Types of Disturbances

A literature survey showed that as early as 1929 Park and Banker[10] reviewed the stability problem in 'the light of recent analytical and experimental studies' accounting for such factors as the short-circuit ratio, voltage regulators, excitation systems, neutral impedance, governors and damper windings, in a two machine as well as a multi-machine system. This paper was written very clearly and is a starting point for almost any study on power system stability. The disturbances considered included sudden application of load on the alternator, opening one of two parallel lines and a short-circuit along a transmission line. Solutions for simple representations were obtained by means of the equal area criterion. When considering features such as saliency, flux decrement, damper windings and regulators, a step-by-step method of solution was used.

In 1932 Crary and Waring[11] set out to establish general equations from which may be derived specific equations applying to a particular disturbance such as changes in excitation voltage, in external reactance and in system voltage. They provided a step-by-step method for calculating the electrical torque at any time of a machine having any number of rotor circuits. Of particular importance was the recognition of unidirectional components of torque developed when a symmetrical three phase short circuit occurred.

Ching and Adkins[12] considered disturbances incorporating the line-to-line, the line-to-neutral and the double line-to-neutral fault.

In 1959 Aldred and Shackshaft[13] considered a sudden change in prime mover shaft torque and used an analogue computer to solve the non-linear equations. Already an attempt was being made to find a relationship between the steady state stability limit and the transient limit, this being in the form of a new set of 'voltage-excitation' characteristics for predetermination of swing curves for a machine with a regulator. The paper also presented comprehensive results on the relationship between the regulator gain and time constant. For the first time then a signal from within the alternator was fed back, in this case the derivative of the field current, which improved the alternator response. The regulator feedback singnals gave a damping effect which might have outweighed the effect of any damper winding.

The performance of a regulator incorporating a voltage signal plus a rotor angle signal was described in 1960 by Easton[14] et. al. in which the transient consisted of a change in the regulator's reference setting. Although relatively small disturbances were used on linearised equations, the main feature of this paper was the useful practical regulator data presented.

Mehta and Adkins[1] in 1960 succeeded mathematically in presenting the various components of electrical torque, following a change in tie-line reactance, in a form which made it possible to relate the components physically to the machine behaviour. They also investigated the unidirectional torque after a three phase fault. Experimental results on micro-machines reasonably confirmed their predictions which made this paper one of the few in which predictions were corroborated by experimental results.

Shackshaft[6] followed in 1963 with a composite mathematical representation of a typical large 30 MW alternator as well as the analogue computer prediction of full scale grid tests including a three phase short circuit.

In 1968 the names of Surana and Hariharan[15] appear in the literature where they show that some regulator parameters that give optimum steady state stability do not necessarily also provide optimum transient stability.

The authors mentioned and many others have considered one or more of the following large disturbances:-

change in the transmission line configuration[1,10,11,13,16]
increasing the load of a synchronous motor[10]
symmetrical short circuit along a
transmission line[1,6,10,11,13,16 - 21].
changing the excitation voltage[6,10,11,14].
unsymmetrical short circuits[12,21]
sudden change in electrical load[6,13,17,18].
sudden change in prime mover torque[13,15]

The rest of this chapter investigates different types of disturbances and compares the transient electrical torque after each disturbance. The disturbance considered in detail in the rest of the thesis is a three-phase short-circuit.

2.2 Basic System, Assumptions and Equations

It is assumed that the system can be represented by a single alternator connected through a transformer and a transmission line (single or twin) to an infinite bus bar as in Fig. 2.1. This relatively simple model is used on order to keep the mathematics manageable and the results understandable. The effects of saturation, eddy currents and hysteresis are neglected throughout the thesis. The motoring sign convention of Adkins[22] is followed.

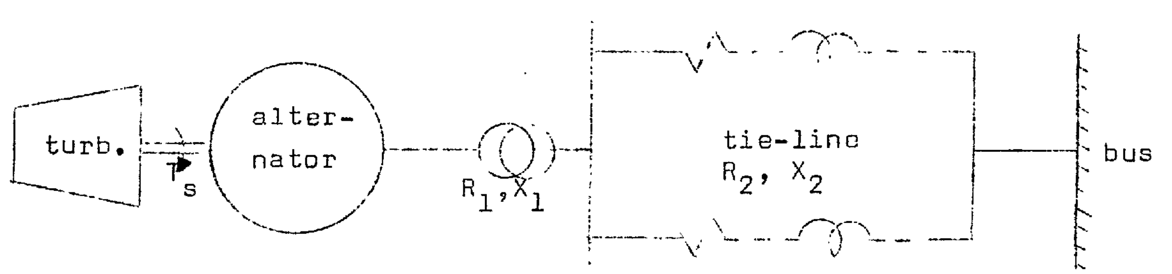

Fig. 2.1 Basic system

According to the "generalized machine theory"[22], the equations for the two-axis representation of the synchronous machine in Fig. 2.2, are (using Heaviside's notation)

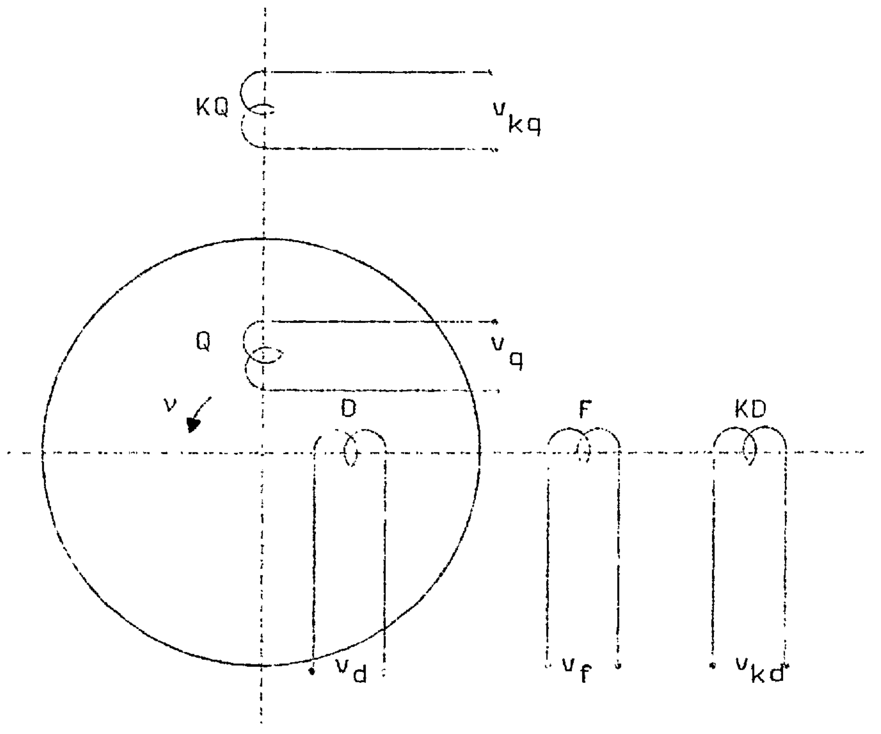

Fig. 2.2 Two axis representation of a three phase synchrous machine

$$v_d = p\Psi_d + \nu\Psi_q + r_a i_d \tag{2.1}$$

$$v_q = -\nu\Psi_d + p\Psi_q + r_a i_q \tag{2.2}$$

$$0 = r_{kd} i_{kd} + p\Psi_{kd} \tag{2.3}$$

$$0 = r_{kq} i_{kq} + p\Psi_{kq} \tag{2.4}$$

$$v_f = r_f i_f + p\Psi_f \tag{2.5}$$

for voltages, and

$$\Psi_d = L_{dd} i_d + L_{md} i_{kd} + L_{md} i_f \tag{2.6}$$

$$\Psi_q = L_{qq} i_q + L_{mq} i_{kq} \tag{2.7}$$

$$\Psi_{kd} = L_{md} i_d + L_{kkd} i_{kd} + L_{md} i_f \tag{2.8}$$

$$\Psi_{kq} = L_{mq} i_q + L_{kkq} i_{kq} \tag{2.9}$$

$$\Psi_f = L_{md} i_d + L_{md} i_{kd} + L_{ffd} i_f \tag{2.10}$$

for the flux linkages, and

$$T_e = \frac{\omega}{2} (\Psi_d i_q - \Psi_q i_d) \tag{2.11}$$

for the electromagnetic torque.

Apart form additonal equations describing the behaviour of regulators, turbines and governors, the equations for mechanical motion and for the transmission network also have to be solved.

During steady state conditions, the generator voltages may be represented by the phasor diagram of Fig. 2.3.

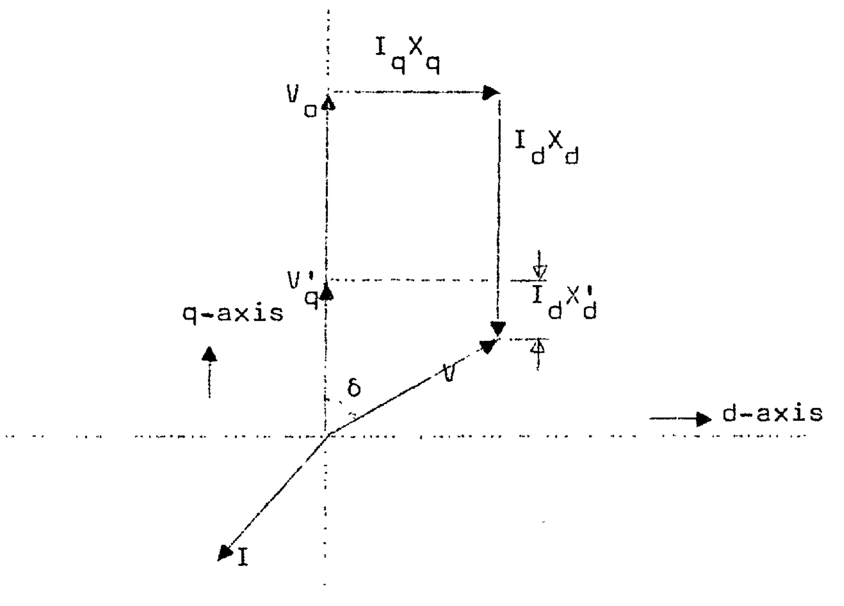

Fig. 2.3 Phasor diagram for generator steady state conditions — allowing for transient saliency

Now Eqns. (2.1),(2.2) and (2.11) are non-linear and can be solved only by means of a numerical method. However, in these equations the speed may be replaced by the rotor angle δ and if δ were a known function of time, it would be possible to determine the currents i_d, i_q and the flux linkages Ψ_d and Ψ_q by solving a set of linear equations in which the applied voltages depend on δ. However, δ is usually not known and a method for solving the machine equations consists of

(a) obtaining a general expression for the eletrical torque T_e in terms of δ, then

(b) writing the equations for mechanical motion and accelerating torque, with or without damping, while finally

(c) integrating the Eqn. in (b) by a step-by-step process to obtain the variation of δ and T_e as functions of time. A fast computing aid is necessary.

The above method gives a result somewhere between a strict analytical solution and a strict computer solution and thus permits some insight into the physical behaviour of the alternator. The various disturbances considered are compared only as regards their relative electrical torques T_e obtained in (a). Much of the foundation for this comparison was laid by Refs. 1 and 11.

The position of a synchronously rotating axis with respect to a fixed reference point is taken as an angle ωt radians, and with varying speed the position of the alternator rotor with respect to the same reference point is θ where $\theta = \omega t - \delta$ from which the speed $\frac{d\theta}{dt} = v = p\theta = \omega - p\delta$. Thus δ is the angle between the rotor and a synchronously rotating reference frame. For a sinusoidally applied terminal phase voltage

$v_a = - V_m \sin \omega t$, Eqns. (2.1) and (2.2) become

$$v_d = V_m \sin\delta = p\Psi_d + \omega\Psi_q + r_a i_d - \Psi_q p\delta \tag{2.12}$$

$$v_q = - V_m \cos\delta = - \omega\Psi_d + p\Psi_q + r_q i_q + \Psi_d p\delta \tag{2.13}$$

It is assumed in the remainder of Chaper 2,

(i) that the transmission line and machine resistance voltage drops are negligible with respect to rotational voltages;

(ii) that during transient conditions the flux linkages change relatively slowly with respect to the supply frequency so that the $p\Psi_d$ and $p\Psi_q$ terms in Eqns.(2.12) and (2.13) may be neglected and

(iii) that the speed remains close to synchronous speed and changes slowly so that the $p\delta$ terms may be neglected as well.

From Eqns. (2.12) and (2.13) we then find

$V_m \sin\delta = \omega\Psi_q$

$V_m \cos\delta = \omega\Psi_d$ during a transient.

Therefore $$\Psi_q = \frac{V_m \sin\delta}{\omega} = \frac{v_d}{\omega} \tag{2.14}$$

and $$\Psi_d = \frac{V_m \cos\delta}{\omega} = \frac{-v_q}{\omega} \tag{2.15}$$

During steady operation, denoted by subscript o,

$$\Psi_{qo} = \frac{V_m \sin\delta_o}{\omega}$$

$$\Psi_{do} = \frac{V_m \cos\delta_o}{\omega}$$

From the phasor diagram in Fig. 2.3 and using the relations[22] between axis and phasor quantities it is seen that

$$i_{do} = \frac{-\sqrt{2}}{X_d} \cdot (V_o - V\cos\delta_o) \tag{2.16}$$

$$i_{qo} = \frac{\sqrt{2}\ V}{X_q} \sin\delta_o \tag{2.17}$$

2.3 Analyses of Disturbances

2.3.1 Switching in additional tie-line reactance

Switching out one of two twin lines has an effect similar to a sudden increase of the tie-line reactance and this can be modelled analytically by having an external reactance X_e suddenly switched into the equivalent circuits of the direct and quadrature axis respectively. Inserting the reactance X_e may be treated as opening a normally closed switch S1 across an inductance L_e in the equivalent axis circuit of Fig. 2.4. By superposition, the effect of opening S1 may first be found and the resultant changes added to the steady state values.

The combination of the machine and the external reactance can be treated as a modified alternator having a leakage reactance $X_a + X_e = \omega(L_a + L_e)$. The Ψ_d and Ψ_q equations for such a modified alternator connected to a fixed supply V are found from Eqns. (2.6) and (2.7) as

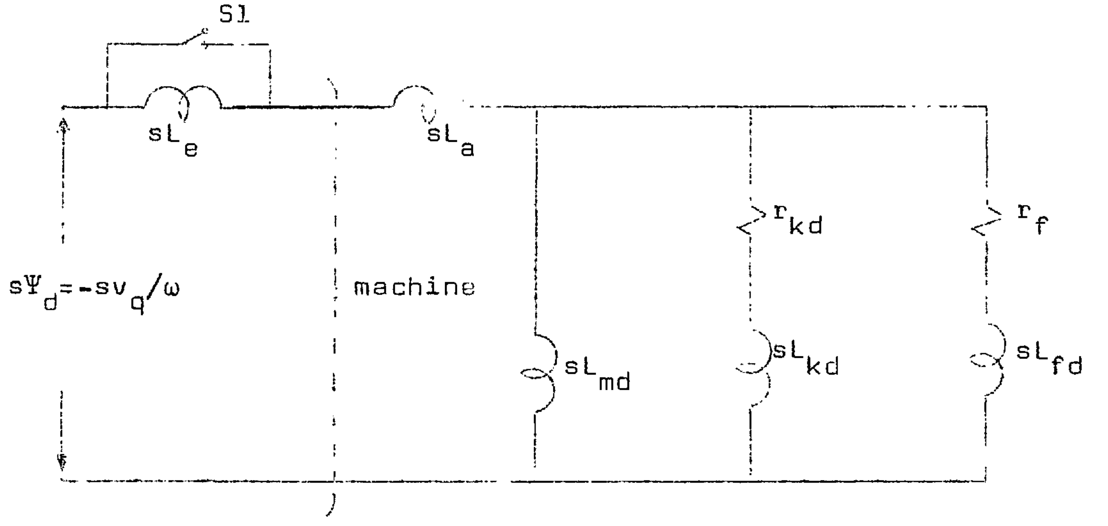

Fig. 2.4 The d-axis circuit for changes only.

$$\begin{aligned}\Psi_{de} &= (L_{md} + L_a + L_e)\, i_d + L_{md} i_{kd} + L_{md} i_f \\ \Psi_{qe} &= (L_{mq} + L_a + L_e) i_q + L_{mq} i_{kq}\end{aligned} \qquad (2.18)$$

while the voltage Eqns. (2.12) and (2.13) become

$$\begin{aligned}v_{de} &= V_m \sin\delta = p\Psi_{de} + \omega\Psi_{qe} + r_a i_d - \Psi_{qe} p\delta \\ v_{qe} &= V_m \cos\delta = -\omega\Psi_{de} + p\Psi_{qe} + r_a i_q + \Psi_{de} p\delta\end{aligned} \qquad (2.19)$$

where V_m is the amplitude of the constant infinite bus voltage. The synchronous reactance of the modified alternator becomes

$$\begin{aligned}X_{de} &= \omega(L_{md} + L_a + L_e) \\ X_{qe} &= \omega(L_{mq} + L_a + L_e)\end{aligned} \qquad (2.20)$$

and likewise for the modified transient and subtransient reactances. The equations (2.14) and (2.15) become

$$\omega\Psi_{qe} = V_m \sin\delta = v_{de} \qquad (2.21)$$

$$\omega\Psi_{de} = V_m \cos\delta = v_{qe} \qquad (2.22)$$

for the modified flux linkages.

During steady operation the equations for the flux linkages and currents are

$$\omega\Psi_{qeo} = V_m \sin\delta_o \qquad (2.23)$$

$$\omega\Psi_{deo} = V_m \cos\delta_o \qquad (2.24)$$

$$i_{do} = \frac{-\sqrt{2}}{X_{de}} (V_o - V\cos\delta_o) \qquad (2.25)$$

$$i_{qo} = \frac{\sqrt{2}}{X_{qe}} V\sin\delta_o \qquad (2.26)$$

where v_{de}, v_{qe}, Ψ_{de} and Ψ_{qe} are associated with the voltage at the infinite bus which has now become the terminal voltage of the modified alternator.

In Laplace notation 's' corresponds to 'p' in Heaviside's notation. By opening S1, a current step $- i_{do}$ is injected throug S1. Since the value of v_{qe} does not stay constant once δ starts changing, the input of Fig. 2.4 connot be regarded as short circuited for the analysis of changes only.

When L_e is switched in, the speed changes and δ increases causing v_{qe} and Ψ_{de} to decrease and consequently i_d.

The change in v_{qe} is (in Laplace transform)

$$\Delta v_{qe}(s) = - V_m \mathcal{L}(\cos\delta - \cos\delta_o) \tag{2.27}$$

The current step becomes $(-\frac{i_{do}}{s})$ in the Laplace domain and may be replaced by an equivalent voltage source in series with L_e. Fig. 2.4 then becomes Fig. 2.5

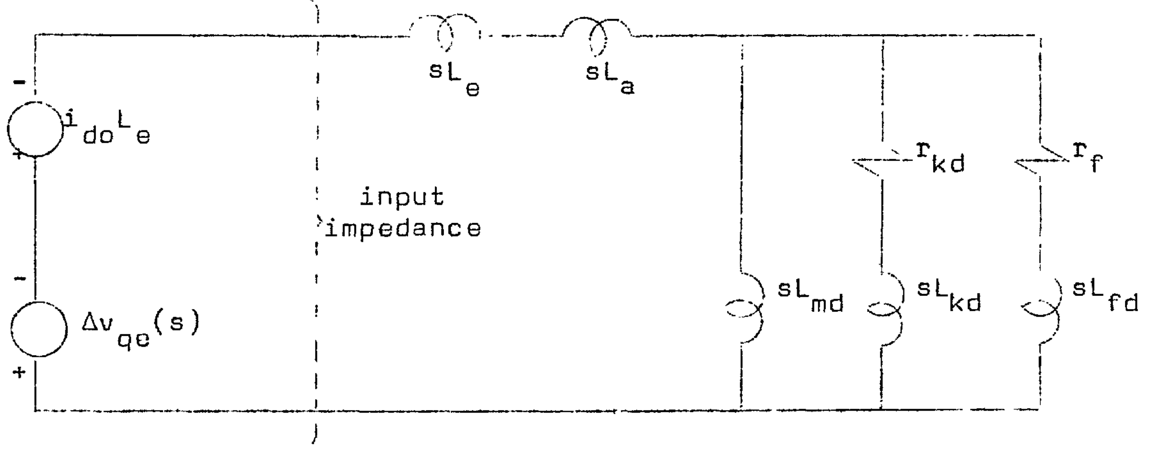

Fig. 2.5 The d-axis circuit for changes only

The operational input impedance in Fig. 2.5 is

$$Z_{de}(s) = \frac{s\ X_{de}(s)}{\omega}$$

The transform of the change in d-axis current is

$$\Delta i_d(s) = (-V_m \mathcal{L}(\cos\delta - \cos\delta_o) + \frac{i_{do}X_e}{s}) \cdot \frac{1}{X_{de}(s)}$$

After the change the transformed direct axis current becomes

$$i_d(s) = \frac{i_{do}}{s} - \Delta i_d(s)$$

$$= \frac{i_{do}}{s} - (-V_m \mathcal{L}(\cos\delta - \cos\delta_o) + \frac{i_{do}X_e}{s}) \cdot \frac{1}{X_{de}(s)} \qquad (2.28)$$

Likewise it can be chown that

$$i_q(s) = \frac{i_{qo}}{s} + (V_m \mathcal{L}(\sin\delta - \sin\delta_o) - i_{qo}\frac{X_e}{s})\ \frac{1}{X_{qe}(s)} \qquad (2.29)$$

Now Ψ_{de} and Ψ_{qe} are simple functions (Eqns.(2.21) and (2.22)) of the δ, but the currents (Eqns. (2.28) and (2.29)) are in Laploce form and have to be inversely transformed into the time domain before T_e can be calculated.

Putting $1/X_{de}(s)$ and $1/X_{qe}(s)$ into partial fractions, Eqn. (2.28) becomes

$$\left.\begin{aligned}
i_d(s) &= \frac{i_{do}}{s} - \frac{A}{X'_{de}} && \ldots\ i_{d1}(s) \\
&+ A\left(\frac{1}{X'_{de}} - \frac{1}{X_{de}}\right) \cdot \frac{1}{(1 + sT'_{de})} && \ldots\ i_{d2}(s) \\
&\dot{-} A\left(\frac{1}{X''_{de}} - \frac{1}{X'_{de}}\right) \cdot \frac{sT''_{de}}{(1 + sT''_{de})} && \ldots\ i_{d3}(s)
\end{aligned}\right\} \qquad (2.30)$$

$$\text{where } A = -\sqrt{2} \quad V \mathcal{L}(\cos\delta) + \frac{\sqrt{2} \quad V \cos\delta_o}{s} + \frac{i_{do}X_e}{s}$$

and Eqn. (2.29) becomes

$$\left.\begin{aligned} i_q(s) &= \frac{i_{qo}}{s} \quad \frac{B}{X_{qe}} && i_{q1}(s) \\ &+ 0 && i_{q2}(s) \\ &+ B\left(\frac{1}{X''_{qe}} - \frac{1}{X_{qe}}\right) \cdot \frac{sT''_{qe}}{(1 + sT''_{qe})} && i_{q3}(s) \end{aligned}\right\} \quad (2.31)$$

$$\text{where } B = \sqrt{2} \cdot V \mathcal{L}(\sin\delta) - \frac{\sqrt{2} \; V \sin\delta_o}{s} - \frac{i_{qo}X_e}{s}$$

The current components i_{d1}, i_{d2}, i_{d3}, etc can now be inversely transformed and, corresponding to each pair of currents (i_{d1}, i_{q1}), (i_{d2}, i_{q2}) etc. Eqn. (2.11) for the electrical torque yields corresponding torque components.

First torque component

Previous literature[1,11] has used Heaviside's calculus which yields basically the same results although approached and solved in a somewhat different form.

Standard transforms may be used for the inverse Laplace transformations of $i_{d1}(s)$ and $i_{q1}(s)$. Therefore from Eqn. (2.30)

$$i_{d1}(t) = \frac{\sqrt{2} \cdot V \cos\delta}{X'_{de}} - \frac{\sqrt{2} \quad V \cos\delta_o}{X'_{de}} + i_{do} \cdot \frac{X'_d}{X'_{de}} \qquad (2.32)$$

From the phasor diagram in Fig. 2.3

$$i_{do}X'_d = -\sqrt{2} \cdot V'_{qo} + \sqrt{2} \cdot V \cos\delta_o \qquad (2.33)$$

and after substituting this expression into equation (2.32) it is found that

$$i_{d1}(t) = - \frac{\sqrt{2}}{X'_{do}} \quad (V'_{qo} - V \cos\delta) \tag{2.34}$$

Likewise i_{q1} $(t) = \frac{\sqrt{2}V}{X_{qe}} \sin\delta$ (2.35)

The torque component corresponding to i_{d1} and i_{q1} is found from Eqns. (2.11),(2.21),(2.22),(2.34) and (2.35) as

$$T_{e1} = \frac{VV'_{qo}}{X'_{de}} \cdot \sin\delta - \frac{V^2}{2} \left(\frac{1}{X'_{de}} - \frac{1}{X_{qe}}\right) \cdot \sin2\delta \tag{2.36}$$

Second torque component

Since $i_{q2} = 0$, the second torque component is a function of i_{d2} only.

$$T_{e2} = \frac{-Vi_{d2}}{\sqrt{2}} \quad \sin\delta \tag{2.37}$$

Effectively i_{d2} introduces a torque term proportional to sinδ which suggests that the first term in Eqn. (2.36) does not have a constant coefficient.

It has been shown that i_{d2} is due to variation of the field flux linkage and consequently of V'_{qo}, while

$$T_{e2} = \frac{VV'_{q2}}{X'_{de}} \cdot \sin\delta$$

$$V'_{q2} = \frac{-X'_{de}}{\sqrt{2}} \cdot i_{d2} \tag{2.38}$$

After substituting for i_{d2} from Eqn. (2.30) into Eqn.(2.38) it is found that

$$-\mathcal{L}(V'_{q2}) = \frac{X'_{de}}{\sqrt{2}}\left(-\sqrt{2}\ .\ V\ .\ \mathcal{L}(\cos\delta) + \frac{\sqrt{2}\ .\ V}{s}\ \cos\delta_o + \frac{i_{do}.X_e}{s}\right)$$

$$\left(\frac{1}{X'_{de}}\quad \frac{1}{X_{de}}\right).\ \frac{1}{(1 + sT'_{de})}$$

$$= (-V\mathcal{L}(\cos\delta) + \frac{V}{s}\cos\delta_o + \frac{i_{do}X_e}{s\sqrt{2}})(\frac{X_{de} - X'_{de}}{X_{de}}).\ \frac{1}{(1 + sT'_{de})}$$

The phasor diagram relationship can be used to show that

$$-(1 + sT'_{de})\ .\ \mathcal{L}(V'_{q2}) = -V\mathcal{L}(\cos\delta)(1 - \frac{X'_{de}}{X_{de}}) - \frac{1}{s}(V_o\frac{X'_{de}}{X_{de}} - V'_{qo})$$

or

$$V'_{q2} + T'_{de}\ \frac{d}{dt}(V'_{q2}) = V\cos\delta(1 - \frac{X'_{de}}{X_{de}}) + V_o\frac{X'_{de}}{X_{de}} - V'_{qo} \qquad (2.39)$$

Assuming constant d-axis flux linkage, V'_{qo} remains constant, but any variation in the flux linkage introduces the additional term T_{e2}. Now V'_{q2} is the amount by which V'_q changes from its steady state value of V'_{qo} so that $V'_q = V'_{qo} + V'_{q2}$, and from Eqn. (2.39) we find

$$\frac{dV'_q}{dt} = \frac{1}{T'_{de}}(-V'_q + \frac{X'_{de}}{X_{de}}V_o + (1 - \frac{X'_{de}}{X_{de}}))\ V\cos\delta \qquad (2.40)$$

and

$$T_{e2} = \frac{V}{X'_{de}}(V'_q - V'_{qo})\sin\delta \qquad (2.41)$$

where $V'_q = V'_{qo}$ at $t = 0$. The value of V'_q is calculated by a step-by-step method using Eqn. (2.40) to find the new value at the end of each interval.

Third torque component

From Eqn.(2.30)it is seen that

$$i_{d3}(s) = -(-\sqrt{2}\ V\mathcal{L}(\cos\delta) + \frac{\sqrt{2}\ V}{s}\ \cos\delta_o + \frac{i_{do}X_e}{s})(\frac{1}{X''_{de}} - \frac{1}{X'_{de}})\frac{sT''_{de}}{1 + sT''_{de}}$$

$$= \sqrt{2} \quad \alpha \, V \quad \frac{sT''_{de}}{(1 + sT''_{de})} \cdot \mathcal{L}(\cos\delta) \qquad \ldots \quad d_1(s)$$

$$- \sqrt{2} \quad \alpha \, V \cos\delta_o \cdot \frac{T''_{de}}{1 + sT''_{de}} \qquad \ldots \quad d_2(s)$$

$$- \alpha \, i_{do} X_e \cdot \frac{T''_{de}}{1 + sT''_{de}} \qquad \ldots \quad d_3(s)$$

where $\alpha = \dfrac{1}{X''_{de}} - \dfrac{1}{X'_{de}}$

Now $d_2(s)$ and $d_3(s)$ are readily transformable, but not $d_1(s)$ which contains the product of two Laplace functions, one of which is an unknown function of 's'

The expression

$$d_1(s) = \frac{s}{1 + sT''_{de}} \quad \mathcal{L}(\cos\delta) \cdot \alpha \sqrt{2} V$$

is of the form

$$L_1(s) = \frac{s}{s + a} \cdot \mathcal{L}(\cos\delta)$$

which can be solved by convolution integral when used in conjunction with the indicial admittance[23]. Therefore if

$$L_1(s) = s \mathcal{L}(A(t) \quad f(t)) \text{ then}$$

$$L_1(t) = (\int_o^t A(t - \lambda) \cdot f'(\lambda) \cdot d\lambda) + A(t)f(o)$$

where $A(t)$ is the indicial admittance. For the purpose of this analysis

$$A(s) = \frac{1}{\frac{1}{T''_{de}} + s} \quad \text{and} \quad A(t) = e^{-t/T''_{de}}$$

while $f(\lambda) = \cos(\delta(\lambda))$ with $f'(\lambda) = -\sin\delta \cdot \dfrac{d\delta}{d\lambda}$

$$\text{So} \quad L_1(t) = e^{-t/T''_{de}} \cdot \cos\delta_o + \int_o^t e^{-(t - \lambda)/T''_{de}} \cdot f'(\lambda) \cdot d\lambda \qquad (2.42)$$

Since T''_{de} is a short time constant, and $f(\lambda)$ changes relatively slowly, the integral in Eqn. (2.42) may be evaluated approximately by giving $f'(\lambda)$ its value at $\lambda = t$ and taking it outside the integral, resulting in

$$L_1(t) = e^{-t/T''_{de}} \cdot \cos\delta_o + \sin\delta \cdot p\delta \cdot T''_{de}(e^{-t/T''_{de}} - 1)$$

$$\text{So} \quad d_1(t) = \sqrt{2}\alpha V \left[T''_{de} \cdot \sin\delta \cdot p\delta(e^{-t/T''_{de}} - 1) + e^{-t/T''_{de}} \cos\delta \right] \qquad (2.43)$$

$$\text{while} \quad d_2(t) = \sqrt{2}\, \alpha V \cos\delta_o \cdot e^{-t/T''_{de}}$$

$$d_3(t) = -\alpha i_{do} X_e^{-t/T''_{de}}$$

The values of $d_2(t)$, $d_3(t)$ and exponential terms in $d_1(t)$ decay rapidly and can be neglected with respect to the other terms of $d_1(t)$, and hence

$$i_{d3}(t) = -\sqrt{2} \;\; \alpha\, V T''_{de} \sin\delta \cdot p\delta \qquad (2.44)$$

It can be shown in a simalar way that

$$i_{q3}(t) = \sqrt{2}\; \beta V T''_{qe} \cos\delta \cdot p\delta \qquad (2.45)$$

$$\text{where} \quad \beta = \frac{1}{X''_{qe}} - \frac{1}{X_{qe}}$$

Eqns. (2.44) and (2.45) combined with Eqns. (2.21) and (2.22) render the torque as

$$T_{e3} = (a.\sin^2\delta + b.\cos^2\delta)S \qquad (2.46)$$

where $a = \omega V^2 T''_{de} \alpha$; and $b = \omega V^2 T''_{qe} \beta$

while $\omega S = \dfrac{d\delta}{dt}$ and S is the slip.

The total electrical torque produced by the machine is the sum of the individual components, so that

$$
\left.
\begin{aligned}
T_e = {} & \frac{VV'_{qo}}{X'_{de}} \cdot \sin\delta - \frac{V^2}{2}\left[\frac{1}{X'_{de}} - \frac{1}{X_{qe}}\right] \sin 2\delta && \ldots\ldots T_{e1} \\
& + \frac{VV'_{q2}}{X'_{de}} \cdot \sin\delta && \ldots\ldots T_{e2} \\
& + (a.\sin^2\delta + b.\cos^2\delta)S && \ldots\ldots T_{e3}
\end{aligned}
\right\} \quad (2.47)
$$

where $V'_{q2} = V'_q - V'_{qo}$ and at $t = 0$, $V'_{q2} = 0$, thereafter being found from Eqn. (2.40) at each interval of a step-by-step solution. Also X'_{de}, X_{qe} etc. is the reactance of a modified alternator which has the external reactance X_e added to the alternator's leakage reactance X_a while the infinite bus voltage has become the terminal voltage of the modified alternator.

In Eqn. (2.47) the component T_{e1} represents the synchronizing and transient saliency torques, T_{e2} allows for a change in field flux linkage while T_{e3} represents a damping torque proportional to slip.

2.3.2 A change in the excitation voltage

In the second type of transient disturbance, the voltage v_f, applied to the alternator field changes by an amount Δv_f. The equivalent two axis circuits are again employed (see Fig. 2.6) to find the components of electrical torque.

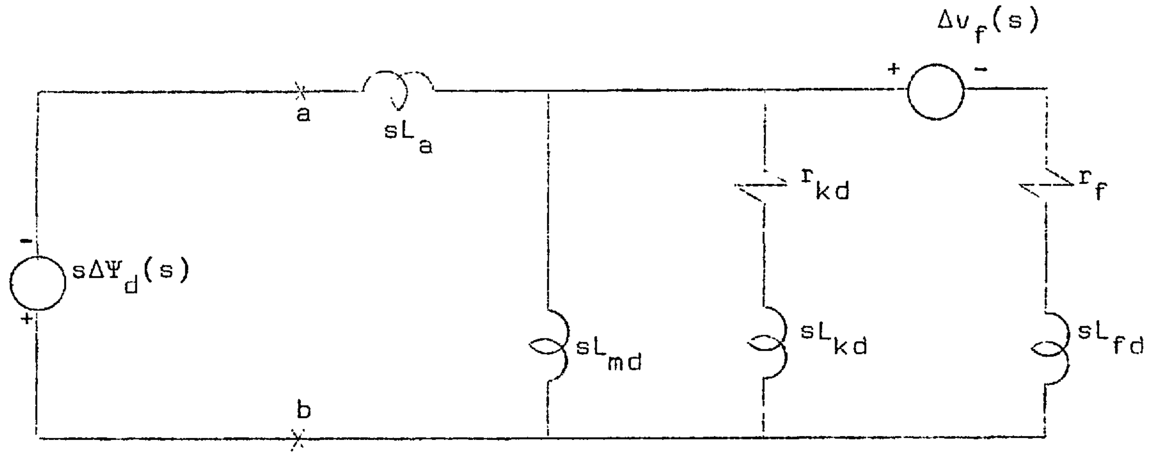

Fig. 2.6 The d-axis circuit for changes in field voltage

The current i_d changes firstly by an amount Δi_{df} due to the change Δv_f, and secondly, by an amount $\Delta i_{d\delta}$ because of a change in the rotor angle δ. According to the generalized machine theory (in Laplace form),

$$\Psi_d(s) = \frac{X_d(s)}{\omega} \cdot i_d(s) + \frac{G(s)}{\omega} \cdot v_f(s) \tag{2.48}$$

from which

$$\Delta i_d(s) = \frac{\omega . \Delta\Psi_d(s)}{X_d(s)} - \frac{G(s)}{X_d(s)} \cdot \Delta v_f(s)$$

$$= \Delta i_{d\delta}(s) + \Delta i_{df}(s) \tag{2.49}$$

Eqn. (2.15) shows that

$$\Delta\Psi_d(s) = \frac{\sqrt{2}\ V}{\omega} \mathcal{L}(\cos\delta - \cos\delta_o)$$

therefore

$$\Delta i_{d\delta}(s) = \frac{\sqrt{2}}{X_d(s)} \quad V \cdot \mathcal{L}(\cos\delta - \cos\delta_o) \tag{2.50}$$

and by putting $\dfrac{1}{X_d(s)}$ into partial fractions as before, $\Delta i_{d\delta}(s)$ may be readily transformed into the time domain. However, in the case of $\Delta i_{df}(s)$ the term $G(s)/X_d(s)$ also needs partial fractioning.

$$\text{Now} \quad \frac{G(s)}{X_d(s)} = \frac{(1 + T_{kd}.s) \quad X_{md}}{(1 + T_d' .s)(1 + T_d''s)r_f X_d}$$

$$= \frac{X_{md}}{r_f X_d} \left(\frac{A}{1 + sT_d'} + \frac{B}{1 + sT_d''} \right)$$

$$\text{where} \quad A = \frac{(1 - T_{kd}/T_d')}{(1 - T_d''/T_d')} \approx 1 \tag{2.51}$$

$$\text{and} \quad B = \frac{T_d'' - T_{kd}}{T_d'' - T_d'} \approx 0 \tag{2.52}$$

Since in Fig. 2.6 the polarity of $\Delta v_f(s)$ is such as to reduce i_d, the total value of $i_d(s)$ after the change is

$$i_d(s) = \frac{i_{do}}{s} - \sqrt{2}\, V \mathcal{L}(\cos\delta - \cos\delta_o) \frac{1}{X_d'} \qquad \ldots\ldots\ i_{d1}(s)$$

$$+ D \left(\frac{1}{X_d'} - \frac{1}{X_d}\right) \cdot \left(\frac{1}{1 + sT_d'}\right) \qquad \ldots\ldots\ i_{d2}(s)$$

$$- D \left(\frac{1}{X_d''} - \frac{1}{X_d'}\right) \cdot \left(\frac{sT_d''}{1 + sT_d''}\right) \qquad \ldots\ldots\ i_{d3}(s)$$

$$- \Delta v_f(s) \frac{X_{md}}{r_f X_d} \cdot \frac{A}{(1 + sT_d')} \qquad \ldots\ldots\ i_{d4}(s)$$

$$- \Delta v_f(s) \frac{X_{md}}{r_f X_d} \cdot \frac{B}{(1 + sT_d'')} \qquad \ldots\ldots\ i_{d5}(s)$$

Likewise

$$i_q(s) = \frac{i_{qo}}{s} + \sqrt{2}\; V \mathcal{L}(\sin\delta - \sin\delta_o) \cdot \frac{1}{X_q} \qquad \ldots\; i_{q1}(s)$$

$$+ \sqrt{2} \cdot V \; \mathcal{L}(\sin\delta - \sin\delta_o)\left(\frac{1}{X''_q} - \frac{1}{X_q}\right) \cdot \frac{sT''_q}{(1 + sT''_q)} \qquad \ldots\; i_{q2}(s)$$

The effect of the current components i_{d1}, i_{d2}, i_{d3}, i_{q1} and i_{q3} upon the torque is the same as in Sect. 2.3.1.

The effect of i_{d4} and i_{d5} due to $\Delta v_f(s)$ connot be assessed in the time domain unless the general disturbance Δv_f is assigned a specific value, which for the purpose of this study is chosen as a step decrease ΔV_f in the field voltage. The result is that

$$i_{d4} = \frac{AX_{md}\Delta V_f}{r_f X_d}\left(1 - e^{-t/T'_d}\right)$$

and $$i_{d5} = \frac{BX_{md}\Delta V_f}{r_f X_d}\left(1 - e^{-t/T''_d}\right)$$

The corresponding torque terms are

$$T_{e4} = -\frac{VA}{\sqrt{2}} \cdot \frac{X_{md}\Delta V_f}{r_f X_d}\left(1 - e^{-t/T'_d}\right)\sin\delta \qquad (2.53)$$

$$T_{e5} = -\frac{V.B}{\sqrt{2}} \cdot \frac{X_{md}\Delta V_f}{r_f X_d}\left(1 - e^{-t/T''_d}\right)\sin\delta \qquad (2.54)$$

With the approximate values for A and B from Eqns. (2.51) and (2.52) substituted in Eqns. (2.53) and (2.54), the value of T_{e5} becomes zero and

$$T_{e4} = \frac{-V}{\sqrt{2}} \cdot \frac{X_{md}\Delta V_f}{r_f X_d}\left(1 - e^{-t/T'_d}\right)\sin\delta \qquad (2.54)$$

So, for a step decrease in the excitation the torque becomes

$$T_e = T_{e1} + T_{e2} + T_{e3}$$

$$- \frac{V}{\sqrt{2}} \quad \frac{X_{md}\Delta V_f}{r_f X_d} (1 - e^{-t/T'_d}) \sin\delta \qquad \ldots\ldots T_{e4} \qquad (2.56)$$

2.3.3 Change in prime mover output

When considering the effect of voltage regulators on the transient performance of the alternator, it has been assumed [13,15] that the disturbance may be a sudden change in the shaft torque or prime mover output. This eliminates some of the additional considerations such as fault type, duration and distance when considering a sudden change on the stator side. In practice this type of prime mover disturbance seems an unlikely one due to the relatively long time constants of the governor and turbine. However, to demonstrate the theoretical value of such investigations, this case has been included in the comparison of large disturbances.

Suppose the shaft torque T_s from the prime mover suddenly increases by an amount ΔT_s while the field voltage as well as transmission line configuration remain unchanged. The rotor angle δ changes and hence the voltage components v_d and v_q. If there is a constant external tie-line reactance X_e in the system, this can be added to the alternator's leakage reactance X_a as in Sect. 2.3.1

The change in v_q is

$$\Delta v_q(s) = - \sqrt{2}V \mathcal{L}(\cos\delta - \cos\delta_o) \qquad (2.57)$$

as in Eqn.(2.27) while the input impedance (analagous to Fig. 2.5) is

$$Z_{de}(s) = \frac{sX_{de}(s)}{\omega}$$

The change in d-axis current is

$$\Delta i_d(s) = -\sqrt{2}V \mathcal{L}(\cos\delta - \cos\delta_o)\frac{1}{X_{de}(s)}$$

and after the change

$$i_d(s) = \frac{i_{do}}{s} - \Delta i_d(s)$$

$$= \frac{i_{do}}{s} + \sqrt{2}V \mathcal{L}(\cos\delta - \cos\delta_o) \cdot \frac{1}{X_{de}(s)} \qquad (2.58)$$

Likewise it can be shown that

$$i_q(s) = \frac{i_{qo}}{s} + \sqrt{2}\ V\ (\sin\delta - \sin\delta_o) \cdot \frac{1}{X_{qe}(s)} \qquad (2.59)$$

When the partial fraction forms of $\frac{1}{X_{de}(s)}$ and $\frac{1}{X_{qe}(s)}$ are used

$$\left.\begin{aligned} i_d(s) = {} & \frac{i_{do}}{s} - \frac{A}{X'_{de}} && \cdots\cdots\ i_{d1}(s) \\ & + A\left(\frac{1}{X'_{de}} - \frac{1}{X_{de}}\right) \cdot \frac{1}{1 + sT'_{de}} && \cdots\cdots\ i_{d2}(s) \\ & - A\left(\frac{1}{X''_{de}} - \frac{1}{X'_{de}}\right) \cdot \frac{sT''_d}{(1 + sT''_{de})} && \cdots\cdots\ i_{d3}(s) \end{aligned}\right) \qquad (2.60)$$

where $A = -\sqrt{2}\ V \mathcal{L}(\cos\delta) + \frac{\sqrt{2}\ V}{s}\cos\delta_o$

$$\left.\begin{aligned} \text{while} \quad i_q(s) &= \frac{i_{qo}}{s} + \frac{B}{X_{qe}} && \cdots\cdots \; i_{q1}(s) \\ &+ 0 && \cdots\cdots \; i_{q2}(s) \\ &+ B\left(\frac{1}{X''_{qe}} - \frac{1}{X_{qe}}\right) \cdot \frac{sT''_q}{(1 + sT''_{qe})} && \cdots\cdots \; i_{q3}(s) \end{aligned}\right) \tag{2.61}$$

where $B = -\sqrt{2}\, V \mathcal{L}(\sin\delta) - \frac{\sqrt{2}\, V}{s} \sin\delta_o$

First torque component

The inverse Laplace transformation of $i_{d1}(s)$ becomes

$$i_{d1}(t) = \frac{\sqrt{2}\, V \cos\delta}{X'_{de}} - \frac{\sqrt{2}\, V \cos\delta_o}{X'_{de}} + i_{do} \tag{2.62}$$

but, from the phasor diagram in Fig. 2.3,

$$i_{do} X'_{de} = -\sqrt{2}\, V'_{qo} + \sqrt{2} \cdot V \cos\delta_o$$

so that

$$i_{d1}(t) = -\frac{\sqrt{2}}{X'_{de}} (V'_{qo} - V \cos\delta) \tag{2.63}$$

Likewise

$$i_{q1}(t) = \frac{\sqrt{2}\, V}{X_{qe}} \sin\delta$$

Hence

$$T_{e1} = \frac{V V'_{qo}}{X'_{de}} \cdot \sin\delta + \frac{V^2}{2} \left(\frac{1}{X'_{de}} - \frac{1}{X_{qe}}\right) \cdot \sin 2\delta \tag{2.64}$$

which is identical to T_{e1} due to switching in external reactance. It can likewise be shown that the second and the third torque components are also identical to those in Sect. 2.3.1

The accellerating torque of the generator is

$$T_{acc} = Jp^2\delta = (T_s \pm \Delta T_s) - (T_{e1} + T_{e2} + T_{e3}) \tag{2.65}$$

$$= T_s - (T_{e1} + T_{e2} + T_{e3} \mp \Delta T_s)$$

so that $T = \pm \Delta T_s$

Thus the machine behaves as it an additional constant electrical torque has suddenly appeared.

2.3.4 A symmetrical short-circuit

2.3.4.1 The single transmission line

In the case of a single transmission line, as shown in Fig. 2.7 the symmetrical three-phase fault isolates the machine from the infinite bus and since the resistances of the machine and transmission line have been neglected, the electromagnetic torque of the alternator becomes zero.

The d-axis equivalent circuit used to study this phenomena is seen in Fig. 2.8. When S1 is closed, the pre-fault

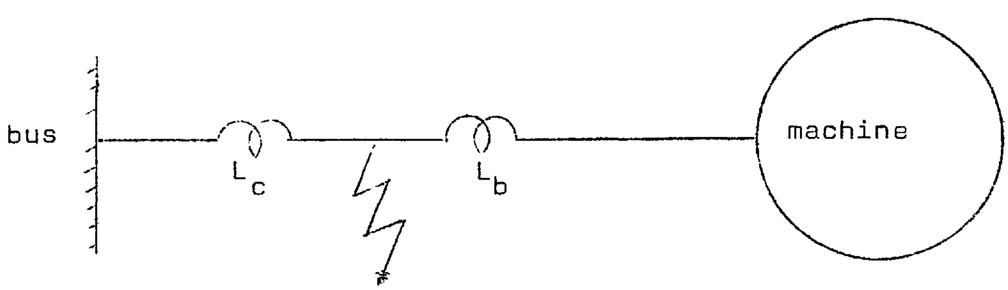

Fig. 2.7 Symmetrical fault on a single transmission line

voltage across the point 'ab' becomes zero and disturbs the current balance in the machine, while shorting any connection to the infinite bus.

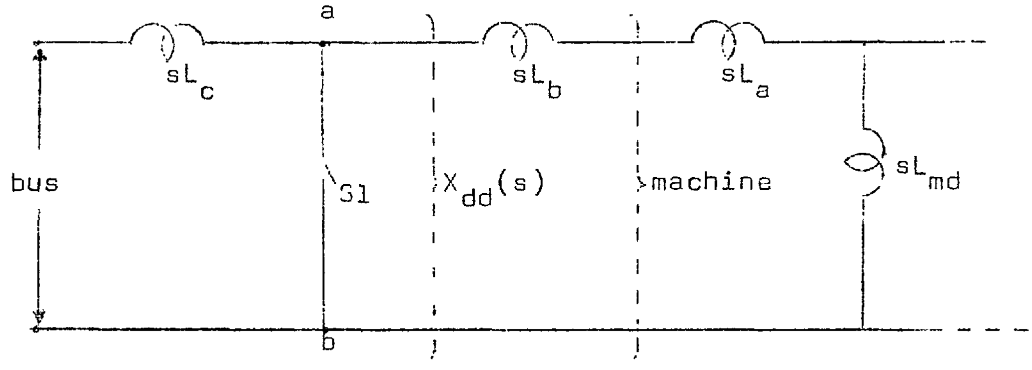

Fig. 2.8 The d-axis circuit for changes only

The voltage

$$V_{ab}(s) = \frac{s\ V_m \cos\delta_o}{\omega} - i_{do} sL_c$$

across 'ab' is made zero by applying a step voltage of opposite polarity in series with S1.

The transformed change in i_{do} is

$$\Delta i_d(s) = \frac{-V_m \cos\delta + i_{do} X_c}{sX_{db}(s)} \tag{2.66}$$

which, after inserting the partial fractions of $X_{db}(s)$, becomes

$$\Delta i_d(s) = (-\sqrt{2}\ V \cos\delta_o + X_c i_{do}) \left[\frac{1}{X_{db}} + \left(\frac{1}{X'_{db}} - \frac{1}{X_{db}}\right) e^{-t/T'_{db}} \right.,$$

$$\left. + \left(\frac{1}{X''_{db}} - \frac{1}{X'_{db}}\right) e^{-t/T''_{db}} \right] \tag{2.67}$$

At no-load

$$\Delta i_d(t) = -\sqrt{2}\ V_q \left[\frac{1}{X_{db}} + \left(\frac{1}{X'_{db}} - \frac{1}{X_{db}}\right) e^{-t/T'_{db}} + \left(\frac{1}{X''_{db}} - \frac{1}{X'_{db}}\right) e^{-t/T''_{db}} \right] \quad (2.68)$$

which is the well known expression for the "alternating component" of the short-circuit current. The "asymmetrical component" is absent because $p\Psi_d$ and $p\Psi_q$ were neglected.

The total post-fault d-axis and q-axis currents are

$$i_d(t) = i_{do} + \frac{A}{X_{db}} + A\left(\frac{1}{X'_{db}} - \frac{1}{X_{db}}\right) e^{-t/T'_{db}} + A\left(\frac{1}{X''_{db}} - \frac{1}{X'_{db}}\right) e^{-t/T''_{db}} \quad (2.69)$$

$$i_q(t) = i_{qo} - \frac{B}{X_{qb}} - B\left(\frac{1}{X''_{qb}} - \frac{1}{X_{qb}}\right) e^{-t/T''_{qb}} \quad (2.70)$$

where $A = -\sqrt{2}\ V \cos\delta_o + i_{do}X_c$; and $B = \sqrt{2}\ V \sin\delta_o - i_{qo}X_c$;

The final steady values of these currents correspond to[21]

$$i_d = \frac{-\sqrt{2}\ V'_{qo}}{X'_{db}} = \frac{-\sqrt{2}\ V_o}{X_{db}} \text{ and } i_q = 0; \text{ (see phasor diagram, Fig.2.3)}$$

The pre-fault flux linkages at the points 'ab' of Fig. 2.8, are

$$\Psi_{do} = \frac{1}{\omega}\left(\sqrt{2}\ V \cos\delta_o - i_{do}X_c\right) \quad (2.71)$$

$$\Psi_{qo} = \frac{1}{\omega}\left(\sqrt{2}\ V \sin\delta_o - i_{qo}X_c\right) \quad (2.72)$$

The changes in flux linkages when the fault is applied, are

$$\Delta\Psi_d(s) = \frac{X_{db}(s)}{\omega} \cdot \Delta i_d(s) \quad (2.73)$$

$$\Delta\Psi_q(s) = \frac{X_{qb}(s)}{\omega} \cdot \Delta i_q(s) \quad (2.74)$$

The total flux linkages after the change are found from Eqns.(2.66) and (2.71) to (2.74) as

$$\Psi_d = \Psi_{do} + \Delta\Psi_d = 0 \tag{2.75}$$

$$\Psi_q = \Psi_{qo} + \Delta\Psi_q = 0 \tag{2.76}$$

which confirms that

$$T_e = T_{e1} = T_{e2} = T_{e3} = 0 \tag{2.77}$$

2.3.4.2 The twin transmission line

In the case of a twin transmission line as shown in Fig.2.9, the healthy line may still be able to provide synchronizing torque, provided the fault is not at either extreme of the faulted line. The torque and current expression are different from Eqns. (2.67) to (2.77).

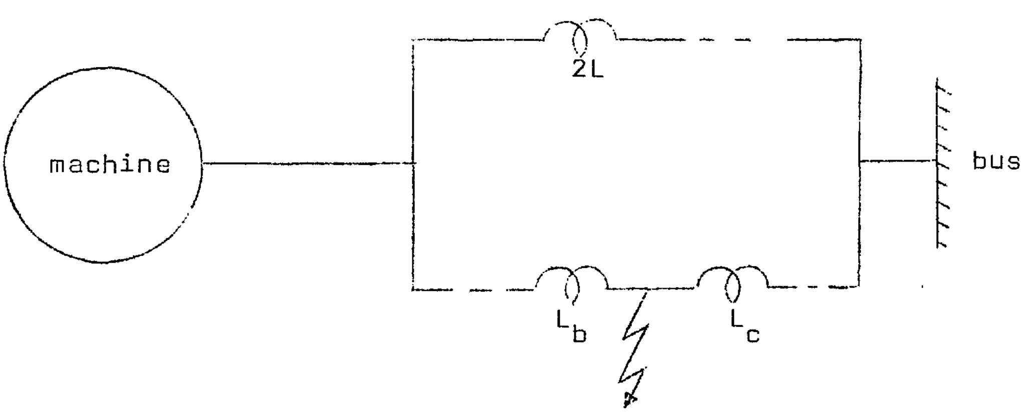

Fig. 2.9 Symmetrical fault on a twin transmission line

The d-axis equivalent circuit portraying these changes is shown in Fig. 2.10. The closing of S1 applies the fault and a delta-star transformation can be made from Fig. (2.10) to (2.11). Mathematical simplification results by taking $L_b + L_c = 2L$, without reducing the comparative significance of the results.

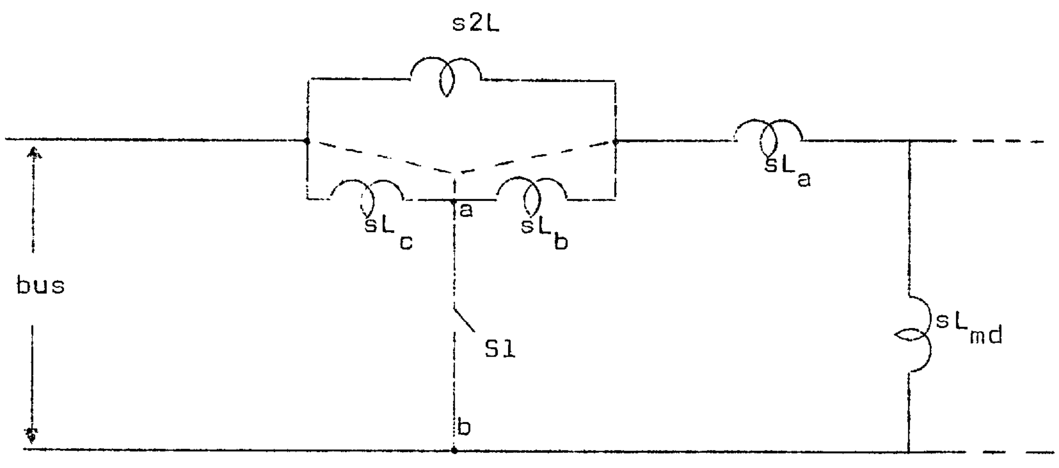

Fig. 2.10 Twin transmission line and d-axis circuit.

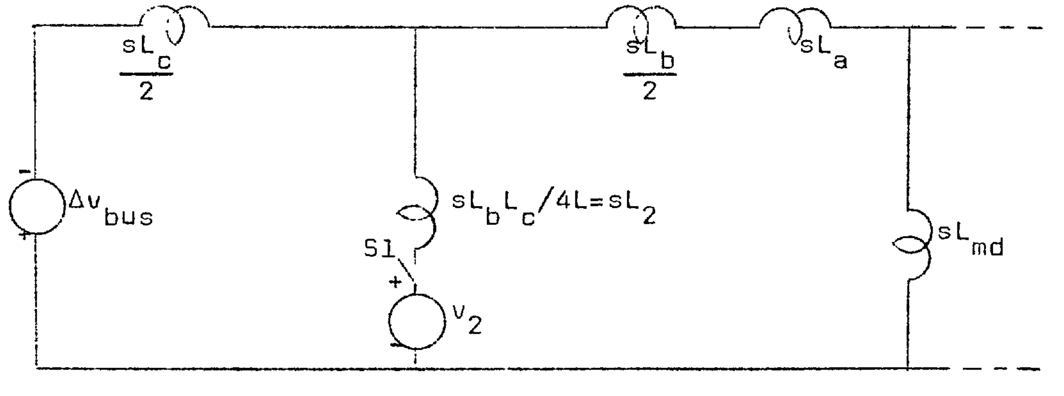

Fig. 2.11 The d-axis circuit with two voltage sources for changes only

Now $v_2 = \frac{1}{\omega}(V_m \cos\delta - i_{do}X_{c2})$, where $X_{c2} = X_c/2$

and $\Delta v_{bus} = \frac{sV_m}{\omega}(\cos\delta - \cos\delta_o)$

and as shown in Fig. 2.11, the two voltage sources have opposite effects on i_d.

Millman's theorem on superposition yields

$$i_d(s) = \frac{i_{do}}{s} - \frac{K_2(V_m \cos\delta_o - i_{do}X_{c2}) - K_1 sV_m \mathcal{L}(\cos\delta - \cos\delta_o)}{sX_{d3}(s)}$$

and

$$i_q(s) = \frac{i_{qo}}{s} - \frac{K_2(V_m \sin\delta_o - i_{qo}X_{c2}) - K_1 sV_m \mathcal{L}(\sin\delta - \sin\delta_o)}{sX_{q3}(s)}$$

where: $X_3 = \dfrac{X_2 X_{c2}}{X_c + X_{c2}}$;

X_{db} includes $\frac{X_b}{2}$ as additional leakage reactance;

X_{d3} includes X_3 in X_{db} as additional leakage reactance and likewise for X_{q3}; while

$$K_1 = \frac{X_2}{X_2 + X_{c2}} \; ; \quad K_2 = \frac{X_{c2}}{X_2 + X_{c2}} \; ; \quad K_1 + K_2 = 1;$$

The flux linkages at the point 'ab', which are now not zero as for the single line, are (see Fig. 2.10)

$$\Psi_d = \frac{K_1}{\omega}(V_m \cos\delta - i_{do}X_{c2}) \tag{2.78}$$

$$\Psi_q = \frac{K_1}{\omega}(V_m \sin\delta - i_{qo}X_{c2}) \tag{2.79}$$

Gathering the corresponding current components and combining them with Eqns. (2.78) and (2.79) yield the torque components as:

$$T_{e1} = \frac{K_1 V V'_{qo} . \sin\delta}{X'_{d3}} - \frac{K_1^2 V^2}{2} \left(\frac{1}{X'_{d3}} - \frac{1}{X_{q3}}\right) \sin 2\delta$$

$$+ \frac{K_1 V X_{c2} \sin\delta (K_1 V'_{qo} - V\cos\delta_o)}{X_{q3}(X'_{db} + X_{c2})}$$

$$+ \frac{K_1 V V'_{qo} X_{c2} \sin\delta_o (K_1 \sin\delta - 1)}{X'_{d3}(X_{qb} + X_{c2})}$$

$$T_{e2} = - K_1 K_2 . M(\delta) \left(\frac{1}{X'_{d3}} - \frac{1}{X_{d3}}\right) e^{-t/T'_{d3}} + \frac{K_1 V V'_{q2} . \sin\delta}{X'_{d3}}$$

(where $M(\delta) = V^2 . \sin\delta . \cos\delta_o - \frac{V}{\sqrt{2}} \cdot i_{do} X_{c2} . \sin\delta + \frac{V}{\sqrt{2}}(i_{qo} X_{c2} . \cos\delta_o)$

$+ i_{qo} i_{do} X_{c2}^2)$

$$T_{e3} = K_1 (a . \sin^2\delta + b . \cos^2\delta) S - K_1 K_2 M(\delta) \left(\frac{1}{X''_{d3}} - \frac{1}{X'_{d3}}\right) e^{-t/T''_{d3}}$$

while $X'_{d3} = X'_{db} + X_3$;

$X'_{d3} + X_{c2} K_2 = X'_{db} + X_{c2}$;

$X_{q3} + X_{c2} K_2 = X_{qb} + X_{c2}$;

Hence neglecting the exponontially decaying terms the complete expression for the torque is

$$T_e = \frac{K_1 VV'_{qo}}{X'_{d3}} \cdot \sin\delta - \frac{K_1^2 V^2}{2}\left[\frac{1}{X'_{d3}} - \frac{1}{X_{q3}}\right] \sin 2\delta$$

$$+ \frac{K_1 VV'_{q2}}{X'_{d3}} \cdot \sin\delta + K_1(a.\sin^2\delta + b.\cos^2\delta)S$$

$$+ \frac{K_1 VX_{c2}.\sin\delta(K_1 V'_{qo} - V\cos\delta_o)}{X_{q3}(X'_{db} + X_{c2})}$$

$$+ \frac{K_1 VV'_{qo} X_{c2}.\sin\delta_o(K_1.\sin\delta - 1)}{X'_{d3}(X_{qb} + X_{c2})} \qquad (2.80)$$

the factor K_1 varies between zero and unity, depending upon the position of the fault along the twin line. It is zero because $X_2 = 0$ for a fault either at the machine terminals or at the bus and in both cases T_e is zero with the assumptions made.

2.4 Comparison of Various Disturbances

The transient electrical torques for the various disturbances considered in Sect. 2.3 follow much the same pattern, permitting certain assumptions in the derived analytical results. The torque in each case has three main components as in Eqn. (2.47), viz:-

$$T_{e1} = \frac{K_1 VV'_{qo}}{X'_{de}} \cdot \sin\delta - \frac{K_1 V^2}{2}\left(\frac{1}{X'_{de}} - \frac{1}{X_{qe}}\right)\sin 2\delta$$

(synchronizing) (saliency)

$$T_{e2} = + \frac{K_1 VV'_{q2}}{X'_{de}} \cdot \sin\delta$$

(field flux decay)

$$T_{e3} = + K_1(a.\sin^2\delta + b.\cos^2\delta)S$$

(damping)

The three components are common to all the disturbances considered, provided

(i) adjustments in X_d, X_{de}, etc. are made when allowing for external reactance to be lumped with the alternator's own leakage reactance, and

(ii) adjustments are made in the value of the coefficent K_1, which is equal to unity except in the case of a short circuit along a transmission line. For a twin line the value of K_1 is between 0 and 1, depending on the position of the fault, but for a single transmission line the value of K_1 is always zero.

There are in addition the following components for each individual disturbance:

$$T_{e4} = -\frac{V}{\sqrt{2}} \frac{X_{md}.\Delta V_f}{r_f X_d} (1 - e^{-t/T'_d}) \sin\delta$$

(step decrease ΔV_f in the alternator field voltage)

$$T_{e5} = \pm \Delta T_s$$

(step change ΔT_s in prime mover output)

$$T_{e6} = + \frac{K_1 V X_{c2}.\sin\delta(K_1 V'_{qo} - V\cos\delta_o)}{X_{q3}(X'_{db} + X_{c2})}$$

$$+ \frac{K_1 V V'_{qo} X_{c2}.\sin\delta_o(K_1 \sin\delta - 1)}{X'_{d3}(X_{qb} + X_{c2})}$$

(three phase fault along a twin transmission line: see note (ii) above for value K_1) (2.81)

The synchronizing, saliency, varying field flux linkage and damping torque components are common to the most commonly accepted disturbances. For each individual disturbance other than the shorting of a reactance, some additional torque terms appear. However for a three phase fault along one of two parallel transmission lines the value of the torque depends on the distance between the fault and the alternator.

So although some authors (see Sect. 2.1) have chosen a rather impractical step-change in prime mover torque as the transient disturbance, it does test the system behaviour as regards the mechanical movement of the rotor in much the same way as a change in alternator excitation (since the term T_{e4} decays fairly rapidly), or changing the tie-line reactance.

As stated in Sect. 2.2 the three main torque components T_{e1}, T_{e2} and T_{e3} of Eqn. (2.81) correspond to a simplified mathematical model. Although theory is approximate, the following significant conclusions can be drawn.

Using only the component T_{e1} corresponds to neglecting damping and assuming that the field flux linkage remains constant and thereby regarding V'_{qo} as a constant voltage. Saliency is however allowed for in T_{e1}, and the two terms of T_{e1} are recognized as the synchronizing and the transient saliency torques respectively.

A more accurate model which allows for changing field flux linkages but no damping, introduces the additional component T_{e2}.

Damping is allowed for approximately by means of the terms T_{e3}. If there is zero subtransient saliency T_{e3} becomes a constant multiplied by the slip. This corresponds to Crary's[24] damping torque which has been used by many authors.

---oOo---

CHAPTER 3

3. CLASSIFICATION OF METHODS OF SOLUTION

The approximate expressions of Eqn. (2.81) in Sect. 2.4, based on the assumptions of Sect. 2.1, are acceptable for many purposes, but situations may arise where a more accurate representation of the machine is needed.

The literature survey not only showed that various types of disturbances have been considered by different authors, but also that various methods of solving the stability problem have been used, as below.

3.1 Methods using Torque-angle Characteristics

Assuming that the voltage V_q' (see Fig. 2.3) behind transient reactance is constant and that the torque is a function of the angle only, stability can be studied by means of the equal area criterion. This corresponds to assuming constant flux linkage and no damping.

3.2 Methods using a Step-by-step Computation

Most stability studies are based on the machine equations and use a step-by-step computation, but there are many variations depending on the assumptions made. The torque is calculated at each step and used to determine the changes in load angle. All the methods require a solution of the second order differential equation for rotor movement and the transient response is found in the form of a swing curve, i.e. a curve of load angle as a function of time.

Methods A to D, in the following classification, neglect the terms $p\Psi_d$, $p\Psi_q$ and resistance r_a in Eqns. (2.1) and (2.2), while methods A to C also neglect any departure in speed from synchronous speed.

A. The earliest methods[24], commonly worked out by means of a network analyser, assumed a constant voltage behind transient reactance (V' in Fig. 3.1) and zero transient saliency i.e. $X_q = X_d'$.

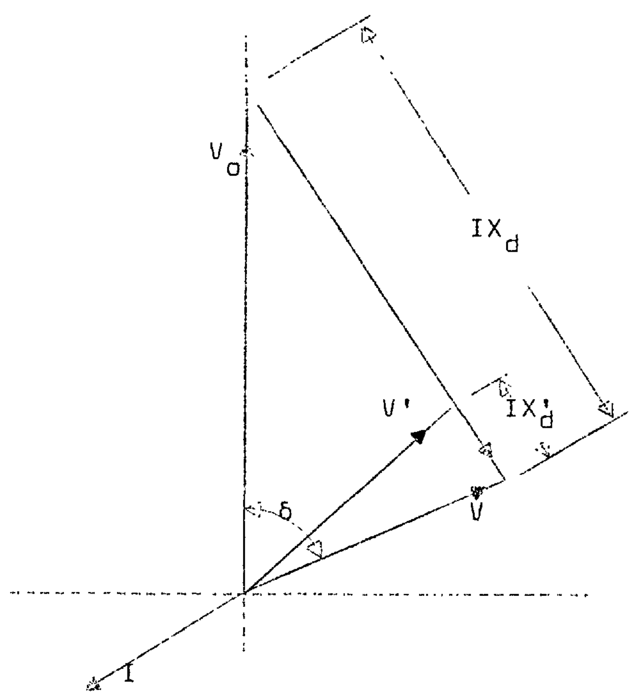

Fig. 3.1 <u>Generator phasor diagram for steady state or for slow transients, assuming zero transient saliency</u>

The assumptions are therefore similar to those in Sect. 3.1 but the method can readily be applied to a multi-machine system. With some extra complication saliency can be taken into account as in Fig. 2.3 from which it is seen that $V_q' = V'$, $V_d' = 0$ and $X_q \neq X_d'$.

For a single machine system the torque becomes the T_{e1} component of Eqn. (2.47).

B. Although the closed circuit field winding reacts to maintain a constant field flux linkage, it does in practice decay slowly because of the losses in the field resistance. A change in the field flux linkage may also be caused by a varying excitation due to voltage regulator action. This effect is allowed for by means of the additional torque component T_{e2} of Eqn. (2.81).

C. Damping can be allowed for approximately by means of a torque component proportional to slip as shown by the component T_{e3} of Eqn. (2.81). The method, corresponds to the "standard method" of Sect. 4.2.1 with the additional assumption that the alternator has zero sub-transient saliency.

D. Damping may be allowed for more accurately by solving directly the complete machine equations (2.1) to (2.10), but still neglecting $p\Psi_d$ and $p\Psi_q$. This corresponds to the "approximate method" of Sect. 4.2.2.

E. For the most accurate treatment the terms $p\Psi_d$, $p\Psi_q$ and r_a are retained in the machine equations. The tie-line's resistance can also be included, as well as the inductive volt drop due to sudden changes in the amplitude of the armature and line current. This is referred to as the "accurate method" in Sect. 4.2.3.

3.3 Lyapunov's Method

This method, which has been applied to non-linear control systems, determines the boundary between a stable and an unstable operating region for a particular type of disturbance. The criterion depends on a performance figure calculated from a "Lyapunov equation". When the performance figure exceeds a critical value it is possible to forecast[25-27] a loss of synchronism after a disturbance, without having to determine the swing curve. The method has the advantage that provided with the correct Lyapunov equation, a stability forcast can be made rapidly in the form of a "GO" or "NO GO" answer.

Lyapunov's method is claimed to be of general application to all systems, but it has hitherto tended to give pessimistic results for transient stability studies. Unfortunately also, the Lyapunov equation as used by various authors, differs from one to the other, indicating that no general equation or any hard and fast rule for generating such an equation, has yet been established. Even these studies had to be confined to simplified systems and alternators without damping or subtransient effects, voltage regulators, or governors.

3.4 Choice of Method of Representation

It is difficult to make any hard and fast rule regarding the choice of any one method of representing a particular system. Some general deductions may be made although each individual case should be treated on its merits.

A fixed excitation system can be studied by using a constant voltage V_q' behind transient reactance and a damping term proportional to slip.

To allow for the effect of voltage regulators, the variation of V_q' must be included. However, if the flux changes slowly, it may still be permissible to assume that the $p\Psi$ terms are negligible in Eqns. (2.1) and (2.2). If the machine equations allow for damping, the voltage behind subtransient ractance has to be adjusted similarly during a step-by-step solution. (see Sect. 4.2.2.)

In the case of a three phase short circuit the value of $p\Psi_d$ or $p\Psi_q$ may rise to a value comparable with $\omega\Psi_d$ and $\omega\Psi_q$. The terms $p\Psi_d$ and $p\Psi_q$ decay with time, but removal of the fault restarts a rapid variation of Ψ_d and Ψ_q.

At the prsent time it seems doubtful whether the Lyapunov method can be applied successfully until it has been developed as a more readily applicable tool, especially to the more complete practical[6] representation as needed for transient studies.

---oOo---

P A R T   T W O

MORE ACCURATE METHODS OF SOLUTION AND COMPARISONS WITH TEST RESULTS OF A THREE-PHASE FAULT

CHAPTER 4

4. THEORY OF MORE ACCURATE METHODS

4.1 General

At an earlier stage stability calculations were made for generators with fixed excitation, assuming the field flux linkages to be constant[24]. Damping could be allowed for by means of a constant damping coefficient. Later methods have been developed to allow for changing field flux linkage, taking account of the action of voltage regulators and governors[28,29]. Such methods involved, in the first place, an inaccurate allowance for damping and, secondly, the assumption that the rate of change of stator flux linkages ($p\Psi_d$ and $p\Psi_q$) can be neglected. This chapter shows how these factors can be included in a digital calculation.

The need for a more accurate method than that shown in Sect. 2.3.4 was clearly shown by tests made at the Cliff Quay Station 1956[30]. A three phase short circuit test, made when the machine was loaded, gave a result illustrated by Fig. 4.1, which did not agree with the calculated curve. The calculated curve shows an immediate rise of the load angle δ, whereas the test curve has a temporary dip, referred to as a "back swing", before an eventual rise. The phenomenon is in fact advantageous in a generator because it allows more time to clear the fault.

In Ref. 1 an acceptable approximate analytical solution of the machine equations was derived for an initial period, retaining the $p\Psi$ terms but assuming constant speed. With the assumption of

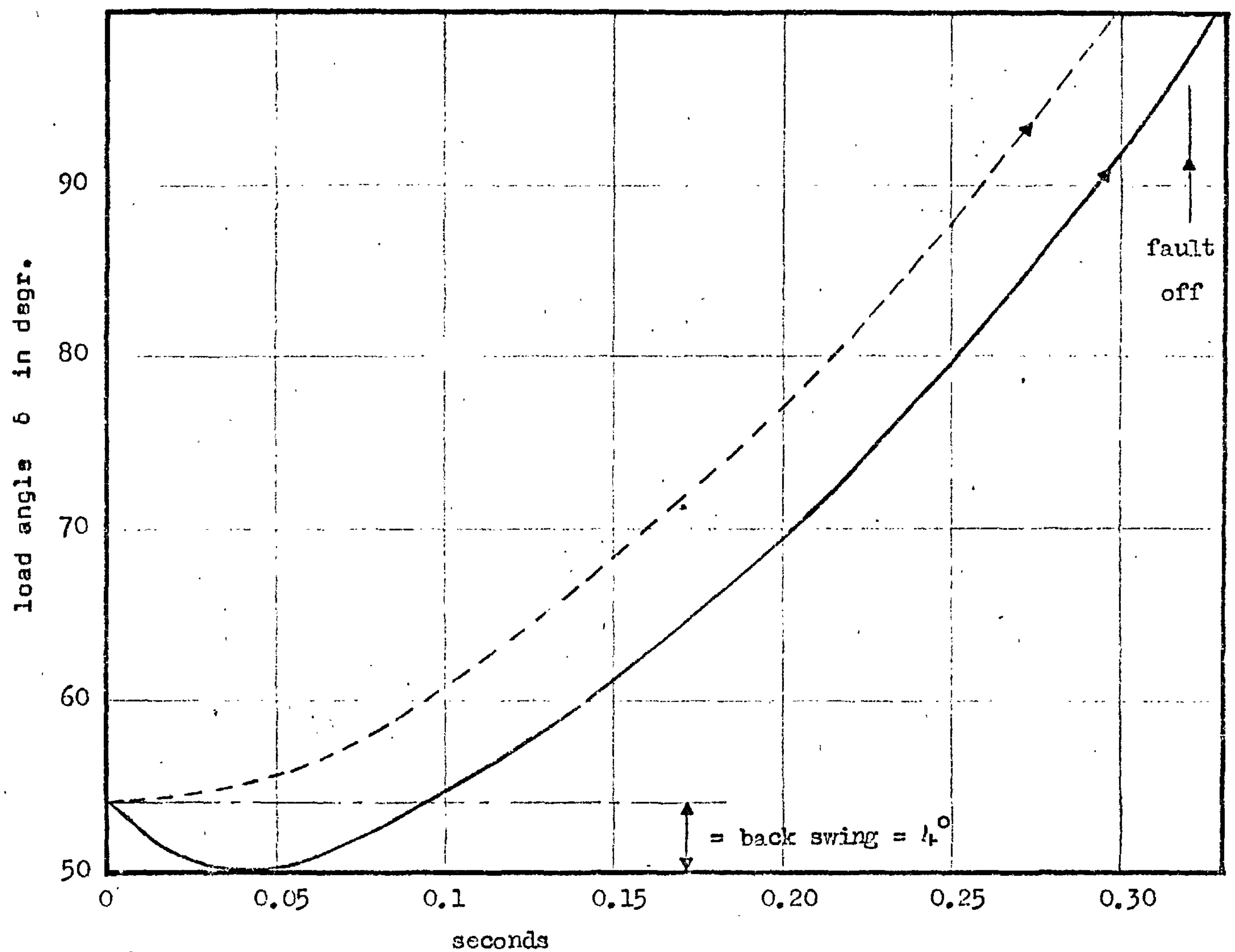

Fig.4.1 Load angle after a short-circuit on a 56 MVA generator at Cliff Quay.

—— Test curve; ----Computed curve;

constant speed the non-linear differential Eqns. (4.1) and (4.2) become linear. The predicted values agreed fairly closely with micro-machine test results and showed that, when a three phase short circuit occurs, there is in addition to oscillating components, a transient unidirectional torque which may, under certain conditions, produce a back swing of the type shown in Fig. 4.1. The study by the above authors highlighted the individual transient torque components and their effects.

An approximate physical picture of the back swing phenomenon may be formed by realising that after a short circuit (isolating the machine from any external busbar) the 'flux wave represented by Ψ_d and Ψ_q' remains as a flux wave stationary with respect to the armature[22]. Voltages are induced in the rotor circuits and the consequent currents cause power losses in the resistance of any closed circuits on the rotor. These losses together with the armature short circuit power losses produce a unidirectional retarding or braking torque which opposes the prime mover torque. Hence there is less torque available to accelerate the rotor after a fault has been applied.

The unidirectional torque decays rapidly and has hitherto been neglected in many studies of transient performance. However the initial value may be considerably larger than the pre-fault prime mover torque and thus be able to produce a retardation or back swing during the short period of its duration. There is evidently a need for a more accurate general method applicable for transient conditions when the speed variation cannot be neglected. Such a method has been developed for analogue computation by Shackshaft[6] and a digital method has been published by Humpage and Saha[17].

The development of an improved digital method in the following sections is made in two stages.

(a) The first stage allows more fully for the action of the damper winding, but neglects $p\Psi_d$ and $p\Psi_q$. This is referred to below as the "approximate method," (see Sect. 3.2, method D).

(b) The second stage accounts for $p\Psi_d$ and $p\Psi_q$ as well and is referred to as the "accurate method", (see Sect. 3.2, method E).

The approximate method gives the results in the same form as earlier ones. The axis currents and the torque are slowly changing quantities, where the changes occurring during an a.c. cycle are small. The stator currents can be regarded as sinusoidal quantities at any instant and can be represented by slowly changing phasors. Thus the time interval in a step-by-step calculation can be relatively long, since the system on the stator side can be treated as an a.c. network in which the complex values change slowly, and the axis quantities in the machine calculations also change slowly.

The situation is quite different when $p\Psi_d$ and $p\Psi_q$ are included in the equations for the accurate method. It is known that, in the calculation of the short circuit current of an unloaded alternator, omission of the $p\Psi$ terms corresponds to neglect of the asymmetrical component of the stator current and to the assumption of slowly changing axis quantities and phasors as explained above. Including the $p\Psi_d$ and $p\Psi_q$ terms therefore results in the axis quantities changing at about supply frequency and it becomes difficult to interpret the oscillating components of a phasor. It also means that the time interval for a step-by-step calculation must be short compared with the period of the a.c. cycle and hence requires a great increase in the computer time.

The first computations performed to obtain results with the "accurate method" made use of the standard Runge- Kutta method of integration and required a very long computer time. By using more efficient methods[31,32] of integration it was possible to reduce the computer time dramatically. This matter is more fully discussed in Chapter 7.

There are several practical operating conditions where the earlier equations do not give sufficiently accurate results. The condition considered in detail in this thesis is the application and removal of a three phase short circuit to a loaded alternator where a back swing may occur. The back swing can also occur in the case of synchronous and induction motors where the effect would be disadvantageous. A further example, not considered here, is an alternator with rectifiers in the field circuit where the current may have sharp discontinuities.

4.2 Alternator Equations and Methods of Solution

The basic system being considered is the single machine case shown in Fig. 2.1. The basic machine equations for such a system are Eqns. (2.1) to (2.10), repeated below as Eqns. (4.1) to (4.10) so that the subsequent mathematical development may be followed with greater ease.

The equations are:

$$v_d = p\Psi_d + \nu\Psi_q + r_a i_d \tag{4.1}$$

$$v_q = -\nu\Psi_d + p\Psi_q + r_a i_q \tag{4.2}$$

$$0 = r_{kd} i_{kd} + p\Psi_{kd} \tag{4.3}$$

$$0 = r_{kq} i_{kq} + p\Psi_{kq} \tag{4.4}$$

$$v_f = r_f i_f + p\Psi_f \tag{4.5}$$

for voltages, and

$$\Psi_d = L_{dd} i_d + L_{md} i_{kd} + L_{md} i_f \tag{4.6}$$

$$\Psi_q = L_{qq} i_q + L_{mq} i_{kq} \tag{4.7}$$

$$\Psi_{kd} = L_{md} i_d + L_{kkd} i_{kd} + L_{md} i_f \tag{4.8}$$

$$\Psi_{kq} = L_{mq} i_q + L_{kkq} i_{kq} \tag{4.9}$$

$$\Psi_f = L_{md} i_d + L_{md} i_{kd} + L_{ffd} i_f \tag{4.10}$$

for the flux linkages, and

$$T_e = \frac{\omega}{2} (\Psi_d i_q - \Psi_q i_d) \tag{4.11}$$

for the electromagnetic torque.

4.2.1 Standard Method

With the assumptions of the "standard method" in Sect. 3.2, Eqn. (2.77) shows that the electromagnetic torque of the alternator immediately becomes zero when a three phase short circut occurs, and the calculated curve of δ is incorrect. The standard method or variants of it has been commonly used in the past, but under certain conditions, as described above, a more accurate solution of the equations is needed.

4.2.2 Approximate Method

The "approximate method" makes full allowance for damping and system resistances and subtransient saliency and for variations in the speed. However the changes in flux linkages represented by $p\Psi_d$ and $p\Psi_q$ are neglected.

The method was worked out by Alford[33], who showed that Eqns. (4.1) to (4.10) can be rearranged as follows.

$$\omega\Psi_d = X''_d i_d + \omega(X''_d - X_a)\left(\frac{\Psi_f}{X_{fd}} + \frac{\Psi_{kd}}{X_{kd}}\right) \tag{4.12}$$

$$\omega\Psi_q = X''_q i_q + \omega(X''_q - X_a)\frac{\Psi_{kq}}{X_{kq}} \tag{4.13}$$

$$p\Psi_{kd} = \left[\frac{(X'_d - X_a)}{\omega} \cdot i_d + \frac{(X'_d - X_a)}{X_{fd}} \cdot \Psi_f - \Psi_{kd}\right] / T''_{do} \tag{4.14}$$

$$p\Psi_{kq} = \left[\frac{X_{mq} i_q}{\omega} - \Psi_{kq}\right] / T''_{qo} \tag{4.15}$$

$$p\Psi_f = v_f + \frac{1}{X'_{do}}\left[\frac{(X''_d - X_a)}{(X'_d - X_a)} \cdot \left[\frac{X_{md} i_d}{\omega} + \frac{X_{md}\Psi_{kd}}{X_{kd}}\right] - \Psi_f\left[1 + \frac{(X''_d - X_a)X_{md}}{X_{kd}X_{fd}}\right]\right] \tag{4.16}$$

when use is made of the following indentities

$$\omega\left(L_{dd} - \frac{L_{md}^2}{L_{ffd}}\right) = X'_d \;; \qquad \omega\left(L_{qq} - \frac{L_{mq}^2}{L_{kkq}}\right) = X''_q \;;$$

$$\omega\left(L_{md} - \frac{L_{md}^2}{L_{ffd}}\right) = X'_d - X_a ; \qquad \frac{L_{mq}}{L_{kkq}} = \frac{(X''_q - X_a)}{X_{kq}} \;;$$

$$\omega\left(L_{kkd} - \frac{L_{md}^2}{L_{ffd}}\right) = \frac{(X'_d - X_a)}{(X''_d - X_a)} \cdot X_{kd} \;; \qquad \frac{L_{md}}{L_{ffd}} = \frac{X'_d - X_a}{X_{fd}} \;;$$

The terminal voltage equations (4.1) and (4.2) can be written (neglecting $p\Psi$ terms) as

$$\left.\begin{aligned} v_{mtd} &= r_a i_d + X_q'' i_q + v_d'' \\ v_{mtq} &= r_a i_q + X_d'' i_d + v_q'' \end{aligned}\right\} \qquad (4.17)$$

Hence, the alternator can be represented by a voltage behind sub-transient reactance and the two axis components are

$$\left.\begin{aligned} v_d'' &= -SX_q'' i_q + \omega(X_q'' - X_a)\frac{\Psi_{kd}}{X_{kq}} \\ v_q'' &= SX_d'' i_d - \omega(1 - S)(X_d'' - X_a)\left(\frac{\Psi_f}{X_{fd}} + \frac{\Psi_{kd}}{X_{kd}}\right) \end{aligned}\right\} \qquad (4.18)$$

The method of representing the machine by a voltage behind sub-transient reactance combined with a step-by-step solution is explained in Ref. 33.

If the alternator is connected through a transformer and transmission line with a total resistance R and a total resistance X, to an infinite bus having a r.m.s. voltage V_b, then the voltage equations for the interconnection tie-line are:

$$v_{mtd} = \sqrt{2}V_{bd} - Ri_d - \frac{X}{\omega} \cdot \nu i_q \qquad (4.19)$$

$$v_{mtq} = \sqrt{2}V_{bq} - Ri_q + \frac{X}{\omega} \cdot \nu i_d \qquad (4.20)$$

where $V_{bd} = V_b \sin\delta$ and $V_{bq} = V_b \cos\delta$ (4.21)

The generator terminal voltage is given by

$$\sqrt{2}V_{mt} = v_{mt} = \sqrt{v_{mtd}^2 + v_{mtq}^2} \qquad (4.22)$$

The equation for mechanical motion is

$$p^2\delta = \frac{\pi f_o}{H} (T_{in} - T_e - T_L) \qquad (4.23)$$

In a step-by-step solution the voltages given by Eqn. (4.18) is applied at time t_n to the tie-line impedance and infinite bus voltage to find the current components i_d and i_q. The electrical torque and the change in the load angle are determined and hence the new value of load angle at t_{n+1}. Equations (4.14) to (4.16) are used to compute the rate of change of the secondary flux linkages and hence Ψ_f, Ψ_{kd} and Ψ_{kq} may be found at t_{n+1} provided the values are known at time t_n. The new values of the flux linkages are then substituted into Eqn. 4.18 together with the currents (value at t_n) in order to obtain v_d'' and V_q'' at t_{n+1}.

By setting $p\Psi_f = p\Psi_{kd} = p\Psi_{kq} = 0$ before a disturbance is applied, the value of the field voltage is found to be

$$v_{fo} = \left[\Psi_{fo} - i_{do} \frac{(X_d'' - X_a)X_{md}}{(X_d' - X_a)\omega} \left(1 + \frac{(X_d' - X_a)}{X_{kd}} \right) \right] / T_{qo}'$$

The damping torque can no longer be separated from the total electromagnetic torque but is automatically taken care of by the rate at which the flux linkages in Eqns. (4.14) to (4.16) are allowed to change.

The calculated results of Chapter 6 show that the improved method of accounting for damping, does not explain the back swing in load angle after a three phase short circuit.

When zero subtransient saliency is assumed $(X_d'' = X_q'')$ for the alternator, the subtransient reactance can be added to the tie-line reactance, and the axis components of voltage in Eqn.(4.18) can conveniently be transformed into a phasor, representing the phase values, so that the alternator can be treated as a network component. The simplification is particularly useful for dealing with a multi-machine system.

4.2.3 Accurate Method

It has been shown that in the event of a three phase fault a significant error is introduced by the assumption that $p\Psi_d$ and $p\Psi_q$ are negligible. Since the inclusion of $p\Psi_d$ and $p\Psi_q$ allows for stator transients, the voltage equations (4.19) and (4.20) must also take into account the transmission line and transformer inductive volt drop after a sudden change.

Hence

$$v_{mtd} = \sqrt{2}V_{bd} - \frac{X}{\omega} pi_d - Ri_d - \frac{X}{\omega}\nu i_q \tag{4.24}$$

$$v_{mtq} = \sqrt{2}V_{bq} - \frac{X}{\omega} \cdot pi_q - Ri_q + \frac{X}{\omega} \nu i_d \tag{4.25}$$

Expressions for $p\Psi_d$ and $p\Psi_q$ can be found by differentiating Eqns. (4.12) and (4.13) and used to obtain a set of first order differential equations. In doing so, either i_d, i_q can be eliminated and $p\Psi_d$, $p\Psi_q$ retained or Ψ_d, Ψ_q can be eliminated and pi_d, pi_q retained. The two methods are equivalent, but it was decided to use the second alternative, because the currents and their derivatives are present in the external network equations.

It is shown in Appendix I that the primary currents i_d, i_q and the secondary flux linkages Ψ_f, Ψ_{kd} and Ψ_{kq}, can be found from five simultaneous first order differential equations, given in Eqn. (4.26)

$$\begin{bmatrix} pi_d \\ pi_q \\ p\Psi_f \\ p\Psi_{kd} \\ p\Psi_{kq} \end{bmatrix} = \begin{bmatrix} a_1 & va_2 & a_3 & a_4 & va_5 & a_6V_{bd} & a_7 \\ vb_1 & b_2 & vb_3 & vb_4 & b_5 & b_6V_{bq} & 0 \\ c_1 & 0 & c_3 & c_4 & 0 & 0 & 1 \\ d_1 & 0 & d_3 & d_4 & 0 & 0 & 0 \\ 0 & e_2 & 0 & 0 & e_5 & 0 & 0 \end{bmatrix} \begin{bmatrix} i_d \\ i_q \\ \Psi_f \\ \Psi_{kd} \\ \Psi_{kq} \\ 1 \end{bmatrix} \tag{4.26}$$

A step of the computation uses the equations to find values of the variables at t_{n+1} from known values at t_n. First a numerical method of integration is applied to the differential equations (4.26) and the values of the integrable variables (IV's)(see Sect. 7.1) i_d, i_q, Ψ_f, Ψ_{kd} and Ψ_{kq} are found at time t_{n+1}. These are used in the algebraic equations (4.12) and (4.13) to compute the non-integrable variables (NIV's)(see Sect. 7.1) Ψ_q and Ψ_d, which together with i_d and i_q are used to compute algebraically the electromagnetic torque T_e from Eqn. (4.11). For a system with a governor, the differential equations are used to find the prime mover shaft torque T_{in}. The new value of the IV's speed and load angle δ, are found from the differential equation (4.23) The non-integrable variables V_{bd}, V_{bq}, v_{mtd}, v_{mtq}, V_{mt} are calculated from the algebraic equations (4.21),(4.24),(4.25) and (4.22). When an a.v.r. is present the value of V_{mt} is substituted into an algebraic equation and the comparator output is used in the a.v.r.

differential equations (see Sect. 5.2.2) to find the value of the integrable variable V_f. Without an a.v.r. the field voltage V_f. remains constant.

The computation described above is an improvement on previous attempts to solve the non-linear system equations by digital computer. Humpage and Saha[17] retained the $p\Psi$ terms but were unsuccessful in extracting a set of simultaneous differential equations and therefore had to use the numerical method of finite differences to calculate at the end of the nth step the derivatives of variables to be used during the (n + 1) th step. As a result the solution of the flux linkages was always one step behind the solution of the currents or vice versa, and required shorter time steps in the integration process.

Expressions for the voltages v''_d and v''_q behind subtransient reactance, like those in Eqn. (4.18) are found as

$$v''_d = \frac{X''_d p i_d}{\omega} + (X''_d - X_a)\left[\frac{p\Psi_f}{X_{fd}} + \frac{p\Psi_{kd}}{X_{kd}}\right] - SX''_q i_q + \omega(X''_q - X_a)\frac{\Psi_{kq}}{X_{kq}} \tag{4.27}$$

$$v''_q = \frac{X''_q p i_q}{\omega} + \frac{(X''_q - X_a)}{X_{kq}T''_{qo}}\left[\frac{X_{mq}}{\omega}\cdot p i_q - p\Psi_{kq}\right]$$

$$+ SX''_d i_d - (1 - S)\left[\omega(X''_d - X_a)\left(\frac{\Psi_f}{X_{fd}} + \frac{\Psi_{kd}}{X_{kd}}\right)\right] \tag{4.28}$$

However there is no advantage in using Eqns. (4.27) and (4.28) since Eqn. (4.26) gives all that is required.

---o0o---

CHAPTER 5

5. EQUIPMENT USED FOR TESTS

5.1 General

Test results about the transient behaviour of a synchronous generator after a three-phase fault were obtained from results about a 30 MW turbo- alternator and also from experiments performed for the purpose fo this thesis on a micro-machine system at Imperial College. The parameters of the micro-machine system were chosen, where possible, to correspond on a per unit basis as closely as practically possible to the values of the large system.

5.2 A Large Practical System

Although the 30 MW system (see Fig. 5.1) at Goldington has been described in Ref. 6, it is necessary to repeat the description of some of the equipment which has a direct bearing on the studies and results in later chapters.

5.2.1 The Alternator

The data used for the computed results of Chapter 6 appear in Table 5.1.

Table 5.1 Data of 30 MW turbo-generator

Base stator voltage		$9.68 \times \sqrt{3}/\sqrt{2}$ kV, r.m.s. line
Base stator current		$2.59 \times \sqrt{3}/\sqrt{2}$ kA r.m.s.
Base power		37.5 MVA
Base stator impedance		3.73 ohm.
Base field voltage		$153.5/\sqrt{2}$ kV
Base field current		$244/\sqrt{2}$ A
Base field impedance		630 ohm.
Mutual reactance, X_{md}, X_{mq} (unsat.)		1.86 p.u.
Armature leakage reactance, X_a		0.14 p.u.
Armature resistance, r_a		0.002 p.u.
Field leakage reactance, X_{fd}		0.14 p.u.
Field resistance, r_f		0.00107 p.u.
Damper leakage reactance, X_{kd}, X_{kq}		0.04 p.u.
Damper resistance, r_{kd}, r_{kq}		0.00318 p.u.
Inertia constant, H		5.3 kWs/kVA
<u>Calculated data</u>		
Subtransient reactance	X''_d	0.1706 p.u.
	X''_q	0.1792 p.u.
Transient reactance	X'_d	0.2702 p.u.
Time constants:	T'_{do}	5.949 sec.
	T'_d	0.8038 sec.
	T''_d	0.1076 sec.
	T''_q	0.0978

5.2.2 The automatic voltage regulator

The physical operation has been described[6] with reference to the block diagram representation of Fig. 5.2. The equations and parameters in this section are in physical units and the values of a.v.r. parameters appear in Table 5.2

Voltage transformer and comparator

Both references 6 and 17 quote a common gain G_{vs} for the reference level V_{re} and the terminal voltage V_{mt}, while in fact Fig. 5.2, which was first published in Ref. 6 and later used in Ref. 17, shows V_{mt} to pass through a voltage transformer before reaching the error sensing element or comparator stage. The comparator's output

$$V_{m1} = - G_{vs}(V_{mt} - V_{re}) \tag{5.1}$$

therefore implies that the fictitious reference voltage V_r in Eqn. (5.1) is on the same side of the voltage transformer as V_{mt}, and is thus of the order of 12,000 volts.

First magnetic amplifier

$$V_{m2} = \frac{G_{m1}}{1 + \tau_{m1}p} \quad (V_{m1} + V_{xs} + V_{ms}) + K_{m1} \tag{5.2}$$

while $V_{m2\ min} \leqslant V_{m2} \leqslant V_{m2\ max}$

Second magnetic amplifier

$$V_x = \frac{G_{m2}}{1 + \tau_{m2}p} \quad V_{m2} + K_{m2} \tag{5.3}$$

while $V_{x\ min} \leqslant V_x \leqslant V_{x\ max}$

The a.c. exciter and rectifiers

$$V_f = \frac{G_x \quad V_x}{1 + \tau_x p} + K_x \tag{5.4}$$

Ampifier stabilizer

$$V_{ms} = - \frac{G_{ms}\tau_{ms}p}{1 + \tau_{ms}p} \quad V_x \tag{5.5}$$

Exciter stabilizer

$$V_{xs} = - \frac{G_{xs}\tau_{xs}p}{1 + \tau_{xs}p} \cdot V_f \tag{5.6}$$

Steady state initial conditions

Before the disturbance is applied, the steady state values of some regulator variables are found from the values of active-and reactive power, and voltage at the generator terminals.

The reference voltage of the voltage regulator is given by

$$\left.\begin{array}{l} V_{reo} = G_{vs}V_{mto} + (V_{fo} - K_x - G_xK_{m2} - G_xG_{m2}K_{m1})/G_xG_{m1}G_{m2} \\ \text{while} \\ V_{xso} = V_{mso} = 0 \\ V_{xo} = (V_{fo} - K_x)/G_x \\ V_{m2o} = (V_{xo} - K_{m2})/G_{m2} \\ V_{m1o} = (V_{m2o} - K_{m1})/G_{m1} \end{array}\right) \tag{5.7}$$

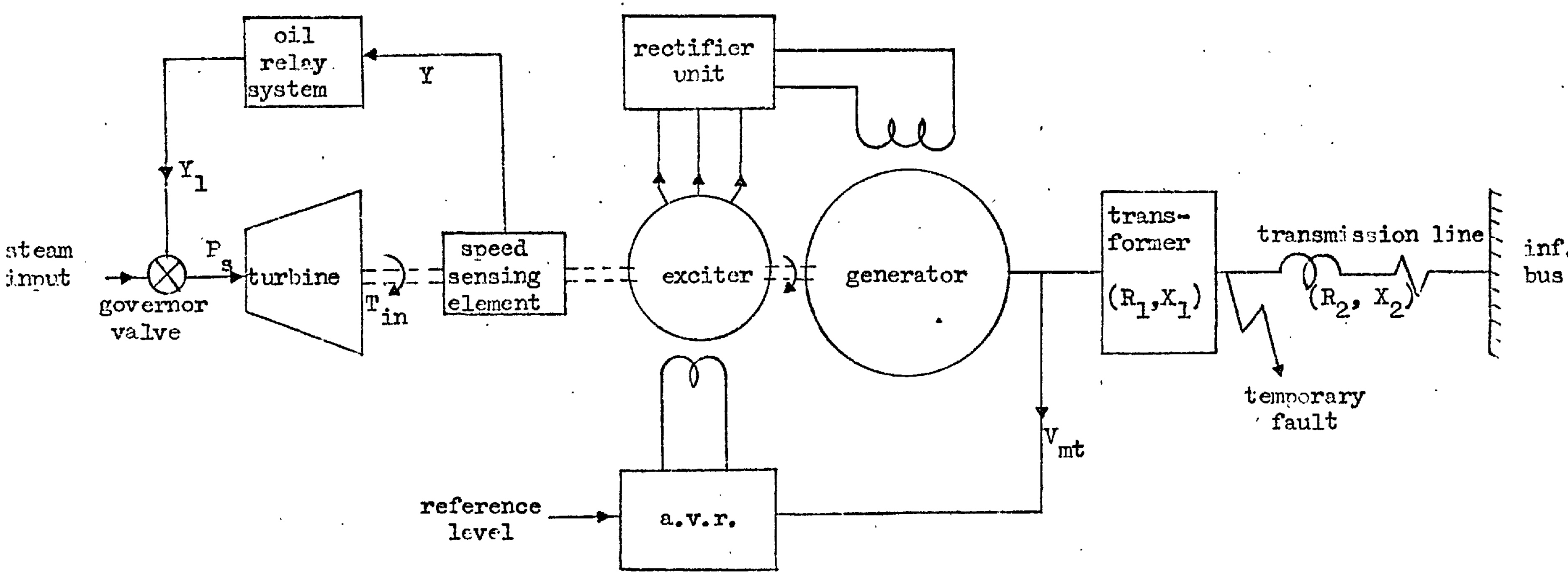

Fig. 5.1 Diagram of the Goldington system.

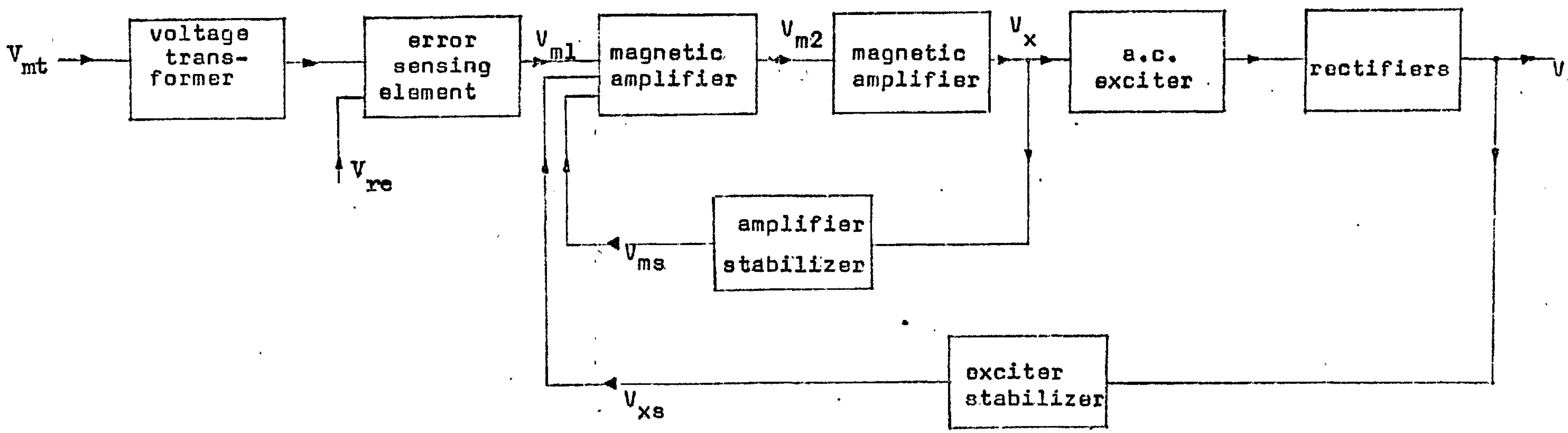

Fig. 5.2 Block diagram of voltage regulator.

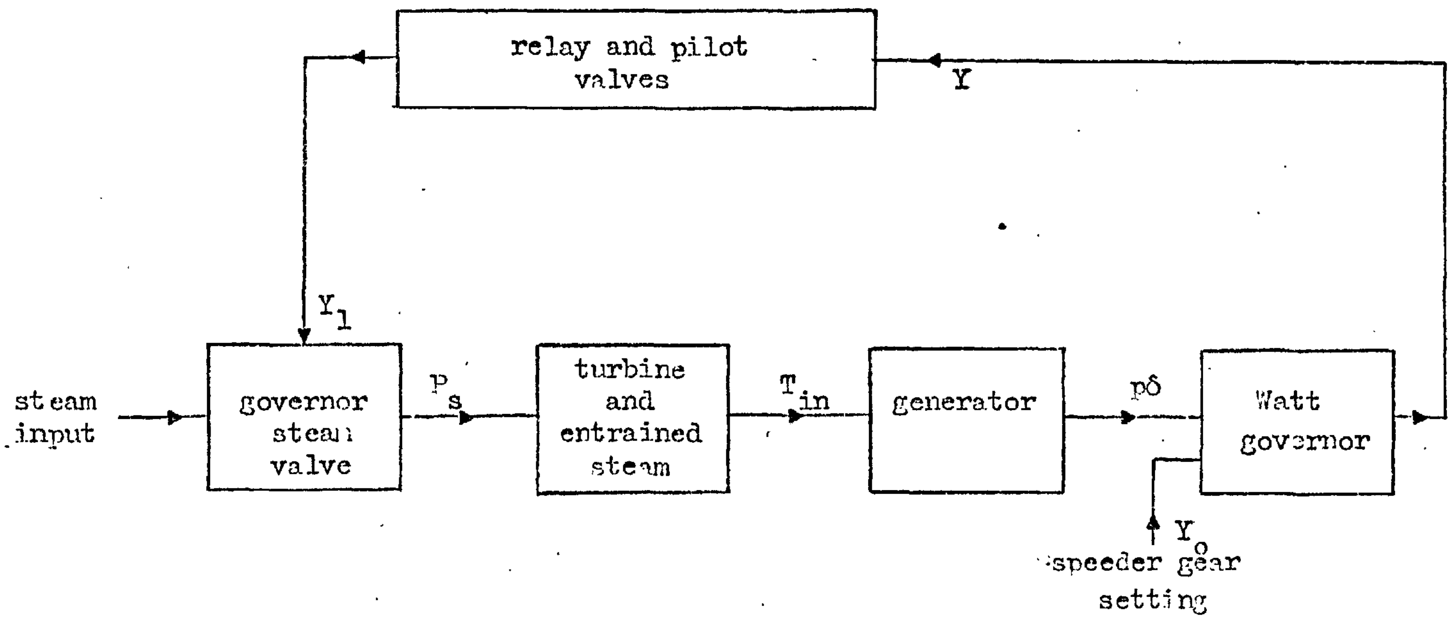

Fig. 5.3 Block diagram of governing system

Table 5.2 Voltage regulator data.

$G_{vs} = 0.00159$	$V_{x\ min} = 0$ V
$G_{m1} = 52$	$V_{x\ max} = 227$ V
$\tau_{m1} = 0.044$ sec.	$G_x = 3.06$
$K_{m1} = 65.4$	$\tau_x = 0.2$ sec.
$V_{m2\ min} = 1.8$ V	$K_x = 15$
$V_{m2\ max} = 51.6$ V	$G_{ms} = 0.0139$
$G_{m2} = 12.2$	$\tau_{ms} = 0.1$ sec.
$\tau_{m2} = 0.1$ sec.	$G_{xs} = 0.00525$
$K_{m2} = -146.7$	$\tau_{xs} = 2.0$ sec.

The value of G_{vs} as listed above is applicable[34] to Eqn. (5.1) when V_{mt} and V_{re} are in line volts r.m.s. G_{ms} and G_{xs} were printed incorrectly in Ref. 6 and corrected values[5] appear in the above table. K_{m2} has a negative value.

5.2.3 The governor and turbine

The physical operation and assumptions for the mathematical model have been described[6] with reference to the block diagram representation of Fig. 5.3, and the values of parameters appear in Table 3.

Centrifugal Watt governor

$$Y = Y_o - G_1 p\delta \tag{5.8}$$

while $0 \leqslant Y \leqslant 1$

Y is proportional to sleeve movement and is zero when the weights are fully out and unity when they are fully in. Y_o is proportional to the speeder gear setting.

Relay and pilot valves

$$Y_1 = \frac{G_2 Y}{(1 + \tau_1 p)(1 + \tau_2 p)} + K_2 \tag{5.9}$$

while $0 \leqslant Y_1 \leqslant 1$

Y_1 is the governor steam valve position and is zero when the valve is fully closed and unity when fully open.

Governor steam valve

$$P_s = G_3 Y_1 \tag{5.10}$$

where P_s is the steam power

Turbine

The turbine output power is delayed by the entrained steam and appears as

$$P_{in} = \frac{P_s}{1 + \tau_3 p} \tag{5.11}$$

The shaft torque transmitted to the alternator is

$$T_{in} = \frac{P_{in}}{(1 + \frac{p\delta}{2\pi f})} \tag{5.12}$$

or, since $\frac{p\delta}{2\pi f}$ is small compared to unity, Eqn. (5.12) can be rearranged by means of the Binomial Expansion Theorem to

$$T_{in} = P_{in}(1 - \frac{p\delta}{2\pi f}) \tag{5.13}$$

which is the form used in Ref. 6.

Steady state initial conditions

At synchronous speed $p\delta = 0$, so

$$\left.\begin{aligned} T_{ino} &= P_{ino} = T_e + T_L = P_{so} = G_3 Y_{1o} \\ \text{Also} \quad Y &= (Y_{1o} - K_2)/G_2 = \left(\frac{P_{ino}}{G_3} - K_2\right)/G_2 = N \\ \text{and the speeder gear setting } Y_o &= N \end{aligned}\right\} \quad (5.14)$$

Table 5.3 Governor and turbine data

$G_1 = 1.088 \times 10^{-3}$	$K_2 = -0.267$
$G_2 = 1.33$	$G_3 = 1.42$
$\tau_1 = 0.1$ sec.	$\tau_3 = 0.49$ sec.
$\tau_2 = 0.188$ sec.	

5.2.4 The tie-line impedance

The tie-line consists of the generator step-up transformer and the transmission line as in Fig. 5.1. The parameters are as follows:

	100 MVA base	37.5 MVA base
R_1	1.35 %	0.506 %
X_1	35.4 %	13.3 %
R_2	4.6 %	1.73 %
X_2	12.65 %	4.74 %

5.3 A Micro-machine System

The micro-machine is connected to the fixed supply, treated as an infinite bus, through series impedance Z_1 and Z_2 as shown in Fig. 5.4. The machine is a small alternator specially designed to give a range of parameters on a per unit (p.u.) basis and values were selected, within limits, to correspond with the large system in Sect. 5.2. The equipment includes a time constant regulator (see Sect. 5.3.2) which controls the effective resistance of the excitation circuit. A governor and a.v.r. were not included in this particular system.

5.3.1 The alternator

The micro-alternator[35] (stator no. 334819, rotor no. 334828) has a laminated cylindrical rotor, although standard test[36] results showed a saliency of about 10%. The machine parameters are given in Table 5.4.

A comparison of Tables 5.4 and 5.1 reveals that the parameters agree fairly well except for the high armature resistance and the small sub-transient time constants. In both cases it was practically impossible to avoid these differences.

Table 5.4 Data of micro-alternator

Base stator voltage	186 V, r.m.s. line
Base stator current	4.3 A r.m.s.
Base armature power	1385 VA
Base stator impedance	25.0 ohm
Base field voltage	1410 V
Base field current	0.491 A
Base field power	692.5 VA
Base field impedance	2870 ohm
Mutual reactance: X_{md}(sat.)	1.71 p.u.
X_{mq}(sat.)	1.51 p.u.
Armature leakage reactance, X_a	0.127 p.u.
Armature resistance, r_a	0.0127 p.u.
Field leakage reactance, X_{fd}	0.095 p.u.
Field resistance, r_f	0.00108 p.u.
Transient reactance, X'_d	0.217 p.u.
Subtransient reactance: X''_d	0.150 p.u.
X''_q	0.170 p.u.
Time constants: T'_{do}	5.34 sec.
T'_d	0.630 sec.
T''_d	0.013 sec.
T''_q	0.013 sec.
Inertia constant, H	5.7 kWs/kVA

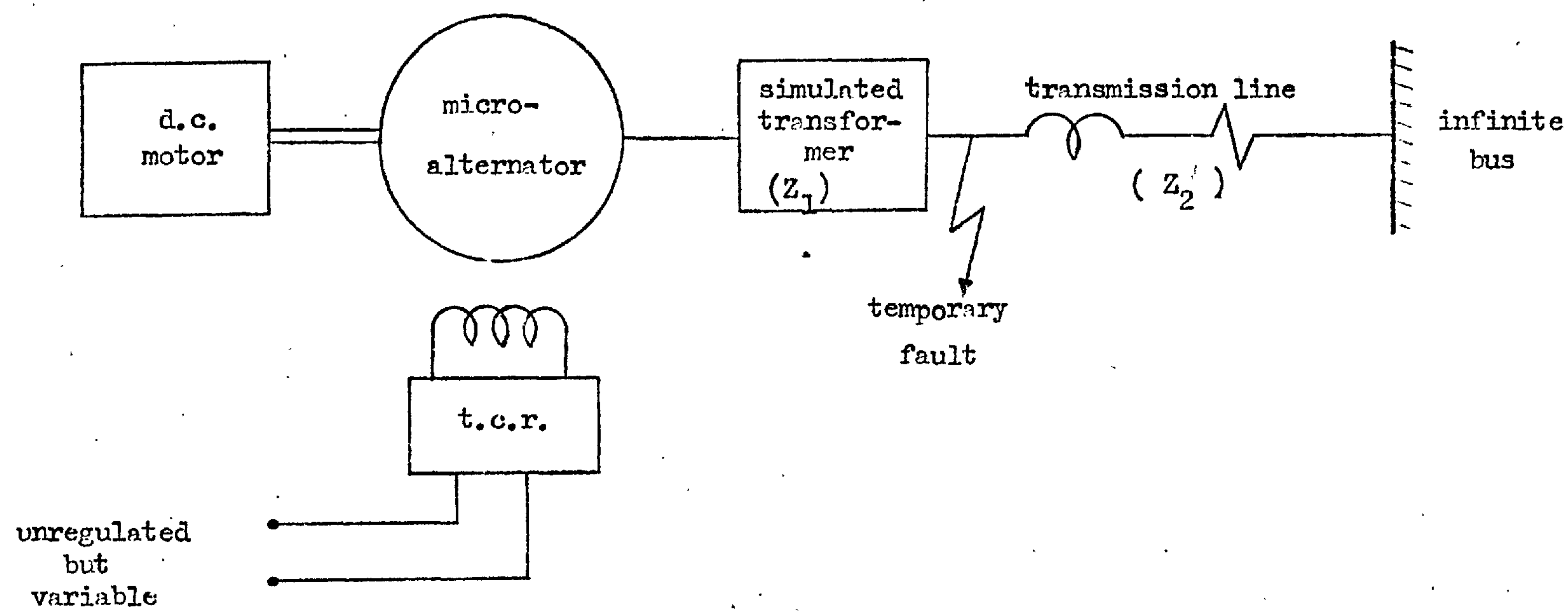

Fig. 5.4 Diagram of the micro-machine system

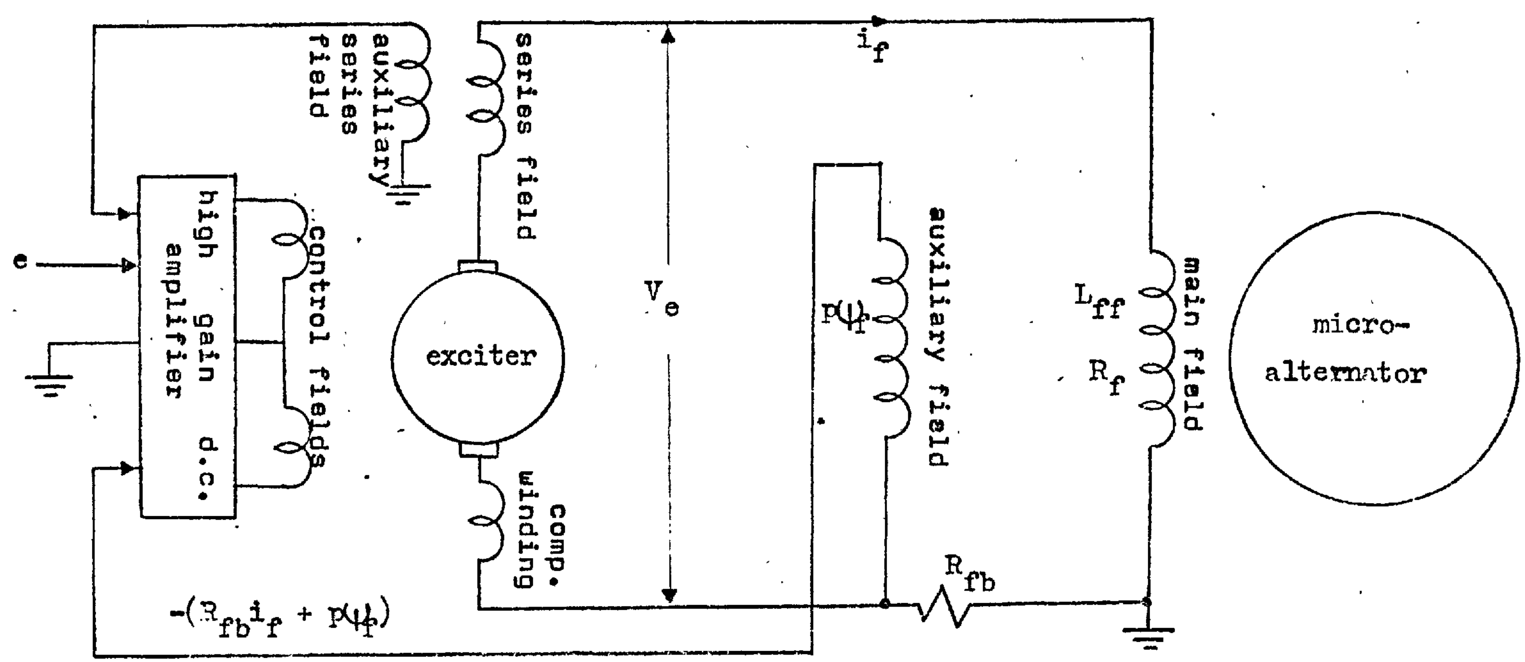

Fig. 5.5 Diagram of time constant regulating system

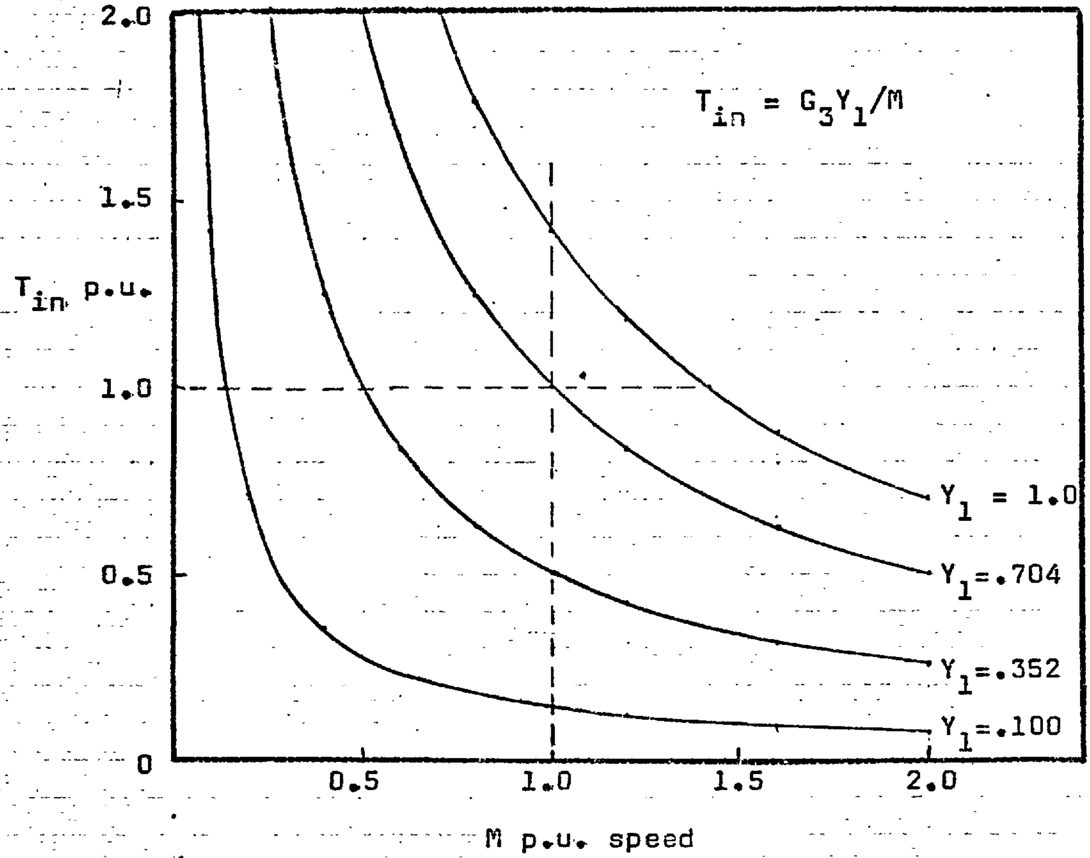

Fig. 5.6 Torque speed characteristics of the prime mover at Goldington

5.3.2 The time constant regulator

The micro-machine has a much higher natural per unit field resistance than a large generator. A time constant regulator (t.c.r.) which reduces the effective field resistance had been developed and used in earlier experiments[33]. The basic elements of such a t.c.r. appear in Fig. 5.5. An auxiliary field winding with the same number of turns as the main field winding but of much smaller copper section has been wound in the same slots as the main field. With nearly perfect coupling between the two windings, the voltage appearing across the auxiliary field is equal to the induced voltage $p\Psi_f$ in the main field. This is added to a voltage $i_f R_{fb}$ and the total fed back through a high gain d.c. amplifier to the control fields of a series exciter. It can be shown that if the open loop gain of this control system is large enough the effective field resistance becomes R_{fb} which may then be set to a suitable value in order to obtain the required time constant.

5.3.3 The prime mover torque-speed characteristic

An important source of damping[24] in a turbo-alternator is the turbine since the torque is a function of the speed. The torque-speed characteristic of the turbine at Goldington can be found for slow changes in speed as shown below.

Eqns. (5.10),(5.11) and (5.12) can be combined to show that

$$T_{in} = \frac{G_3 Y_1}{M} = \frac{1.42\ Y_1}{M} \tag{5.15}$$

$$M = \frac{\nu}{\omega} = \text{per unit speed.}$$

$$= (1 + \frac{p\delta}{2\pi\ f})$$

The torque/speed relationship of Eqn. (5.15) is therefore a function of the steam valve position Y_1 and Fig. 5.6 shows this relationship for various values of Y_1.

The slope of a torque/speed curve in Fig. 5.6 can be found by differentiation of Eqn. (5.15) i.e.

$$\frac{dT_{in}}{dM} = - \frac{G_3 Y_1}{M^2} = K_{TM} \qquad (5.16)$$

and this determines the damping effect[24].

At synchronous speed, $M = 1$ and the slope becomes

$$K_{TM} = - G_3 Y_1 \qquad (5.17)$$

but from Eqn. (5.15) it is seen that when $M = 1$,

$$Y_1 = T_{in}/G_3$$

which, when substitute into Eqns. (5.17), yields the slope as

$$K_{TM} = - T_{in} \qquad (5.18)$$

According to Eqn. (5.18) the torque/speed slope at synchronous speed is 1 at 1 p.u. torque and speed, and the numerical value is less than 1 at reduced torques.

The micro-alternator is driven by a separately excited D,C. motor, the characteristics of which are different from those of a turbine and have an important effect on the machine behaviour under transient operation. Equipment has been designed and tested to control the D.C. driving motor in such a way as to simulate a turbine drive. The control equipment was not fully operational however, at the time when the system stability tests described in Chapter 6, were carried out.

For the purpose of the micro-machine tests, a constant value of the torque/speed slope therefore had to be used. The natural torque/speed slope of the D.C. motor at 1 p.u. torque is in the order of -30, but it is possible to reduce this value by adding resistance in series with the armature. An attempt was made to achieve the value of - 1 (also suggested in Ref. 24), but because of d.c. sypply voltage limitations it was not possible to reduce the slope further than - 2.68.

5.3.4 The tie-line impedance

Use was made of a three-phase transmission line simulating network which consists of resistance-, inductance-, conductance- and capacitance "units". Each unit consists of a number of fixed "elements" so that a range of values are possible.

The capacitance and conductance units of the simulator were not used since there are no details about these parameters in the practical system of Sect. 5.2 and a series combination of only resistance and inductance was used. However, the exact tie-line parameters could not be modelled, because

(a) the simulator elements have fixed finite values. Furthermore, the inductance elements have a finite Q which varies from 10 to 30 and thus have appreciable resistance.

(b) the transmission line of the Goldington system has only 4.74% reactance. Hence, the short circuit current from the infinite bus is about 20.0 p.u. On the micro-machine system, this corresponds to a current of approximately 90 A which exceeds the maximum rating of the transmission line elements and of the air circuit breaker. Moreover, the inductance elements have iron cores and at the higher fault currents there are errors due to saturation.

To overcome the above limitations a vacuum breaker capable of clearing 200 A (a.c.) was purchased and a larger transmission line reactance was used. On the transmission line simulator, a choice had to made between a 4 ohm (16%) and a 2 ohm reactance. Due to saturation and consequently the unknown upper limit of fault current, the 4 ohm reactance was used. This also allowed rapid repetition of the fault application without overheating of the low-Q reactance element or any other auxiliary equipment.

The transformer in Fig. 5.1 was simulated by a high-Q reactance which has an iron core with an air gap. The final values of the micro-machine transmission line parameters are listed below

	Micro-machine system	30 MW system
R_1	0.56%	0.506%
X_1	13.2%	13.3%
R_2	1.9%	1.73%
X_2	16%	4.74%

Tests were also made with $X_2 = 8\%$, but were not analysed because it was discovered that the t.c.r. was not functioning satisfactorily (see Sect. 6.3)

---oOo---

CHAPTER 6

6. COMPARISON OF CALCULATED AND TEST RESULTS

6.1 General

The results presented in this chapter are for the case of a three-phase short-circuit close to the alternator. Test results for a large system (Sect. 5.2) as well as for a micro-machine system (see Sect. 5.3) are compared with computed results.

6.2 Results for a Large System (Goldington)

The tests conducted by the C.E.G.B. on a 30 MW alternator at Goldington (see Sect. 5.2) included a short circuit test applied at the high voltage terminals of the transformer (see Fig. 5.1) with the generator operating at full load. In Ref. 6, the results of the test are recorded and calculations of the performance are made by means of an analogue computer. The complete equations are used with allowance for regulator and governor action and for the effect of saturation.

In the present section, digital computations are used to verify the results, using the approximate and accurate methods described in Sect. 4.2. The calculations do not allow for saturation. Further computations are made for different conditions on the same system. Particular emphasis is placed on the initial period for a detailed study of the back swing phenomenon.

6.2.1 Three-phase short-circuit at rated load.

Fig. 6.1 shows the swing curves determined by the site tests and by the approximate and accurate methods of calculation. The angle on the test curve does not swing back noticeably but is almost horisontal for the first 0.1 sec. showing that there are losses which neutralise the turbine torque, but are not sufficient to cause a back swing. The angle determined by the approximate method commences to rise immediately, because it does not allow for any losses, and the peak value of δ is too high. The accurate method shows much better agreement with the test curve during the first swing, although there is some discrepancy during later swings, probably because of uncertainty in the turbine and governor parameters and because saturation is neglected.

Fig. 6.2 shows computed curves for the two flux linkages calculated by the two methods. The flux linkages Ψ_d and Ψ_q determined by the accurate method (Curves (a) and (c)) are decaying sinusoids at supply frequency and are 90^0 out of phase with each other. When calculated by the approximate method, on the other hand, each flux linkage has an initial step change (Curves (b) and (d)) followed by a gradual decay which agrees closely with the mean value of the corresponding sinusoid.

From Eqn. (4.1)

$$p\Psi_d + \nu\Psi_q = v_d - r_a i_d$$

or approximately v_d, if $r_a i_d$ is neglected. Curve (g) shows v_d as a slowly decaying curve. The quantity $p\Psi_d$, (Curve (e)) which is neglected in the approximate method, is seen to be of the same order of magnitude as $v\Psi_q$. Curve (h) shows the quantity

$$- p\Psi_q + v\Psi_d = - v_q + r_a i_q \ .$$

The value of v_q is nearly the same for both methods while again $p\Psi_q$ is of the same order of magnitude as $v\Psi_d$. The curves for v_d and v_q show that, although the axis fluxes oscillate, the axis voltages are slowly changing unidirectional quantities.

Fig. 6.3 shows curves of $v\Psi_d$ for a time period longer than the fault time. After the fault is removed the accurate curve is again a decaying oscillation but now the approximate value is not the mean value of the accurate sinusoid as it was during the fault. This is because the two methods yield different results for the rotor angle at the instant of fault clearance and thus lead to different currents, torques and flux linkages when the generator is back on the system, Fig. 6.3 also shows the axis currents calculated by the two methods.

Figure 6.4 shows the axis components of voltage, v_d and v_q , and also the terminal voltage V_{mt}. The 50 Hz oscillations in v_d and v_q initially after application and again initially after removal of the fault, are present when the numerical calculations take the $r_a i_d$ and $r_a i_q$ terms into account. These terms are only appreciable for short periods when i_d and i_q are relatively large.

The variation of electrical torque T_e according to Eqn. (4.11) appears in Fig. 6.5. The accurate method shows a 50 Hz oscillating torque with a first peak of about 4 p.u. while the approximate method shws T_e to decreace step-wise initially to about 0.15 p.u.

The mean value of the envelopes of the accurate solution, tends towards the value of the approximate curve after about 60 milli-secs.

The semi-log plot of the envelope of T_e is a straight line and by extrapolating back to zero time, it is possible to find an initial value for the rapidly decaying unidirectional or mean torque T_{eu}. The time constant of the decaying envelope is about 130 milli-seconds which agrees fairly well with the value of 125 milli-seconds which was calculated by using the expression[1] for the armature time constant T_a.

Fig. 6.6 shows the approximate value of T_e, which has an initial step change of 0.7 p.u. followed by a decay to a constant value 0.08 p.u., while the unidirectional torque T_{eu} obtained by the accurate method has an initial value of about 0.68 p.u. Since T_{eu} is less than the shaft torque of 0.8 p.u. the machine is not retarded and no clear back swing is seen in Fig. 6.1.

6.2.2 Three-phase short-circuit at various system conditions

No site test results for a three-phase short-circuit were available except those already given, but calculations were made for other conditions, and the results are shown below.

(a) Effect of reduced load

Fig. 6.7(a) shows calculated curves similar to those of Fig. 6.1 but for the case of 0.2p.u. active power and 0.6 p.u. reactive power. The back swing is now clearly visible. There is not only a significant difference in the amplitude of the first peak as calculated by the two methods, but also considerable phase shift during the first few swings. The difference in the angle δ_f when the fault is removed, is 11^o on Fig. 6.1 and 12^o on Fig. 6.7(a).

The steady shaft torque of 0.2 p.u. is smaller than the unidirectional torque and the machine is temporarily retarded. The lower the steady pre-fault power level, the more severe is the back swing. At no load the angle swings only into the negative region.

(b) Effect of increased tie-line reactance

Figure 6.7(b) shows the effect of a transmission line whose reactance is ten times that of the Goldington system. In comparison with Fig. 6.7(a) the discrepancy between approximate and accurate calculations has increased and continues longer. With P = 0.2 p.u. and Q = 0.6 p.u. the larger tie-line reactance requires increased excitation and higher terminal volts. Hence the airgap flux, which is trapped when the short circuit occurs is larger and the initial transient losses and the initial unidirectional torque are increased.

(c) Effect of reduced inertia

The results of Fig. 6.7(b) were recalculated for a reduced inertia constant of 3 sec. which is slightly lower than that of a modern 600 MW turbo-alternator. The results are shown in Fig. 6.7(c) The back swing lasts for the entire fault period of 0.38 secs., the difference in δ_f between the two methods in now about 22 degrees and the amplitude error is also larger. The phenomenon of lower inertia permitting a larger back swing supports the results shown in the next section.

6.2.3 Detailed assessment of the back swing

The curves in Fig. 6.8 apply to the system condition of Sect. 6.2.2(c) and show the torque, the slip, and the load angle when the calculation is made with the accurate and approximate methods.

According to the approximate method the slip increases from zero when the fault is applied because the prime mover torque is larger then the armature copper loss torque by itself. Upon removal of the fault, the slip decreases again. Hence the load angle δ increases initially and reaches a maximum when the slip is zero.

On the other hand, the accurate method shows the first peak of the pulsating electromagnetic torque T_e to rise to about 5.4 p.u. while the turbine output T_{in} is only about 0.2 p.u. Figure 6.9 shows the variation of the unidirectional torque T_{eu} which has an initial value of about 0.68 p.u. which is larger than the shaft torque of 0.2 p.u. and hence the retardation or back swing occurs. It is significant that the initial value of T_{eu} for these system conditions is about the same as for the original conditions of the site test (Sect. 6.2.1). However the different effects of T_{eu} depend on the pre-fault shaft torque and the machine inertia. Fig. 6.9 also shows the step decrease in the approximately calculated value of T_e. A semi-log plot of the torque envelope of Fig. 6.8 is again a straight line with a time constant of 135 milli-seconds. This value corresponds to that found in Sect. 6.2.1 since the armature and field circuits are the same for the two conditions while the fault is on.

The variation of T_e when the fault is removed is shown in Fig. 6.10 for various values of fault time. It is seen that after fault removal, T_e invariably first goes negative due to synchronising power from the infinite bus.

In addition to factors like pre-fault load, excitation level and inertia, the amount of back swing is increased when the fault is closer to the machine and thus permits a larger armature short-circuit current and losses. The duration of the unidirectional torque is also affected by such quantities as armature resistance and the field and damper winding time constants.

6.3 Results for a Micro-machine System

Three-phase faults were applied to the c.w.r. micro-machine system of Fig. 5.4 on the transmission line side of the simulated transformer. No governor or a.v.r. is used in this section, digital computations are used to verify the results using the accurate method described in Sect. 4.2 but not allowing for saturation.

Figure 6.11 shows the accurately calculated as well as the measured swing curve for the micro-alternator when the field is excited directly from a steady battery supply. The agreement is good apart from some discrepancy during the first swing, which may be due to other losses not allowed for.

Figure 6.12 shows the accurately calculated swing curve for a reduced field resistance and the measured curve when the t.c.r. (see Sect. 5.3.2) was used. The discrepancy between calculated and test results of Fig. 6.12 is too large to have been caused by uncertainty of the parameters. Closer investigation of the recordings of the alternator field current and the t.c.r. exciter output voltage V_e (see Fig. 5.5) showed that the existing t.c.r. was not responding fast enough when applying and removing the short circuit, especially when close to the alternator. In practice this meant that the effective field resistance was not being kept constant at the value R_{fb} as used in the calculations.

The exciter output voltage V_e should respond in such a way that under all conditions the power dissipation $i_f^2R_f$ is supplied by the exciter set. However, due to the slow response of V_e after application of the fault, a certain amount of the $i_f^2R_f$ loss is not supplied from the exciter but is drawn from the kinetic energy of the alternator's rotating rotor. This effectively decreases the available accelerating torque from the prime mover and makes the braking effect larger. A similar effect in the reverse direction occurs when the fault is subsequently removed. The test curve of Fig. 6.12 shows a larger and longer back swing and a higher peak value of δ after the fault has been removed, thus confirming the above deductions.

The t.c.r. had previously been used for less severe conditions than the short circuit. Plans are in progress to replace the rotating machine type of t.c.r. by one using transistors.

It is interesting to note that the calculated curves of Figs. 6.11 and 6.12 show the difference between a typical small laboratory machine with a high field resistance (Fig. 6.11) and a typical large alternator with a low field resistance (Fig. 6.12). The results indicate the type and magnitude of error involved when conclusions drawn from a small commerial machine are extended to a large practical machine.

According to the calculated curves of Fig. 6.13 the unidirectional torque is initially of similar magnitude for both values of field resistance, but decays more rapidly with high field resistance.

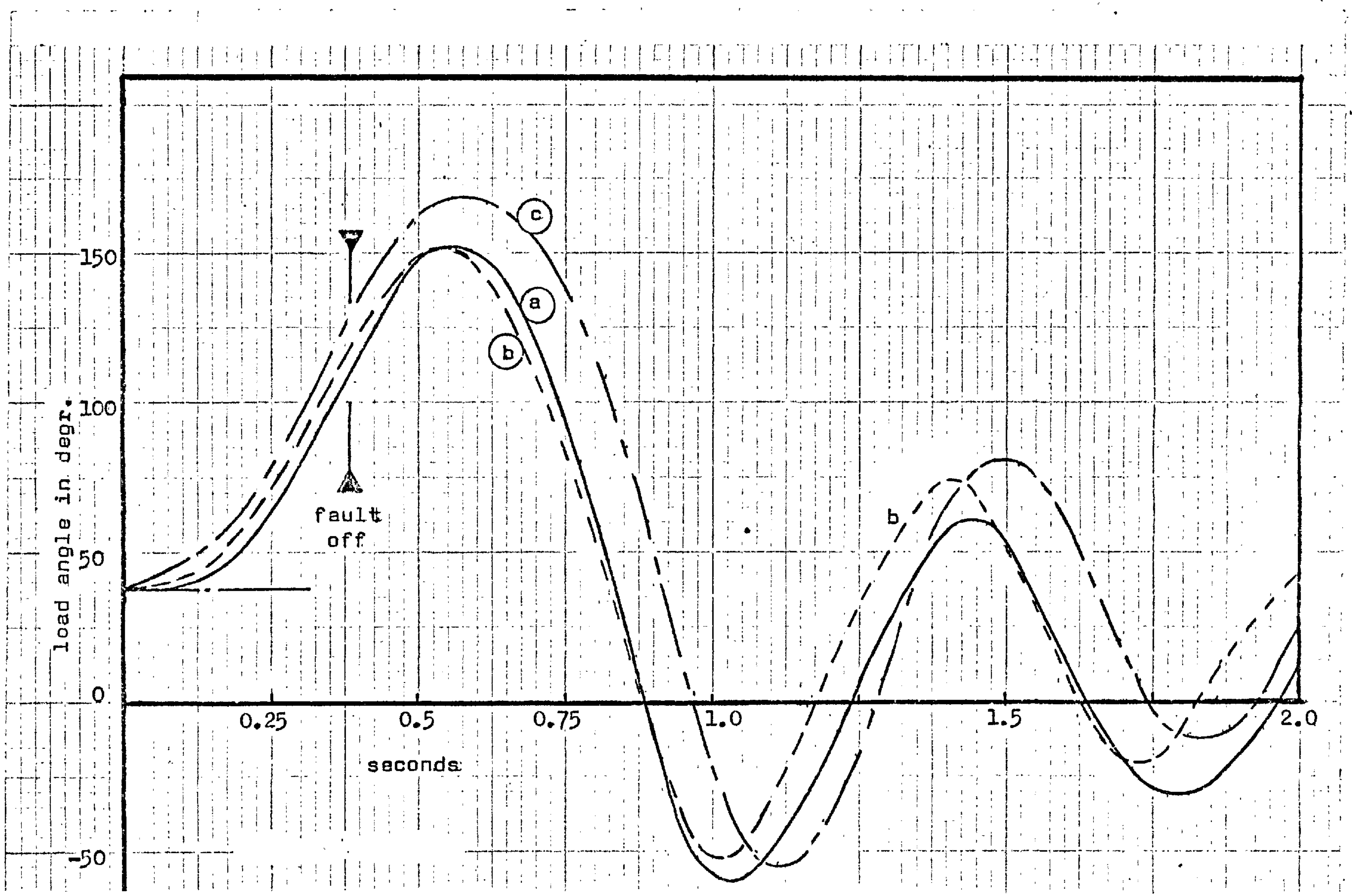

Fig. 6.1 Load angle after a short-circuit on the Goldington system.
$P = 0.8$ p.u., $Q = 0.6$ p.u., $H = 5.3$ sec.

Curves: (a) Test, (b) Accurate method (c) Approx. method.

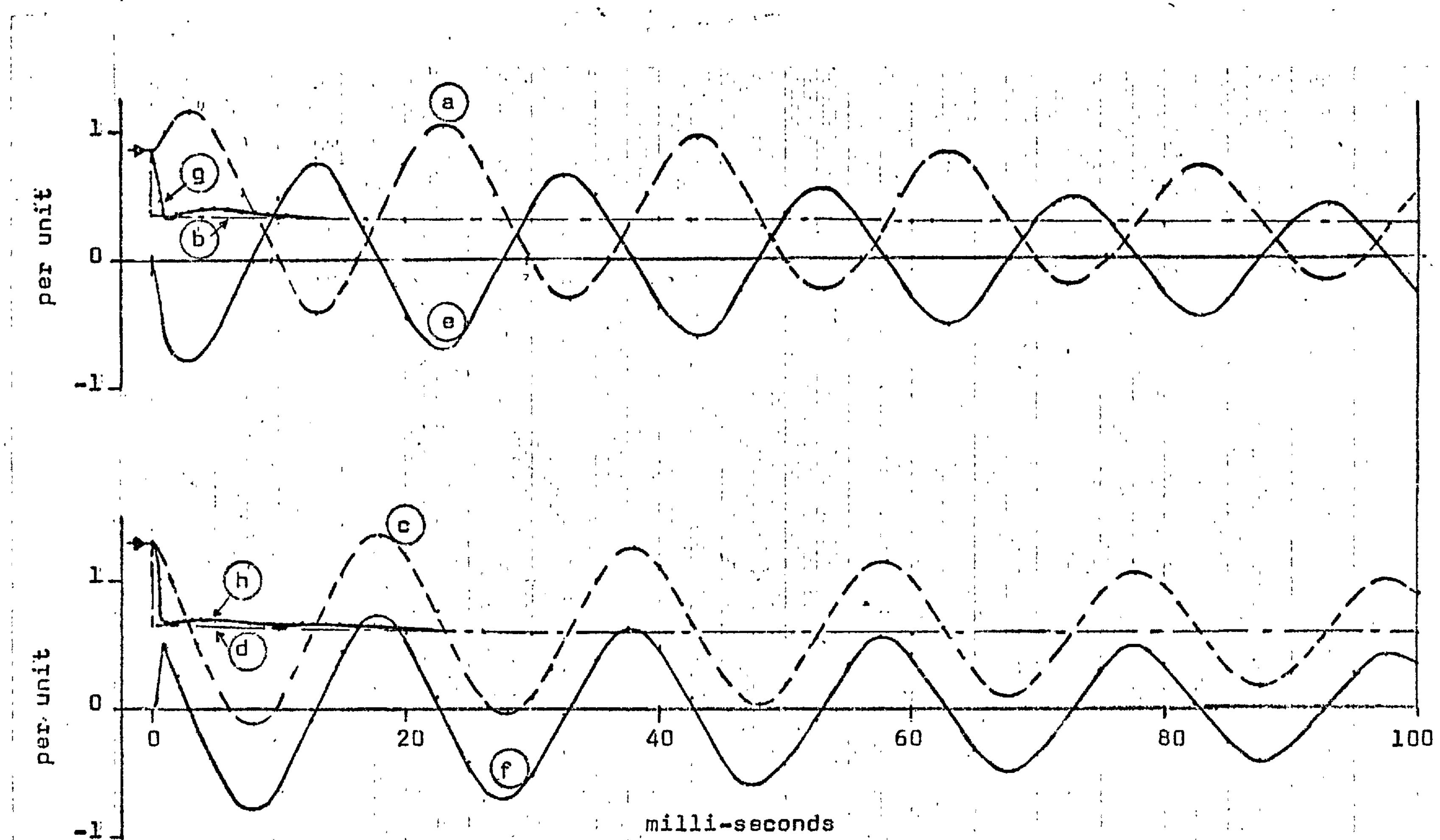

Fig. 6.2 Flux linkages for the Goldington generator.
$P = 0.8$ p.u., $Q = 0.6$ p.u.

	Accurate method. Curve.	Approximate method. Curve.
$\nu\psi_d - p\psi_q$	h	
$\nu\psi_q$	a	b
$\nu\psi_d$	c	d
$p\psi_d$	e	
$p\psi_q$	f	
$\nu\psi_q + p\psi_d$	g	

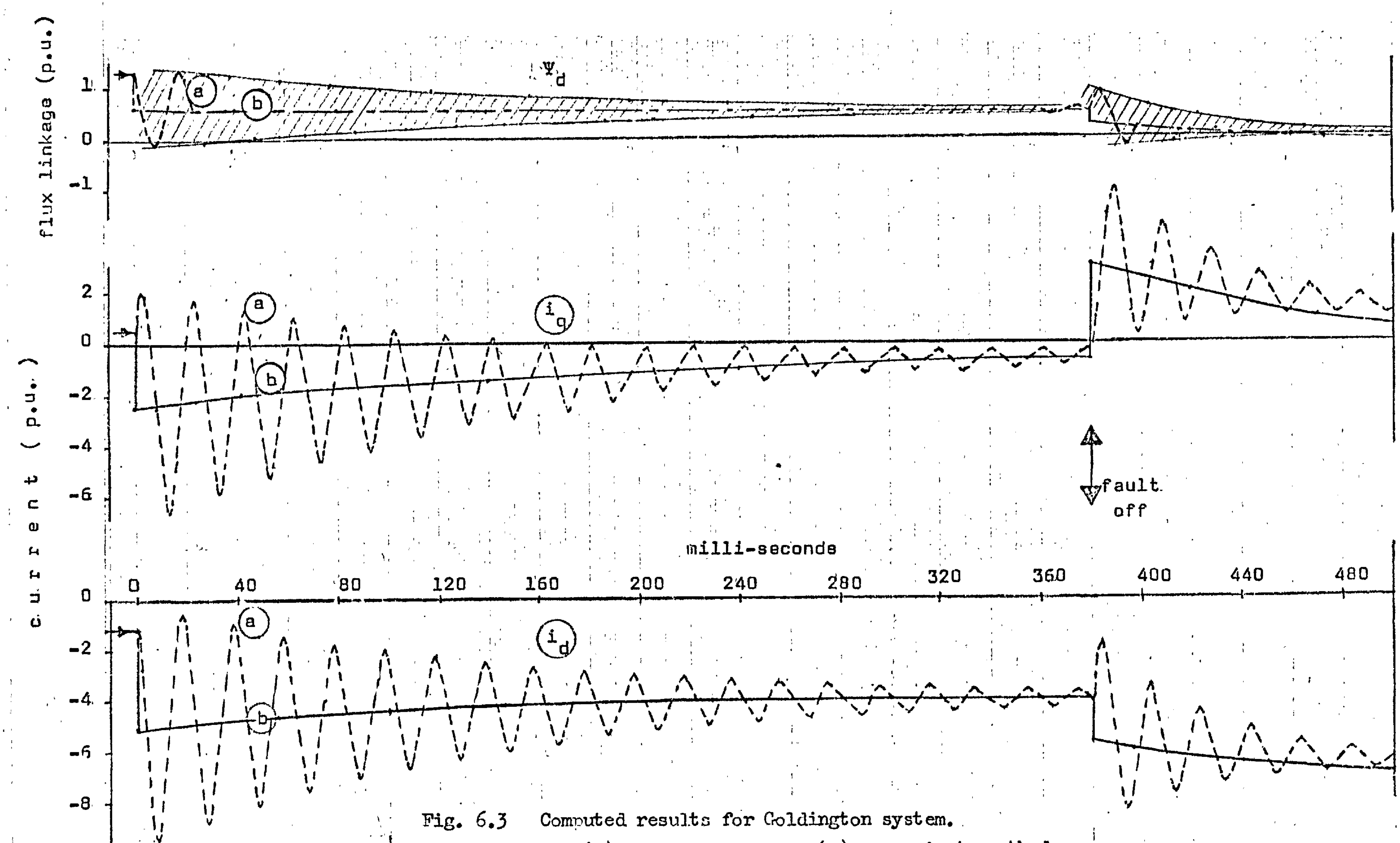

Fig. 6.3 Computed results for Goldington system.
(a) Accurate method; (b) Approximate method.

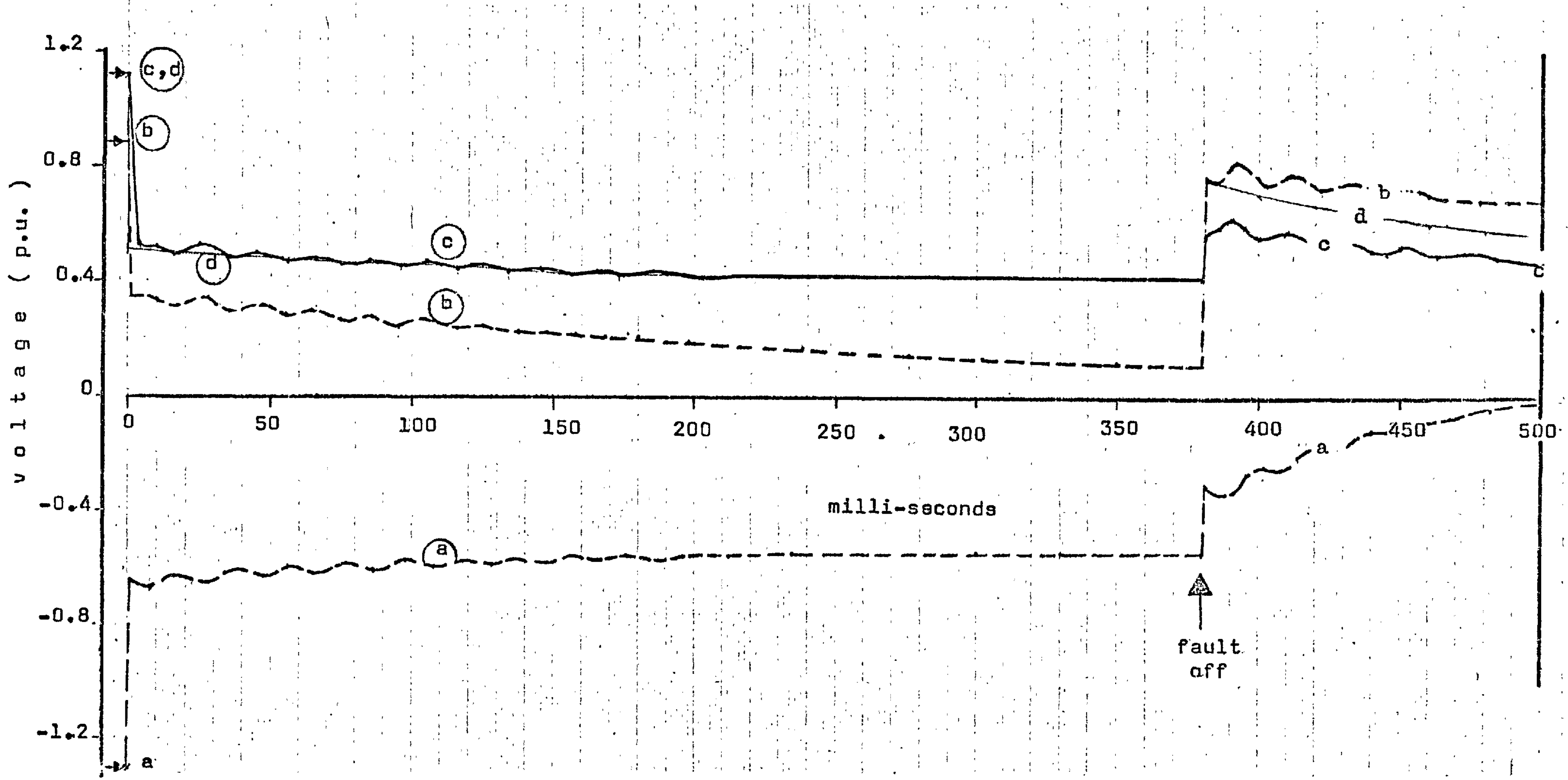

Fig. 6.4 Goldington system

Curves: (a) v_q (acc.), (b) v_d (acc.)

(c) V_{mt} (acc.), (d) V_{mt} (app.)

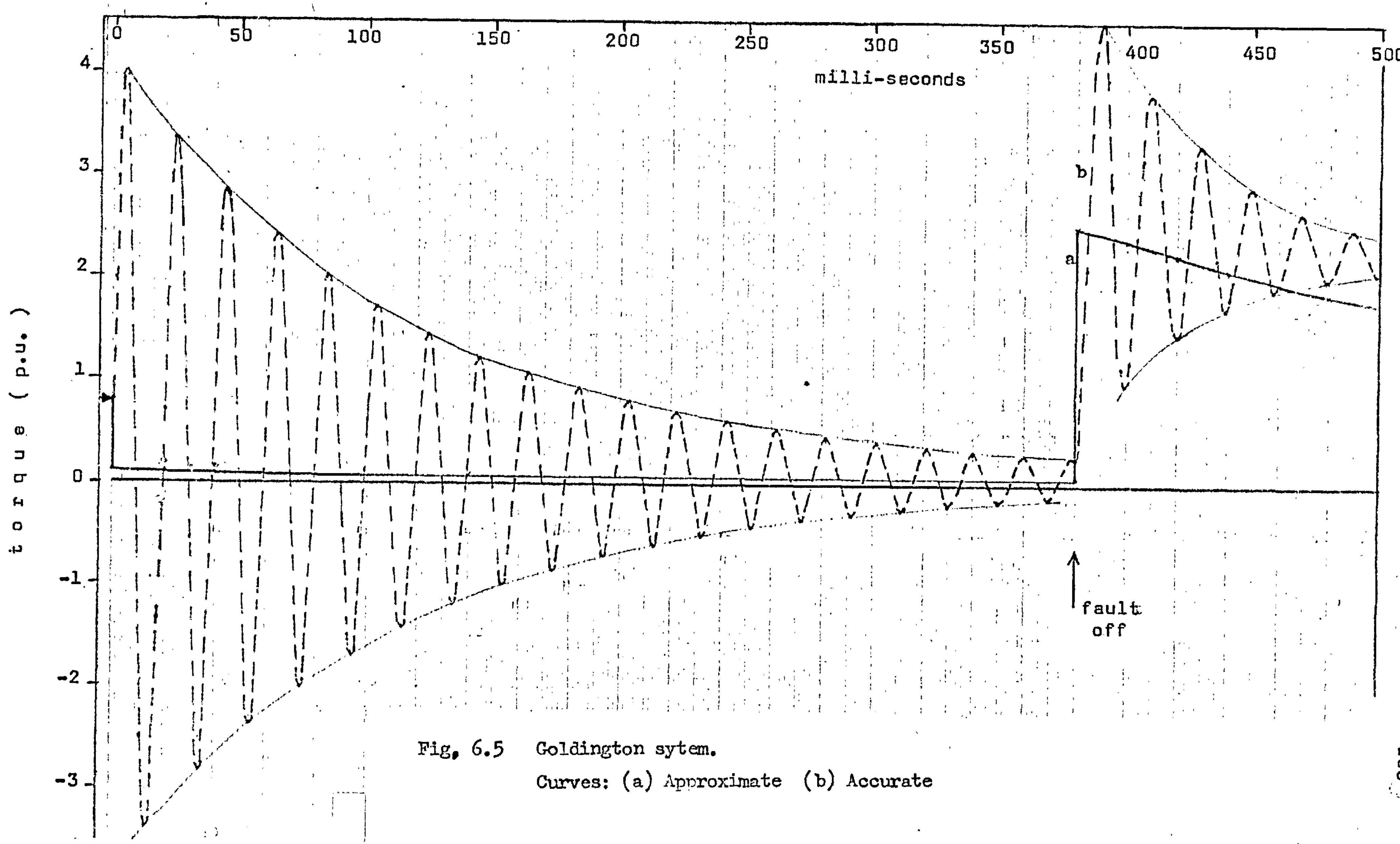

Fig. 6.5 Goldington sytem.
Curves: (a) Approximate (b) Accurate

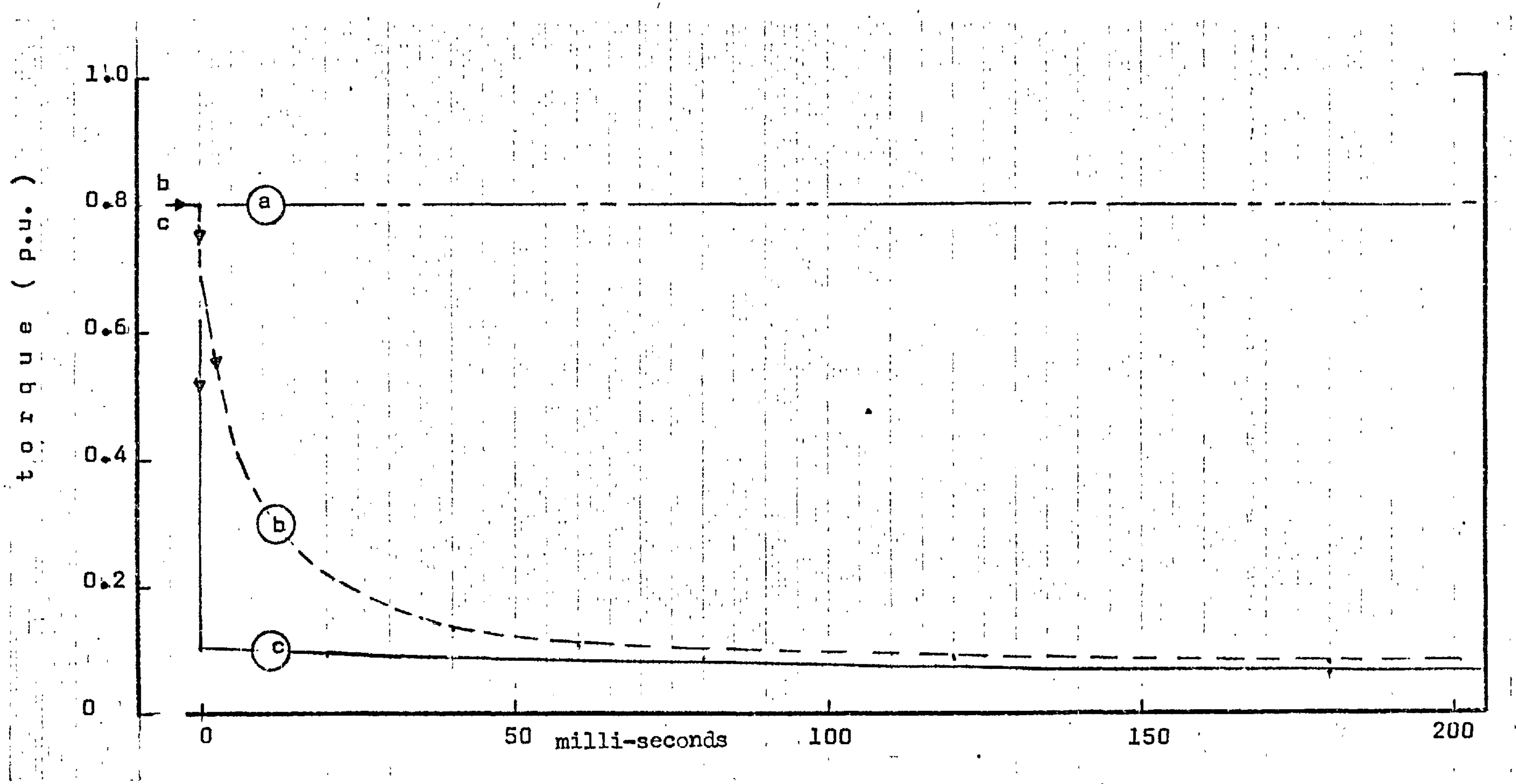

Fig. 6.6 Goldington system.

Curves: (a) Steady shaft torque (b) T_{eu} (accurate method)

(c) T_e (approximate method)

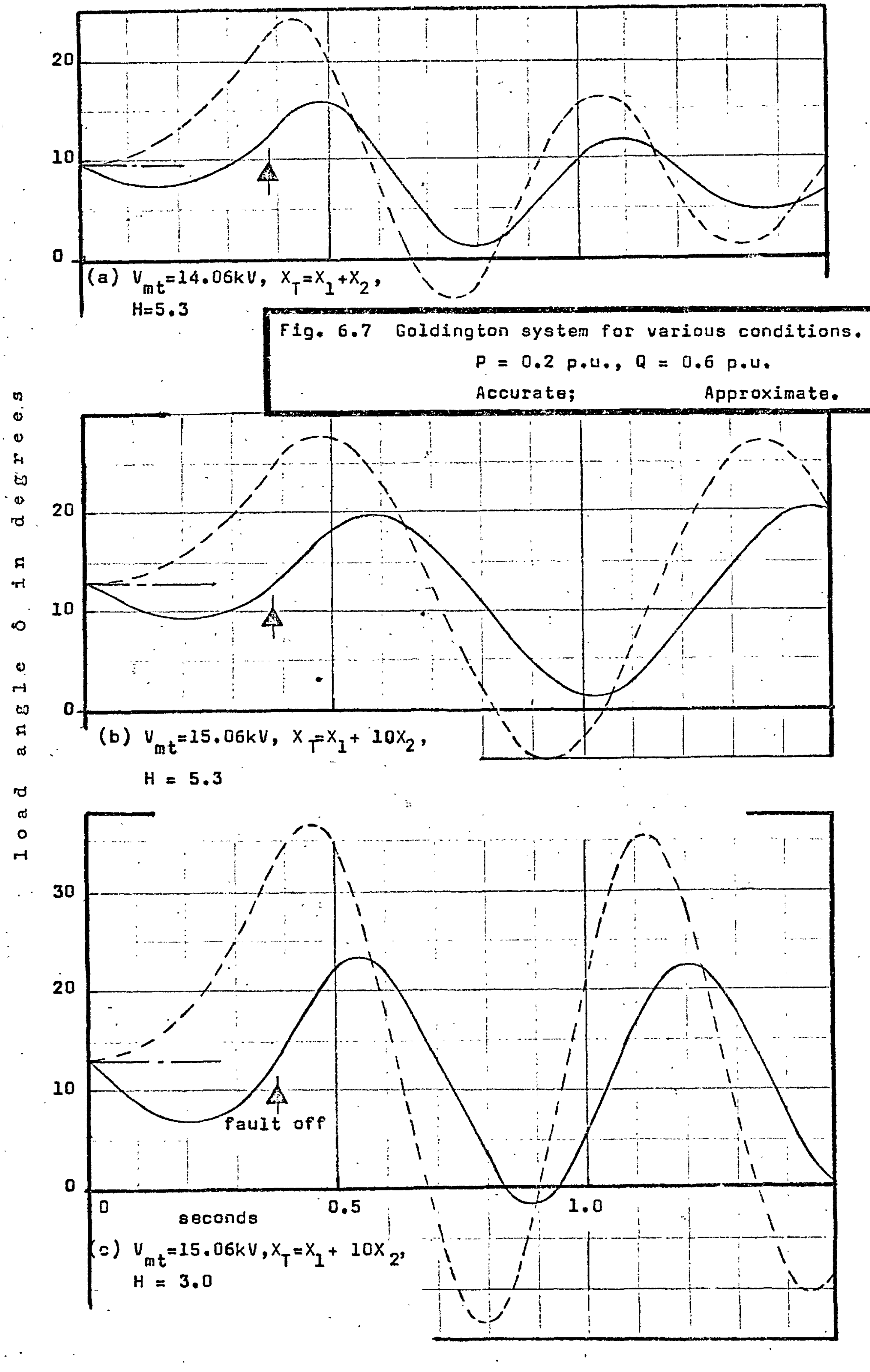

Fig. 6.7 Goldington system for various conditions.
P = 0.2 p.u., Q = 0.6 p.u.
Accurate; Approximate.

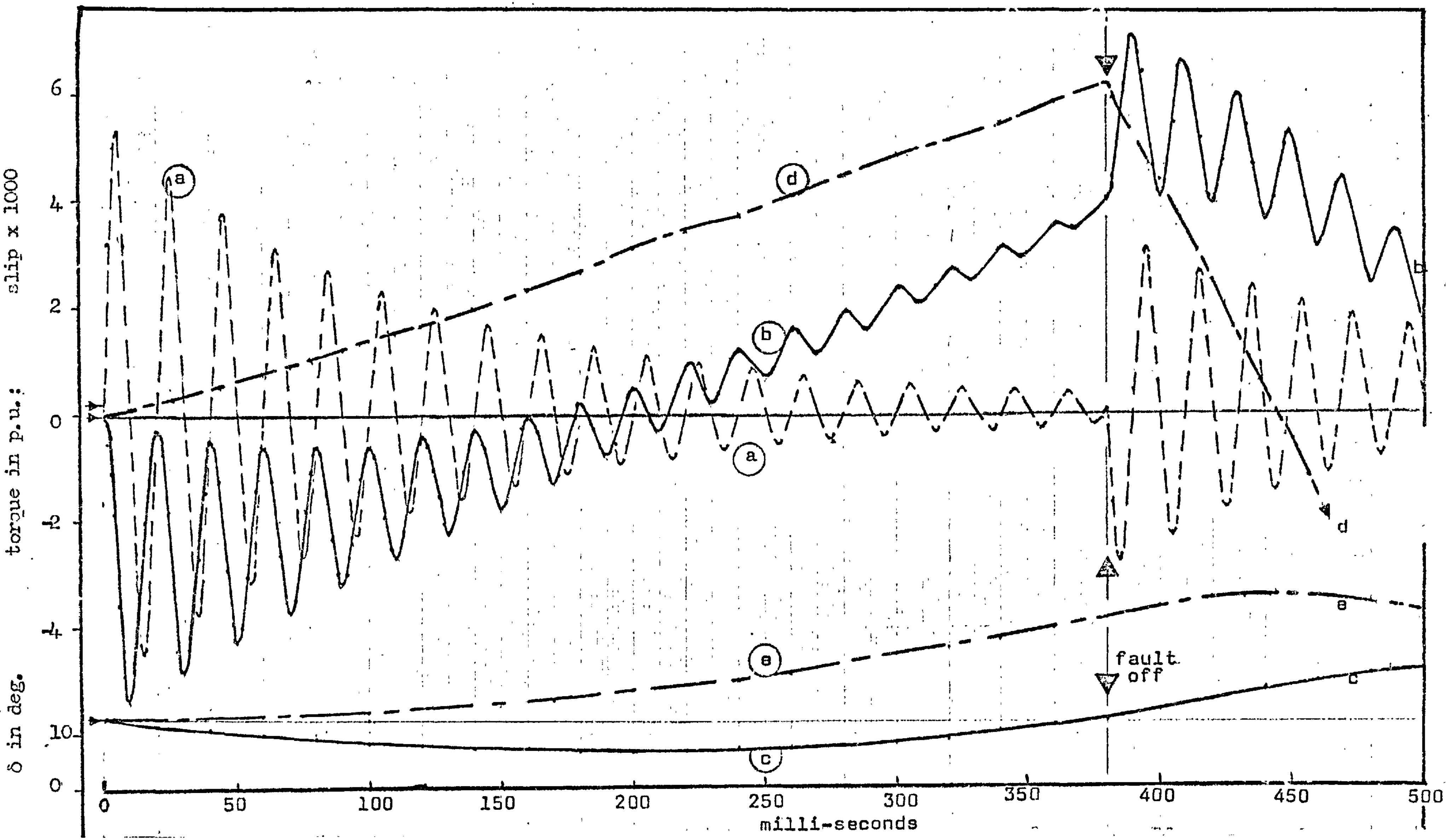

Fig. 6.8 Goldington system.

V_{mt} = 15.06 kV, $X_T = X_1 + 10X_2$, P = 0.2 p.u. Q = 0.6 p.u., H = 3 sec.

Curves: (a) T_e (b) slip (acc.) (c) δ (acc.) (d) slip (app.) (e) δ (app.)

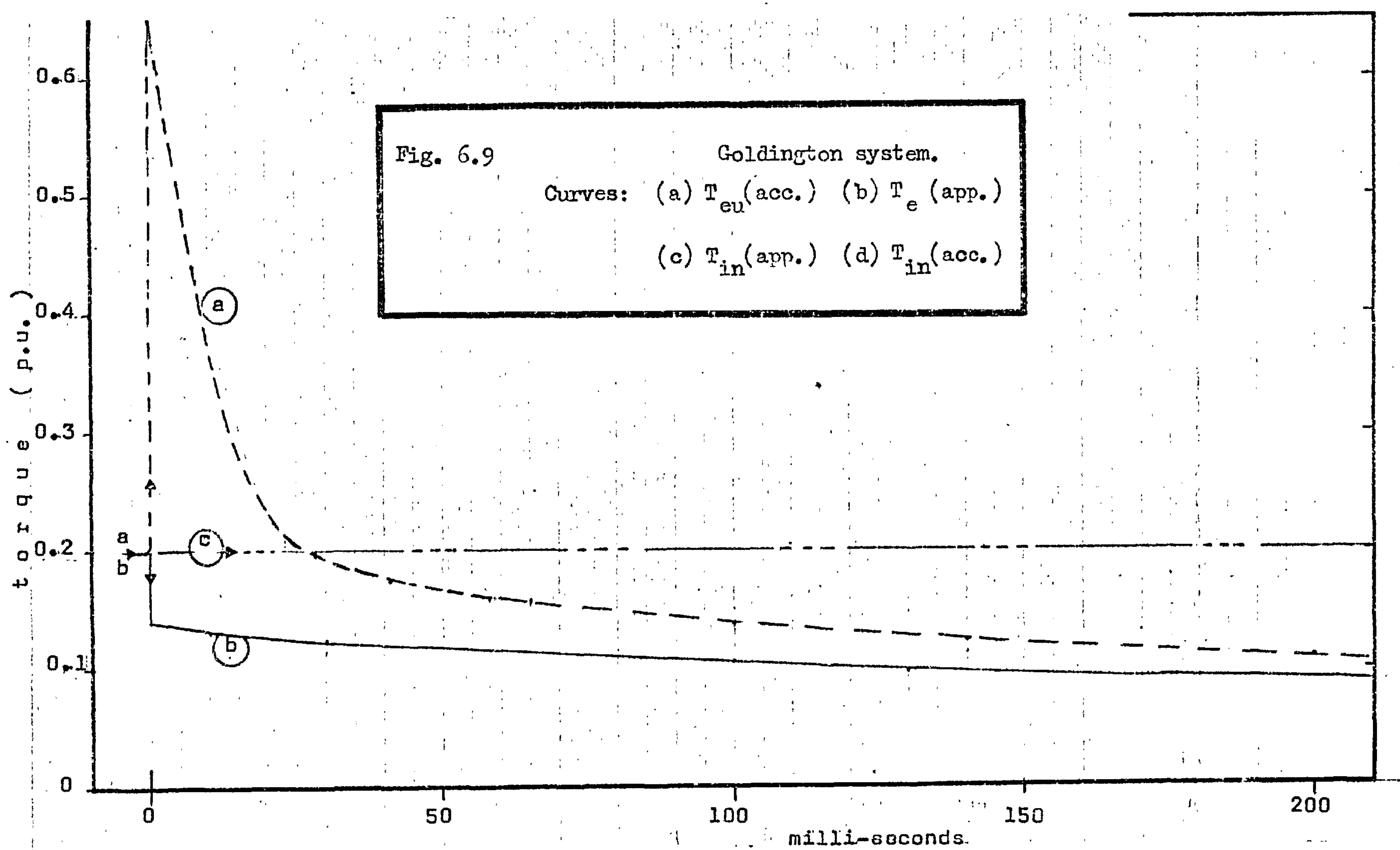

Fig. 6.9 Goldington system.

Curves: (a) T_{eu}(acc.) (b) T_e (app.)

(c) T_{in}(app.) (d) T_{in}(acc.)

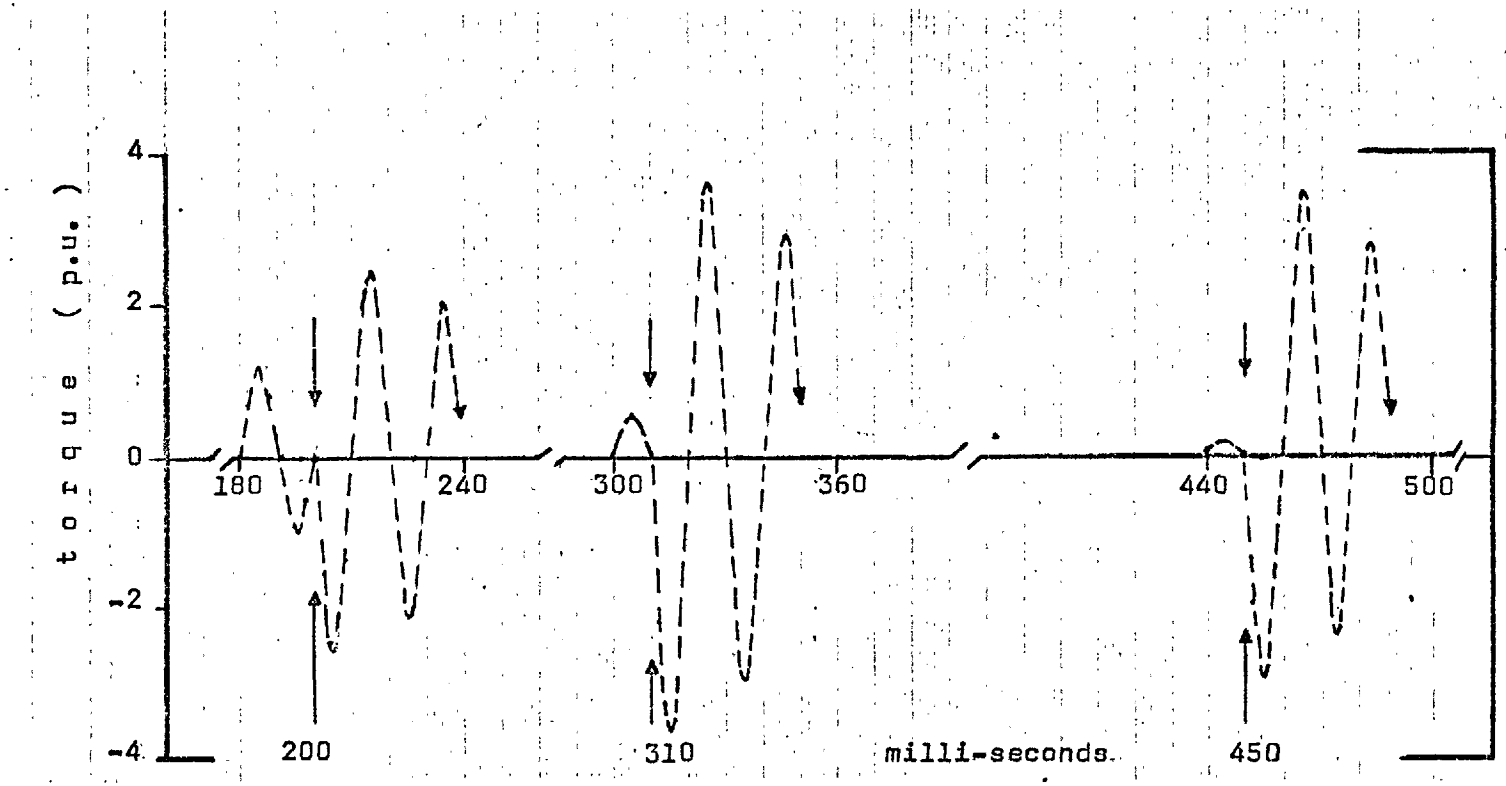

Fig. 6.10 Goldington system.

T_e after fault removal for various fault times.

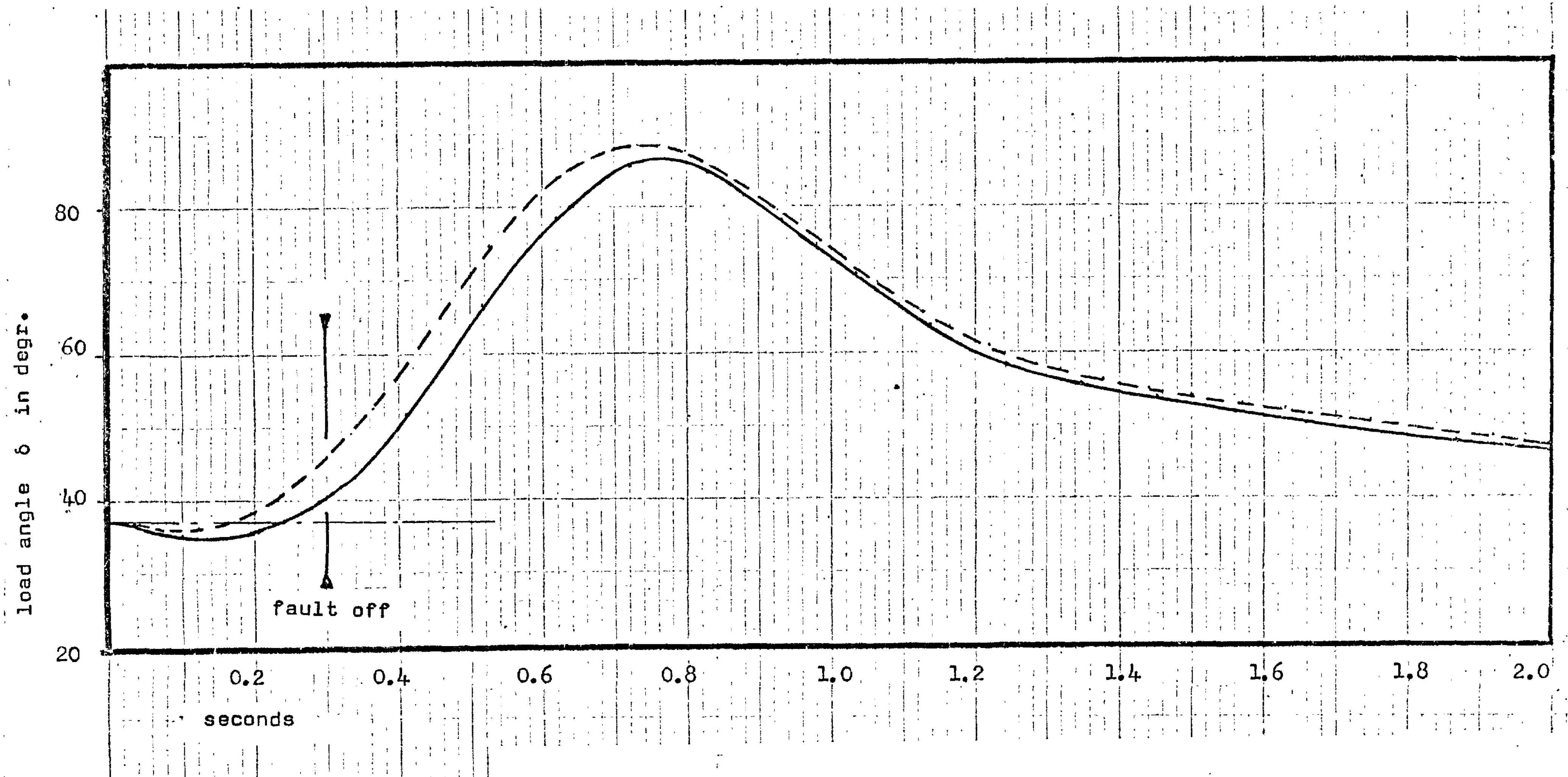

Fig. 6.11 Load angle after a short circuit on the micro-machine operating without a t.c.r.
P = 0.32 p.u. and Q = - 0.13 p.u. at infinite bus;
—— Test curve; - - - - Computed curve.

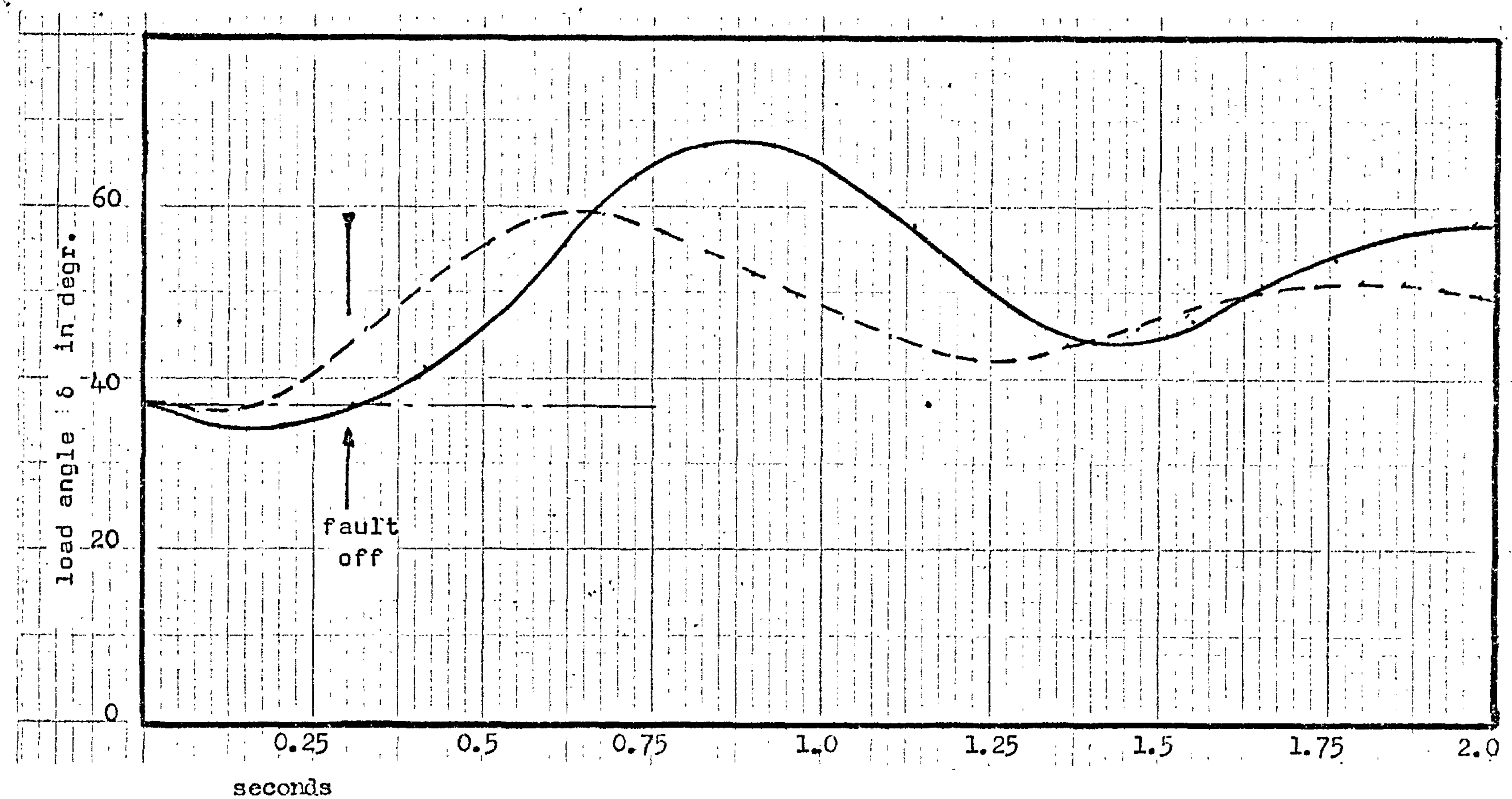

Fig. 6.12 Load angle after a short-circuit on the micro-machine operating with the t.c.r, P = 0.32 p.u., and Q = - 0.13 p.u. at infinite bus;
Test curve; Computed curve.

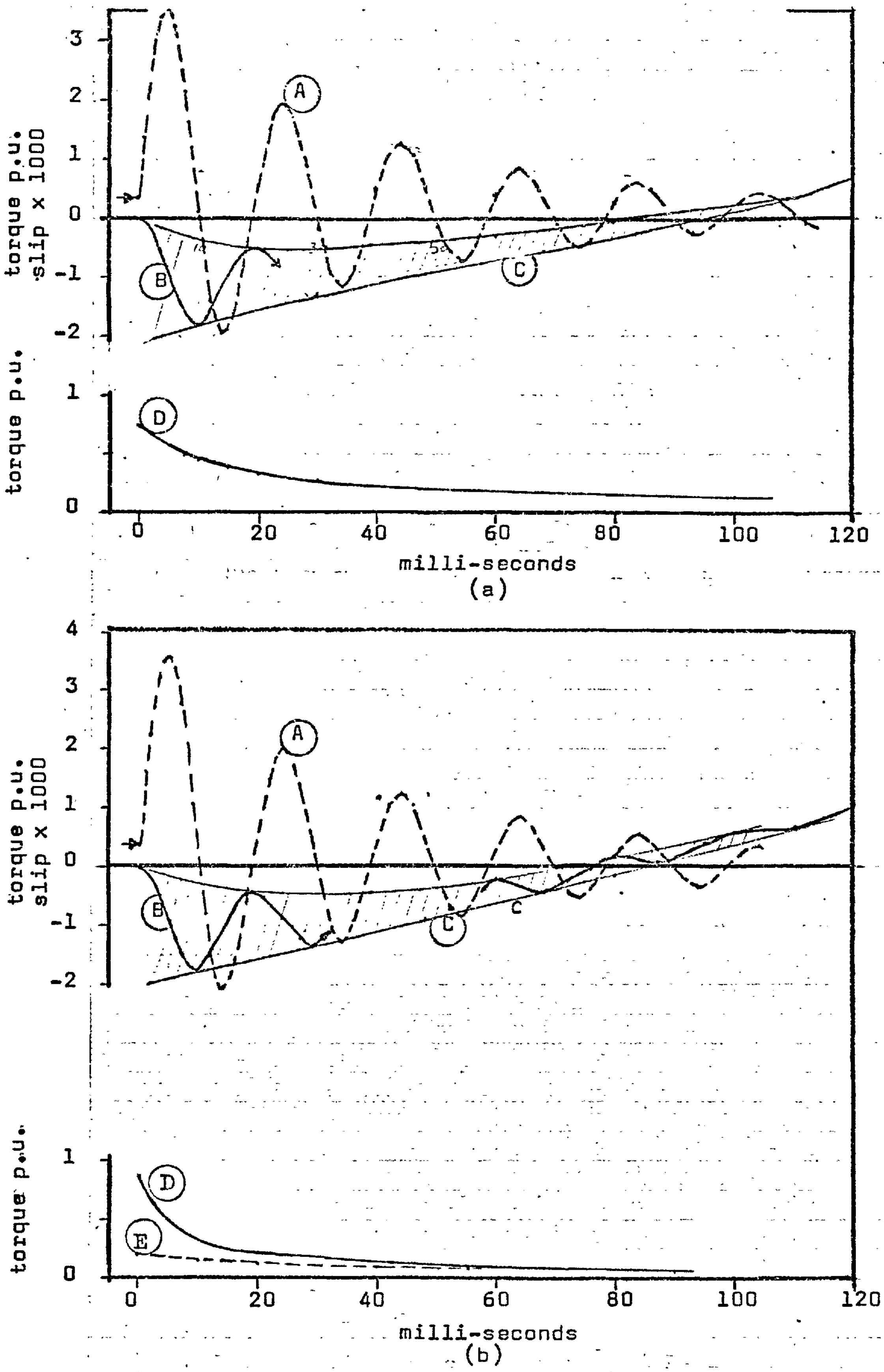

Fig. 6.13 Micro-machine calculations.

(a) Effective field resistance of 3 ohm(with t.c.r.)
(b) Effective field resistance of 27 ohm(without t.c.r.)

Curves: (A) T_e (acc.); (B) slip (acc.);
(C) Envelope of slip curve.
(D) Unidirectional torque (acc.)
(E) Unidirectional torque (app.)

CHAPTER 7

7. NUMERICAL INTEGRATION TECHNIQUES

7.1 General

The transient response of a synchronous machine is described by non-linear equations which can be solved by using a numerical method and a fast computing aid. The time taken to solve the equations is therefore directly related to their complexity, the order of the numerical method and the speed of the computing device. This chapter presents the results of studies about the accuracy and overall digital computer time, when various integration routines are used to solve the machine and system equations.

The solution of an "integrable variable" (IV) is found by integrating the derivative of the variable, for which the expression is a differential equation in terms of other system variables. The solution of a "non-integrable variable" (NIV) is found by calculating its value from an algebraic expression in terms of other system variables.

The "approximate method" (see Sect. 4.2.2) uses algebraic equations (4.11) to (4.13) and (4.17) to (4.21) in conjunction with differential equations (4.14) to (4.16) and the dynamic equation of motion (4.23). Ψ_{kd}, Ψ_{kq} Ψ_f and δ are obtained from the differential equations by a relatively simple step-by-step method of integration.

The "accurate method" (see Sect. 4.2.3) uses algebraic equations (4.11) to (4.13), (4.21),(4.24) and (4.25) in conjunction with differential equation (4.26) and the dynamic equation of motion (4.23). Ψ_{kd}, Ψ_{kq}, Ψ_f, δ, i_d and i_q are obtained from the differential equations by a complicated numerical method of integration.

In the practical system at Goldington, the machine is equipped with an automatic voltage regulater and the prime mover has a governor. These regulating devices have additional differential equations of both first and second order as explained in Sect. 5.2.

Several methods of solution were used for the Goldington system. Using the experience so gained, calculations for the c.w.r. micro-machine were worked out to reduce the computer time. The micro-machine had no regulator or governor, but they could readily be included.

7.2 Methods of solution for the Goldington system

7.2.1 The approximate method

The second order differential equation of motion can be rea - ranged as suggested by Crary[24]. When the approximate method is used to represent the machine, the additional differential equations can also be rearanged in a form suitable for the trapezoidal rule of integration. This rule consists of adding the product of Δt and Y'_n (the slope of y at t_n) to y_n in order to find Y_{n+1}. The approximate curve in Fig. 6.1 has been calculated in this way, using a time step of 0.001 sec. and the ratio of computer execution time to real time of 3 seconds, is approximately 14.1 (the CR ratio) on an IBM 7090 digital computer. The maximum step length is limited by the feedback circuits of the control mechanisms rather than by the machine equations. This is the simplest method of solving the approximate representation of such a single machine system.

7.2.2 The accurate method

When the accurate method is used, it is possible to "arrange" the equations and the sequence of the solution in several ways to suit the particular numerical method of integration.

The terms "method of integration" or "integration routine" refer to Euler's trapezoidal method, the Runge-Kutta method, or the Kutta-Merson method. By "arrangement" is meant the arranging or grouping together of certain equations in a form most suitable for a particular method of integration. As an example, Fig. 7.1 shows an arrangement where the machine's five differential equations (Eqn. 4.26) are grouped together in a "block" and solved by the method of .Runge-Kutta while the turbine, a.v.r., torque and load angle equations are arranged or grouped into three other "blocks" and solved by the trapezoidal method.

Only one arrangement was us'd in the study of the Goldington system but two methods of integrating the machine's differential equations were investigated, viz. a fourth order Runge-Kutta and a fifth order Kutta-Merson method. During the solution the fifth order method provides information which may be used to adjust the time step and hence decrease the CR-ratio even further. However, a fixed value of time step was used for both methods for comparative purposes.

The main feature of Fig. 7.1 is that one of these higher order

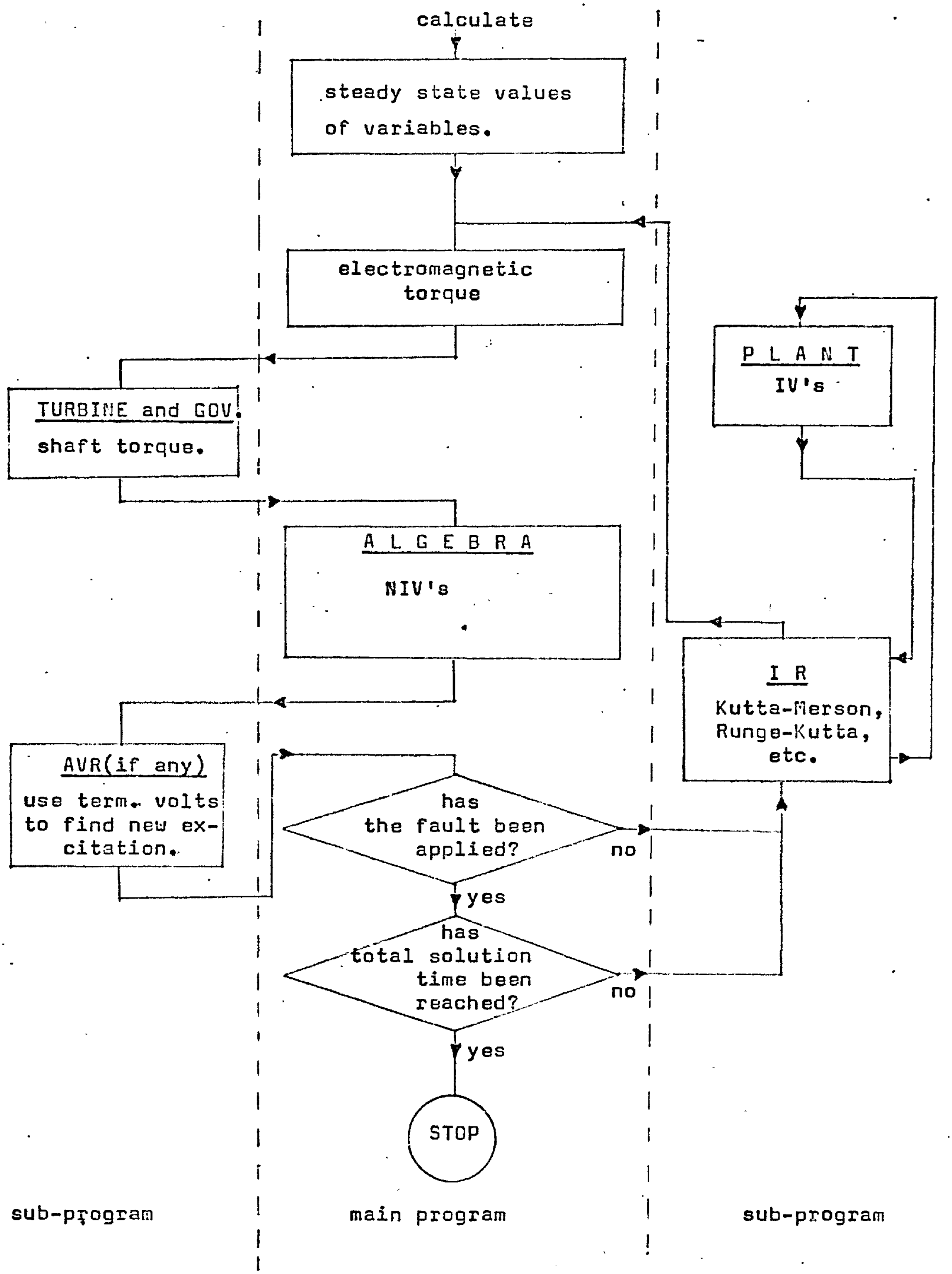

Fig. 7.1 Flow chart for a short circuit calculation (accurate method).

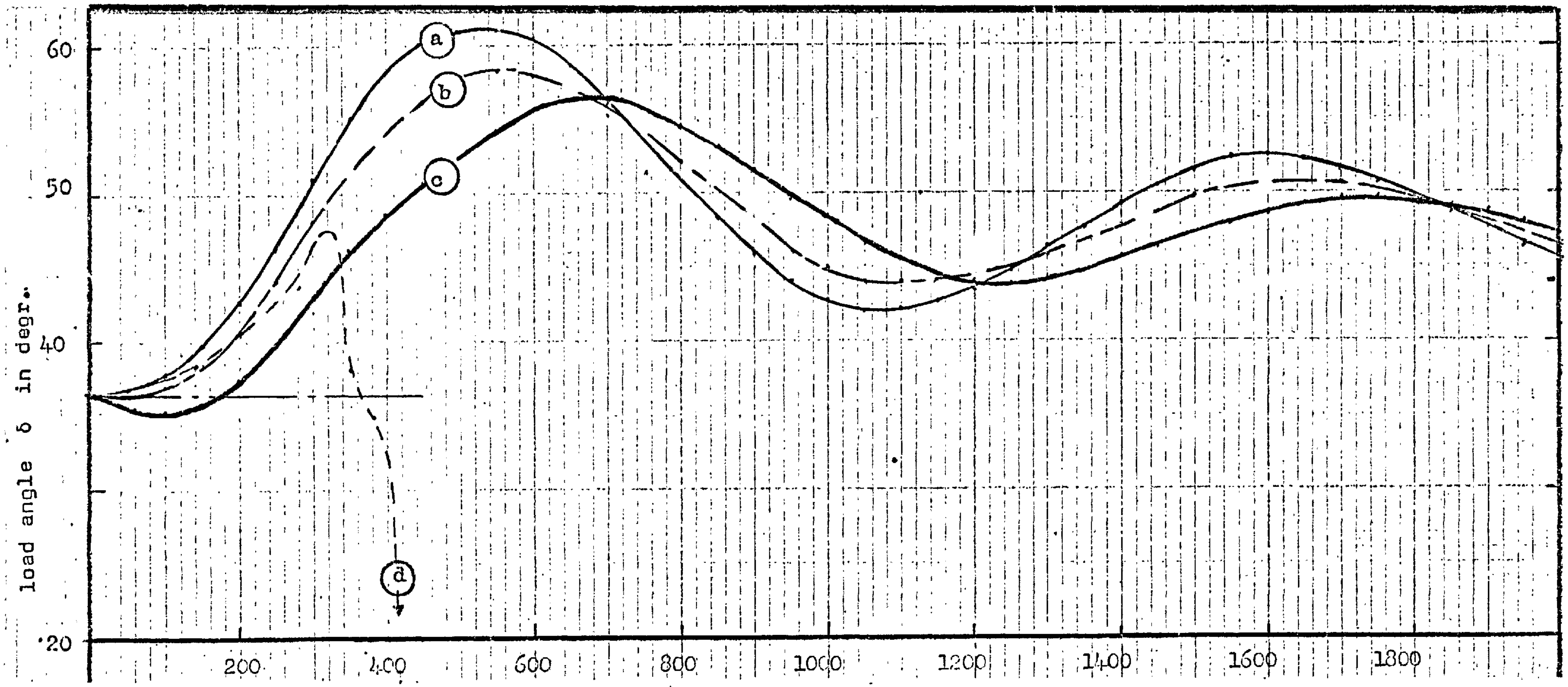

Fig. 7.2 Load angle curves for micro-machine system as computed by various numerical techniques. (see Table 7.1)

Approximate method	Accurate method (Arrangement 1)
(a) Δt of 0.0005 to 0.01 sec.	(b) Δt = 0.005
(d) Δt = 0.035 sec.	(c) Δt = 0.0005 to 0.001 sec.

integration routines is applied only to the block labelled 'PLANT'. At the end of each step, the solution transfers to the main program and the algebraic quantities (NIV's) are calculated while the differential equations of motion , and the equations of the turbine and governor and of the automatic voltage regulator are solved by the first order trapezoidal method.

The accurate curve of Fig. 6.1 was calculated according to the flow chart in Fig. 7.1 while using a Kutta-Merson routine with a time step of 0.0002 sec. The step length may be increased but accuracy would be lost. A Runge-Kutta routine required a time step of 0.0001 sec. to render the same accuracy. The CR-ratio using Kutta-Merson on the IBM 7090 was approximately 80 while it was 30 on an IBM 7094-11 computer. However this ratio may be improved significantly by using Predictor-Corrector methods (see Sect. 7.3) to solve the differential equations in 'PLANT' since the major portion of computer time is spent on this subprogram.

7.3 The Micro-machine System

The micro-machine system of Sect. 5.3, which has no governor or automatic voltage regulator to add any additional differential equations to those of the machine, is used to examine the merits of different ways of arranging the computation.

7.3.1 The approximate method

The equation of motion can be rearranged and together with the other algebraic equations of the approximate method (see Sect. 4.2.2) may then be solved by the trapezoidal method.

Curve (a) in Fig. 7.2 has been calculated for the micro-machine with reduced field resistance. A comparison of the CR-ratio , accuracy etc. as a function of the step length Δt, appears in Table 7.1.

7.3.2 The accurate method

As mentioned in Sect. 7.2.2 there are several possible ways in which the system equations may be arranged when using the "accurate method" (see Sect. 4.2.3). In this section the effect of various arrangements is considered for the single micro-machine system having two types of equations viz. the differential equations for the IV's like i_d, i_q and the algebraic equations for the NIV's like torque and terminal voltage, as explained in Sect.4.2.3. The different arrangements are illustrated by the flow charts of figures 7.1 and 7.3.

(1) In Fig. 7.1 the algebraic equations in the block named 'ALGEBRA' are kept separate from the differential equations in the block named 'PLANT'. The integrating routine (IR) solves the differential equations in 'PLANT' after which the program transfers to 'ALGEBRA' where the NIV's are calculated. Some NIV's for example V_{bd}, V_{bq} and ν, appear on the right hand side of the IV equations in 'PLANT'. Since values for the NIV's are only calculated at the end of each step, the method assumes in effect that the values at the end of the (n)th step remain constant during the (n+1)th step during which the IV equations in 'PLANT' are solved. Hence the solution of the NIV equations is always one step behind that of the IV equations. In order to maintain accuracy,

Table 7.1 Ratios of computer time to real time.

Arrangement of equations	Time step Δt, seconds	CR ratio	Accuracy within 1.0%	Graphical display	
				Fig.	Curve
Approximate Method.	0.0005	2.710	YES	7.2	a
	0.001	1.800	YES	7.2	a
	0.005	1.055	YES	7.2	a
	0.010	0.965	YES	7.2	a
	0.035	-	Mathm. Unstable	7.2	d
Accurate method. Arrangement (1) Figure 7.1	0.0005	8.312	YES	7.2, 7.4	c
	0.001	4.712	YES	7.2, 7.4	c
	0.005	1.828	NO	7.2, 7.4	b
	0.010	-	NO	7.4	a
	0.012	-	Mathm. Unstable	7.4	d
Arrangement (2) Figure 7.3	0.0005	13.758	YES	7.4	c
	0.001	7.438	YES	7.4	c
	0.005	2.360	YES	7.4	c
	0.010	1.734	NO(2%)	7.4	c
	0.012	-	Mathm. Unstable	7.4	e
Arrangement(3) Figure 7.3 with Predictor-Corrector method	0.0005	7.516	YES	7.4	c
	0.001	4.322	YES	7.4	c
	0.002	2.712	YES	7.4	c
	0.005	-	Mathm. Unstable	7.4	f

the solution has to use a relatively small step length.

(2) An improvement on the arrangement of Fig.7.1 is that shown in Fig. 7.3 where the NIV and IV equations appear together in the 'PLANT' block. This means that when the integrating routine solves the differential equations at various intermediate stages within an interval Δt, the algebraic calculations for new values of the NIV's are also performed.

In the execution of a digital computer program the Runge-Kutta routine transfers the execution through 'PLANT' four times during each interval. Since the major portion of computer time is spent by the integration routine going through 'PLANT', a computation with the same time interval would generally increase the CR-ratio if the number of equations in 'PLANT' were increased. However, in this particular example the results show that a longer interval may be used without forfeiting accuracy, since the NIV's and IV's are solved simultaneously within each step.

In order to establish which arrangement required less overall computer time, the following computational test was performed using the Kutta-Merson routine. In Fig. 7.2 Curve (c) is the accurate numerical solution according to both arrangements. An appreciable error shown by Curve (b) is introduced when using the arrangement of Fig. 7.1 with a time step of 0.005 sec., whereas the error is less than 1% when the same time step is used in the arrangement of Fig. 7.3.

For Δt = 0.005 sec. the CR-ratios are 1.828 and 2.36 respectively. However, the arrangement of Fig. 7.1 does not meet the requirement of 1%

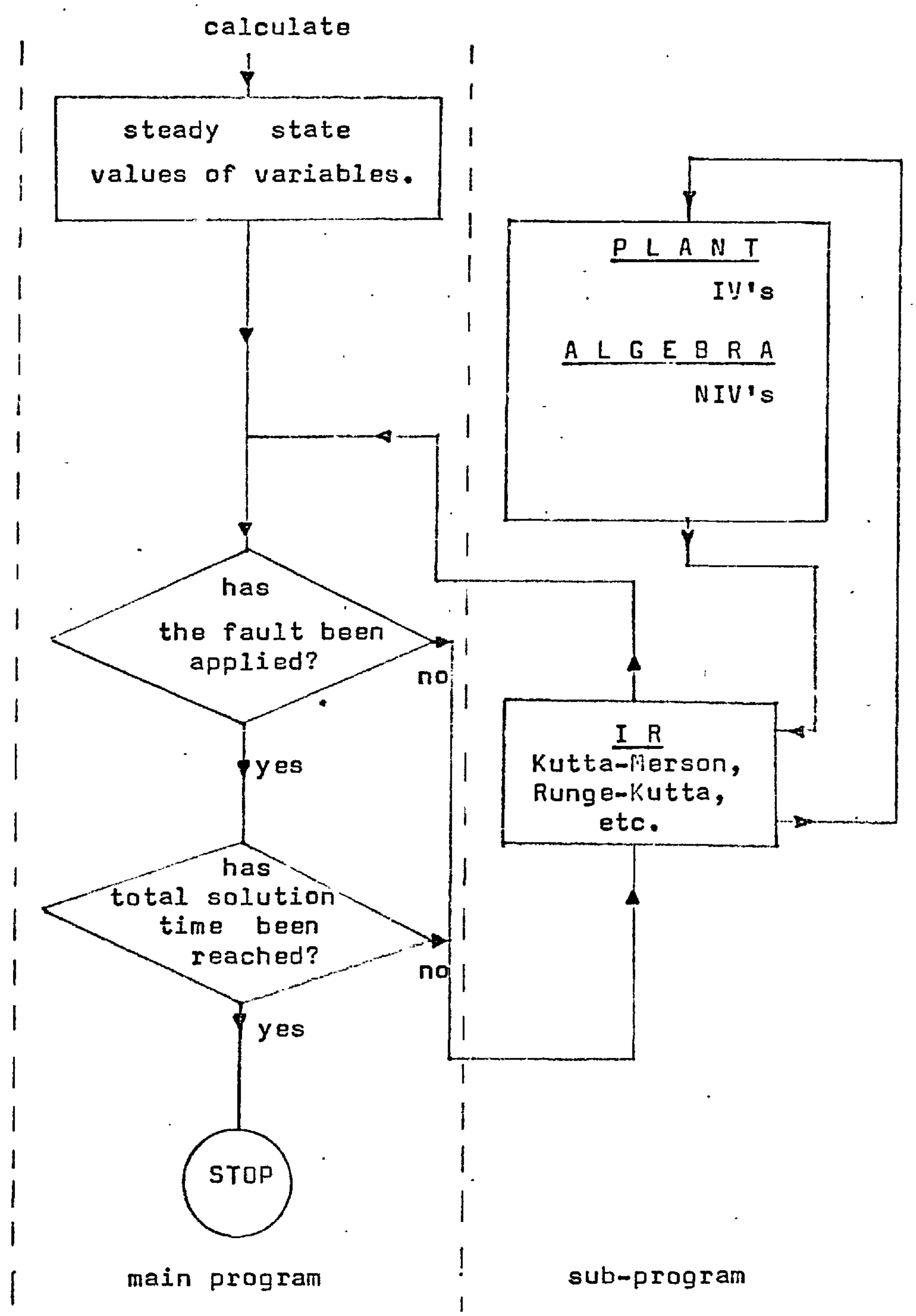

Fig. 7.3 Flow chart for accurate solution when the algebraic and differential equations are solved simultaneously.

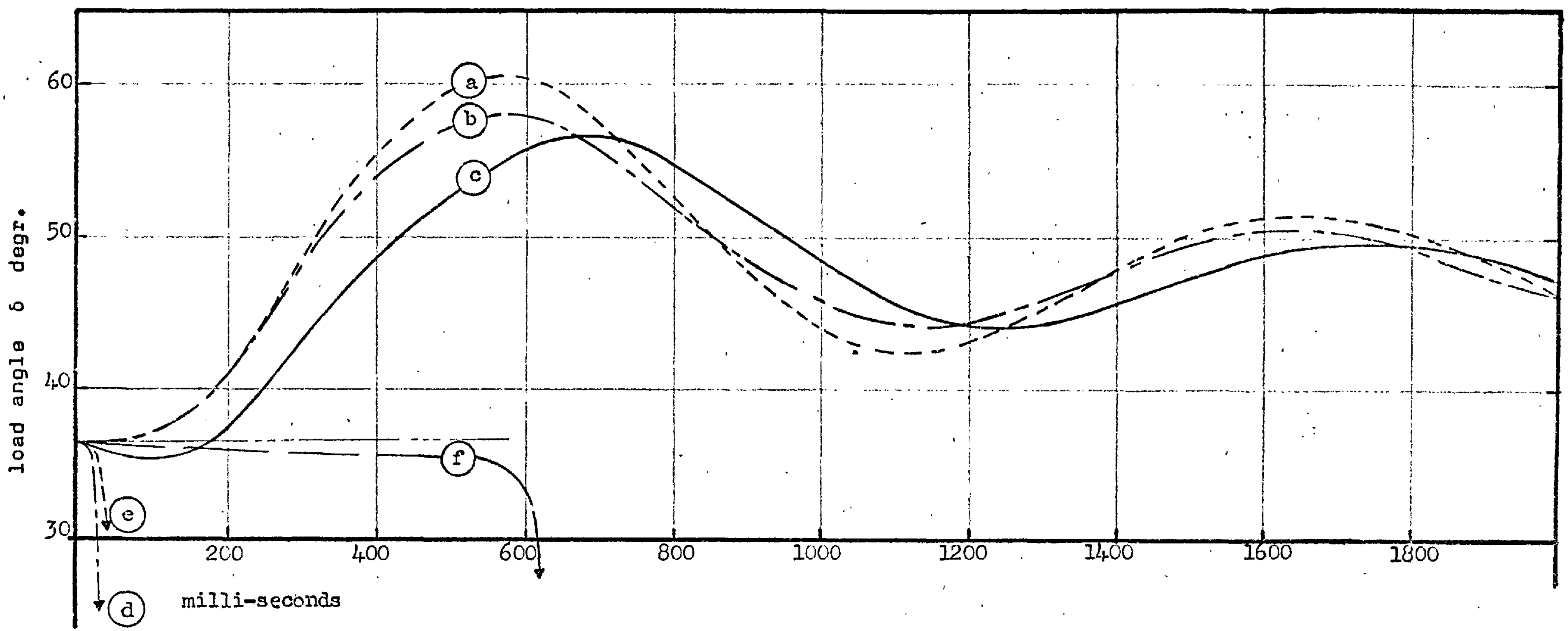

Fig.7.4 Load angle curves for the micro-machine system as computed by various numerical techniques (see Table 7.1)

Arrangement	(1)	(2)	(3)
Curves:	(a) t = 0.01 (b) t = 0.005 (c) t = 0.0005, 0.001 (d) t = 0.012	(c) t = 0.0005 to 0.01 (e) t = 0.012	(c) t = 0.0005 to 0.002 (f) t = 0.005

accuracy, and Δt must be reduced to 0.001, for which the CR-ratio is 4.712. The results (see Table 7.1) of various computations show that the CR-ratio is not directly proportional to Δt, because different parts of the program are differently related to Δt.

(3) Whether Fig. 7.3 gives a smaller CR-ratio than Fig.7.1 for the same accuracy, depends upon the number and complexity of the differential and algebraic equations. Depending upon the ratio of differential to algebraic equations, a lower CR-ratio may be achieved by the use of integrating routines belonging to the Predictor-Corrector class. Such a routine would solve the equations in 'PLANT' only once or twice during each step, instead of four or five times.

The fifth order Kutta-Merson method may be used as a starter for the fifth order Predictor-Corrector method of Hamming . When a discontinuity occors the solution is temporarily transferred back to Kutta-Merson for a few steps after which Hamming takes over again. Table 7.1 shows the comparative results of such an arrangement.

A 4^{th} order Runge-Kutta would not be satisfactory as a starter for a higher order Predictor-Corrector method.

7.4 Resume of integration methods and arrangements

The results in Table 7.1 for the micro-machine only are obtained from five basic differential equations of the alternator plus two first order differential equations for the mechanical motion.

The CR-ratios do not include compitation time and therefore give some qualitative indication of the CR-ratio that could be expected from an on-line computation assuming that the entire program is not compiled before every execution. For an accuracy of within 1% the minimum CR-ratio is 0.965 when using the "approximate method" of Sect. 7.3.1. The choice between arrangements (2) and (3) depends upon the equations of the particular system and has to be found by test runs. In the present study on the micro-machine system it is evident that (2) is faster when Δt = 0.005 sec.

According to the approximate method the currents and flux linkages vary slowly in relation to the a.c. cycle while the accurate method shows (see Sect. 6.2) that these quantities contain a fundamental frequency component. This accounts for the large difference in the time step required for the two methods.

Curve (d) in Fig. 7.2 and Curves (d), (e) and (f) in Fig.7.4 show how rapidly mathematical instability occurs for the higher order integrating routines as Δt is increased.

Further computations have shown that when arrangement (2) is used to solve the complete Goldington system, the CR-ratio is 3.5 when Δt = 0.005 sec., while arrangement (3) produces a CR-ratio of 4.1 when Δt = 0.002 sec. The fifth order Adams-Bashforth method was also used in arrangement (3) as a starter for the Hamming method but the CR-ratio was higher than when using Kutta-Merson as a starter. Another possible way of reducing the CR-ratio is to change the step length during the solution. However the step length of 0.005 sec. in arrangement (2) is already too large to permit the drawing of a smooth 50 Hz wave and step length would have to be decreased to 0.001 sec. for display purposes, in which case arrangement (3) becomes more useful.

---o0o---

P A R T   T H R E E

STABILITY PROBLEMS OF A SYNCHRONOUS MACHINE WITH A DIVIDED WINDING ROTOR.

CHAPTER 8

8. CALCULATIONS OF TRANSIENT STABILITY

8.1 Instroduction

Developments in electrical-supply systems have brought about a change in the conditions under which generators have to operate. During lightly loaded conditions, the generator often has a leading power factor because of increased charging currents in the modern high-voltage transmission networks, and may have to operate beyond the normal stability limit of the conventional synchronous machine. Moreover, the modern economic large turbo-generator sets have higher reactances and less inertia so that normal stable operation in the leading region is reduced.

The normal range of stable operation of a generator with fixed excitation is severely limited at leading current if a reasonable margin is allowed, but it is well known that the range can be extended, by means of an automatic voltage regulator (a.v.r.) acting on the single direct-axis field winding[3] of a machine with a conventionally wound rotor (c.w.r.). The limitations of all such systems at light load however, has been proved elsewhere[4].

The use of a second field winding on the quadrature-axis of the rotor, was first suggested as a means of improving the transient performance[39]. The idea of a quadrature axis regulated (q.a.r.) machine was pursued[4] for steady operating conditions and a dramatic improvement in the steady-state stability margin was obtained when a suitable continuous feedback control signal (the rotor angle) was used to excite the q-axis winding. Another scheme to extend the range of steady-state stability and also to improve the transient stability, has been developed by the C.E.G.B.[5] In this scheme, the generator has a 'divided winding rotor' (d.w.r.), that is, the rotor winding is divided into two sections, one displaced from the other. One section which is called a "torque winding" and performs a similar function to the quadrature winding of Ref. 5, is excited by a feed-back signal derived from the generator terminal load angle. The other section, called the var-winding or reactive-winding, is excited by a voltage regulator. In the light of the stability limitations of the c.w.r. machine, and the recent above mentioned developments of the d.w.r. machine, it was decided not to pursue the stability studies of the former (see PART TWO) any further but rather to investigate the stability problems of the latter.

PART THREE of this thesis deals with the stability problems, steady-state and transient, of such a divided winding rotor machine. The equations are developed, following the generalized machine theory, for the case of a field winding on the d-axis as well as on the q-axis. The field windings of the d.w.r. machine are not necessarily on the d and q-axes, but a transformatiom matrix is used to replace the physical field windings by two fictitious windings, one on each axis. The transient and steady-state performace of the d.w.r. machine is then studied by treating it as a fictitious q.a.r. machine. Steady-state stability computations are corroborated by test results on a new 3 kW d.w.r. micro-machine (see Chapter 10) at Imperial College.

8.2 Transformations for the Field Windings

The divided winding arrangement can be accommodated in the conventional turbogenerator-rotor slots by using, instead of the single conventional concentric type winding, two double layer lap-windings. Fig. 8.1 is a winding diagram the 3 kW d.w.r. micro-machine which was designed to simulate a large d.w.r. turbo-alternator. The T-winding in Fig. 8.1 is used as the torque-winding and R as the reactive-winding; the windings are identical and symmetrical and the angle between their axes is 67.5 degrees.

A schematic layout of the d.w.r. machine appears in Fig. 8.2. Windings a,b,c, are the conventional three-phase stator windings while t and r represent the torque- and reactive windings respectively. The damping effect is represented by the conventional kd- and kq-windings.

Fig. 8.3(a) shows the equivalent generalized machine representation of the actual field coils r and t. Fig. 8.3(c) shows two fictitious field coils fd, fq which are used in the following sections to replace mathematically coils r and t. In a general case where $N_r \neq N_t$, it is possible to use the same base quantities for the various field coils by reducing them to equivalent coils with equal numbers of turns. In a per unit system where

$$N_{fd} = N_{fq} = N_t \qquad (8.1)$$

only the r-coil need be replaced by an equivalent coil r_{eq} as shown in Fig. 8.3(b), such that

$$i_{req} = i_r N$$

where $N = N_r/N_t$ (8.2)

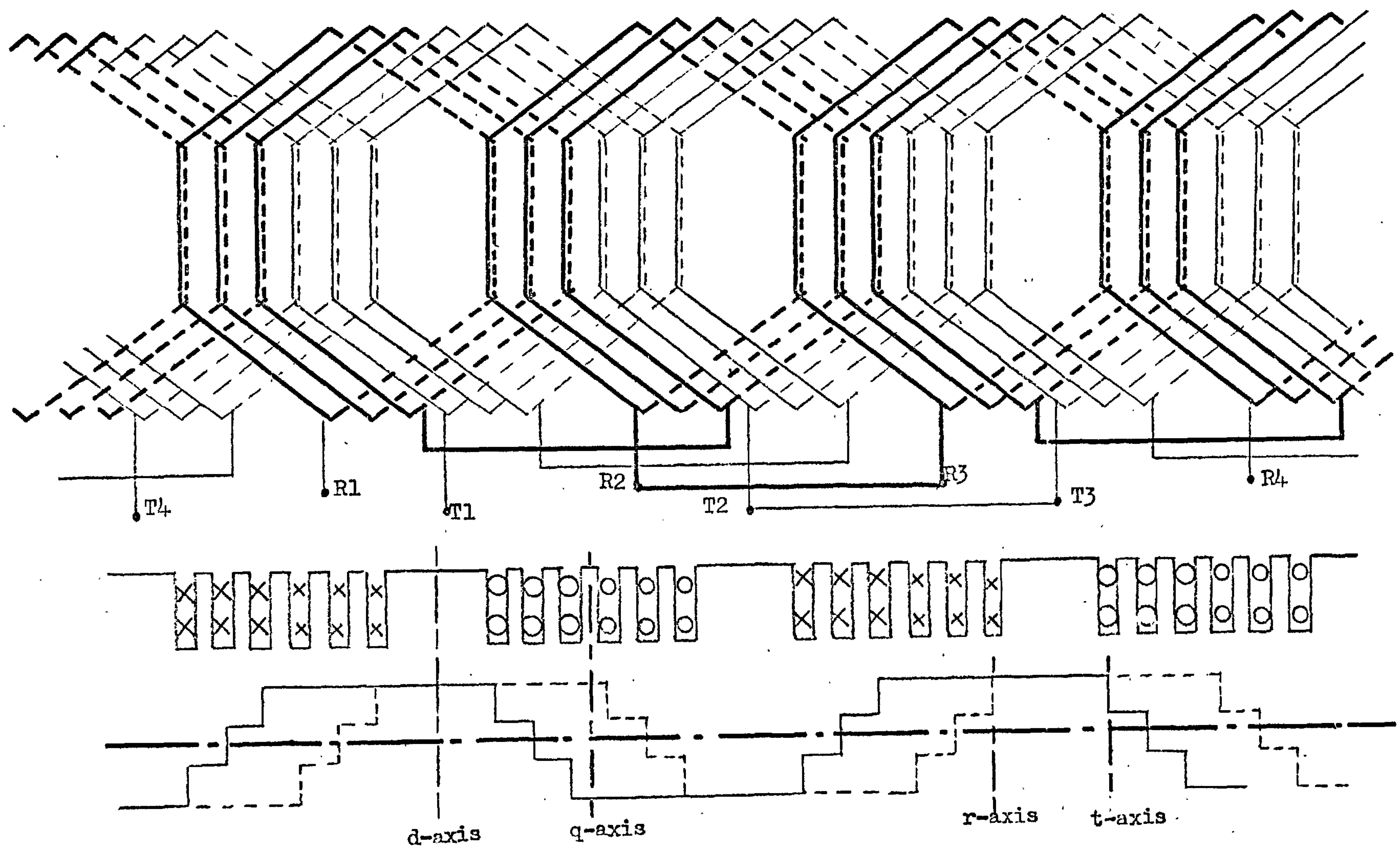

Fig. 8.1 Divided rotor winding of the micro-machine.

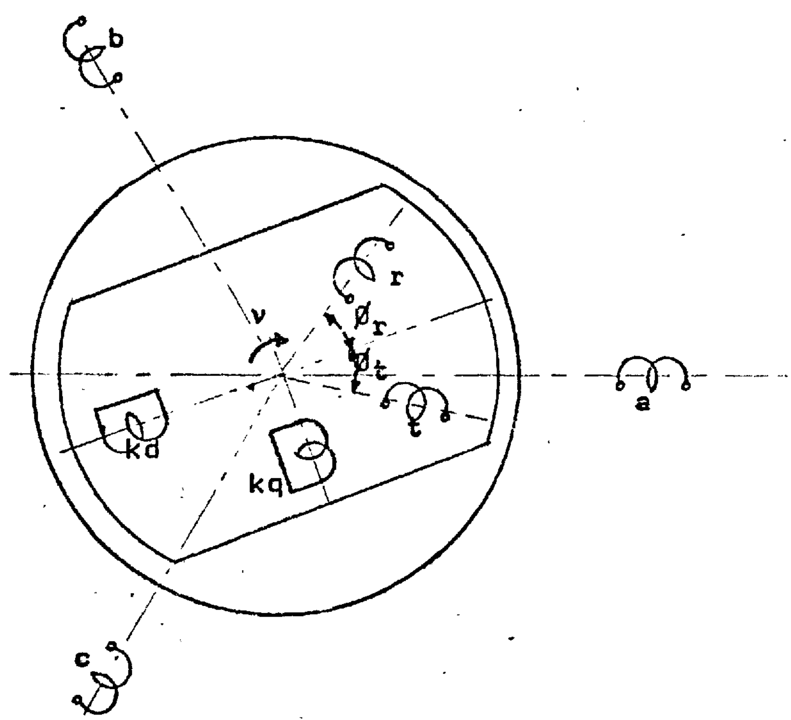

Fig. 8.2 Schematic layout of divided winding rotor generator.

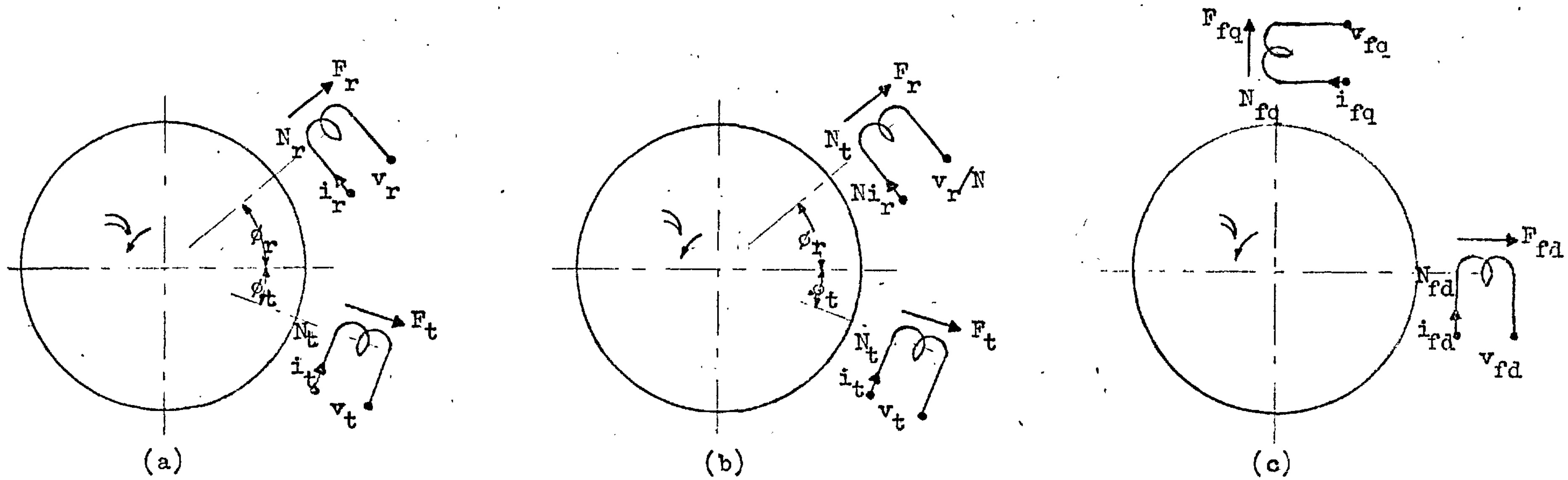

Fig, 8.3 Equivalent diagram of the d.w.r. field windings with rotating armature and stationary field.

(a) Actual field windings r and t.

(b) Actual winding t and equivalent winding r_{eq}.

(c) Fictitious field windings fd and fq.

The effect of saturation is neglected in the following transformations. The sign convention is according to that of Ref.22 where positive applied voltage causes positive current to flow which produces positive M.M.F. and flux linkage outwards along the coil axis in Fig. 8.3.

8.2.1 The current transformation

The axis field currents i_{fd} and i_{fq} are defined as the currents in fictitious coils, located on the axes, which would set up the same rotor M.M.F. wave as the actual field currents i_t and i_r.

The maximum of the sinusoidal M.M.F. wave due to the current i_t in coil t of Fig. 8.3 is proportional to i_t and occurs at the axis of the coil, that is at the angular position ϕ_t. The M.M.F. wave due to i_t may be resolved into two components, one along each of the direct and quadrature axes. The amplitude of the direct-axis component is $i_t\cos\phi_t$ and the amplitude of the quadrature-axis component is $-i_t\sin\phi_t$.

The direct-axis component of the resultant rotor M.M.F. wave due to the combined action of the r and t-coil currents, is equal to the amplitude of the M.M.F. wave due to the current i_{fd} in the direct-axis field coil. Hence i_{fd} is given by

$$i_{fd} = i_t\cos\phi_t + Ni_r\cos\phi_r \tag{8.3}$$

Similarly the quadrature-axis field current i_{fq} is given by

$$i_{fq} = - i_t\sin\phi_t + Ni_r\sin\phi_r \tag{8.4}$$

The "transformation" equations giving the fictitious currents in terms of the actual currents are therefore expressed by the following matrix equations:

$$\begin{bmatrix} i_{fd} \\ i_{fq} \end{bmatrix} = \begin{bmatrix} \cos\phi_t & N\cos\phi_r \\ -\sin\phi_t & N\sin\phi_r \end{bmatrix} \begin{bmatrix} i_t \\ i_r \end{bmatrix} \tag{8.5}$$

The equations of the "inverse transformation", giving the actual currents i_t, i_r in terms of the fictitious currents i_{fd}, i_{fq}, are obtained by solving the above equations.

$$\begin{bmatrix} i_t \\ i_r \end{bmatrix} = \begin{bmatrix} \frac{\sin\phi_r}{\lambda} & \frac{-\cos\phi_r}{\lambda} \\ \frac{\sin\phi_t}{N\lambda} & \frac{\cos\phi_t}{N\lambda} \end{bmatrix} \begin{bmatrix} i_{fd} \\ i_{fq} \end{bmatrix} \tag{8.6}$$

where $\lambda = \sin(\phi_t + \phi_r)$ (8.7)

8.2.2 The voltage transformations

In the units chosen, the power dissipation of the fictitious coils is the same as for the actual coils. Hence

$$v_r i_r + v_t i_t = v_{fd} i_{fd} + v_{fq} i_{fq} \tag{8.8}$$

By substituting the expressions for the currents given by Eqns. (8.5) and (8.6), it can be shown that the voltage transformation equations are

$$\begin{bmatrix} v_{fd} \\ v_{fq} \end{bmatrix} = \begin{bmatrix} \frac{\sin\phi_r}{\lambda} & \frac{\sin\phi_t}{N\lambda} \\ \frac{-\cos\phi_r}{\lambda} & \frac{\cos\phi_t}{N\lambda} \end{bmatrix} \begin{bmatrix} v_t \\ v_r \end{bmatrix} \tag{8.9}$$

The equations of the inverse transformation are:

$$\begin{bmatrix} v_t \\ v_r \end{bmatrix} = \begin{bmatrix} \cos\phi_t & -\sin\phi_t \\ N\cos\phi_r & N\sin\phi_r \end{bmatrix} \begin{bmatrix} v_{fd} \\ v_{fq} \end{bmatrix} \qquad (8.10)$$

8.3 General Equations for the D.W.R. machine

The d.w.r. machine is studied by using the generalized machine theory[22] and taking account of the additional field winding on the q-axis. It is assumed that there is no saturation. Speed changes are allowed for in the voltage equations as well as the $p\Psi_d$ and $p\Psi_q$ terms.

8.3.1 Basic equations

The fundamental equations for the machine only are as follows:

$$v_d = p\Psi_d + \nu\Psi_q + r_a i_d \qquad (8.11)$$

$$v_q = \nu\Psi_d + p\Psi_q + r_a i_q \qquad (8.12)$$

$$v_{fd} = (r_{fd} + (L_{md} + L_{fd})p)i_{fd} + L_{md}pi_d + L_{md}pi_{kd} \qquad (8.13)$$

$$v_{fq} = (r_{fq} + (L_{mq} + L_{fq})p)i_{fq} + L_{mq}.pi_q + L_{mq}.pi_{kq} \qquad (8.14)$$

$$v_{kd} = 0 = L_{md}.pi_{fd} + (r_{kd} + p(L_{md} + L_{kd}))\, i_{kd} + L_{md}pi_d \qquad (8.15)$$

$$v_{kq} = 0 = (r_{kq} + (L_{mq} + L_{fq})p)\, i_{kq} + L_{mq}.pi_q + L_{mq}.pi_{fq} \qquad (8.16)$$

for the voltages, and

$$\Psi_d = L_{md}i_{fd} + L_{md}i_{kd} + L_{dd}i_d \tag{8.17}$$

$$\Psi_q = L_{mq}i_{fq} + L_{mq}i_{kq} + L_{qq}i_q \tag{8.18}$$

$$\Psi_{kd} = L_{kkd}i_{kd} + L_{md}i_{fd} + L_{md}i_d \tag{8.19}$$

$$\Psi_{kq} = L_{kkq}i_{kq} + L_{mq}i_{fq} + L_{mq}i_q \tag{8.20}$$

$$\Psi_{fd} = L_{ffd}i_{fd} + L_{md}i_d + L_{md}i_{kd} \tag{8.21}$$

$$\Psi_{fq} = L_{ffq}i_{fq} + L_{mq}i_q + L_{mq}i_{kq} \tag{8.22}$$

for the flux linkages,

while the electromagnetic torque is given by Eqn. (4.11).

If during a step of the calculation, i_{fd} etc. are obtained using the axis equations, they are readily transformed to i_r, i_t ect. by the transformation equations and used in the regulator equations; or vice versa.

8.3.2 Equivalent circuits and operational impedances

Figure 8.4 shows two equivalent circuits, one for each axis, which can be used to assist in the analysis of the d.w.r. synchronous machine. The quantities in the network of Fig. 8.4(a) satisfy Eqns. (8.13), (8.15) and (8.17), and the quantities in the network of Fig. 8.4(b) satisfy Eqns. (8.14), (8.16) and (8.18).

The expressions for Ψ_d and Ψ_q can be written as

$$\Psi_d = \frac{X_d(p)}{\omega}\, i_d + \frac{G_d(p)}{\omega}\, v_{fd} \tag{8.23}$$

$$\Psi_q = \frac{X_q(p)}{\omega}\, i_q + \frac{G_q(p)}{\omega}\, v_{fq} \tag{8.24}$$

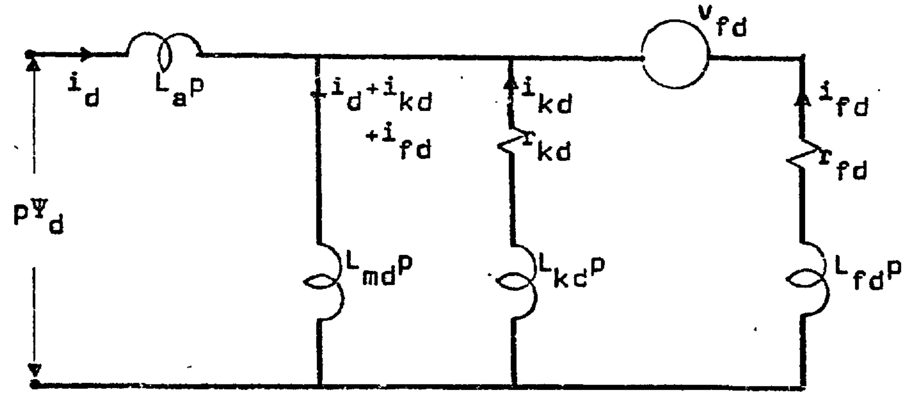

(a) Direct axis

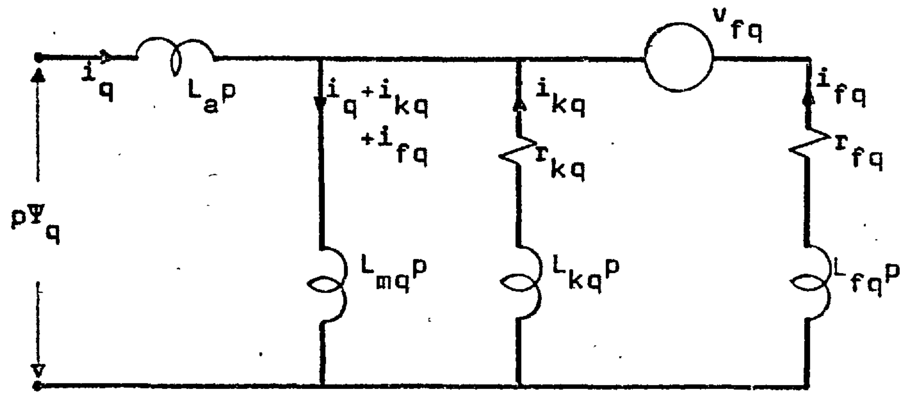

(b) Quadrature axis

Fig. 8.4 Equivalent circuits of a d.w.r. synchronous machine.

where

$$X_d(p) = \frac{(1 + T'_d p)(1 + T''_d p)X_d}{(1 + T'_{do} p)(1 + T''_{do} p)} \tag{8.25}$$

$$X_q(p) = \frac{(1 + T'_q p)(1 + T''_q p)X_q}{(1 + T'_{qo} p)(1 + T''_{qo} p)} \tag{8.26}$$

$$G_d(p) = \frac{(1 + T_{kd} p)}{(1 + T'_{do} p)(1 + T''_{do} p)} \cdot \frac{X_{md}}{r_{fd}} \tag{8.27}$$

$$G_q(p) = \frac{(1 + T_{kq} p)}{(1 + T'_{qo} p)(1 + T''_{qo} p)} \cdot \frac{X_{mq}}{r_{fq}} \tag{8.28}$$

8.3.3 Fundamental machine constants

Listed below are some of the generalized machine theory q-axis constants which differ from the values given in Ref. 22.

$$T'_{qo} = \frac{1}{\omega r_{fq}} (X_{fq} + X_{mq})$$

= quadrature-axis transient open-circuit time constant.

$$T'_q = \frac{1}{\omega r_{fq}} \left(X_{fq} + \frac{X_{mq} X_a}{X_{mq} + X_a}\right)$$

= quadrature-axis transient short-circuit time constant.

$$T''_{qo} = \frac{1}{\omega r_{kq}} \left(X_{kq} + \frac{X_{mq} X_{fq}}{X_{mq} + X_{fq}}\right)$$

= quadrature-axis subtransient open-circuit time constant.

$$T''_q = \frac{1}{\omega r_{kq}} \left(X_{kq} + \frac{X_{mq} X_{fq} X_a}{X_{mq} X_a + X_{mq} X_{fq} + X_a X_{fq}}\right)$$

= quadrature-axis subtransient short-circuit time constant.

$$T_{kq} = \frac{X_{kq}}{\omega r_{kq}}$$

= quadrature-axis damper leakage time constant.

$$X'_q = \frac{X_q T'_q}{T'_{qo}} = X_a + \frac{X_{mq} X_{fq}}{X_{mq} + X_{fq}}$$

= quadrature-axis transient reactance

$$X''_q = \frac{X_q T'_q T''_q}{T'_{qo} T''_{qo}} = X_a + \frac{X_{mq} X_{fq} X_{kq}}{X_{mq} X_{fq} + X_{mq} X_{kq} + X_{fq} X_{kq}}$$

= quadrature-axis subtransient reactance.

8.4 Parameters of the Fictitious Field Windings

During a step of the computation, the excitation voltages v_r and v_t are transformed to v_{fd} and v_{fq} which are substituted in the basic machine equations. It is therefore necessary to know the numerical values of the following fd, fq parameters which can be calculated either by transforming known r, t parameters, or from experiments described in Sect. 10.1.2;

r_{fd}, L_{ffd}, r_{fq}, L_{ffq} in Eqns (8.13), (8.14), (8.21) and (8.22).

The "parameter transformation" can be found by transforming the following r, t voltage expressions into fd, fq quantities:

$$\left.\begin{aligned} v_r &= (r_r + L_{rr}p)i_r + NL_{mtr}pi_t \\ v_t &= (r_t + L_{tt}p)i_t + NL_{mtr}pi_r \end{aligned}\right) \qquad (8.29)$$

where L_{rr}, L_{tt} is the complete[22] inductance of windings r, t and L_{mtr} is the mutual inductance between windings r_{eq} and t.

Eqns. (8.29) can be rewritten as

$$[v]_{r,t} = [Z]_{r,t}\,[i]_{r,t}$$

where the r,t-impedance matrix is

$$[Z]_{r,t} = \begin{array}{c|c} r & t \\ \hline r_r + L_{rr}p & L_{mtr}p \\ \hline L_{mtr}p & r_t + L_{tt}p \end{array}$$

The current and voltage transformation Eqns. (8.6) and (8.9) are used to find the fd, fq-impedance m trix (8.30)

$$[Z]_{fd,fq} = \begin{array}{c|c} fd & fq \\ \hline r_{fd} + L_{ffd}p & 0 \\ \hline 0 & r_{fq} + L_{ffq} \end{array} \qquad (8.30)$$

where

$$\left.\begin{aligned}
r_{fd} &= (r_{req}\sin^2\phi_t + r_t\sin^2\phi_r)/\lambda^2 \\
r_{fq} &= (r_{req}\cos^2\phi_t + r_t\cos^2\phi_r)/\lambda^2 \\
L_{ffd} &= (L_{rreq}\sin^2\phi_t + L_{tt}\sin^2\phi_r + L_{mtr}\sin(\phi_r + \phi_t))/\lambda^2 \\
L_{ffq} &= (L_{rreq}\cos^2\phi_t + L_{tt}\cos^2\phi_r - L_{mtr}\cos(\phi_r - \phi_t))/\lambda^2 \\
r_{req} &= r_r/N^2 \\
L_{rreq} &= L_{rr}/N^2
\end{aligned}\right\} \qquad (8.31)$$

8.5 Equations for a Transient Disturbance

The basic system being considered is the single machine case shown in Fig. 2.1 except that the alternator is a d.w.r. machine. As in the analysis of the c.w.r. machine of Sect. 4.2, there is a "standard method", an "approximate method" and an "accurate method" of solution. Only the "approximate" and "accurate" methods are studied here in detail.

8.5.1 The approximate method

The assumptions of Sect. 4.2.2 are valid and the $p\Psi_d$ and $p\Psi_q$ terms are neglected.

It may be seen from Appendix II that when the secondary currents i_{fd} and i_{kd} are eliminated from Eqns. (8.17),(8.19) and (8.21), the flux linkage is obtained as

$$\omega\Psi_d = X_d''i_d + \omega(X_d'' - X_a)\left(\frac{\Psi_{fd}}{X_{fd}} + \frac{\Psi_{kd}}{X_{kd}}\right) \tag{8.32}$$

(compare Eqn. (4.12)).

Similarly, if i_{fq} and i_{kq} are eliminated from Eqns.(8.18),(8.20) and (8.22)

$$\omega\Psi_q = X_q''i_q + \omega(X_q'' - X_a)\left(\frac{\Psi_{fq}}{X_{fq}} + \frac{\Psi_{kq}}{X_{kq}}\right) \tag{8.33}$$

(compare Eqn. (4.13))

When the "approximate method" is used, the damping torque can not be separated from the total electromagnetic torque but is automatically taken care of by the rate at which the secondary flux linkages Ψ_{fd}, Ψ_{fq}, Ψ_{kd} and Ψ_{kq} are allowed to change. When the four secondary currents i_{kd}, i_{kq}, i_{fd} and i_{fq} are eliminated from the basic equations (see Appendix II), the expressions for the rates of change become:-

$$p\Psi_{fd} = v_{fd} + \frac{1}{T'_{do}} \left[\frac{(X''_d - X_a)}{(X'_d - X_a)} \left[\frac{X_{md} i_d}{\omega} + \frac{X_{md}\Psi_{kd}}{X_{kd}} \right] - \Psi_{fd} \left(1 + \frac{(X''_d - X_a)X_{md}}{X_{kd}X_{fd}}\right) \right] \tag{8.34}$$

(compare Eqn. (4.16))

$$p\Psi_{fq} = v_{fq} + \frac{1}{T'_{qo}} \left[\frac{(X''_q - X_a)}{(X'_q - X_a)} \left[\frac{X_{mq} i_q}{\omega} + \frac{X_{mq}\Psi_{kq}}{X_{kq}} \right] - \Psi_{fq} \left[1 + \frac{(X''_q - X_a)X_{mq}}{X_{kq}X_{fq}}\right] \right] \tag{8.35}$$

$$p\Psi_{kd} = \frac{1}{T''_{do}} \left[\frac{(X'_d - X_a)i_d}{\omega} + \frac{(X'_d - X_a)\Psi_{fd}}{X_{fd}} - \Psi_{kd} \right] \tag{8.36}$$

(compare Eqn. (4.14))

$$p\Psi_{kq} = \frac{1}{T''_{qo}} \left[\frac{(X'_q - X_a)i_q}{\omega} + \frac{(X'_q - X_a)\Psi_{fq}}{X_{fq}} - \Psi_{kq} \right] \tag{8.37}$$

(compare Eqn. (4.15))

The relationship between the voltage behind subtransient reactance and the machine terminal voltage is (see Sect. 4.2.2)

$$\left.\begin{aligned} v_{mtd} &= r_a i_d + X''_q i_q + v''_d \\ v_{mtq} &= r_a i_q + X''_d i_d + v''_q \end{aligned}\right) \tag{8.38}$$

where v''_d and v''_q for a d.w.r. machine are given by:

$$\left.\begin{aligned} v''_d &= -SX''_q i_q + (X''_q - X_a)\omega(1-S)\left[\frac{\Psi_{fq}}{X_{fq}} + \frac{\Psi_{kq}}{X_{kq}}\right] \\ v''_q &= SX''_d i_d - \omega(1-S)(X''_d - X_a)\left[\frac{\Psi_{fd}}{X_{fd}} + \frac{\Psi_{kd}}{X_{kd}}\right] \end{aligned}\right\} \quad (8.39)$$

(compare Eqn. (4.18))

The relationship between the terminal voltage and the infinite bus voltage V_b is given by Eqns. (4.19) and (4.20) as

$$v_{mtd} = \sqrt{2}\, V_{bd} - Ri_d - \frac{X}{\omega} \nu\, i_q \quad (4.19)$$

$$v_{mtq} = \sqrt{2}\, V_{bq} - Ri_q + \frac{X}{\omega} \nu\, i_d \quad (4.20)$$

The step-by-step solution of a transient disturbance can be computed as follows:-

Steady-state Conditions

From a knowledge of the active and reactive power at the machine terminals, it is possible to find the bus power factor, -load angle and voltage. The values of i_d, i_q, v''_q, v''_d are found from Eqns. (4.19), (4.20) and (8.38). Under steady-state conditions, $p\Psi_{fd} = p\Psi_{fq} = p\Psi_{kd} = p\Psi_{kq} = 0$. Using Eqns. (8.34) to (8.37), the steady-state values of the secondary flux linkages are:-

$$\Psi_{fdo} = T'_{do} v_{fdo} + \frac{X_{md}(X''_d - X_a)}{\omega}\left[\frac{1}{(X'_d - X_a)} + \frac{1}{X_{kd}}\right] i_{do} \quad (8.40)$$

$$\Psi_{fqo} = T'_{qo} v_{fqo} + \frac{X_{mq}(X''_q - X_a)}{\omega}\left[\frac{1}{(X'_q - X_a)} + \frac{1}{X_{kq}}\right] i_{qo} \quad (8.41)$$

$$\Psi_{kdo} = \left(\frac{X'_d - X_a}{\omega}\right)i_{do} + \left(\frac{X'_d - X_a}{X_{fd}}\right)\Psi_{fdo} \tag{8.42}$$

$$\Psi_{kqo} = \left(\frac{X'_q - X_a}{\omega}\right)i_{qo} + \left(\frac{X'_q - X_a}{X_{fq}}\right)\Psi_{fqo} \tag{8.43}$$

In Eqn. (8.39), Ψ_{kd} and Ψ_{kq} are replaced by their values from Eqns. (8.42) and (8.43). v''_q and v''_q known and the slip is zero before the disturbance. This leaves Ψ_{fdo} and Ψ_{fqo} as:-

$$\Psi_{fdo} = - \frac{X_{fd}\left[v''_q + \dfrac{(X''_d - X_a)(X'_d - X_a)i_d}{X_{kd}}\right]}{\omega(X''_d - X_a)\left[1 + \dfrac{(X'_d - X_a)}{X_{kd}}\right]} \tag{8.44}$$

$$\Psi_{fqo} = \frac{X_{fq}\left[v''_d - \dfrac{(X''_q - X_a)(X'_q - X_a)i_q}{X_{kq}}\right]}{\omega(X''_q - X_a)\left[1 + \dfrac{(X'_q - X_a)}{X_{kq}}\right]} \tag{8.45}$$

The values of Ψ_{do} and Ψ_{qo} are found from Eqns. (8.31) and (8.32) and Eqn. (4.11) is used to compute the electrical torque.

The steady-state values of v_{fd} and v_{fq} are found from Eqns. (8.40) and (8.41):

$$v_{fdo} = \Psi_{fdo} - i_{do}\left[\frac{(X''_d - X_a)X_{md}}{(X'_d - X_a)\omega}\left(1 + \frac{(X'_d - X_a)}{X_{kd}}\right)/T'_{do}\right] \tag{8.46}$$

$$v_{fqo} = \Psi_{fqo} - i_{qo}\left[\frac{(X''_q - X_a)X_{mq}}{(X'_q - X_a)\omega}\left(1 + \frac{(X'_q - X_a)}{X_{kq}}\right)/T'_{qo}\right] \tag{8.47}$$

The transformation Eqns. (8.10) are used to find v_{to} and v_{ro}.

Transient conditions

After a disturbance to the system, the flux linkages Ψ_{fd}, Ψ_{kd}, Ψ_{fq} and Ψ_{kq}, the voltages v''_d and v''_q and the speed ν are all assumed constant for the first step of the calculation. The change in transmission line impedance is introduced into Eqns. (4.19) and (4.20) which, together with Eqn. (8.38), are used to find the new values of i_d and i_q. New values for Ψ_d and Ψ_q are found and used with i_d and i_q to compute the electrical torque.

The acceleration and change in load angle are computed for the period Δt while the time rates of change of secondary flux linkages given by Eqns. (8.34) to (8.37) are used to find the new values of Ψ_{fd}, Ψ_{kd}, Ψ_{fq} and Ψ_{kq} after a time Δt. These new flux linkages are then used in Eqn. (8.39) to find the new v''_d and v''_q and the whole process is repeated for the next interval.

This method of step-by-step computation agrees with that described in Ref. 33 except for the additional equations of the fq coil.

8.5.2 <u>The accurate method</u>

As in Sect. 4.2.3, this method includes the $p\Psi_d$ and $p\Psi_q$ terms and the terms which allow for the transmission line and transformer inductive volt drop after a sudden change.

Expressions for $p\Psi_d$ and $p\Psi_q$ are found by differentiating Eqns. (8.32) and (8.33) and used to obtain first order differential equations (8.48) for the primary currents i_d, i_q and secondary flux linkages Ψ_{fd}, Ψ_{kd}, Ψ_{fq} and Ψ_{kq} as shown in Appendix III.

$$\begin{bmatrix} pi_d \\ pi_q \\ p\Psi_{fd} \\ p\Psi_{fq} \\ p\Psi_{kd} \\ p\Psi_{kq} \end{bmatrix} = \begin{bmatrix} a_1 & \nu a_2 & a_3 & \nu a_4 & a_5 & \nu a_6 & a_7 V_{bd} & a_8 & 0 \\ \nu b_1 & b_2 & \nu b_3 & b_4 & b_5 & b_6 & b_7 V_{bq} & 0 & b_9 \\ c_1 & 0 & c_3 & 0 & c_5 & 0 & 0 & 1 & 0 \\ 0 & d_2 & 0 & d_4 & 0 & d_6 & 0 & 0 & 1 \\ e_1 & 0 & e_3 & 0 & e_5 & 0 & 0 & 0 & 0 \\ 0 & f_2 & 0 & f_4 & 0 & f_6 & 0 & 0 & 0 \end{bmatrix} \begin{bmatrix} i_d \\ i_q \\ \Psi_{fd} \\ \Psi_{fq} \\ \Psi_{kd} \\ \Psi_{kq} \\ 1 \\ v_{fd} \\ v_{fq} \end{bmatrix} \tag{8.48}$$

The voltage expressions for the interconnection tie-line are:

$$V_{mtd} = \sqrt{2}\ V_{bq} - \frac{X}{\omega}\ pi_d - Ri_d - \frac{X}{\omega}\ \nu i_q \tag{4.24}$$

$$V_{mtq} = -\sqrt{2}\ V_{bq} - \frac{X}{\omega}\ pi_q + \frac{X}{\omega}\ \nu i_d \tag{4.25}$$

where $V_{bd} = V_b \sin\delta$ and $V_{bq} = V_b \cos\delta$

A step-by-step computation which uses the above equations is described in Sect. 4.2.3.

8.6 Calculated Results of a Fault on a Large System

In order to verify the validity of the theory and transformations derived in the earlier parts of this chapter, it was neccessary to compare the calculations with test results. However, no test results on a large practical d.w.r. machine were available. A micro-machine with a divided winding, described in Chapter 10, was available but could not be used for the present purpose because the existing t.c.r. was too slow in its action (see Sect.6.3). The verification had to be done by using the analogue computer results[5] of a hypothetical 30 MW d.w.r. system shown in Fig. 8.5.

8.6.1 System details

The hypothetical 30 MW system includes a governor and turbine, transformer and transmission line similar to the 30 MW c.w.r. system in Sect. 5.2. Table 8.1 shows the physical parameters together with the fictitious machine parameters calculated from the transformation in Sect. 8.4 and expressions in Sect. 8.3.3.

The main feature of the d.w.r. control is that the torque winding has a closed-loop rotor angle control, adjusted so that the reactive winding generates no torque ideally. The angle control is an essential part of the scheme and all the other features depend on it.

In Fig. 8.6 the terminal rotor angle δ_t is derived from a phase-sensitive detector which measures the phase relationship of the generator terminal voltage to the output of a tacho-generator on the turbo-generator shaft. The form of the rotor angle control after the error-sensing or comparator stage is similar to that of the conventional voltage regulator of Sect. 5.2.2.

The angle regulator equations are as follows in degrees, volts and seconds:

Power-bias filter

$$P_f = \frac{P_m}{1 + \tau_p p} \tag{8.49}$$

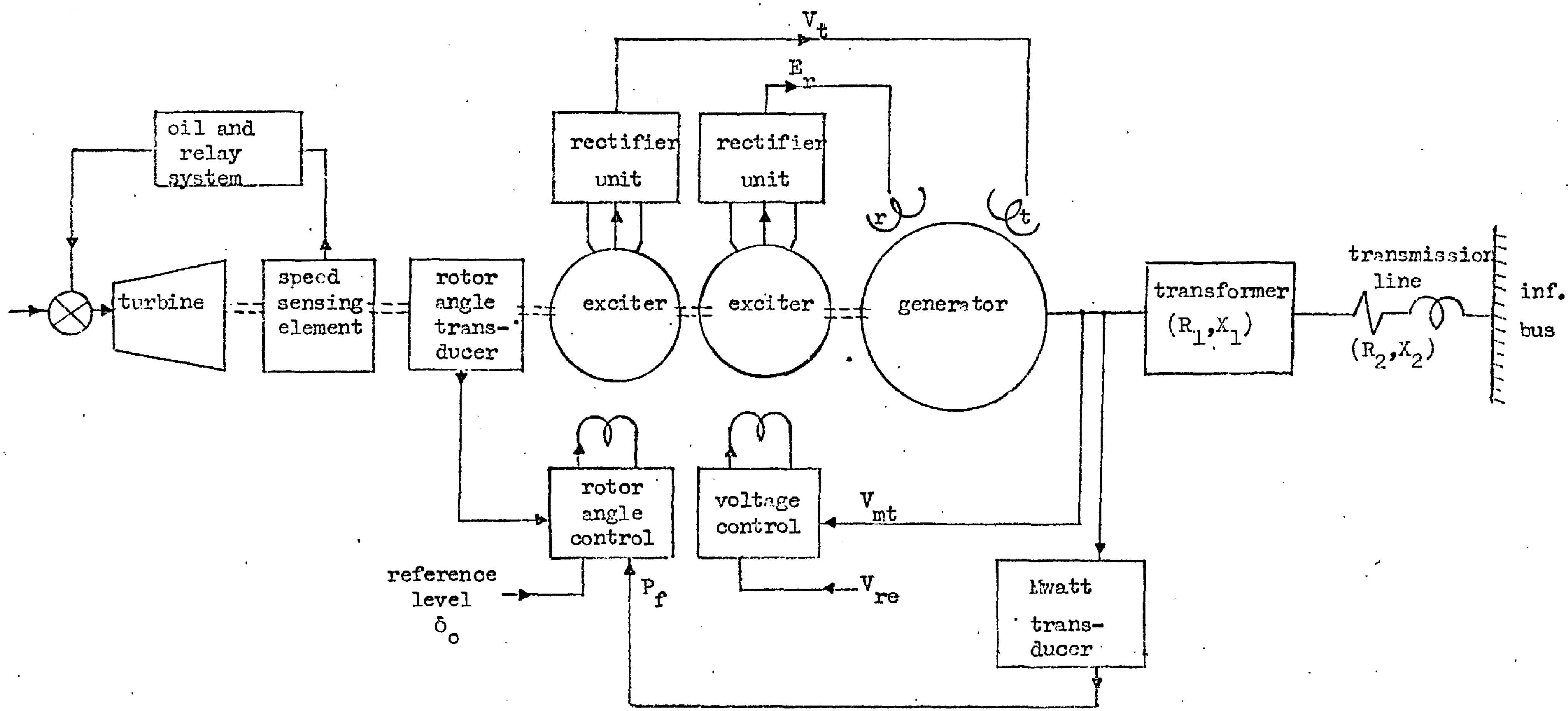

Fig. 8.5 Block diagram of 30 MW d.w.r. system.

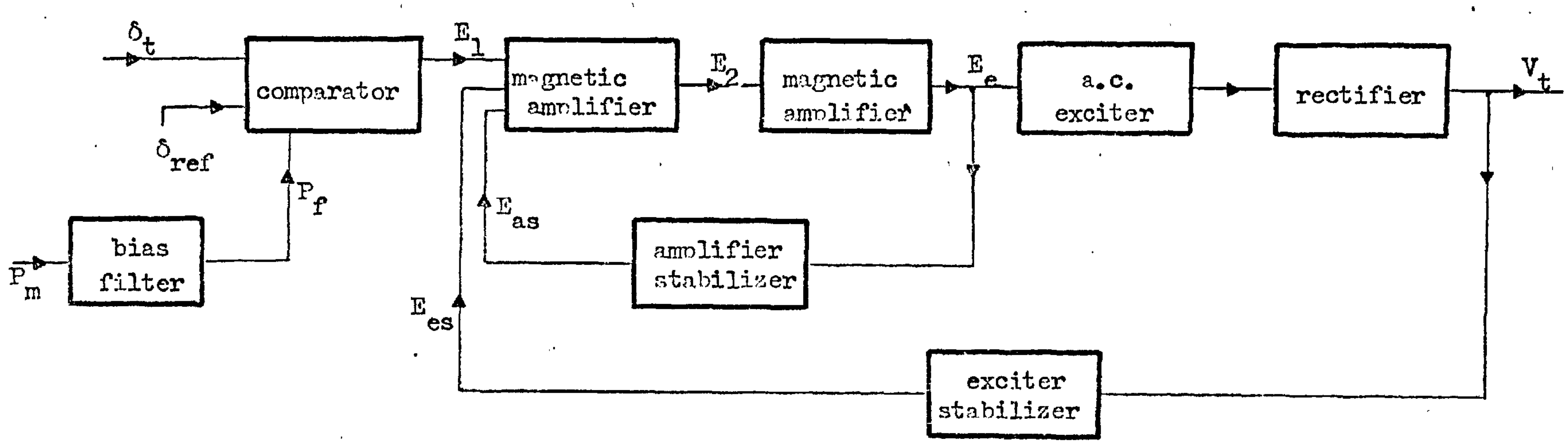

Fig. 8.6 Block diagram of rotor-angle control.

Table 8.1 Generator and system data

For base armature values see Table 5.1	
Base r- and t-current	$422.6/\sqrt{2}$ A
Base r- and t-voltage	$88.63/\sqrt{2}$ kV
Base r- and t-impedance	209.7 ohm
Mutual reactance	
r, t-axis X_{mr}, X_{mt}	1.79 p.u.
Reactive-torque winding X_{trm}	1.00 p.u.
Leakage reactance	
X_a	0.14 p.u.
X_r, X_t	0.21 p.u.
X_{kd}, X_{kq}	0.04 p.u.
Transformer	
Reactance X_1	0.1154 p.u.
Resistance R_1	0.0044 p.u.
Transmission line	
Reactance X_2	0.333 p.u.
Resistance R_2	0.1215 p.u.
Governor gain G_1	0.000472
Calculated fictitious values	
X''_d	0.171 p.u.
X'_d	0.270 p.u.
T'_{do}	6.58 sec.
T'_d	0.889 sec.
T''_d	0.027 sec.
X''_q	0.1757 p.u.
X'_q	0.472 p.u.
T'_{qo}	2.6 sec.
T'_q	0.69 sec.
T''_q	0.035 sec.
X_{fq}	0.42 p.u.
X_{fd}	0.14 p.u.
r_{fq}	0.00245 p.u.
r_{fd}	0.000975 p.u.

Table 8.2 Control system data

Common data	
G_{ms}, G_{as}	0.0139
G_{xs}, G_{es}	0.00525
τ_{m1}	0.044 sec.
τ_{m2}	0.1 sec.
τ_{x}	0.2 sec.
τ_{ms}, τ_{as}	0.1 sec.
τ_{xs}, τ_{es}	2.0 sec.
G_{m1}	52
G_{m2}	12.2
G_{x}	2.65
Voltage regulator	
G_{vs}	0.000795
K_{m1}	56.6 V
K_{m2}	- 278.7 V
$V_{m2\ max}$	45.7 V
$V_{m2\ min}$	0.0 V
$V_{x\ max}$	131 V
$V_{x\ min}$	- 131 V
Angle regulator	
$E_{2\ max}$	28.1 V
$E_{2\ min}$	- 17.45 V
$E_{e\ max}$	131 V
$E_{e\ min}$	0 V
G_{e}	0.0417
G_{b}	2.41×10^{-9} V/MW
τ_{p}	7.0 sec.

Comparator

$$E_1 = G_e(\delta_t - \delta_{ref}) + G_b P_f \tag{8.50}$$

First magnetic amplifier

$$E_2 = \frac{G_{m1}}{1 + \tau_{m1} p} (E_1 + E_{as} + E_{es}) \tag{8.51}$$

$$E_{2\ min} \leqslant E_2 \leqslant E_{2\ max}$$

Second magnetic amplifier

$$E_e = \frac{G_{m2}}{1 + \tau_{m2} p} E_2 \tag{8.52}$$

$$E_{e\ min} \leqslant E_e \leqslant E_{e\ max}$$

Exciter and Rectifiers

$$V_t = \frac{G_x}{1 + \tau_x p} E_e \tag{8.53}$$

Amplifier stabilizer

$$E_{as} = \frac{- G_{as} \tau_{as} p}{1 + \tau_{as} p} E_e \tag{8.54}$$

Exciter stabilizer

$$E_{es} = \frac{-G_{es} \tau_{es} p}{1 + \tau_{es} p} V_t \tag{8.55}$$

Steady-state initial conditions

The steady-state values of the regulator variables are found from the following expressions:

$$\left.\begin{aligned}
\delta_{ref} &= (\delta_t + P_m \frac{G_b}{G_e} - V_{to}/(G_e G_{xd} G_{m1} G_{m2})) \\
E_{eso} &= E_{aso} = 0 \\
E_{eo} &= V_{to}/G_x \\
E_{2o} &= E_{eo}/G_{m2} \\
E_{1o} &= E_{2o}/G_{m1}
\end{aligned}\right) \qquad (8.56)$$

V_{fdo} and V_{fqo} are found from Eqns. (8.46) and (8.47) and used in the transformation Eqn. (8.10) to calculate V_{to} for the angle regulator and V_{ro} for the voltage regulator.

The same automatic voltage regulator of Sect. 5.2 is used, but the amplifier limits are different so that excitation current can flow in either direction. The values of voltage - and angle regulator parameters appear in Tables 5.2 and 8.2

8.6.2 Results for a three-phase short-circuit

In this section digital computations are made and compared for a three-phase fault, using the "approximate method" and the "accurate method" described in Section 8.5. The calculations do not allow for saturation. Further computations are made for different conditions on the same system. Particular emphasis is placed on the initial period to determine the effect of a "back swing" in the rotor angle (Sect. 6.2.3)

The initial conditions for the results in Fig. 8.7, appear in Table 8.3.

Table 8.3 Steady state initial conditions

P_t p.u.	Q_t p.u.	V_{mt} p.u.	I p.u.	V_b p.u.	δ_t deg.	δ deg.	I_r A	I_t A
0.8	-.225	0.963	0.863	1.044	30	52.65	-90.3	421.4
0.2	-.225	0.963	0.313	1.049	30	36.7	75.9	91.4

In Fig. 8.7 (a) the results calculated by the approximate- and accurate methods agree closely enough for a single curve to be drawn except where the accurate method gives 50 Hz oscillations. However, sime of the results are repeated in Figs.8.7(b) and (c) which clearly show the error introduced by the ap roximate method. The results are similar to that shown in Sect. 6.2 for a c.w.r. machine. There is no clear back swing, although the rotor angle remains constant for about 50 milli-seconds. Moreover the effect seems less severe on the rest of the system perhaps because the rotor angle is being controlled. In general the results of Fig. 8.7 agree with those of Ref. 5, the main source of error being the neglect in saturation.

The curves for the two field currents I_t and I_r (see Fig. 8.7(c)) show a phase difference of 60^o which is also the angle between the axes of the two field windings on the rotor. This supports the statement in Sect. 4.1, that "after a short-circuit the flux wave represented by Ψ_d and Ψ_q remains as a flux wave stationary with respect to the armature". The voltages induced in the field windings and the consequent currents are therefore of fundamental frequency.

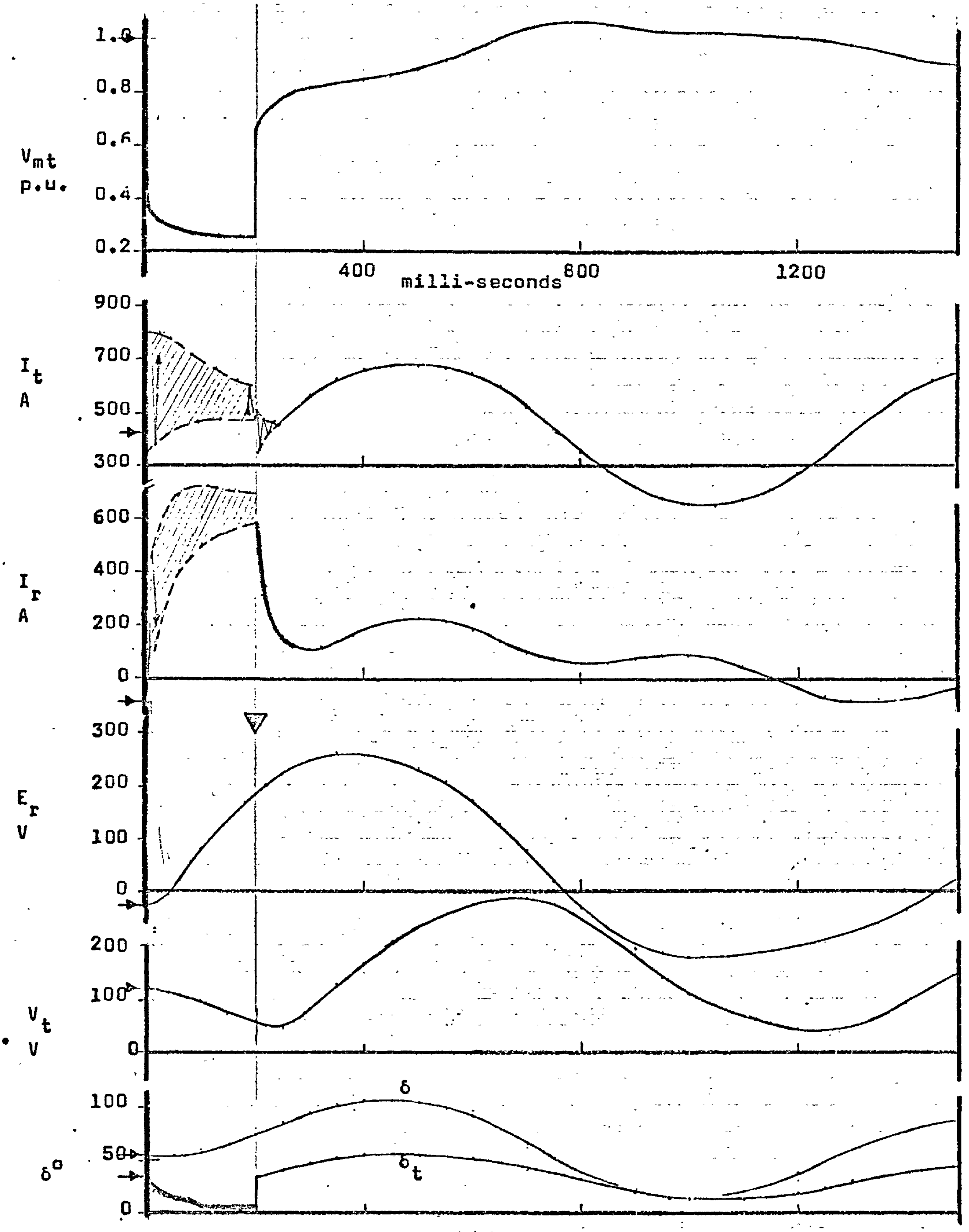

Fig. 8.7(a) The hypothetical d.w.r. system after a three-phase short-circuit.
P = 0.8 p.u., Q = -0.225 p.u.

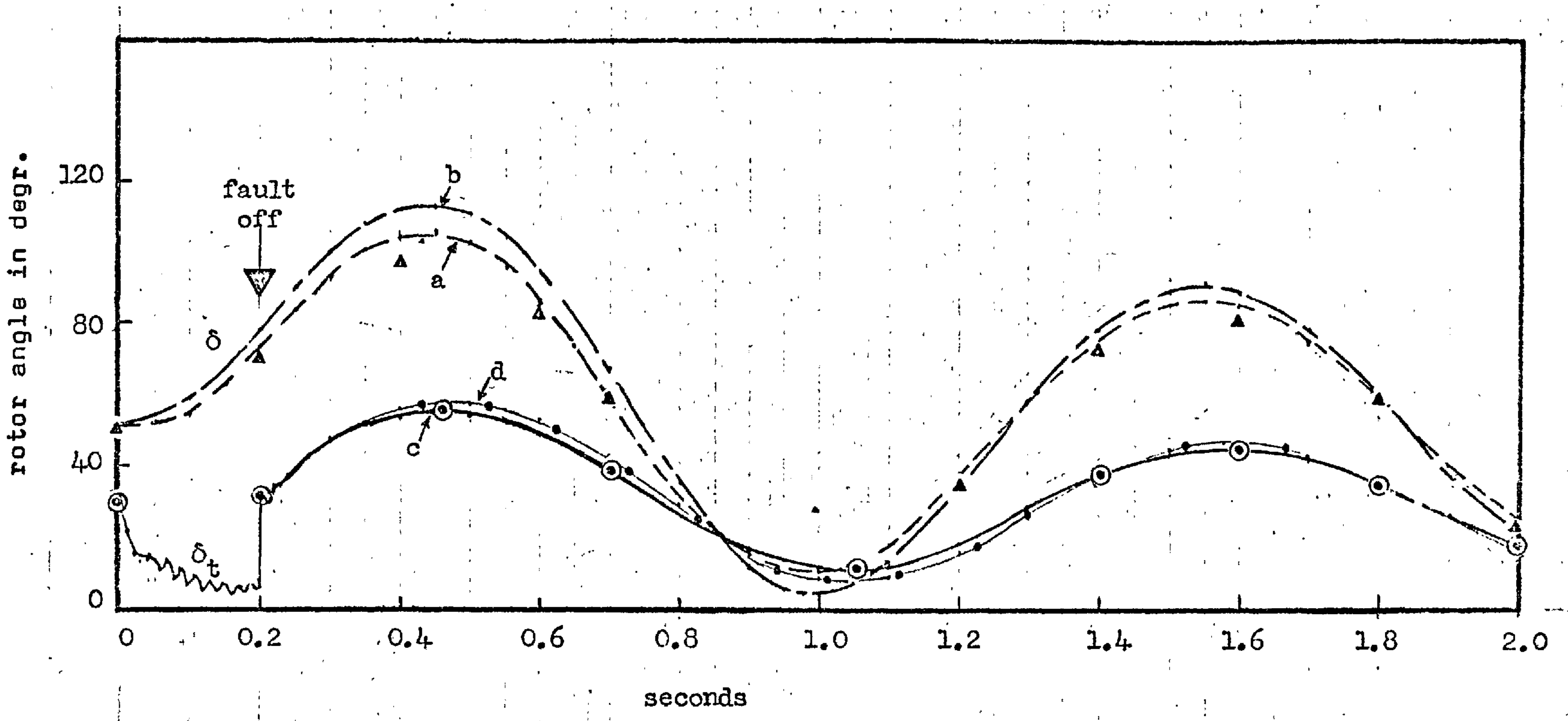

Fig. 8.7(b) Rotor angles of the hypothetical 30 MW d.w.r. turbo-alternator after a short-circuit.

$P = 0.8$ p.u., $Q = -0.225$ p.u.

Curves: (a),(c) accurate method; (b),(d) approximate method.

⊙ ⊙ ▲▲ Points from Reference 5.

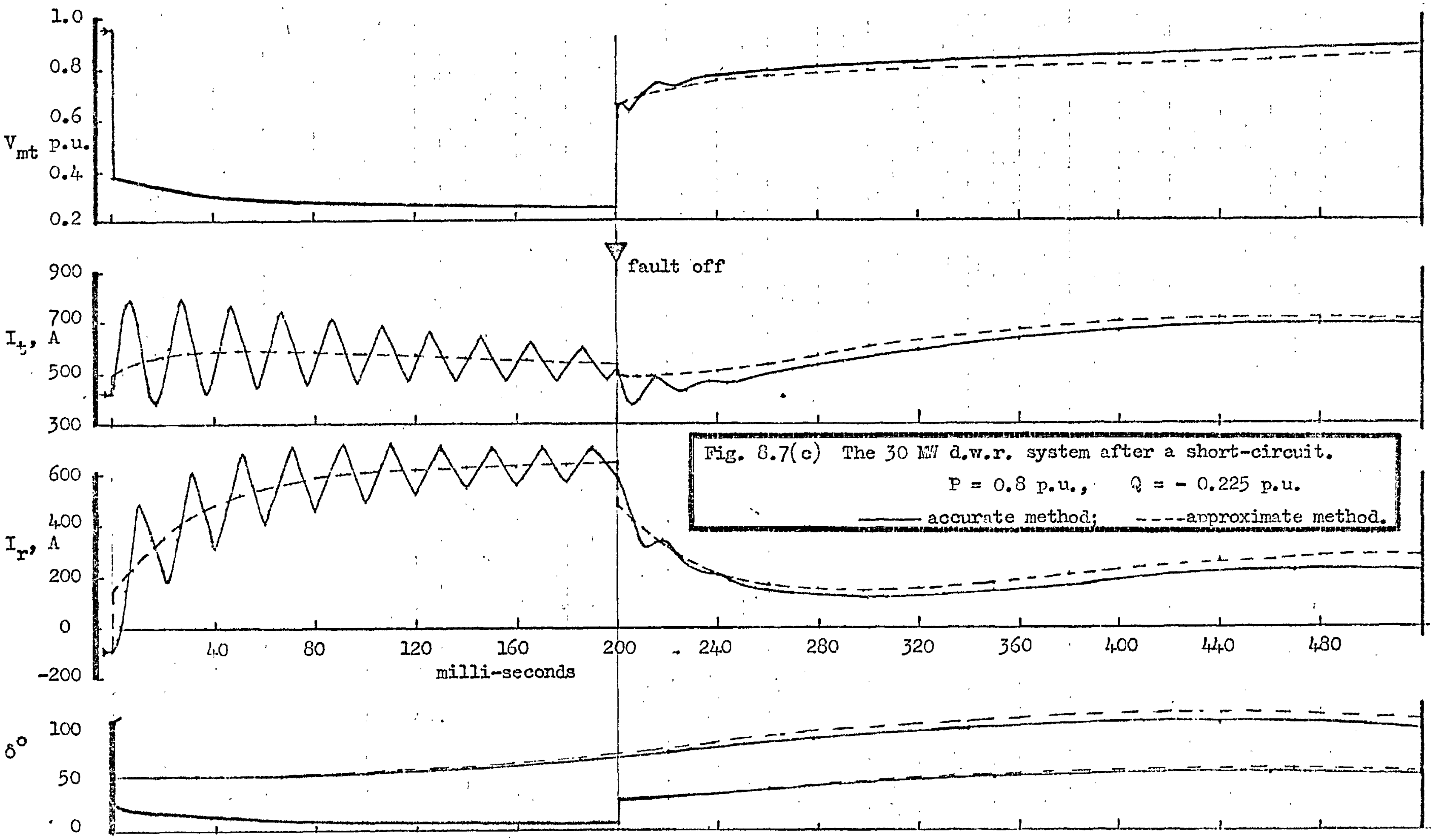

Fig. 8.7(c) The 30 MW d.w.r. system after a short-circuit.
P = 0.8 p.u., Q = - 0.225 p.u.
——— accurate method; - - - - approximate method.

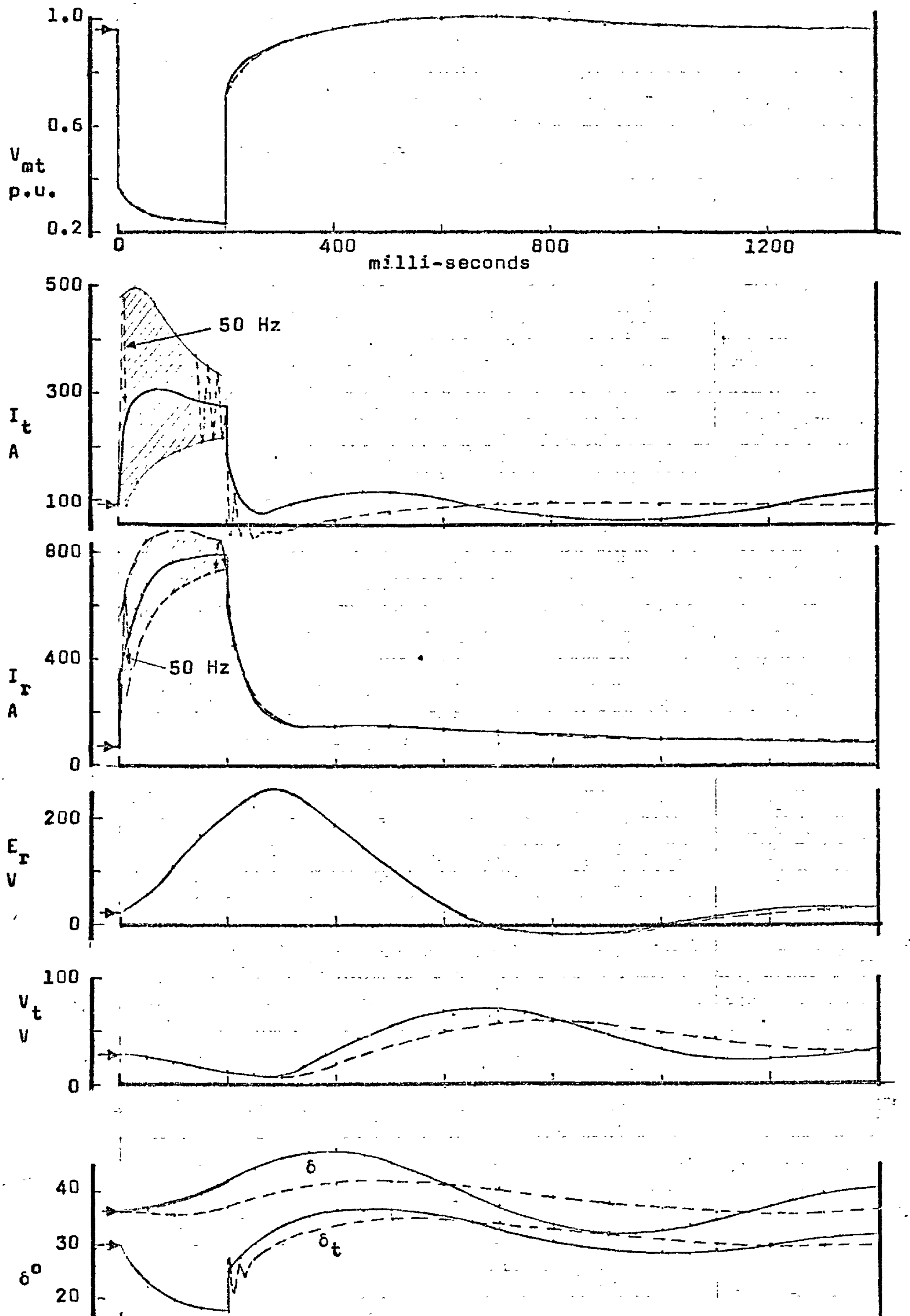

Fig. 8.8 The hypothetical 30 MW d.w.r. system after a three-phase short-circuit.

P = 0.2 p.u., Q = -0.225 p.u.
----accurate, ——approximate.

The torque winding quantities are ahead in time because the torque winding axis is ahead of the reactive winding axis (see Fig. 8.2), in the direction of rotation. During the fault the approximate method gives values of field current which agree very closely with the mean value of the field current envelope.

Figure 8.8 shows calculated curves similar to those of Fig. 8.7 but for the case of 0.2 p.u. active power. The initial conditions are listed in Table 8.3. The clear back swing for a lower active power confirms the earlier results of the c.w.r. system.

The results of this section show that the transient response of a d.w.r. system can be studied by replacing the two actual coils r, t by two fictitious coils fd, fq. It also shows that the discrepancies which arise between the accurate method and approximate method are similar to those of a c.w.r. system.

---oOo---

CHAPTER 9

9. STEADY-STATE STABILITY THEORY OF D.W.R. REGULATION

9.1 General

Reference 4 showed that the steady-state stability of an alternator can be improved by using a suitable feedback signal to control the excitation of a field winding on the q-axis when the excitation of the d-axis field winding is adjustable but unregulated. It also showed that the q-axis field controls the active power and the d-axis field controls the reactive power. The equations for a machine with a field winding on each axis were linearized for small disturbances and the Nyquist criterion was used to calculate stability limits which were verified by experimental results. Different feedback signals and regulators were used. The calculated results showed the effect of neglecting saturation and armature resistance.

This Chapter uses the field transformation equations of Sect. 8.2 in conjunction with the linearized equations in Ref. 4 to develop the open loop transfer function of a d.w.r. machine with a voltage regulator controlling the reactive winding excitation and an angle regulator controlling the torque winding excitation. The Nyquist criterion is used to study the steady state stability of such a d.w.r. system. However, as an intermediate stage the stability is investigated firstly for an angle regulator on the torque winding while the reactive winding excitation is adjustable but unregulated, and this is referred to as an "angle regulator only"; and secondly, a voltage regulator on the reactive winding while the torque winding excitation is adjustable but unregulated, and this is referred to as a "voltage regulator only". The angle feedback tries to keep the rotor at a fixed angle, referred to as the "reference angle" with reference to the infinite bus or the terminal voltage. The value of the "reference angle" can be changed by the angle regulator. Stability calculations are made to show the effect of different values of reference angle as well as different values of tie-line reactance. The combined operation of an angle- and a voltage regulator is then investigated with particular interest in the influence of the regulators upon one another.

The d.w.r. excitation control system shown in Fig. 9.1 can be represented by the block diagram for small oscillations in Fig.9.2. The input quantities in Fig. 9.2 are the torque and reactive winding excitation voltages and the transformed output quantities are terminal voltage v_{mt} and rotor angle δ_t. Feedback derived from v_{mt} and δ_t are used to regulate the excitation. For convenience v_{mt} is taken as the value after the rectifier conversion. The system in Fig. 9.2 can however be rearranged in a more suitable form as shown in Fig. 9.3 where the input quantities are v_{fd} and v_{fq} while the physical excitation voltages and field transformations are treated as part of the feedback loops.

9.2 System Equations

All quantities are expressed in per unit. The linearised system equations around the point of equilibrium give the operational relations, i.e., the transfer functions between the input and output quantities. Using such relations the multifeedbacks are reduced to an equivalent single loop configuration and the system is analysed with the aid of conventional control systems theory.

9.2.1 The machine equations

The principle assumptions in the mathematical development are: no saturation, sinusoidal airgap fluxes and no slot effects. Also, since the frequency of oscillations in the system is quite low, the frequency dependant terms $p\Psi_d$, $p\Psi_q$ and $p\delta$ in the armature voltage equations are justifiably neglected. For the purpose of the analyses and subsequent calculation, the external tie-line reactance X_c is lumped with the machine's armature leakage reactance and the modified alternator is studied. The input transformation equation (9.1) for small perturbations is obtained from the linearized machine equations, (see Appendix IV.).

$$\begin{bmatrix} G_d(p).\Delta v_{fd} \\ \Delta T_m \\ G_q(p).\Delta v_{fq} \end{bmatrix} = \Big[C(p)\Big] \begin{bmatrix} \Delta i_d \\ \Delta\delta \\ \Delta i_q \end{bmatrix} \tag{9.1}$$

and

$$\Big[C(p)\Big] = \begin{bmatrix} -X_d(p) & v_{bdo} & r_a \\ -\frac{1}{2}v_{bdo} + r_a i_{do} & -(Q_o + Jp^2) & -\frac{1}{2}v_{bqo} + r_a i_{qo} \\ -r_a & v_{bqo} & -X_q(p) \end{bmatrix} \tag{9.2}$$

where the suffix o denotes the steady state conditions, and

$$Q_o = V_{bdo}I_{qo} - V_{bqo}I_{do} \tag{9.3}$$

which is the reactive power at the infinite bus.

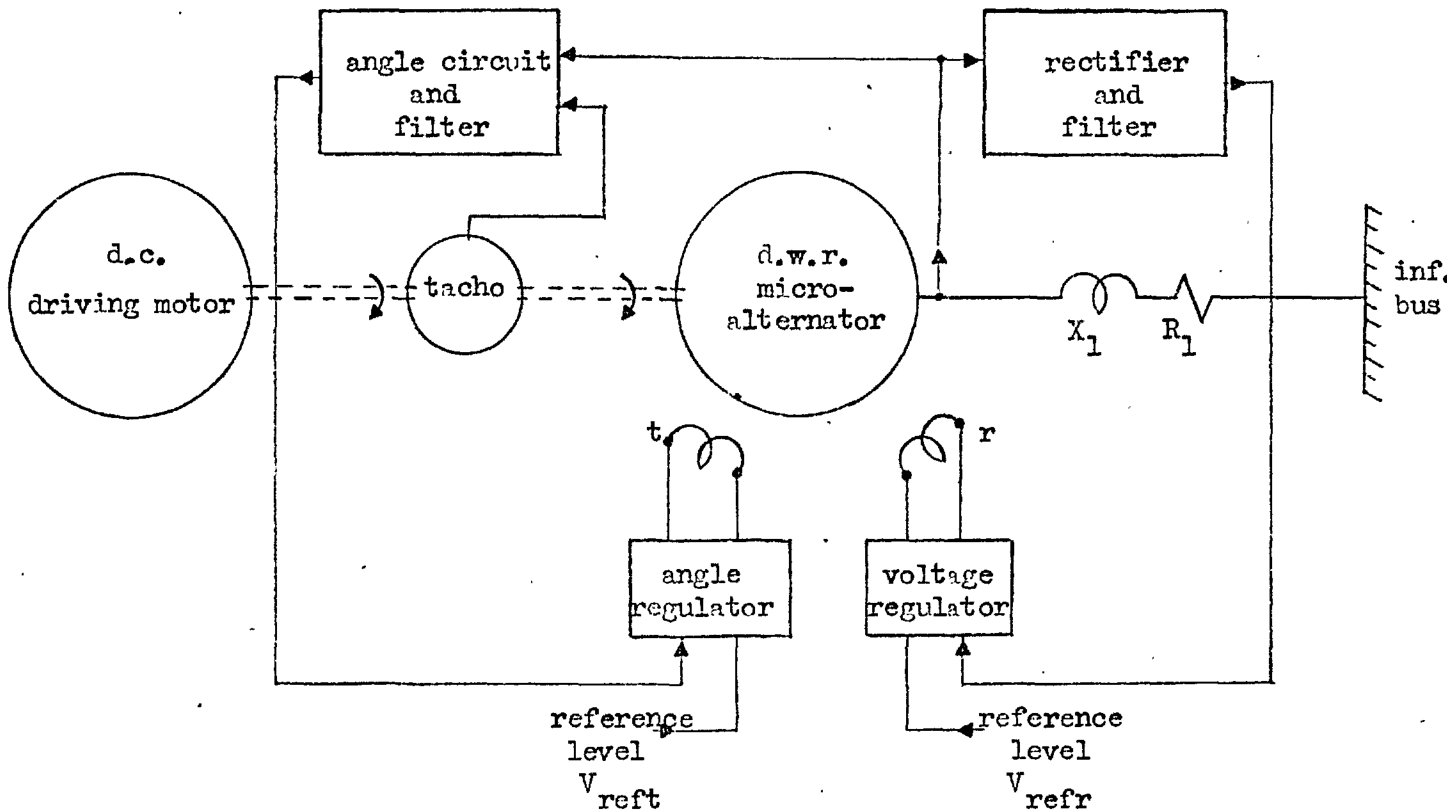

Fig. 9.1 Schematic diagram of d.w.r. micro-machine system.

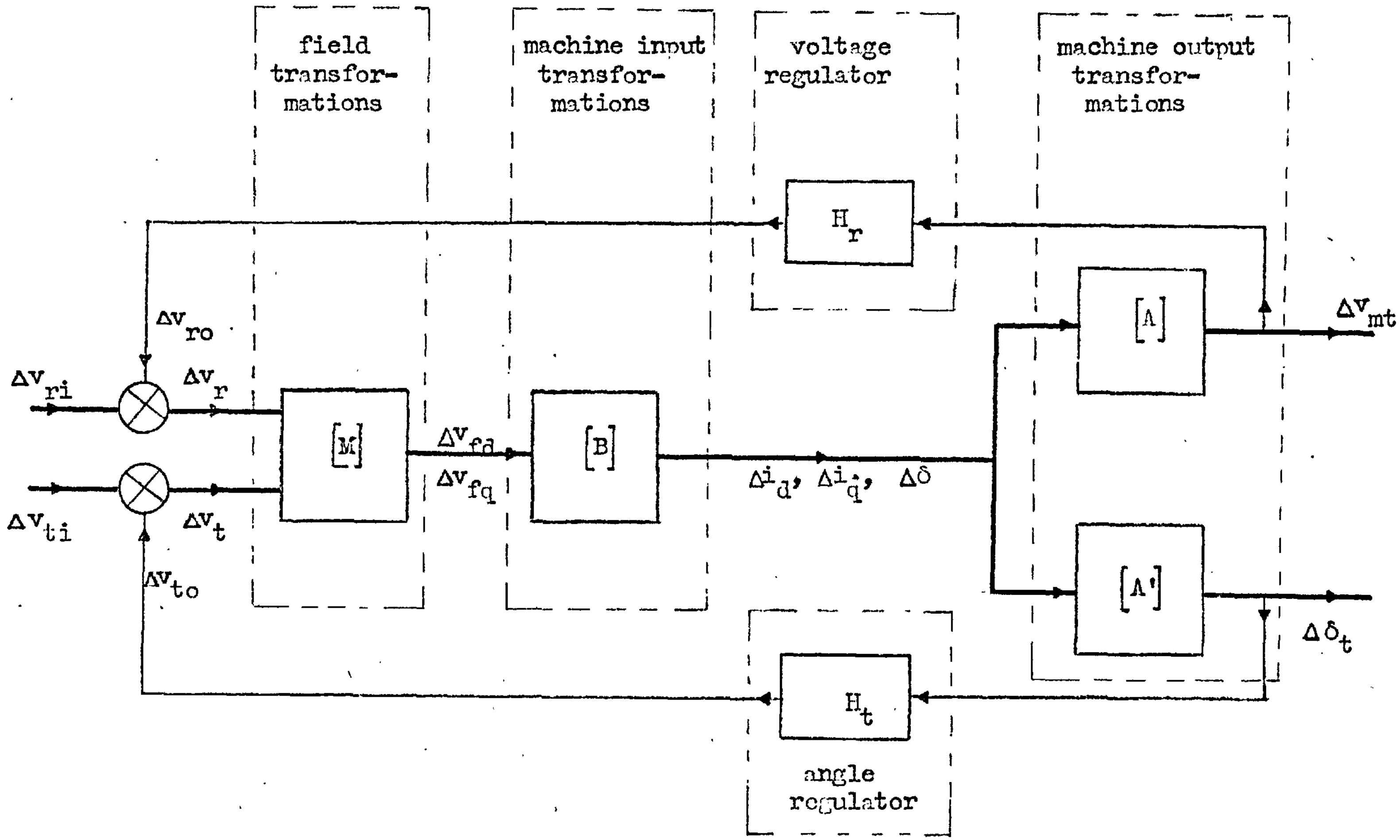

Fig. 9.2 Single line block diagram for divided winding excitation control.

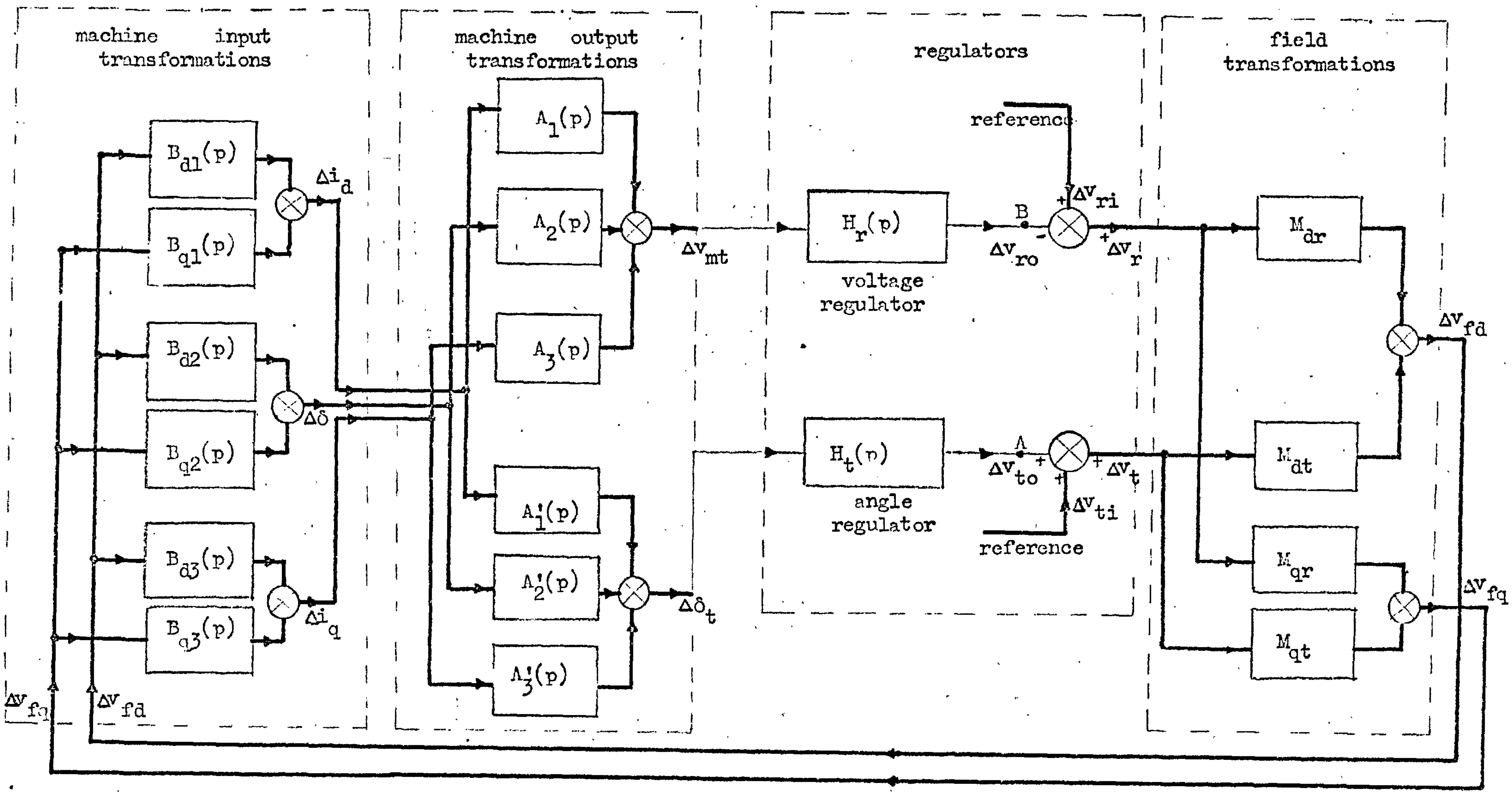

Fig. 9.3 Rearranged block diagram of divided winding excitation control.

There are three basic output quantities Δi_d, $\Delta\delta$ and Δi_q and in general, three input quantities Δv_{fd}, ΔT_m and Δv_{fq}. Inversion of the matrix (9.2) gives operational relations from Eqn. (9.1) between the output and the input quantities as

$$\begin{bmatrix} \Delta i_d \\ \Delta\delta \\ \Delta i_q \end{bmatrix} = \begin{bmatrix} B_{d1}(p) & B_{t1}(p) & B_{q1}(p) \\ B_{d2}(p) & B_{t2}(p) & B_{q2}(p) \\ B_{d3}(p) & B_{t3}(p) & B_{q3}(p) \end{bmatrix} \begin{bmatrix} \Delta v_{fd} \\ \Delta T_m \\ \Delta v_{fq} \end{bmatrix} = \left[B(p)\right] \begin{bmatrix} \Delta v_{fd} \\ \Delta T_m \\ \Delta v_{fq} \end{bmatrix} \quad (9.4)$$

where

$$\left[B(p)\right] = \left[C(p)\right]^{-1} \begin{bmatrix} G_d(p) & 0 & 0 \\ 0 & 1 & 0 \\ 0 & 0 & G_q(p) \end{bmatrix} \quad (9.5)$$

The elements of the input transformation matrix (9.5) are given by the following expressions

$$B_{d1}(p) = (X_q(p)(Q_o + Jp^2) + V_{bqo}^2 - 2r_a V_{bqo} I_{qo}) G_d(p)/D(p)$$

$$B_{d2}(p) = (-X_q(p)V_{bdo} + r_a(2X_q(p)I_{do} - V_{bqo}) + r_a^2\, 2I_{qo})\, G_d(p)/D(p)\sqrt{2}$$

$$B_{d3}(p) = (V_{bdo}V_{bqo} - r_a(2V_{bqo}I_{do} + Q_o + Jp^2))G_d(p)/D(p)$$

$$B_{t1}(p) = (X_q(p)V_{bdo} - r_a V_{bqo})/\sqrt{2}D(p)$$

$$B_{t2}(p) = (X_d(p)X_q(p) + r_a^2)/D(p)$$

$$B_{t3}(p) = (-X_d(p)V_{bqo} - r_a V_{bdo})/\sqrt{2}D(p)$$

$$B_{q1}(p) = (V_{bdo}V_{bqo} + r_a(Q_o + Jp^2 - 2V_{bdo}I_{qo}))G_q(p)/D(p)$$

$$B_{q2}(p) = (X_d(p)V_{bqo} - r_a(2X_d(p)I_{qo} + V_{bdo}) + r_a^2\, 2I_{do})G_q(p)/D(p)\sqrt{2}$$

$$B_{q3}(p) = (X_d(p)(Q_o + Jp^2) + V_{bdo}^2 - 2r_a V_{bdo} I_{do})G_q(p)/D(p)$$

(9.6)

where

$$D(p) = -X_d(p)X_q(p)\Big[Q_o + Jp^2 + V_{bqo}^2 Y_q(p) + V_{bdo}^2 Y_d(p)$$
$$- 2r_a(V_{bqo}I_{qo}Y_q(p) + V_{bdo}I_{do}Y_d(p))$$
$$- r_a^2(V_{bdo}I_{qo} - V_{bqo}I_{do} - Jp^2)Y_d(p)Y_q(p)\Big]$$
$$= X_d(p)X_q(p)D'(p) \tag{9.7}$$

while $G_d(p)$ and $G_q(p)$ are given by Eqns. (8.27) and (8.28)

If it is assumed that T_m is constant, the general input transformation equation (9.4) reduces to

$$\begin{bmatrix} \Delta i_d \\ \Delta\delta \\ \Delta i_q \end{bmatrix} = \begin{bmatrix} B_{d1} & B_{q1} \\ B_{d2} & B_{q2} \\ B_{d3} & B_{q3} \end{bmatrix} \begin{bmatrix} \Delta v_{fd} \\ \Delta v_{fq} \end{bmatrix} \tag{9.8}$$

which is the input transformation relation for the system in Fig.9.3.

9.2.2 Expressions for the feedback quantities

The feedback signals or transformed output quantities are definite functions of the three basic alternator output quantities. The small changes of terminal voltage and rotor angle are related to the basic output quantities as follows

$$\Delta v_{mt} = A_1(p).\Delta i_d + A_2(p).\Delta\delta + A_3(p).\Delta i_q \tag{9.9}$$

$$\Delta\delta_t = A_1'(p).\Delta i_d + A_2'(p).\Delta\delta + A_3'(p).\Delta i_q \tag{9.10}$$

The following expressions for $A(p)$ are the same as for a c.w.r system with voltage feedback because they are not affected by the angle feedback signal in the d.w.r. system;

$$\left.\begin{aligned} A_1(p) &= (I_{do}X_c - V_{bqo})X_cR_e/V_{mto} \\ A_2(p) &= -\sqrt{2}P_oX_cR_e/V_{mto} \\ A_3(p) &= -(V_{bdo} + I_{qo}X_c)X_cR_e/V_{mto} \end{aligned}\right) \tag{9.11}$$

The expressions of A'(p) derived in Appendix V, are

$$\left.\begin{aligned} A_1'(p) &= \frac{-X_cV_{mtdo}}{\sqrt{2}\,V_{mto}^2} \\ A_2'(p) &= \frac{V_{bqo}V_{mtqo} + V_{bdo}V_{mtdo}}{V_{mto}^2} = \frac{V_b^2 + Q_oX_c}{V_{mto}^2} \\ A_3'(p) &= \frac{X_cV_{mtqo}}{\sqrt{2}\,V_{mto}^2} \end{aligned}\right) \tag{9.12}$$

In these equations

$$\left.\begin{aligned} P_o &= V_{mdo}I_{do} + V_{bqo}I_{qo} \\ V_{mtdo} &= V_{bdo} + I_{qo}X_c \\ V_{mtqo} &= V_{bqo} - I_{do}X_c \\ V_{bdo} &= V_b\sin\delta_o \\ V_{bqo} &= V_b\cos\delta_o \\ R_e &= \text{rectifier constant.} \end{aligned}\right) \tag{9.13}$$

The values of Δv_{fd} and Δv_{fq} in Eqn. (9.8) are found from the voltages Δv_r and Δv_t and the field voltage transformation (8.9) as

$$\begin{bmatrix} \Delta v_{fd} \\ \Delta v_{fq} \end{bmatrix} = \begin{bmatrix} M_{dt} & M_{dr} \\ M_{qt} & M_{qr} \end{bmatrix} \begin{bmatrix} \Delta v_t \\ \Delta v_r \end{bmatrix} \tag{9.14}$$

where

$$\left.\begin{aligned} M_{dt} &= \frac{\sin \phi_r}{\lambda N} \\ M_{dr} &= \frac{\sin \phi_t}{\lambda N} \\ M_{qt} &= \frac{-\cos \phi_r}{\lambda} \\ M_{qr} &= \frac{\cos \phi_t}{\lambda N} \end{aligned}\right) \qquad (9.15)$$

From Eqns. (9.8),(9.9),(9.10) and (9.14), it can be shown that if the armature and tie-line resistances are neglected,

$$\begin{bmatrix} \Delta v_{mt} \\ \Delta \delta_t \end{bmatrix} = \begin{bmatrix} E_{11}(p) & E_{12}(p) \\ E_{21}(p) & E_{22}(p) \end{bmatrix} \begin{bmatrix} \Delta v_r \\ \Delta v_t \end{bmatrix} \qquad (9.16)$$

where

$$\begin{aligned} E_{11}(p) &= M_{dr} \sum_{n=1}^{3} A_n(p) B_{dn}(p) + M_{qr} \sum_{n=1}^{3} A_n(p) B_{qn}(p) \\ &= \frac{R_e X_c}{V_{mto} D(p)} \Bigg[\Big[-((Q_o + 3p^2) X_q(p) + V_{bqo}^2) V_{mtqo} \\ &\quad + P_o V_{bdo} X_q(p) - V_{bdo} V_{bqo} V_{mtdo} \Big] G_d(p) M_{dr} \\ &\quad + \Big[(- V_{bqo} V_{bdo} V_{mtqo} - P_o V_{bqo} X_d(p) \\ &\quad - V_{mtdo}((Q_o + 3p^2) X_d(p) + V_{bdo}) \Big] \; G_q(p) M_{qr} \Bigg] \end{aligned} \qquad (9.17)$$

$$E_{12}(p) = M_{dt} \sum_{n=1}^{3} A_n(p) B_{dn}(p) + M_{qt} \sum_{n=1}^{3} A_n(p) B_{qn}(p) \qquad (9.18)$$

$$E_{21}(p) = M_{dr} \sum_{n=1}^{3} A_n'(p)B_{dn}(p) + M_{qr} \sum_{n=1}^{3} A_n'(p)B_{qn}(p)$$

$$= \frac{X_c}{\sqrt{2}V_{mto}^2 D(p)} \Bigg[\Big[(-(Q_o + Jp^2)X_q(p) + V_{bqo}^2)V_{mtdo}$$

$$- V_{bdo}X_q(p)(Q_o + \frac{V_b^2}{X_c})$$

$$+ V_{bdo}V_{bqo}V_{mtqo}\Big] G_d(p)M_{dr}$$

$$+ \Big[- V_{bdo}V_{bqo}V_{mtdo} + V_{bqo}X_d(p)(Q_o + \frac{V_b^2}{X_c})$$

$$+ ((Q_o + Jp^2)X_d(p) + V_{bdo}^2)V_{mtqo} \Big] G_q(p)M \Bigg] \tag{9.19}$$

$$E_{22}(p) = M_{dt} \sum_{n=1}^{3} A_n'(p)B_{dn}(p) + M_{qt} \sum_{n=1}^{3} A_n'(p)B_{qn}(p) \tag{9.20}$$

The two regulator output voltages are

$$\left.\begin{aligned} \Delta v_{ro} &= H_r(p) . \Delta v_{mt} \\ \Delta v_{to} &= H_t(p) . \Delta \delta_t \end{aligned}\right) \tag{9.21}$$

which can be combined with equation (9.16) to show that

$$\begin{bmatrix} \Delta v_{ro} \\ \Delta v_{to} \end{bmatrix} = \begin{bmatrix} H_r(p)E_{11}(p) & H_r(p)E_{12}(p) \\ H_t(p)E_{21}(p) & H_t(p)E_{22}(p) \end{bmatrix} \begin{bmatrix} \Delta v_r \\ \Delta v_t \end{bmatrix} \tag{9.22}$$

which can be used to find the stable operating region of the system in Fig. 9.3.

During the rest of this chapter it is assumed that the armature and tie-line resistance effect can be neglected.

9.2.3 The open-loop transfer function

The stability of the d.w.r. system in Fig. 9.3 can be studied by means of the Nyquist criterion when one of the feedback-loops is regarded as open while the other is left closed and regarded as part of the forward-loop. During steady-state operation at the point of equilibrium the reference voltages v_{ti} and v_{ri} do not change, so that

$$\Delta v_{ti} = \Delta v_{ri} = 0$$

If the angle feedback-loop is considered open at 'A' (see Fig. 9.3) while the voltage feedback-loop remains closed, then

$$\Delta v_{ro} = - \Delta v_r \tag{9.23}$$

and if this value for Δv_{ro} is replaced in Eqn. (9.22), it is found that

$$\Delta v_r = - \frac{E_{12}(p)H_r(p)}{1 + E_{11}(p)H_r(p)} \cdot \Delta v_t \tag{9.24}$$

Hence the open-loop transfer function is

$$\frac{\Delta v_{to}}{\Delta v_t} = F_t(p) = H_t(p) \left[E_{22}(p) - \frac{E_{21}(p)E_{12}(p)H_r(p)}{1 + E_{11}(p)H_r(p)} \right] \tag{9.25}$$

Similarly, the voltage feedback loop can be considered open at 'B' (see Fig. 9.3) while the angle feedback loop remains closed.

Now $\Delta v_{to} = \Delta v_t$ and

$$\frac{\Delta v_{ro}}{\Delta v_r} = F_r(p) = H_r(p) \left[E_{11}(p) + \frac{E_{21}(p)E_{12}(p)H_t(p)}{1 - E_{22}(p)H_t(p)} \right] \tag{9.26}$$

The regulator transfer functions are

$$\left.\begin{aligned} H_r(p) &= K_r \cdot \text{(a ratio of polynomials in p)} \\ H_t(p) &= K_t \cdot \text{(a ratio of polynomials in p)} \end{aligned}\right\} \qquad (9.27)$$

where K_r is the voltage regulator gain and K_t is the angle regulator gain (see Figs.10.9 and 10.10).

9.3 The Equilibrium Diagrams

For any possible operating condition, that is, any point on the active-power/reactive-power chart (P - Q chart) in Fig. 9.11 , a phasor diagram, referred to as an 'equilibrium diagram', can be drawn, but the system may or may not be stable. The distinction between equilibrium and stability is important in any control system. The phasor diagram tells nothing about the stability, which must be determined by one of the stability criteria of control-system theory. If, however, the system is in fact stable, the equilibrium diagram is useful in indicating relations between variables as the operating condition changes.

Figure 9.4(a) is the conventional phasor diagram for a c.w.r. generator operating at a lagging power factor, with excitation on the direct axis. For equilibrium, the rotor angle δ must be such that the diagram can close, and δ therefore varies as the current phasor changes. With fixed excitation, the system becomes unstable if δ exceeds about 90^o, but phasor diagrams can still be drawn for larger angles, and stability can often be maintained by using an appropriate regulator.

Figure 9.4(b) shows the phasor diagram for the same operating condition when the machine has a torque winding control which holds δ

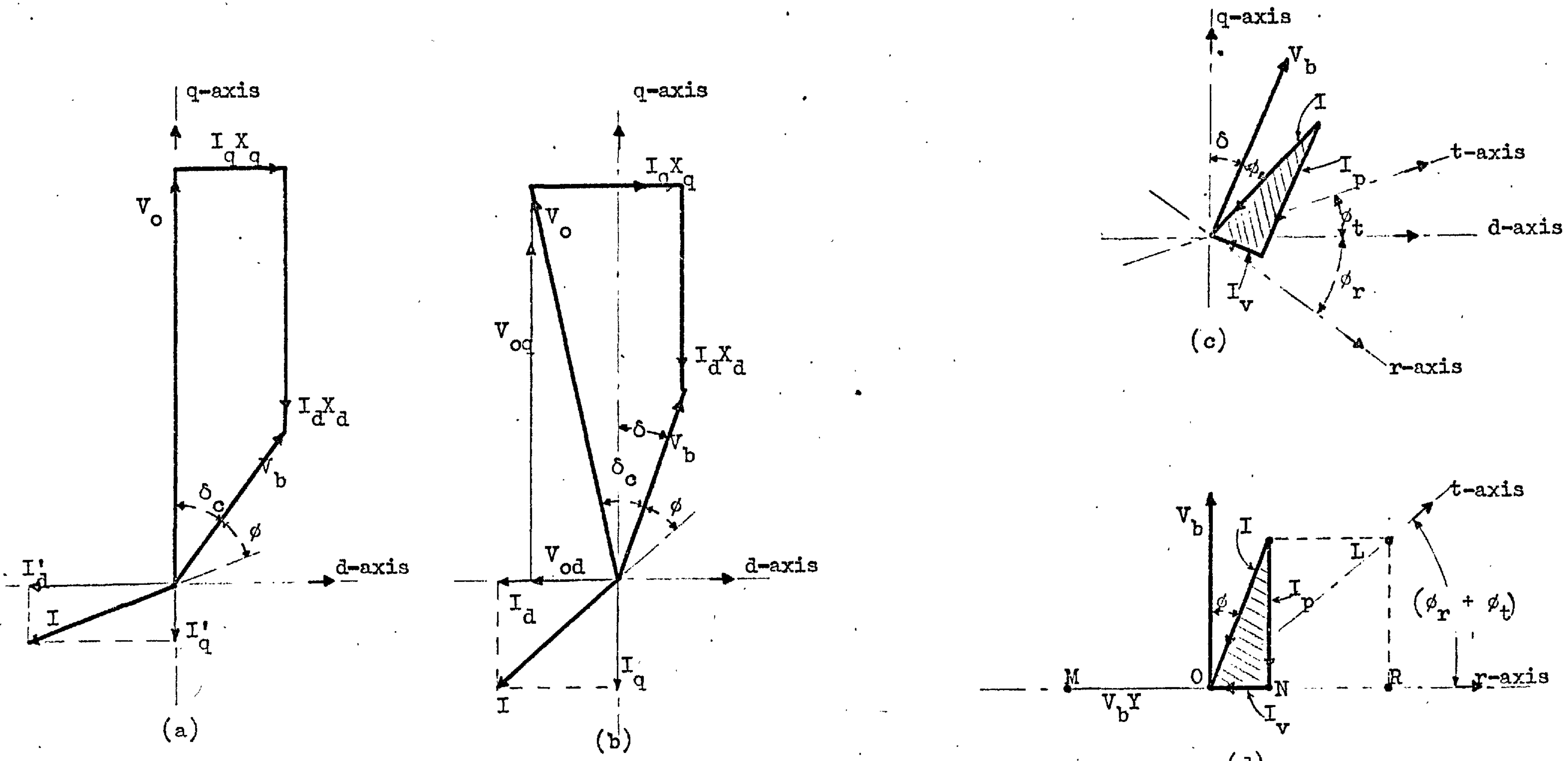

Fig. 9.4 Lagging current condition with bus angle control,
(a) Axis diagram of normal machine (conventional machine)
(b) Axis diagram of d.w.r. machine with angle control on torque winding.
(c),(d) Armature-current phasor diagram.

at a constant value with reference to the infinite bus voltage. Figure 9.4(c) shows the resultant armature current I, the power component I_p in phase with V_b, and the reactive component I_v at right angles to V_b.

From Fig. 9.4(b)

$$V_{od} = V_b \sin\delta - I_q X_q \tag{9.28}$$

$$V_{oq} = V_b \cos\delta + I_d X_d \tag{9.29}$$

where X_d and X_q include the tie-line reactance.

The voltage V_o in a d.w.r. machine, consists of two components, namely V_{oq} which depends on the fictitious direct-axis field current I_{fd}, and V_{od} which depends on the fictitious quadrature axis field current I_{fq}, as follows:

$$V_{oq} = \frac{X_{md}}{\sqrt{2}} I_{fd}$$

$$V_{od} = \frac{X_{mq}}{\sqrt{2}} I_{fq}$$

The field transformation Eqn. (8.5) is used to find that V_{od} and V_{oq} depend on the physical field currents as follows:

$$V_{oq} = \frac{X_{md}}{\sqrt{2}} (I_t \cos\phi_t + N I_r \cos\phi_r) \tag{9.30}$$

$$V_{od} = \frac{X_{mq}}{\sqrt{2}} (I_t \sin\phi_t + N I_r \sin\phi_r) \tag{9.31}$$

If armature and tie-line losses are neglected, the machine's electrical torque is equal to the power P_o at the infinite bus.

Now

$$P_o = V_b I_p$$

and $Q_o = V_b I_v$

also $$I_p = I_d \sin\delta + I_q \cos\delta \tag{9.32}$$

$$-I_v = -I_d \cos\delta + I_q \sin\delta \tag{9.33}$$

The expressions for $I_d\sin\delta$, $I_d\cos\delta$, $I_q\sin\delta$ and $I_q\cos\delta$, in terms of the actual field currents can be found from Eqns. (9.28) to (9.31) and substituted in Eqns. (9.32) and (9.33) to show that

$$I_p = I_t(K_d\sin\delta\cos\phi_t + K_q\cos\delta\sin\phi_t) + NI_r(K_d\sin\delta\cos\phi_r - K_q\cos\delta\sin\phi_r) - \frac{V_b}{2}\sin 2\delta(Y_d - Y_q) \tag{9.34}$$

and $$I_v = -I_t(K_q\sin\delta\sin\phi_t - K_d\cos\delta\cos\phi_t) + NI_r(K_q\sin\delta\sin\phi_r + K_d\cos\delta\cos\phi_r) - V_b(Y_q\sin^2\delta + Y_d\cos^2\delta) \tag{9.35}$$

where

$$K_d = \frac{X_{md}}{\sqrt{2}X_d}$$

$$K_q = \frac{X_{mq}}{\sqrt{2}X_q}$$

Assuming that δ is held constant at a reference value equal to the angle ϕ_r between the r-winding and the d-axis, and that the machine has zero saliency, so that $K_d = K_q = K$, and $Y_d = Y_q = Y$, Eqns. (9.34) and (9.35) become

$$I_p = I_t K \sin(\phi_r + \phi_t) \tag{9.36}$$

$$I_v = KI_t\cos(\phi_r + \phi_t) + NKI_r - V_b Y \tag{9.37}$$

Hence, the active power $P_o = V_b I_p$ is controlled only by the current I_t in the 'torque winding', while the reactive power $Q_o = - V_b I_v$ is controlled by both field currents. With zero excitation in both field windings $Q_o = - V_b^2 Y$. These results are only obtained because there is an independent control holding δ equal to $\emptyset_r$ and also because there is zero saliency

Fig. 9.4(d) shows the relationship between field currents and the components of armature current. Now

$$LR = I_p,$$

$$OL = KI_t,$$

$$OR = I_t \sin(\emptyset_r + \emptyset_t) ,$$

$$MN = K(I_r N + I_t \sin(\emptyset_r + \emptyset_t)).$$

At any operating condition therefore,

$$KI_t = OL$$

$$NKI_r = MN - OR.$$

The conditions are somewhat modified when the generator angle δ_t is used as a feedback signal, since δ is not held exactly equal to the reference value $\emptyset_r$, although it is still approximately true that only the torque winding controls the active power.

9.4 Steady-state Stability of a D.W.R. Micro-machine

The stability of the d.w.r. micro-machine system in Fig. 9.3 (see also Fig. 10.1) is studied by applying Nyquist's criterion to the open-loop frequency response to determine the stability of the closed-loop. The closed-loop system is stable if its open-loop response locus encloses the (-1,0) point in the complex plane counter clockwise a number of times equal to the unstable poles of the open-loop transfer function.

The open-loop response locus depends on the gains of the two regulators and on the steady state operating condition determined by the machine terminal voltage. Eqn. (9.25) can be used to find the limiting K_t for a given value of K_r, active power P_o and reactive power Q_o, and curves relating K_t to Q_o at the stability limit can be obtained for different values of P_o and K_r. Eqn. (9.26) can likewise be used to find the limiting K_r for a given value of K_t and similar sets of stability limit curves are obtained. However, the two groups of curves give the same information and for the purpose of this thesis it was decided to use Eqn. (9.25).

The micro machine has two idendical field windings r and t, and

$$N_t = N_r \quad ; \quad N = 1;$$

$$\phi_t = \phi_r = \phi \quad ; \quad \lambda = 2\sin\phi\cos\phi;$$

so that the elements in the voltage transformation matrix (9.14) reduce to

$$\left.\begin{aligned} M_{dt} = M_{dr} &= \frac{1}{2\cos\phi} \\ -M_{qt} = M_{qr} &= \frac{1}{2\sin\phi} \end{aligned}\right\} \qquad (9.38)$$

This section is devoted to a steady-state stability study of the following combinations of regulators and some useful analytical expressions are derived where possible:

1. A proportionate bus "angle regulator only". Computations are made to show that the maximum negative reactive absorption dependson the value of the "reference angle" (see Sect. 9.1).

2. A proportionate terminal angle regulator only. Computations are made, as in (1) above, to show the effect of different values for the reference angle, and also that the stability limit is least sensitive to changes in P_o when the reference angle is equal to the angle ϕ_r.

3. A proportionate "voltage regulator only" to show that, although the torque winding has a fixed excitation, the system is controlled in the same way as a voltage regulator controls a c.w.r. machine.

4. A proportionate angle regulator and a proportionate voltage regulator.

5. A derivative angle regulator, with proportionate terms plus first- and second derivative terms, and a proportionate voltage regulator. The importance of time delays in the regulators are examined.

9.4.1 Proportionate bus angle regulator only

Consider the case of the divided winding control system in Fig. 9.2 with the torque winding excitation regulated by a bus angle signal while the reactive winding excitation is adjustable but unregulated, i.e., bus "angle feedback only" (see Sect.9.1). The voltage regulator transfer function $H_r(p)$ is zero and

$$\left.\begin{aligned} A_1'(p) &= 0 \\ A_2'(p) &= 1 \\ A_3'(p) &= 0 \end{aligned}\right) \qquad (9.39)$$

Hence, the transfer function becomes

$$F_t(p) = \frac{(-X_q(p)V_{bdo}G_d(p)M_{dt} + X_d(p)V_{bqo}G_q(p)M_{qt})H_t(p)}{-X_d(p)X_q(p)\left[Q_o + Jp^2 + V_{bqo}^2Y_q(p) + V_{bdo}^2Y_d(p)\right]} \tag{9.40}$$

$$= \frac{-V_{bdo}M_{dt}X_{md}Y_d(1 + pT_{kd})H_t(p)}{\sqrt{2}r_{fd}(1 + pT_d')D'(p)}$$

$$+ \frac{V_{bqo}M_{qt}X_{mq}Y_q(1 + pT_{kq})H_t(p)}{\sqrt{2}r_{fq}(1 + pT_q')(1 + pT_q'')D'(p)} \tag{9.41}$$

For a given value of Q_o the transfer function given by Eqn.(9.40) does not contain the active power P_o, hence the same result is obtained at any power level.

A Nyquist plot of $F_t(jw)$ where w is the small oscillation frequency, is used to determine the maximum and minimum stable values of the gain K_t as a function of Q_o. The value of $K_{t\ min}$ required to stabilize the otherwise unstable system is given when the zero frequency point of $F_t(jw)$ crosses the (0, -1) point in the complex plane.

Therefore, Q_o at $K_{t\ min}$ can be obtained from Eqn. (9.41) by putting

$$p = jw = 0$$

and $\mathrm{Real}(F_t(0)) = -1$

So that

$$Q_o = \left[\frac{X_{mq}Y_qM_{qt}V_{bqo}}{\sqrt{2}\ r_{fq}} - \frac{X_{md}Y_dV_{bdo}M_{dt}}{\sqrt{2}\ r_{fd}}\right] K_{t\ min}$$

$$- V_{bqo}^2Y_q - V_{bdo}^2Y_d \tag{9.42}$$

or

$$K_{t\,min} = \frac{\sqrt{2}\,(Q_o + V_{bqo}^2 Y_q + V_{bdo}^2 Y_d)}{\dfrac{X_{mq} Y_q V_{bqo} M_{qt}}{r_{fq}} - \dfrac{X_{md} Y_d V_{bdo} M_{dt}}{r_{fd}}} \tag{9.43}$$

Thus the minimum gain is proportional to the amount by which the reactive compensation $(-Q_o)$ exceeds $-(V_{bqo}^2 Y_q + V_{bdo}^2 Y_d)$

The maximum gain $K_{t\,max}$ is reached when the Nyquist locus of $F_t(j\omega)$ reaches the (0,-1) point. To satisfy this condition the imaginary part of $F_t(j\omega)$ must be zero and the real part equal to -1. Equating the imaginary part to zero also yields the natural mode of oscillation at a frequency ω_n. However, the expression containing ω_n is of sixth order and is cumbersome to solve.

Eqn. (9.42) shows that the relation between Q_o and $K_{t\,min}$ depends on V_{bdo} and V_{bqo} which are functions of the reference angle δ. Results of calculations to find the value of δ for maximum negative reactive absorption, are given in the rest of this section. It is seen that this value does not equal ϕ_r (see Sect. 9.3) and that the reactive winding current affects the active power.

9.4.1.1 Bus angle δ held at 33.75^o

If the "reference angle" is chosen as 33.75^o it means that the axis of the r winding coincides with the resultant air-gap M.M.F. The M.M.F. determines the flux and hence corresponds to the infinite bus voltage if leakage reactance and tie-line impedance are neglected (see Figs. 9.7(a) and 9.4(d)).

The numerical values of the system parameters are substituted in Eqn. (9.40) and the Nyquist loci of $F_t(j\omega)$ are calculated by a digital computer. The values of $K_{t\ min}$ and $K_{t\ max}$ are obtained for various values of Q_o and Fig. 9.5 shows the stability limit curves for the system described by Eqn. (9.40).

The region AB is defined by $K_{t\ min}$ in Eqn. (9.43) and corresponds to the zero frequency point on the Nyquist plot. The region BC for the ideal angle device and no damping is defined by $K_{t\ max}$, obtained when $F_t(j\omega_n)$ goes through the (0, 1) point on the Nyquist plot. If a linear scale was used for K_t the region AB would be a straight line. For $K_t < K_{t\ min}$, instability is of the drifting type because it is associated with zero frequency; whereas at a gain $K_t > K_{t\ max}$, instability is oscillatory with a natural frequency ω_n.

When the practical angle device with filter time delays is considered as part of the transfer function, the high gain limiting curve BC without damping in Fig. 9.5, is shifted to DC because the delays add to the total system phase shift and at a particular frequency the gain margin is reduced.

The curve DE was calculated with damping while FG allows for an external time delay τ_t of 0.5 seconds (see Sect. 10.4.1).

9.4.1.2 Bus angle δ held at 0^o

If the "reference angle" is chosen so that the d-axis (the mid-point between r and t windings) coincides with the resultant air-gap M.M.F., (see Fig. 9.7(b)), then $\delta = 0$, $V_{bdo} = 0$, and $V_{bqo} = V_b$. Under these conditions for the ideal angle device, Eqn. (9.43) becomes

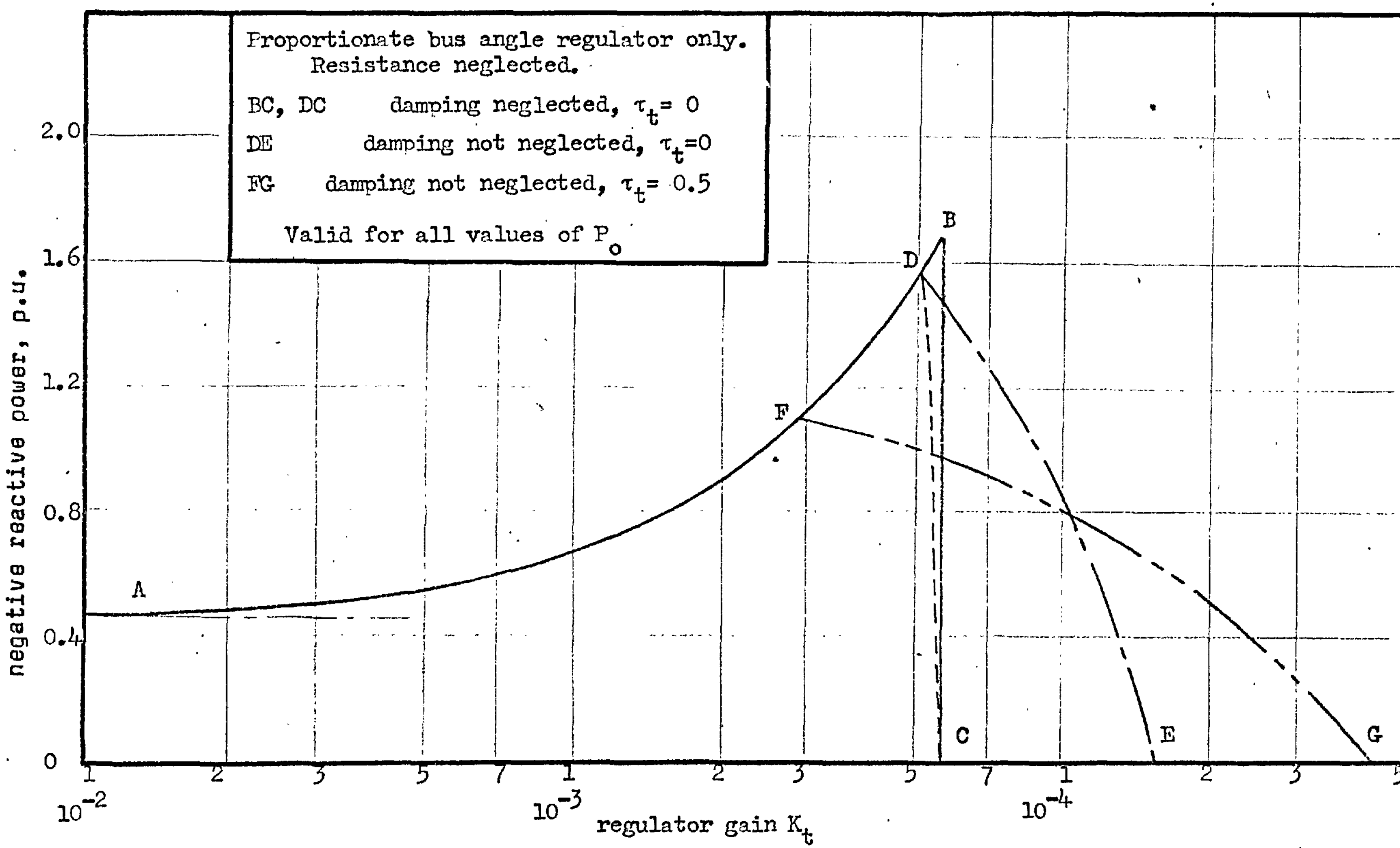

Fig. 9.5 Steady-state stability limit curves.

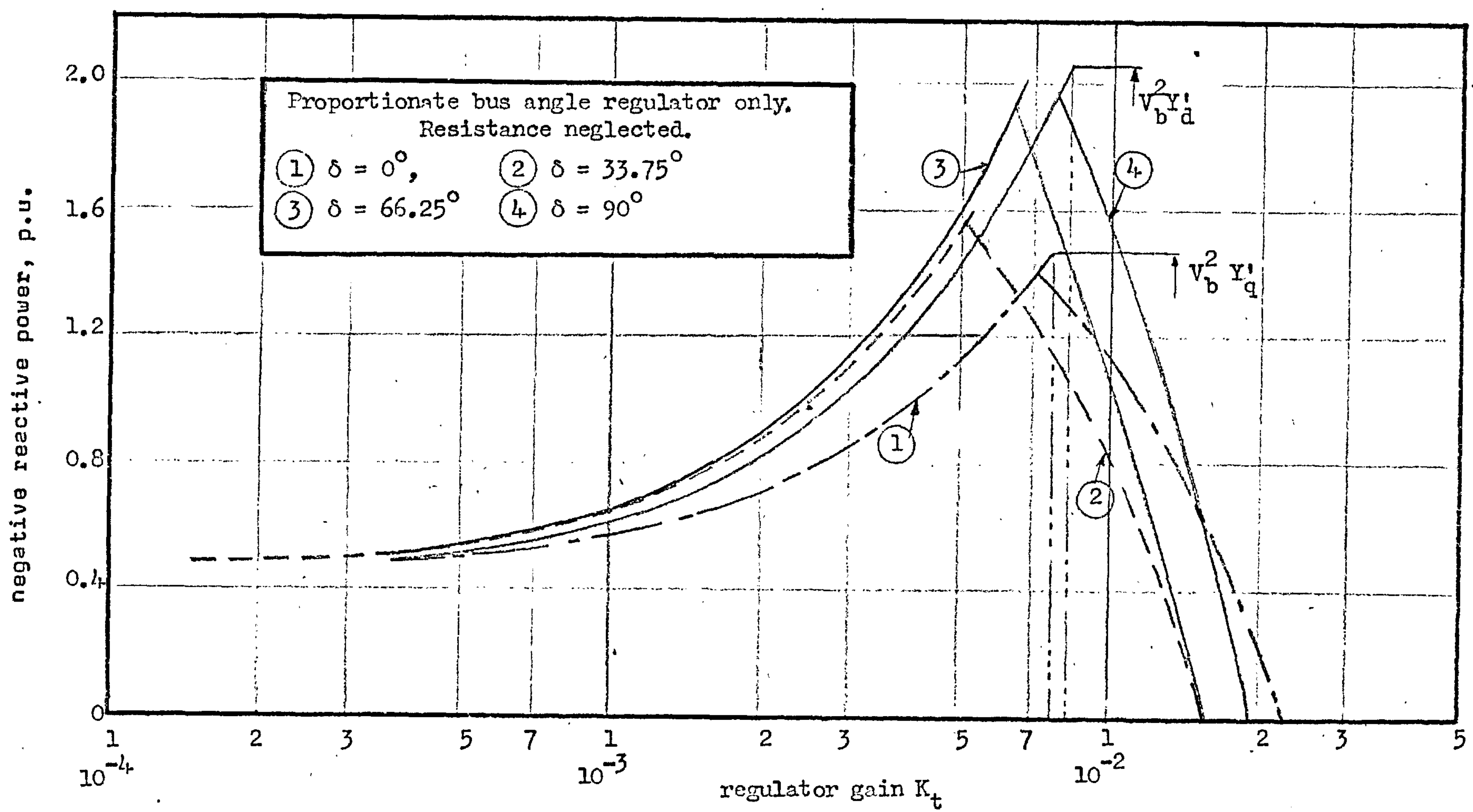

Fig. 9.6 Steady-state stability limit curves for various control angles δ.

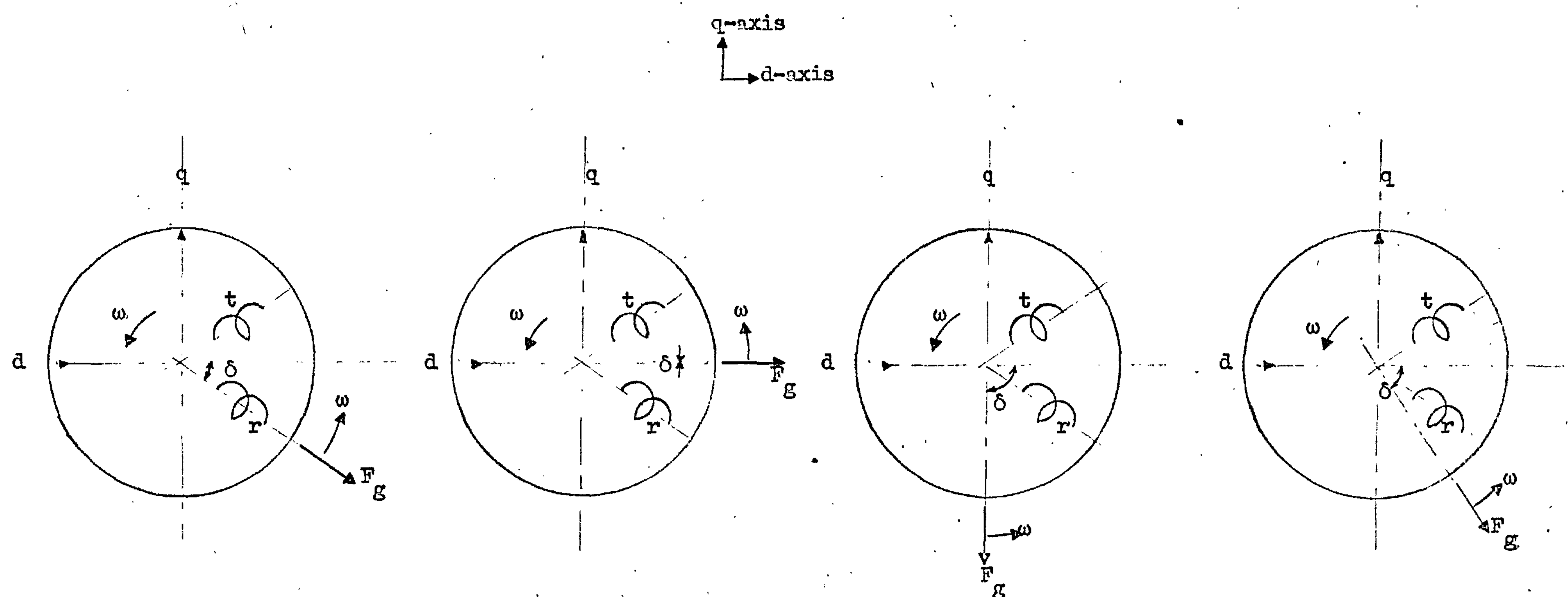

(a) $\delta = 33.75^{\circ}$ (b) $\delta = 0$ (c) $\delta = 90^{\circ}$ (d) $\delta = 66.25^{\circ}$

Fig. 9.7 Schematic diagrams showing various reference angles.

$$K_{t\ min} = \frac{\sqrt{2}(Q_o + V_{bqo}^2 Y_q) r_{fq}}{X_{mq} V_{bqo} Y_q M_{qt}} \tag{9.44}$$

when damping is neglected and the time delay is zero. Furthermore, the natural frequency is

$$\omega_n = \sqrt{\frac{Q_o + V_b^2 Y_q}{J}} \tag{9.45}$$

and

$$K_{t\ max} = - \frac{\sqrt{2} V_b (Y_q' - Y_q) r_{fq}}{Y_q M_{qt} X_{mq}} \tag{9.46}$$

Eqn. (9.46) therefore shows that, subject to the assumptions made, the maximum gain is a constant value at all values of active and reactive power.

The maximum steady state reactive absorption limit is reached when $K_{t\ min} = K_{t\ max}$, and Eqns. (9.44) and (9.46) yield

$$Q_{o\ max} = - V_b^2 Y_q'$$

This limiting point on Curve (1) in Fig. 9.6 is marked at $Q_o = - 1.48$ p.u. However, the effect of damping and the delays of the practical angle device decrease this maximum to $- 1.4$ p.u.

9.4.1.3 Bus angle δ held at 66.25^o

If the reference angle is 66.25^o, the resultant airgap M.M.F. is displaced by about 90^o from the axis of the torque winding as seen in Fig. 9.7(d). The stability limit for this condition is found from Eqn.(9.41) and shown by Curve (3) in Fig. 9.6.

9.4.1.4 Bus angle δ held at 90^o

The reference angle can also be held at 90^o as in Fig. 9.7(c). The transfer function is given by Eqn. (9.41) while the minimum gain is

$$K_{t\ min} = - \frac{\sqrt{2}(Q_o + V_b^2 Y_d) r_{fd}}{X_{md} Y_d V_b M_{dt}} \tag{9.47}$$

and the maximum gain is

$$K_{t\ max} = - \frac{\sqrt{2} V_b (Y'_d - Y_d) r_{fd}}{Y_d M_{dt} X_{md}} \tag{9.48}$$

Equations (9.47) and (9.48) yield the maximum reactive absorption as

$$Q_{o\ max} = - V_b^2 Y'_d$$

This limiting point is shown on Curve (4) in Fig. 9.6 as - 2.07 p.u., but the damping effect and practical angle device reduce it to -1.96 p.u.

The roles of the d and q-axes are therefore reversed compared with a reference angle of zero as in Sect. 9.4.1.2.

9.4.2 Proportionate terminal angle regulator only

For the case of terminal "angle feedback only" the value of $A_n'(p)$ is given by Eqn. (9.12) and the expression for $E_{22}(p)$ is given by Eqn. (9.20). The open-loop transfer function given by Eqn. (9.28) becomes

$$F_t(p) = \frac{X_c H_t(p)}{\sqrt{2}V_{mt}^2 D'(p)} \quad (-Q_o V_{mtdo} - V_{bdo}(Q_o + V_b^2 Y_c)$$

$$- X_c Y_q(p) V_{bqo} P_o)\frac{X_{md} Y_d(p) M_{dt}}{r_{fd}}$$

$$+ (Q_o V_{mtqo} + V_{bqo}(Q_o + V_b^2 Y_c)$$

$$+ X_c Y_d(p) V_{bdo} P_o)\frac{X_{mq} Y_q M_{qt}}{r_{fq}} \qquad (9.49)$$

$$K_{t\ min} = \sqrt{2}(Q_o + V_{bqo}^2 Y_q + V_{bdo}^2 Y_d)/\beta$$

$$\text{where}\quad \beta = \frac{X_c X_{md} Y_d(-Q_o V_{mtdo} - V_{bdo}(Q_o + V_b^2 Y_c) - X_c Y_q V_{bqo} P_o) X_{md} Y_d M_{dt}}{r_{fd} V_{mt}^2}$$

$$+ \frac{(Q_o V_{mtqo} + V_{bqo}(Q_o + V_b^2 Y_c) + X_c Y_d V_{bdo} P_o) X_{mq} Y_q M_{qt}}{r_{fq} V_{mt}^2}$$

(9.50)

Hence when δ_t is used as the angle feedback signal, it is no longer true that $F_t(p)$, and hence the limiting gain, is independent of P_o. At zero load the function $F_t(p)$ in Eqn. (9.49) is similar to that of Eqn. (9.40) but contains additional factors; $K_{t\ min}$ is given by Eqn. (9.41), so that the curve AB in Fig. 9.5 is also valid for the terminal angle feedback at zero load. Furthermore, $K_{t\ min}$ also depends on the reference angle δ_t and the tie-line reactance X_c. Calculations were made to determine the influence of δ_t and X_c.

Fig. 9.8 shows the calculated stability limit cirves when damping is allowed for. The high gain limit is more sensitive to load then the low gain limit and at no load the maximum reactive absorption is equal to the value obtained for the bus angle regulator

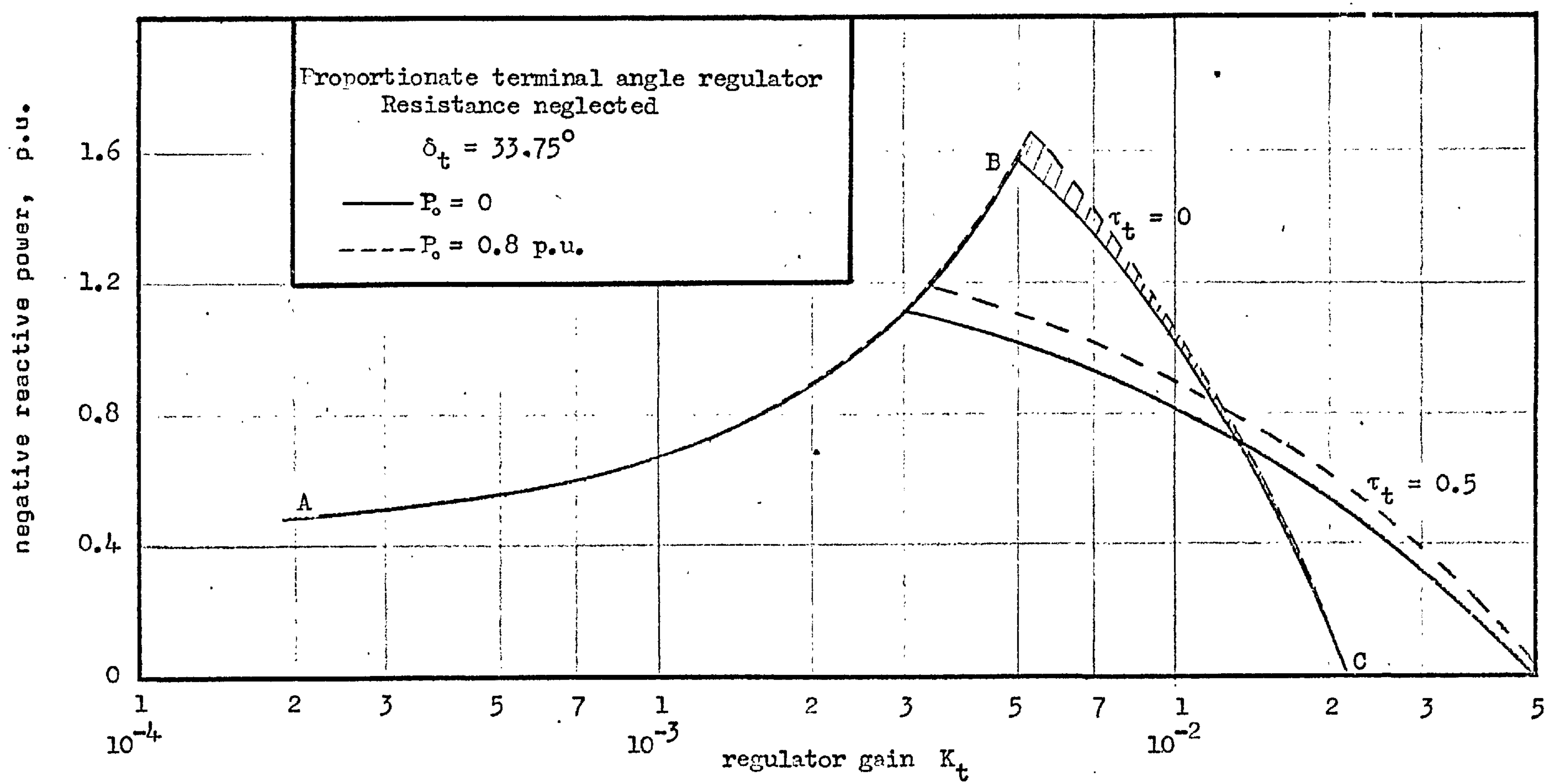

Fig. 9.8 Steady-state stability limit curves for various load conditions.

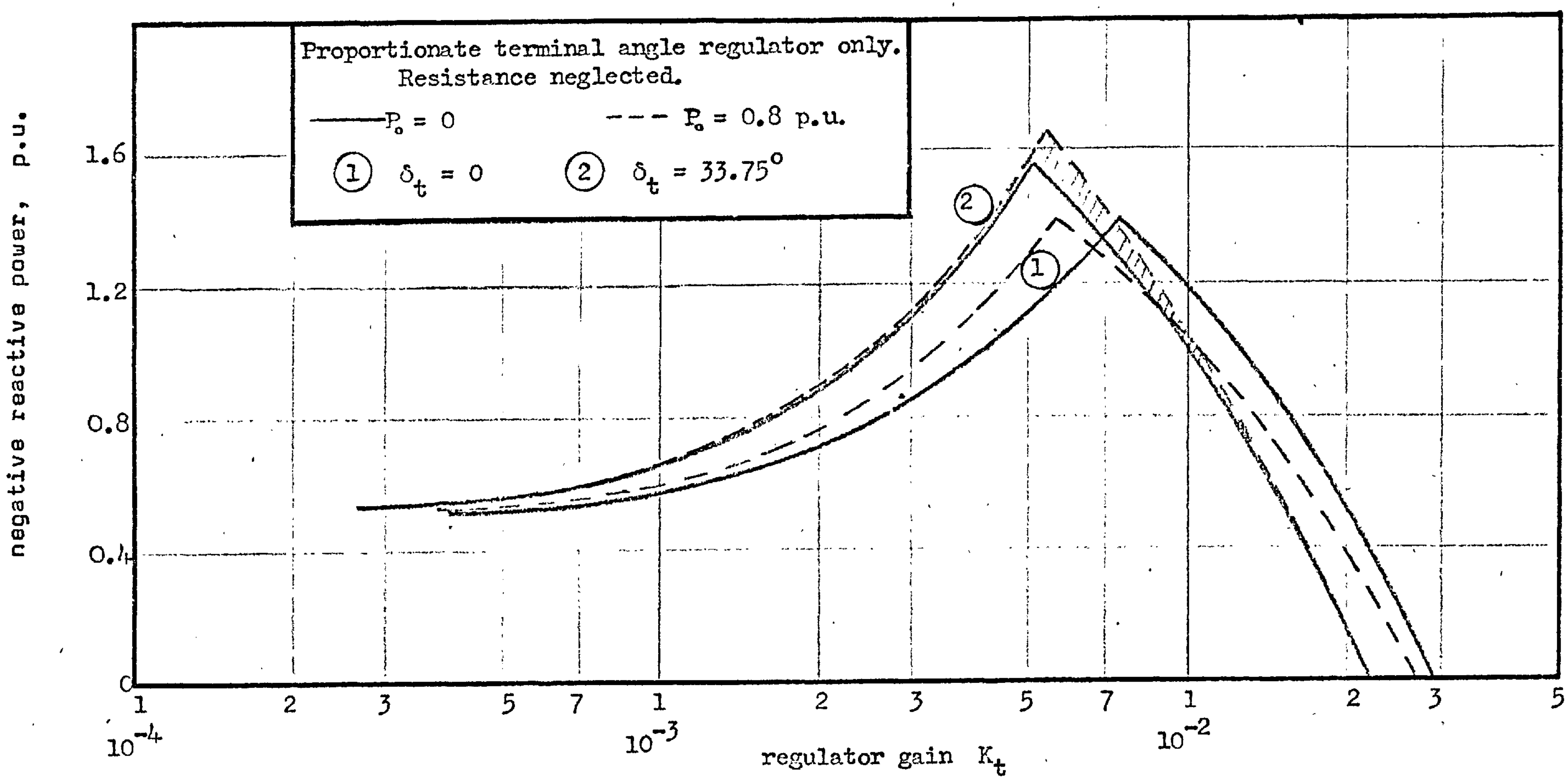

Fig. 9.9(a) Steady-state stability limit curves for various terminal load angles.

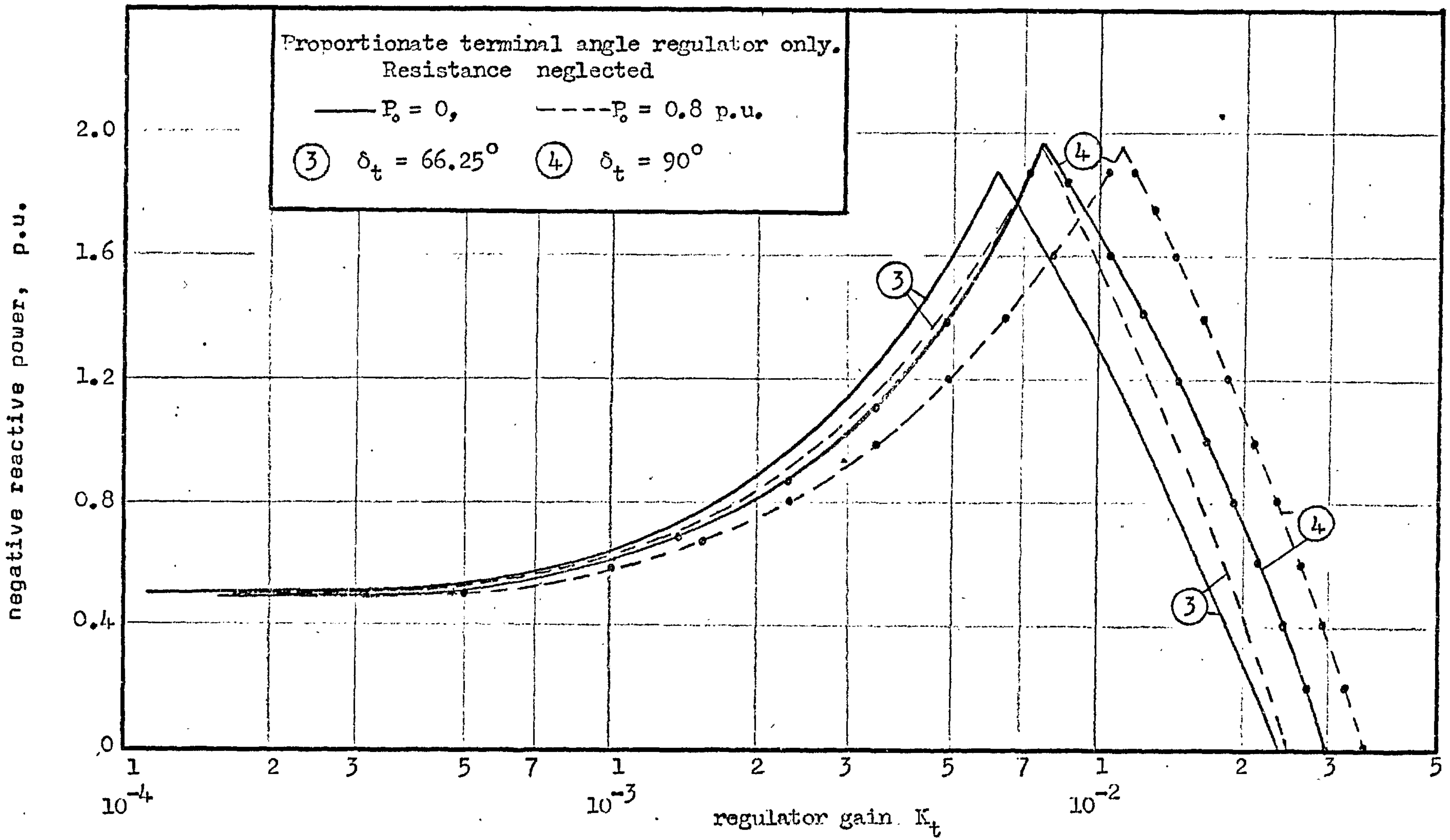

Fig. 9.9 (b) Steady-state stability limit curves for various terminal load angles.

only, at about the same value of gain (see Fig. 9.5). The rotor angle is 33.75° at zero load but as the load increases, δ increases slightly because the terminal voltage changes due to the drop in the 0.186 p.u. external tie-line reactance. The steady-state stability limit curve therefore changes as the load varies. The two curves in Fig. 9.8 have been calculated for zero- and 0.8 p.u. load respectively. The difference between them is quite small in this case, but would be greater for a larger tie-line reactance.

9.4.2.1 The effect of different values of δ_t

Figs. 9.9(a) and (b) show curves similar to those of Fig. 9.6 but for terminal angle control, when δ_t is held at various values. The low gain limit curve at $P_o = 0$ is identical with that for bus angle feedback. There is a small difference in the maximum reactive absorption though, because the high gain limits are functions of Q_o.

The electrical torque of the d.w.r. machine is proportional to the component F_{tgn} of the torque winding M.M.F. F_t in Fig. 9.10, and to the component F_{rgn} of the reactive winding M.M.F. After a small increase $\Delta\delta_t$ in the angle, the regulator increases F_t by an amount $\Delta F_t = K_t.\Delta\delta_t$. The ability of the d.w.r. machine to remain stable depends on the increase

$$\Delta F_{tgn} = K_t.\Delta\delta_t.\sin\phi_2$$

For a given $\Delta\delta_t$, ΔF_{tgn} is a maximum when ϕ_2 is 90° ($\delta = 90^{\circ} - \phi_2$). In other words, for the same ΔF_{tgn}, K_t is a minimum when $\phi = 90^{\circ}$, which is confirmed by the results for zero power in Figs. 9.6 and 9.9. These show that for a given Q_o the values of $K_{t\ min}$ and $K_{t\ max}$ are a minimum when δ or δ_t is 66.25° ($\phi = 90^{\circ}$).

Now $V_b^2 Y'_d = V_b^2 Y'_q$ if there is no transient saliency and the maximum reactive absorption should also be obtained when $\delta = 66.25^o$ which means that a δ or δ_t equal to $\emptyset_r = 33.75^o$ does not yield the maximum value for the maximum reactive absorption.

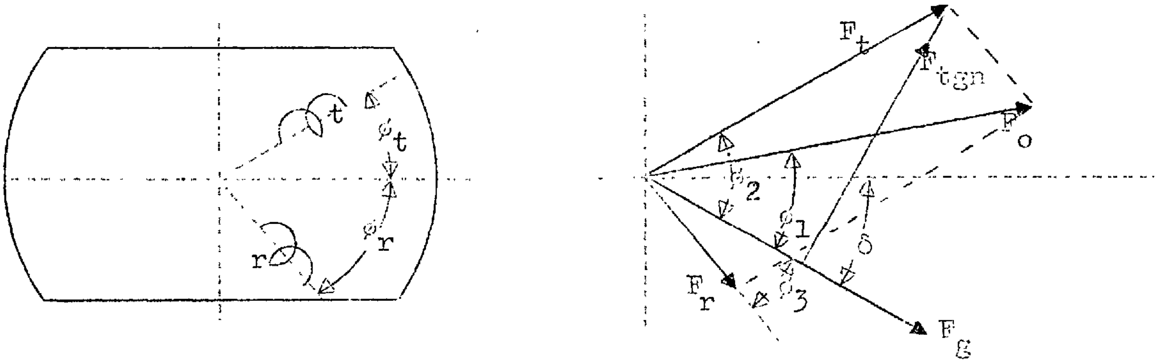

Fig. 9.10 Phasor diagram of d.w.r. M.M.F.'s

For the four cases shown in Fig. 9.9, Curve (2) for $\delta_t = 33.75^o$ shows the least variation when P_o varies from 0 to 0.8 p.u. but it does not have the highest reactive absorption. Furthermore, when P_o is increased, the low gain regions for Curves(1) and (2) move in a direction opposite to that of Curves (3) and (4) and correspond to voltage regulator action on a c.w.r. machine, where, for a given $K_{t\ min}$, the reactive absorption increases as P_o increases (see Fig. 9.11).

Therefore, holding $\delta_t = \emptyset_r$ does not necessarily give the largest stable operating range in the negative current region, although the limit of stable operation is relatively insensitive to load variations.

9.4.2.2 The effect of additional tie-line reactance

The effect of increasing the tie-line reactance X_l (see Fig. 10.1) can be seen from the calculated results in Fig. 9.12. The lower value of X_l represents a typical tie-line while the larger value is an extreme case to illustrate the reduction in reactive aborption when P_o increases for a fixed value of $K_{t\ min}$.

9.4.3 Comparison of d.w.r.- and q.a.r.- system results

The results of Sect. 9.4.1 and 9.4.2 for a d.w.r. system agree in general with those of Ref. 4 for a q.a.r. system. The common points are:

(a) A sharp cut-off of the high-gain limit for bus angle feedback when damping is neglected.

(b) The low gain limit of $\delta_t = 66.25^o$ moves to the right (Fig. 9.9) when P_o increases. For both systems the P-Q relation is similar to Curve (c) in Fig. 9.11.

(c) For terminal angle feedback the high gain limit flattens out somewhat.

(d) The expressions for $K_{t\ min}$, $Q_{o\ max}$ and ω_n are similar.

9.4.4 Proportionate voltage regulator only

A d.w.r. machine with a "voltage regulator only" gives results which are similar to those of a conventional machine. The transfer fuction is obtained from Eqn. (9.26) as

$$F_r(p) = H_r(p)E_{11}(p) \tag{9.51}$$

where

$$E_{11}(p) = \frac{R_e X_c}{V_{mto} D'(p)} \Bigg[\Big[- (Q_o + Jp^2 + V^2_{bqo}(p)) V_{mtqo}$$

$$+ P_o V_{bdo} - V_{bdo} V_{bqo} V_{mtdo} Y_q(p) \Big] \; G_d(p) Y_d(p) M_{dr}$$

$$+ \Big[- V_{bqo} V_{bdo} V_{mtqo} Y_d(p) - P_o V_{bqo}$$

$$- V_{mtdo}(Q_o + Jp^2 + V_{bdo} Y_d(p)) \Big] \Bigg] \; G_q(p) Y_q(p) M_{qr} \qquad (9.52)$$

Now

$$\beta_d = X_{md} Y_d M_{dr} R_e X_c / r_{fd}$$

$$\beta_q = X_{mq} Y_q M_{qr} R_e X_c / r_{fq}$$

K_r = the voltage regulator gain

$$\left.\begin{aligned} K_{vd} &= \beta_d K_r \\ &\text{and} \\ K_{vq} &= \beta_q K_r \end{aligned}\right) \qquad (9.53)$$

The low gain stability limit occurs where the

Real $(F_r(j0)) = -1$

and the relation between reactive absorption Q_o and $K_{r\ min}$ is given

$$Q_o = - K_{vd\ min}(-V^2_{bqo} Y_q V_{mtqo} + P_o V_{bdo} - V_{bdo} V_{bqo} V_{mtdo} Y_q)/\alpha V_{mto}$$

$$- K_{vq\ min}(-V^2_{bdo} Y_d V_{mtdo} - P_o V_{bqo} - V_{bqo} V_{bdo} V_{mtqo} Y_d)/\alpha V_{mto}$$

$$- (V^2_{bqo} Y_q + V^2_{bd} Y_d)/\alpha \qquad (9.54)$$

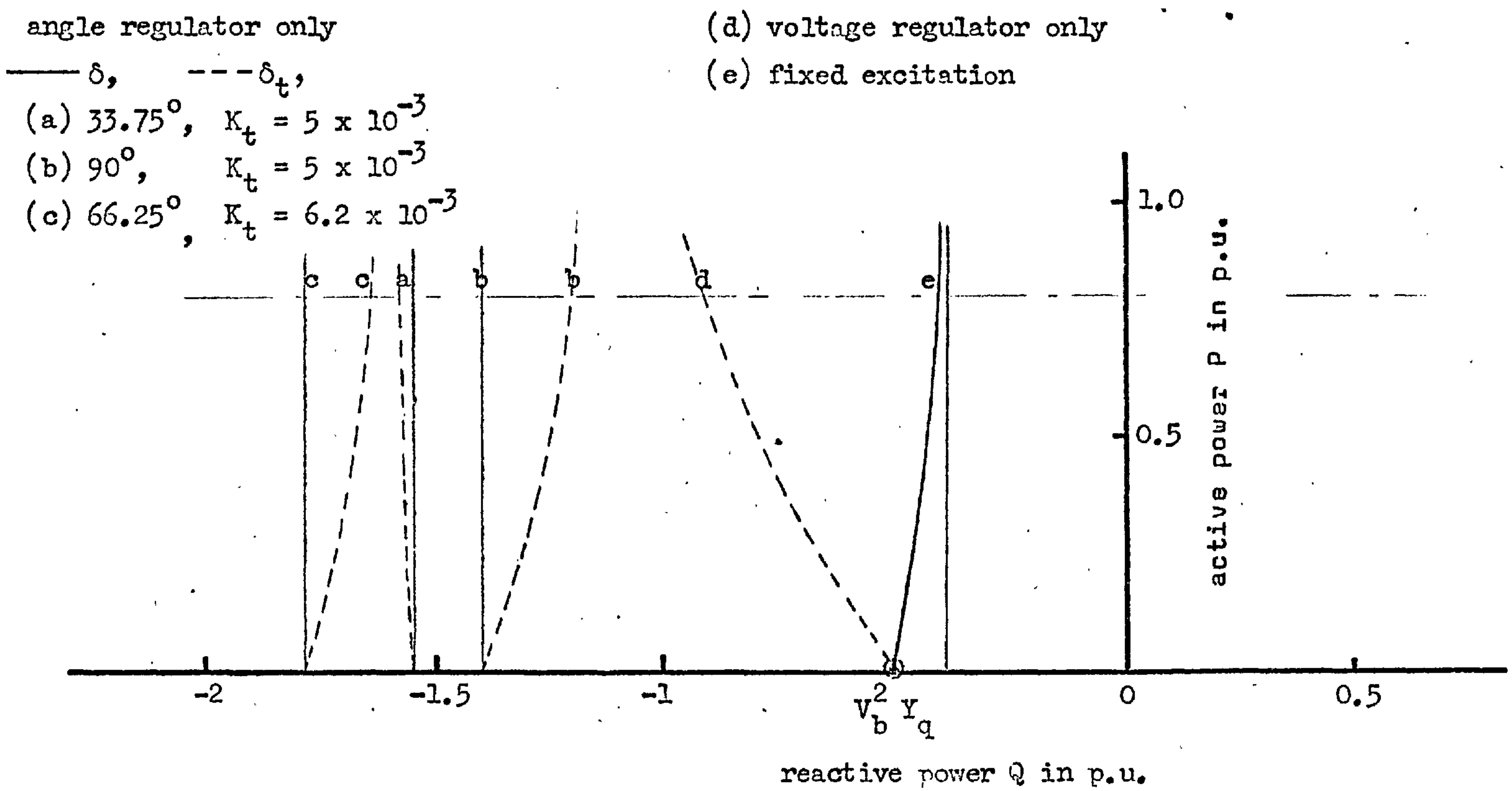

Fig. 9.11 Power-var chart showing stability limit curves.

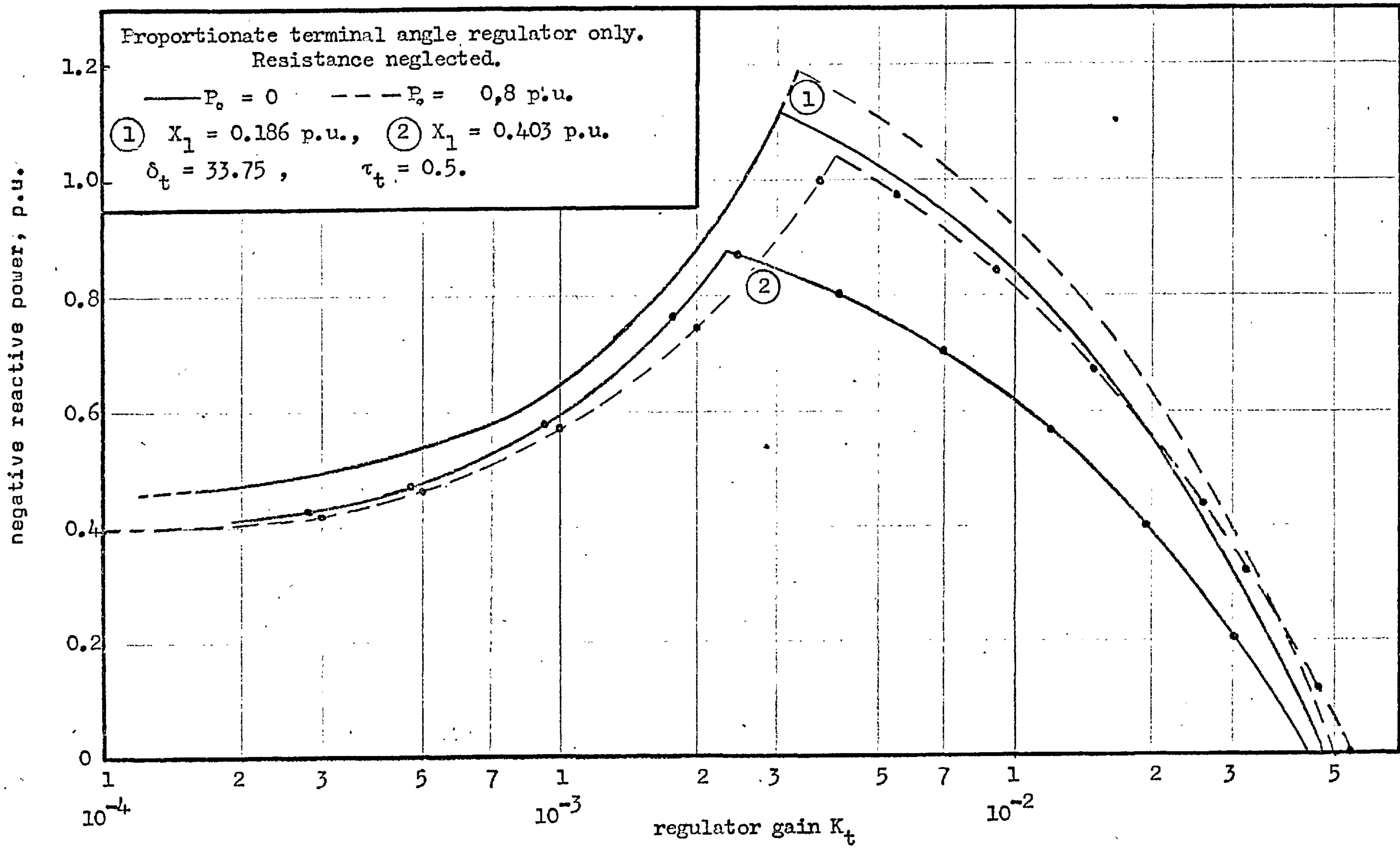

Fig. 9.12 Steady-state stability limit curves for various tie-line reactances.

where

$$\left.\begin{aligned} K_{vd\ min} &= \beta_d K_{r\ min} \\ K_{vq\ min} &= \beta_q K_{r\ min} \\ \alpha &= 1 - K_{vd}\cos\delta_t - K_{vq}\sin\delta_t \end{aligned}\right) \qquad (9.55)$$

At zero active load, $P_o = 0$ and the resultant airgap M.M.F. coincides with the axis of the reactive winding and not with the d-axis, so that $\delta_t = 33.75°$. The reactive absorption is given by

$$\begin{aligned} Q_o &= K_{vd\ min}(V^2_{bqo}Y_q V_{mtqo} + V_{bdo}V_{bqo}V_{mtdo}Y_q)/\alpha V_{mto} & \ldots\ Q_{o1} \\ &+ K_{vq\ min}(V^2_{bdo}Y_d V_{mtdo} + V_{bqo}V_{bdo}V_{mtqo}Y_d)/\alpha V_{mto} & \ldots\ Q_{o2} \\ &- (V^2_{bqo}Y_q + V^2_{bdo}Y_d)/\alpha & \ldots\ Q_{o3} \end{aligned}$$

(9.56)

For an unregulated system, $K_{vd\ min} = K_{r\ min} = K_{vq\ min} = 0$

$\alpha = 1,$

and the reactive absorption is

$$Q_{ou} = -V^2_{bqo}Y_q - V^2_{bdo}Y_d \qquad (9.57)$$

For a regulated system, however,

$$Q_o = Q_1 + Q_2 + Q_{ou}/\alpha \qquad (9.58)$$

which shows that the excitation regulation of the reactive winding affects the reactive absorption at zero load because of saliency. With zero saliency ($Y_d = Y_q = Y$) the d-axis of the machine can be chosen to coincide with the r-axis, and at no load

$V_{bdo} = V_{mtd} = \delta_t = 0, \quad \alpha = 1 - K_{vd\ min},$

$V_{bqo} = V_{mtqo} = V_{mt}$

Eqn. (9.57) simplifies to

$$Q_o = - V_b^2 Y \tag{9.59}$$

which agrees with results for a c.w.r. machine, i.e. the reactive absorption at zero load can not be increased beyond $- V_b^2 Y_q$ irrespective of the type of regulator on the d-axis.

Fig. 9.13 shows calculated stability limit curves for a "voltage regulator only". The low gain region AB is associated with a drifting type of instability and the high gain region BC with an oscillatory type of instability.

9.4.5 Proportionate angle regulator and proportionate voltage regulator

The complete excitation control scheme of the d.w.r. system shown in Fig. 9.2 consists of both an angle and a voltage feedback circuit. In practice the more convenient terminal angle δ_t, rather than the infinite bus angle δ, is used for the angle feedback. The transfer function for small disturbances to such a system, is given by equation (9.25) or (9.26).

Consider a system which has a proportionate voltage regulator with the following transfer fuctions:

$$H_t(p) = K_t/(1 + \tau_t p) \tag{9.60}$$

$$H_r(p) = K_r/(1 + \tau_r p) \tag{9.61}$$

where τ_t and τ_r represent delays in the excitation system (see

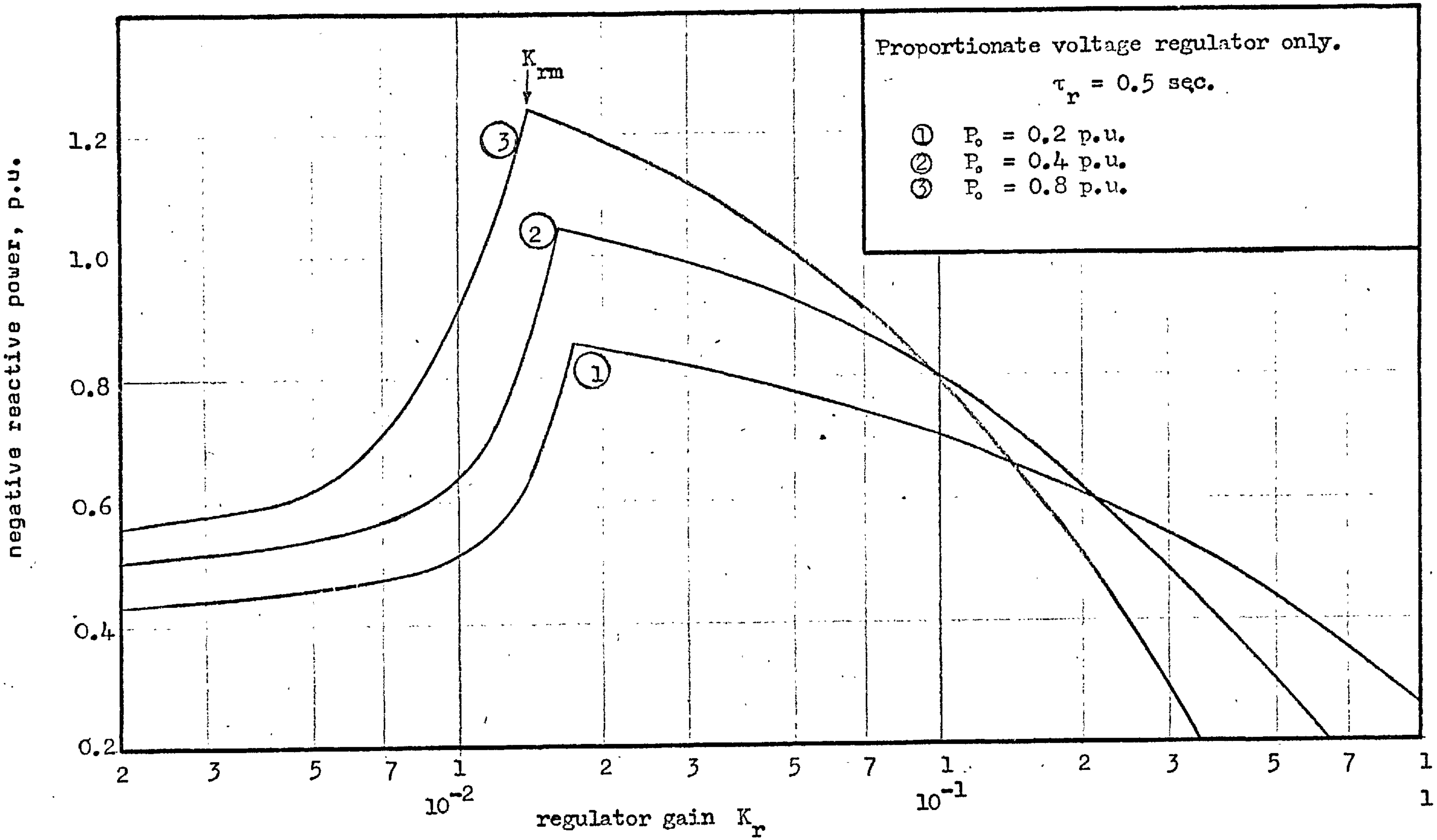

Fig. 9.13 Steady-state stability limit curves.

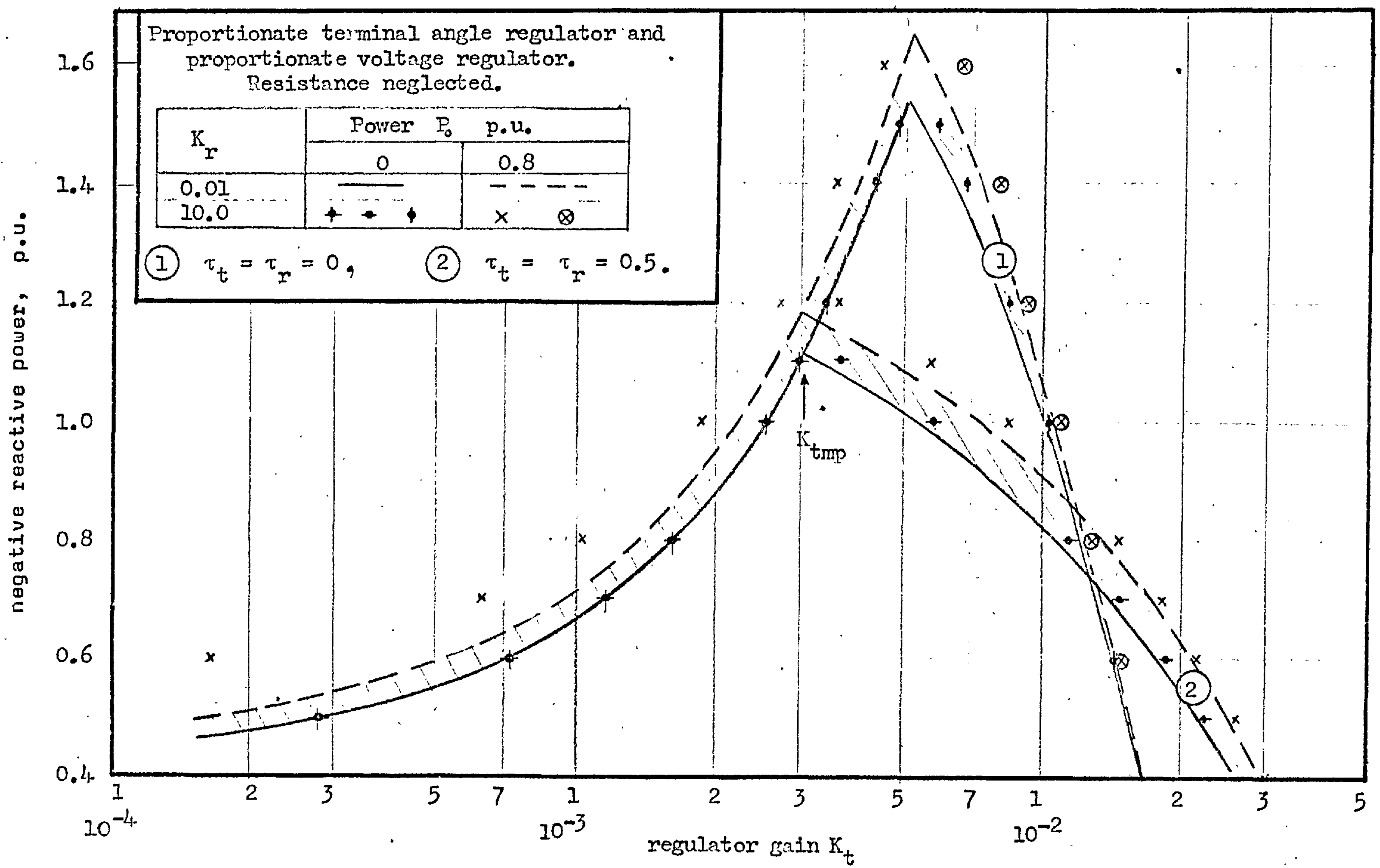

Fig. 9.14 Steady-state stability limit curves.

Sect. 10.4.1). The steady state stability limit curves can be found when the Nyquist criterion is applied to the frequency response loci of Eqns. (9.25),(9.60) and (9.61). The results in Fig. 9.14 have been calculated for different values of K_r, τ_t and τ_r.

A comparison of the results in Figs. 9.8 and 9.14 show that the addition of a voltage regulator to control the reactive winding excitation allows slightly more reactive absorption in the $K_{t\ min}$ region and little or no change in the $K_{t\ max}$ region. The changes are less significant with low values of K_r than with high values and are also proportional to the value of P_o. The voltage regulator (a.v.r.) response when used in conjunction with an angle regulator therefore depends in the same way on P_o as without an angle regulator. However, an a.v.r. gain of 10, which is beyond the steady state stability limit of the a.v.r. without angle regulator (see Fig. 9.13), does not cause instability because the angle regulator stabilises the otherwise unstable voltage regulator system.

From the point of view of steady-state stability, the design consideration for the voltage regulator are similar to those for a c.w.r. generator. Although the results in Fig. 9.14 indicate that K_r can be varied over an extremely wide range, the value should be chosen with due regard to terminal voltage recovery requirements on the one hand, and on the other hand guarding against voltage regulator high gain instability in case of angle regulator failure.

9.4.6 Derivative angle regulator and proportionate voltage regulator

A voltage regulator only, with 0.5 sec. delay, can increase $Q_{o\ max}$ to about - 1.25 p.u. at $K_r = K_{rm}$ and $P_o =$ 0.8 p.u. (see Fig. 9.13), In the previous section the 0.5 sec. delay a.v.r. together with the 0.5 sec. delay proportionate ange regulator increased $Q_{o\ max}$ at $K_t = K_{tmp}$ to a value of - 1.1 p.u. (see Fig. 9.14) which is almost insensitive to changes in P_o and K_r. In an actual system the values of K_r and K_t are fixed and not adjustable to suit each particular operating condition. Hence, if the criterion is maximum negative reactive absorption, the fixed values should be

$$K_r = K_{rm}$$

$$K_t = K_{tmp}$$

when

$$\tau_t = \tau_r = 0.5 \text{ sec.}$$

These results, however, rely upon the fact that δ_t is exactly 33.75^o, i.e. that the r-axis always coincides with the airgap M.M.F., irrespective of P_o. However, any finite value of K_t causes an error in δ_t. Moreover a large K_t would tend to cause oscillatory instability.

The value of K_{tmp} in Fig. 9.14 can be improved by using first and second derivative angle compensations to increase the gain margin and consequently the reactive absorption. The transfer function of the practical derivative angle regulator considered (see Sect. 10.4.1) is

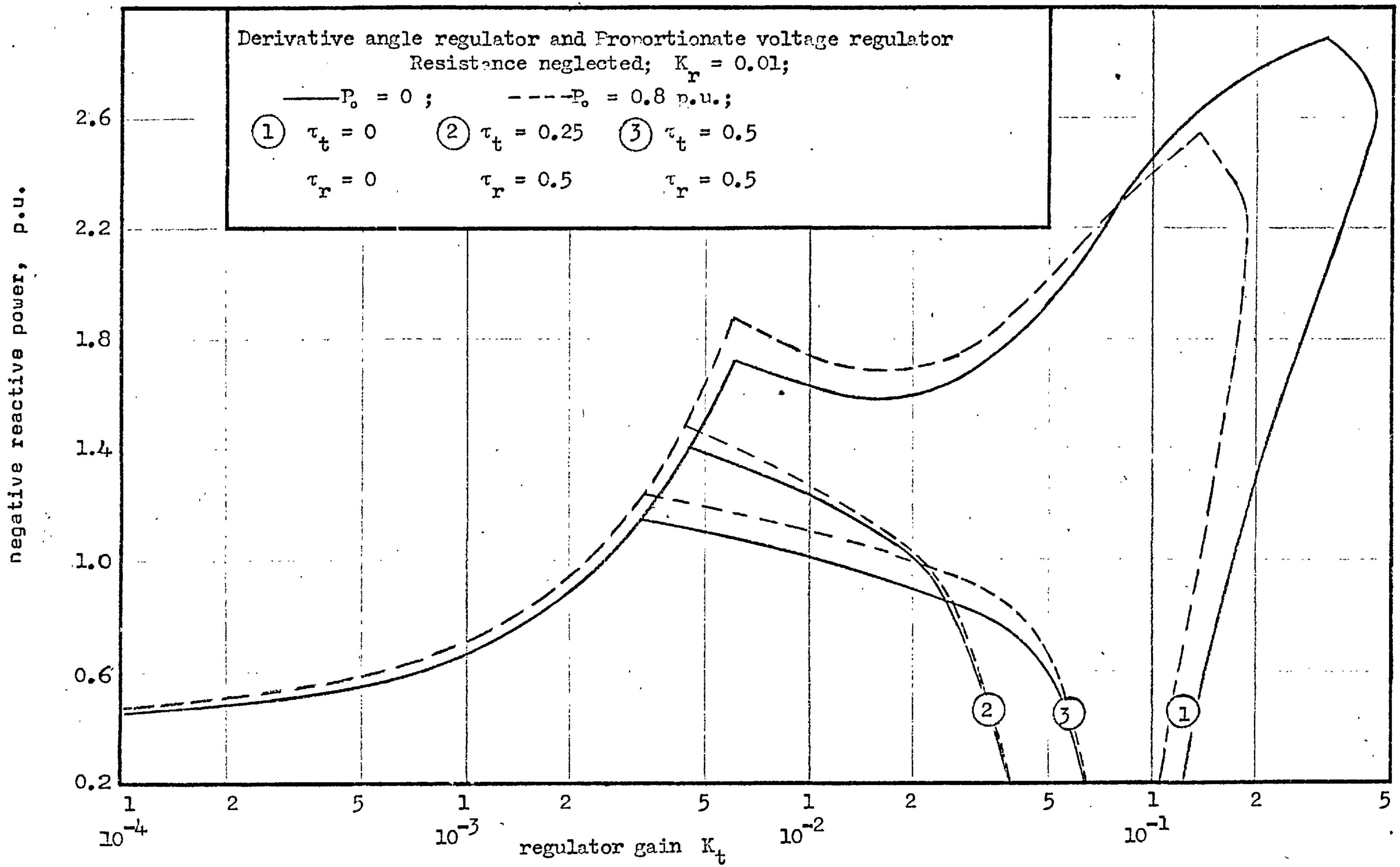

Fig. 9.15 Steady-state stability limit curves.

$$H_t(p) = \left[1 + \frac{.1p}{(1 + .01p)(1 + .01p)} \right.$$

$$\left. + \frac{.02p^2}{(1 + .01p)(1 + .01p)(1 + .01p)(1 + .02p)} \right] \frac{K_t}{(1 + \tau_t p)}$$

(9.62)

The above transfer function gives significant compensation when $\tau_t = 0$ for a system with an angle regulator only.

Equations (9.25),(9.60) and (9.62) have been used to find the stability limit curves in Fig. 9.15 for the derivative angle regulator and proportionate voltage regulator. It is seen that the derivative angle regulator allows a significant increases in $K_{t\ max}$ and $Q_{o\ max}$ when $\tau_t = \tau_r = 0$. Although a practical delay of 0.5 sec. in each regulator almost eliminates the compensation of the derivative signals, it does allow an increase in $K_{t\ max}$, depending on the required $Q_{o\ max}$. For a minimum $Q_{o\ max}$ of - 1 p.u., $K_{t\ max}$ is about twice the value of the maximum gain without compensation. The amount gained in $K_{t\ max}$ and $Q_{o\ max}$ depends very much on the regulator delays and especially on τ_t since a change in τ_r from 0.25 to 0.5 makes little difference to Curve (3) or to Curve (2) while a change in τ_t from 0.25 to 0.5 changes Curve (3) to Curve (2).

The results of the present and the previous section show that the degree of overall d.w.r. system steady-state stability corresponds to the degree of stability of a d.w.r. system with only an angle regulator.

---o0o---

CHAPTER 10

10. THE D.W.R. MICRO-MACHINE EQUIPMENT

At Imperial College the "old" micro-machine (see Sect. 5.2) has only one winding on the rotor d-axis and can therefore only be used as a c.w.r. alternator. The "new" micro-machine has two symmetrical field windings t and r, which can be used in series for the purpose of a .w.r. alternator, or separately for the purpose of a d.w.r. alternator. The electrical angle between a field winding axis and the d-axis is the same for both windings i.e. $\phi_t = \phi_r = \phi = 33.75^\circ$ (see Fig. 8.1). For a divided winding connection the angle between the two winding axes is 67.5°.

Test results about the steady-state stability limits of a divided winding rotor (d.w.r.) synchronous generator were obtained from the "new" micro-machine system (see Fig. 10.1) No parameters were available for a practical large d.w.r. alternator although parameters have been published[5] for a "hypothetical" 30 MW d.w.r. turbo-alternator. The choice of per unit values for the micro-machine system parameters was based on discussions with the C.E.G.B., South Eastern Region.

10.1 The Micro-alternator

The new micro-alternator has a Mawdsley's[40] stator. The divided rotor winding has auxiliary field windings for time constant regulation (see Sect. 5.3.2) and a squirrel cage damper winding. The cylindrical rotor is laminated an non-uniformly slotted.

The design of the micro-machine was influenced by the following factors:

(1) A fixed airgap diameter and a fixed stator design for a 4-pole machine.

(2) Although the number of rotor slots per pole could not be greater than 6, the spacing and dimensions of the slots were chosen so that the machine simulated a large alternator as far as possible.

10.1.1 Connection of the field windings

Each one of the divided field windings in Fig. 8.1 consists of two portions which can either be connected in parallel or in series. For the purpose of this thesis the series connection was used because it presents a higher resistance which limits the effect of brush contact fluctuations at the alternator sliprings and exciter commutator.

For c.w.r. operation the two field windings can be connected in series in two ways viz. so that the resultant M.M.F. coincides with the d-axis (cumulatively), or so that it coincides with the q-axis (differentially), These connections are shown in Fig.10.2 together with the vector diagrams of the fundamental M.M.F.'s The machine parameters are measured by connecting the windings cumulatively as well as differentially and performing the standard[36] d-axis tests for both connections.

From the vector diagrams it is seen that

$$F_d = 2F_t\cos\phi \qquad (10.1)$$

and $$F_q = 2F_t\sin\phi \qquad (10.2)$$

if $F_r = F_t$ as in the case of identical symmetrical windings.

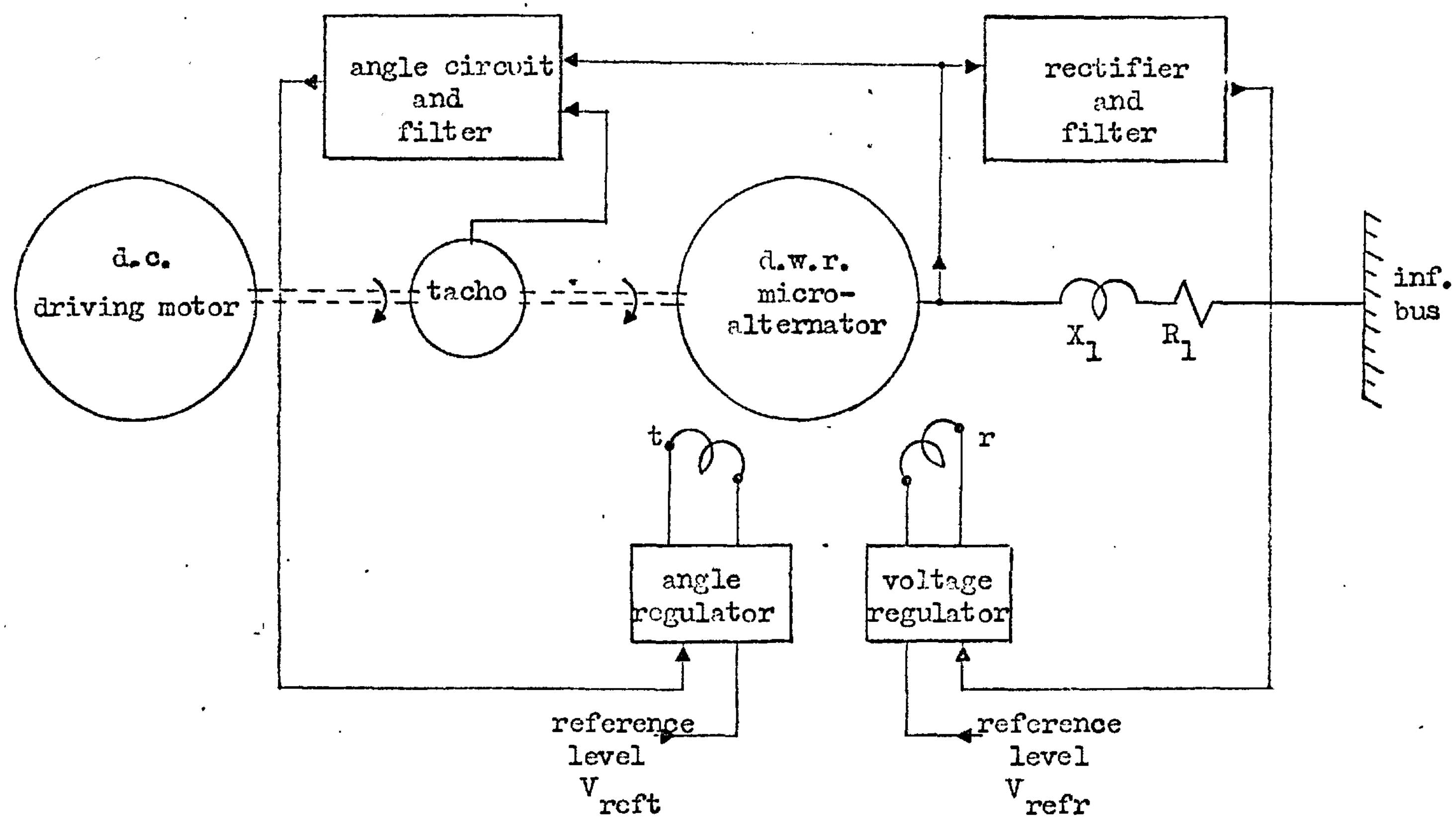

Fig. 10.1 Schematic diagram of d.w.r. micro-machine system.

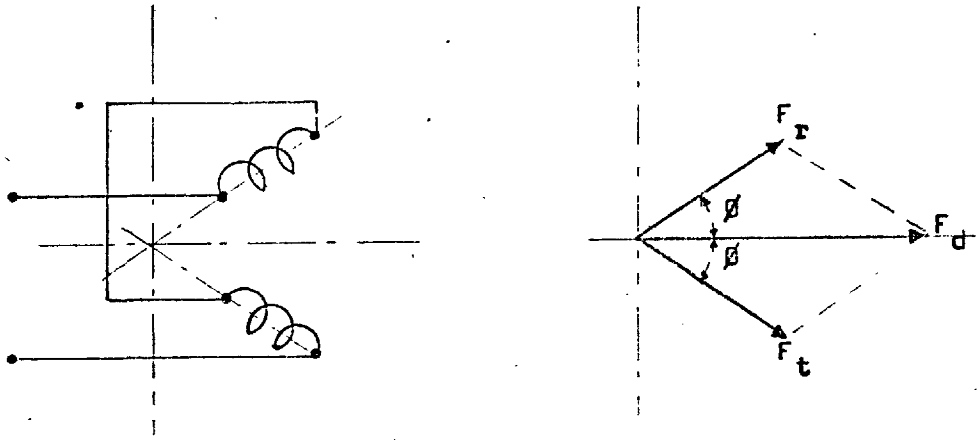

(a) Cumulatively

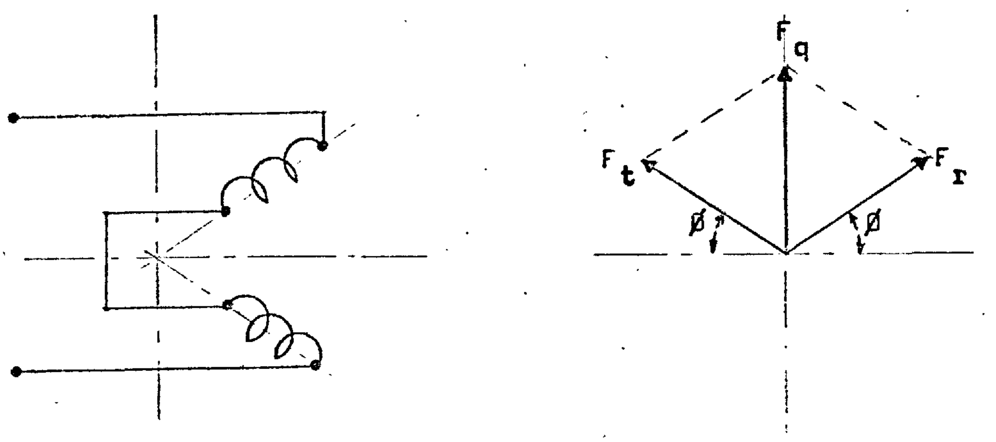

(b) Differentially

Fig. 10.2 Connections of the field windings.

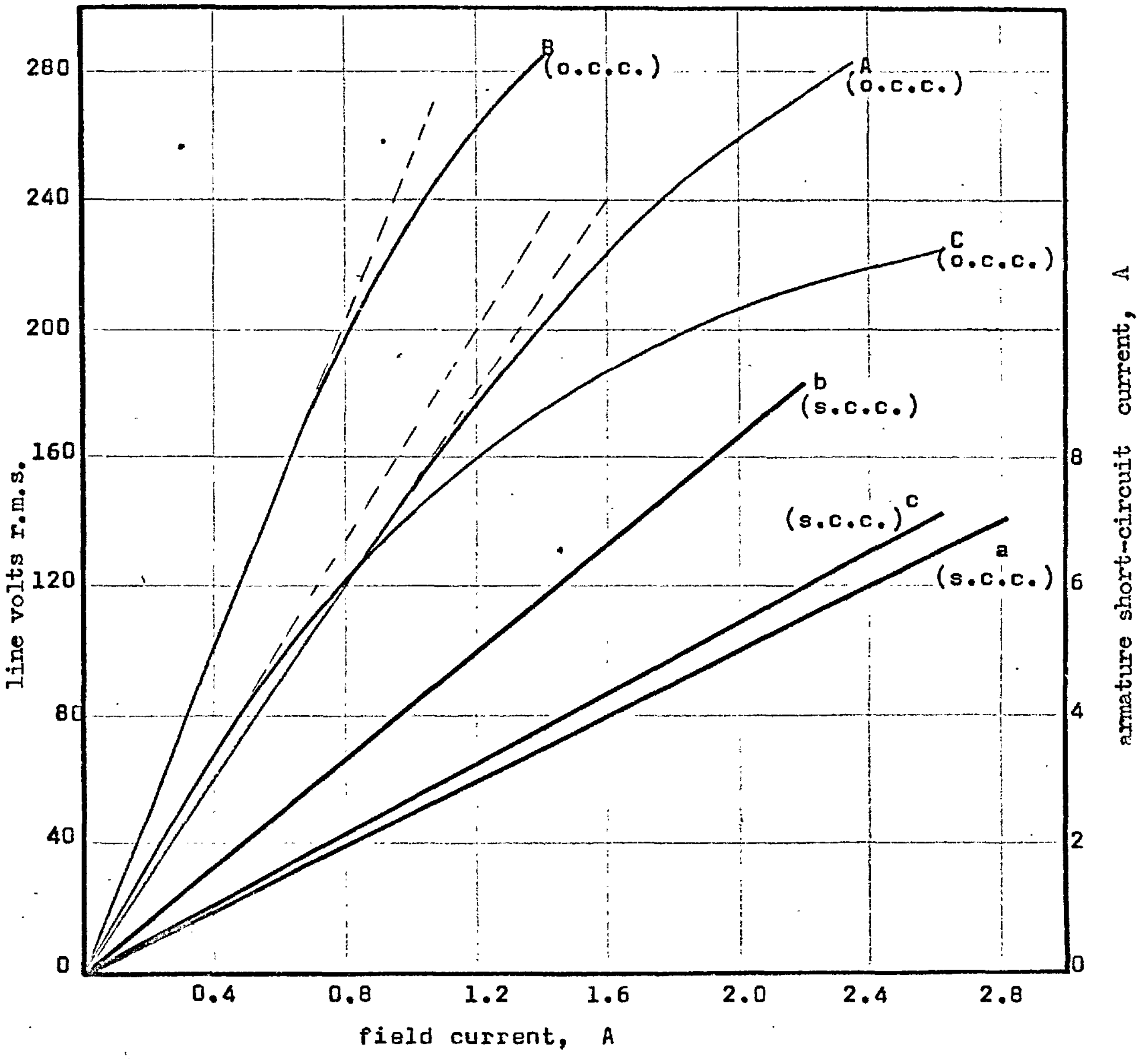

Fig. 10.3 Open-circuit and short-circuit characteristics for the d.w.r. micro-machine.

Curves: (A,a) one winding, r or t only
(B,b) windings t and r cumulatively
(C,c) windings t and r differentially

10.1.2 Determination of parameters

Magnetisation and short-circuit characteristics

The magnetisation characteristics for the new micro-machine are different from those of a large turbo-alternator because the degree of saturation in the teeth is much larger. The open-circuit and short-circuit characteristics for one winding only and for the two windings in series cumulatively as well as differentially, appear in Fig. 10.3. Points on the three airgap lines satisfy Eqns.(10.1) and (10.2) to yield a value of ϕ which is very close to 33.75°. The results of Fig. 10.3 are used to find the unsaturated values of X_{md}, X_{mq} and $X_{mt} = X_{mr}$.

Effective field resistance

As in the case of the existing c.w.r. micro-machine (see Sect. 5.3.2) the per unit field resistance of the d.w.r. micro-machine is too large and one time constant regulator (t.c.r.) per field winding is used to control the effective resistance when the machine operates in the d.w.r. mode. However, during the parameter tests when the two fields are in series, i.e. in the c.w.r. mode, only one t.c.r. is used as the source of excitation. The existing t.c.r.'s function satisforalily at the frequencies of the small oscillations.

The feedback resistance R_{fb} (see Fig. 5.5) is adjusted until T'_{do} (when the fields are cumulatively) corresponds to that of a large machine. For this connection the effective number of turns of the two windings is $2N\cos\phi$ (see also Sect. 8.2). If however, the two divided windings were excited separately (d.w.r. mode) but carrying the same current in the cumulative sense che same M.M.F. as for c.w.r. operation would result on the d-axis. The latter effect can be represented by a fictitious fd-winding of N turns (see Sect. 8.2.1).

Therefore if R_{fb2} is the feedback resistance in ohms for the 2Ncos$\emptyset$-turn winding of the cumulative c.w.r. connection, then the feedback resistance for a fictitious N-turn winding fd on the d-axis is

$$R_{fbN} = \frac{R_{fb2}}{4\cos^2\emptyset}$$

In order to maintain the above-mesured value of T'_{do} in the d.w.r. mode, the resistance R_{fbN} must remain unchanged. Use of the parameter transformation Eqn.(8.31)shows that the feedback resistance R_{fbrt} of a single winding in d.w.r. mode becomes

$$R_{fbrt} = \frac{R_{fbN}}{2} \text{ ohm} \qquad (10.3)$$

The value of T'_{do} measured from tests for the c.w.r. connedtion has a maximum value of 4.17 sec. which cannot be exceeded because of limitations in the t.c.r. Furthermore the low loop gain of the t.c.r. permits the residual voltage of the exciter to circulate an alternator field current without any applied field voltage 'e' (see Fig. 5.5). Hence, the relationship between field voltage and field current becomes non-linear at low values of e. To off-set this, a bias in series with e, but of opposite polarity, is used to reduce i_f to zero when e is zero.

When a t.c.r. supplies one field winding only, the natural field resistance is less than the critical resistance[41] for the series exciter in Fig. 5.5. Only the feedback signal to the exciter control fields limits the exciter output below an acceptable level when e (see Fig. 5.5) is zero. However, when a transient causes i_f to increase, the electronic amplifier feeding the control field soon reaches its output limit in the process of counteracting the series field effect. For higher values of i_f the effective field resistance is therefore no longer R_{fb}. Since there are no taps on the exciter series field the problem was overcome by deliberately adding external resistance into the exciter load circuit.

Inertia constant

The inertia of the micro-alternator and d.c. driving motor was altered by adding a flywheel to the rotating system in order to have an inertia constant typical of a large alternator. Values of inertia constants for large turbo-alternators appear in Table 10.1.

Table 10. 1 Inertia constants

Machine rating, MW	H, sec.
660	3.84
660	3.47
500	4.1
500	3.6
500	2.8

The parameters for the d.w.r. micro-machine with two time constant regulators appear in Table 10.2

Table 10.2 D.W.R. micro-machine and system data

Base stator voltage	220 V, r.m.s. line
Base stator current	7.87 A
Base armature power	3000 VA
Base stator impedance	16.14 ohm
Base field voltage	683.4 V
Base field current	2.19 A
Base field.power	1500VA
Basē field impedance	311.4 ohm
Mutual reactance X_{md}(unsat.)	2.22 p.u.
X_{mq}(unsat.)	1.97 p.u.
Armature leakage reactance, X_a	0.1 p.u.
Armature resistance, r_a	0.0061 p.u.
Field leakage readtances, X_{fd}	0.217 p.u.
X_{fq}	0.486 p.u.
X_t, X_r	0.300 p.u.
Field resistances, r_{fd},	0.00186 p.u.
r_{fq}	0.00416 p.u.
r_t, r_r	0.00257 p.u.
Transient reactance, X'_d	0.298 p.u.
X'_q	0.490 p.u.
Subtransient reactance, X''_d	0.172 p.u.
X''_q	0.203 p.u.
Time constant: T'_{do}	4.17 sec.
T'_d	0.536 sec.
T''_d	0.029 sec.
T'_{qo}	1.88 sec.
T'_q	0.447 sec.
T''_q	0.035 sec.
Inertia constant : H	3.48 sec.
Divided winding angle	67.5°
Transmission line:	
Resistance R_1	0.0086 p.u.
Reactance X_1	0.186 p.u.

10.1.3 Comparison with large hypothetical machine

A comparison between the main parameters in Tables 8.1 and 10.2 reveals important points summarized in Table 10.3

Table 10.3 Comparative data for a d.w.r. micro-machine, a d.w.r. 30 MW machine[5] and two large c.w.r. turbo-generators[42].

Parameter	d.w.r. micro-machine	d.w.r. 30 MW	c.w.r. 275 MW	c.w.r. 500 MW
s.c.r	0.43	0.5	0.45-0.55	0.40-0.48
H	3.48	5.3	3.5 -4.75	3.5 -4.65
X'_d	0.298	0.27	0.2 -0.3	0.23-0.33
X''_d	0.172	0.172	0.17-0.21	0.17-0.23
X'_q	0.490	0.472		
X''_q	0.203	0.176		
T'_{do}	4.17	6.59		
T'_{qo}	1.88	2.60		
r_a	0.0061	0.002		
T''_d	0.029	0.027		
T''_q	0.035	0.035		

The only significant difference of parmameters in Table 10.3 is still the high value of micro-machine armature resistance, although it is about three times smaller than the resistance of the "old" c.w.r. micro-machine. A significant improvement on the damping performace of the old micro-machine is seen in the close agreement between the subtransient time constants of the "new" micro- machine and the 30 MW machine. The results of Table 10.3

indicate that the d.w.r. micro-machine parameters as a whole agree closely with the hypothetical 30 MW d.w.r. parameters and in some respects even better with the c.w.r. 500 MW turbo-generator parameters. Hence the test results of the new micro-machine in either the d.w.r. or c.w.r. mode should be closer to the results of a large machine than hitherto.

10.2 The Prime Mover

The new micro-alternator is driven by a 4.94 h.p. 220 V, compound wound d.c. motor. The torque speed characteristic was not changed (see Sect. 5.3.3) because tests were confined to steady state stability only. Provision was made in the wiring of the d.c. motor supply for the turbine simulator mentioned in Sect.5.2.2 to be swintched in easily. However, although the simulator was operational, it was not ready for general use at the time of the tests.

10.3 Feedback Signals

For a d.w.r. machine to operate successfully as explained in Sect. 8.1, the excitation for the torque winding is controlled by a feedback signal proportional to the rotor angle while the reactive winding excitation is regulated either by the terminal voltage or manually for test purposes.

10.3.1 The angle feedback circuit

A signal proportional to the angle of the rotor with reference to either the infinite bus (fixed supply) or the terminal voltage (see Fig. 10.1), is developed. A shaft driven a.c. tacho-generator which generates the frequency of the system gives a wave form whose phase with respect to the reference wave changes in accordance with the rotor position. Thus the rotor angle problem is converted into phase detection and generation of a voltage proportional to phase variation. A specially constructed phase detection circuit is described below.

10.3.1.1 The angle device

The angle device measures the angle between the rotating rotor body and a rotating reference axis i.e. the "rotor angle". The "load angle" is defined as the angle between the rotating resultant rotor M.M.F. F_o and a rotating reference axis. In a c.w.r. machine F_o is produced by a single field winding and is stationary with respect to the rotor body so that the "load angle" and "rotor angle" are equal. However, in a d.w.r. machine F_o is produced by two field windings and can therefore be moved around the rotor body so that the "load angle" and "rotor angle" are not necessarily equal. In fact, a suitable control system will keep the rotor angle almost constant for variations in load and load angle.

In the closed loop angle control of a d.w.r. generator, the loop gain depends on the slope of the angle device output characteristic (see Fig. 10.7) and the sinewave output of the "old" angle device[4] therefore introduces a variable gain which complicates the stability study. The "new" angle device described in this section has a linear output giving constant gain and the zero- output point on the calibration curve in Fig. 10.7 can be adjusted by the level control in Fig. 10.5(b) The output of the "new" circuit in contrast to the "old" one, does not detect a change of up to 70% in the amplitude of the signal voltage. This is particularly useful when measuring rotor angle to the terminals while the terminal voltage changes as a function of load and excitation.

There are various ways[7], of determining the rotor angle depending upon the method used to obtain a signal indicative of the rotor's position. The available 4-pole, two-phase sine wave tacho-generator was found most convenient.

The tacho-generator output is connected to any one input of the block diagram shown in Fig. 10.4 and the reference voltage to the other input. The reference voltage can be taken either from the generator terminals or the fixed supply, depending on the type of control required and an isolating transformer is used in both cases so that the transmission line is not earthed by the angle device.

The circuit in Fig. 10.4 consists of two identical channels which each produce a pulse every time its incoming signal crosses through zero. The pulses trigger a bistable circuit whose output has a mark-to-space ratio proportional to the phase angle. Suitable filtering follows at the output stages. A detailed circuit diagram appears in Fig. 10.5 and its operation is described below.

The incoming signal is zenered by D1 to limit the inverse base-emitter voltage of the transistor amplifier stage T1. Capacitor C1 accelerates the switching of T2 between the "ON" and "OFF" state. The maximum amplitude of the incoming signal is determined by the power dissipation capability of D1 which can be increased if necessary. The minimum signal amplitude should cause a negligible time lapse between zero-crossover of the signal and the output of

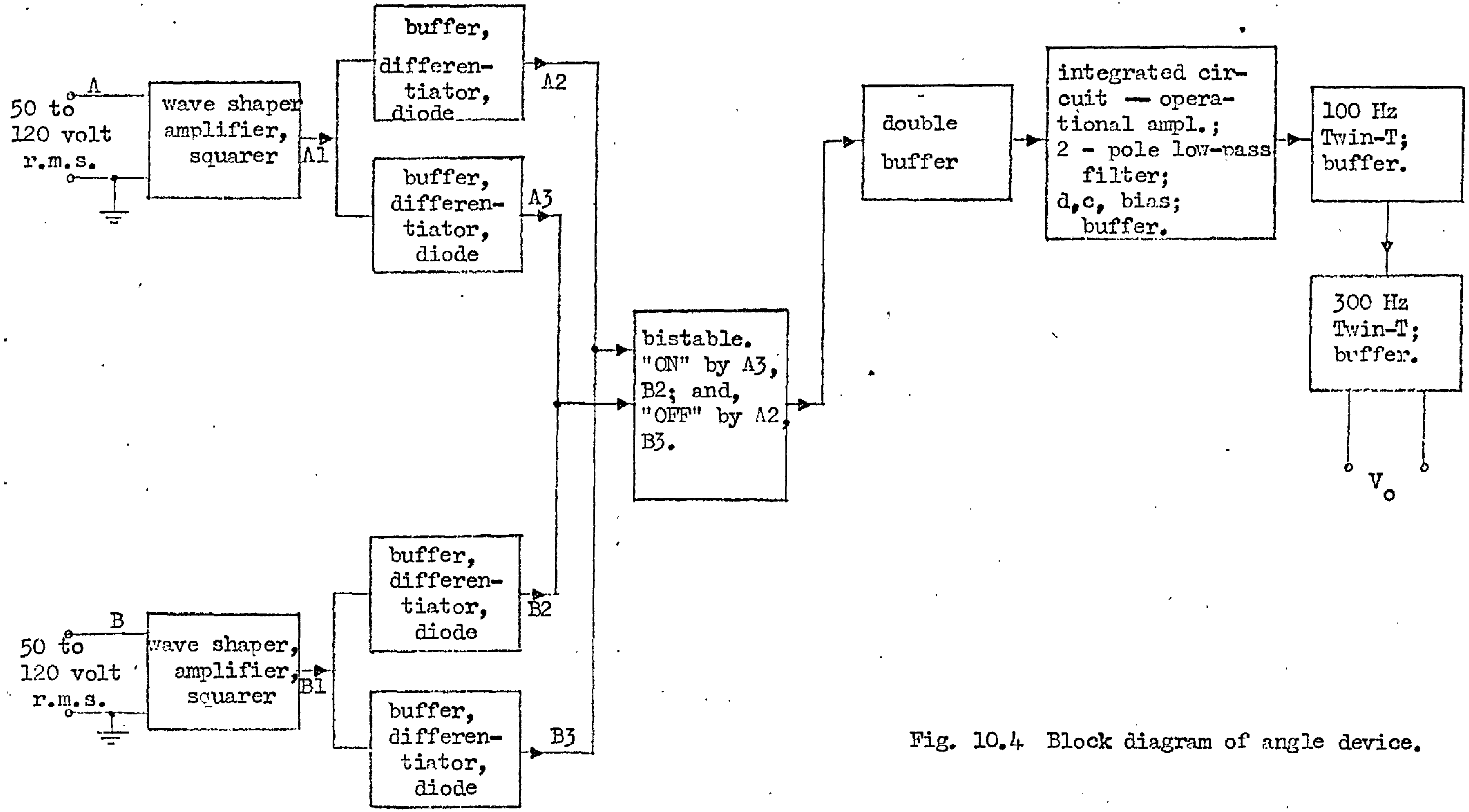

Fig. 10.4 Block diagram of angle device.

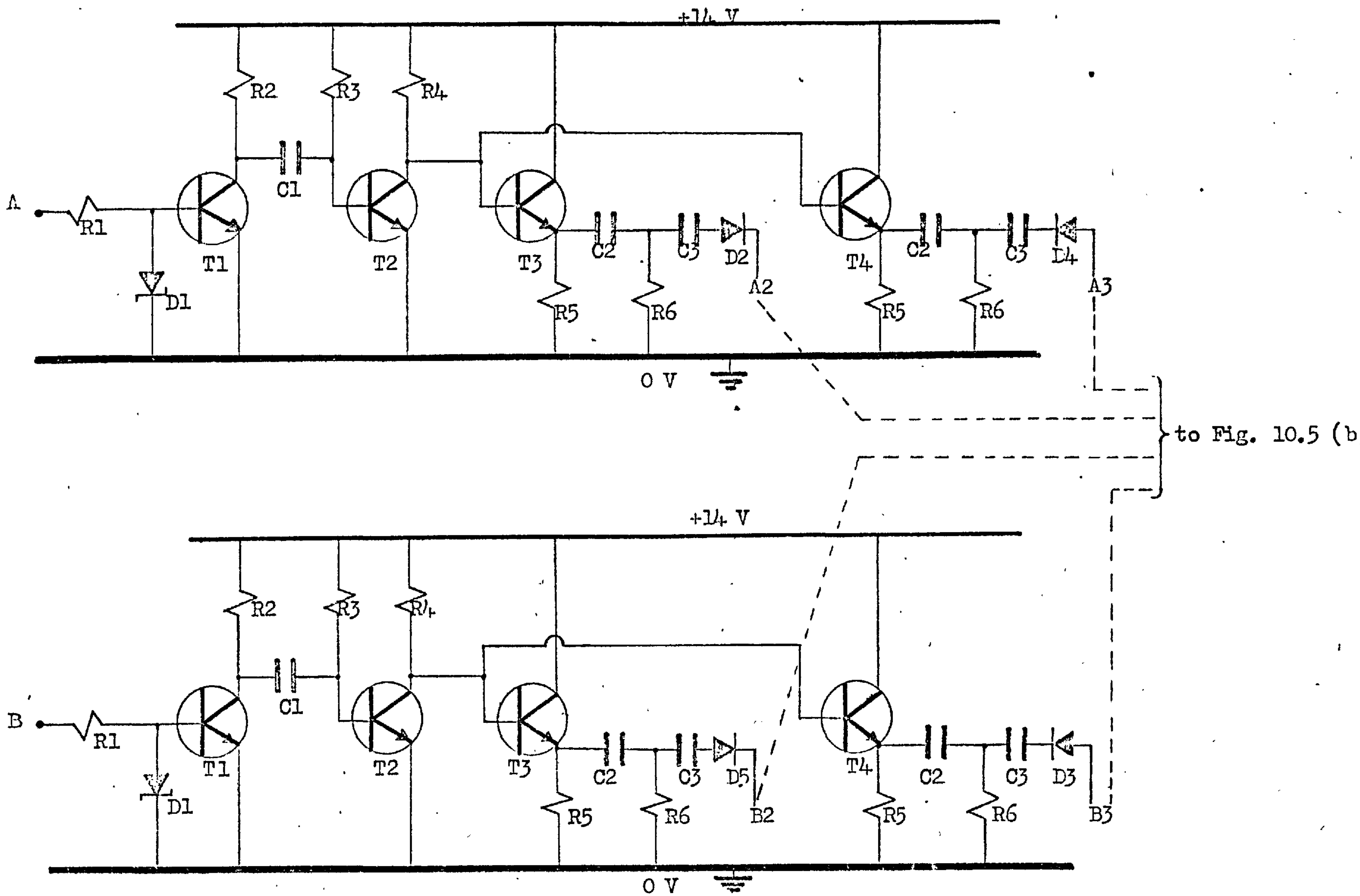

+14 V
A
R1
D1
T1
R2
C1
R3
T2
R4
T3
R5
C2
R6
C3
D2
A2
T4
R5
C2
R6
C3
D4
A3
0 V
to Fig. 10.5 (b)
+14 V
B
R1
D1
T1
R2
C1
R3
T2
R4
T3
R5
C2
R6
C3
D5
B2
T4
R5
C2
R6
C3
D3
B3
0 V

Fig. 10.5 (a)

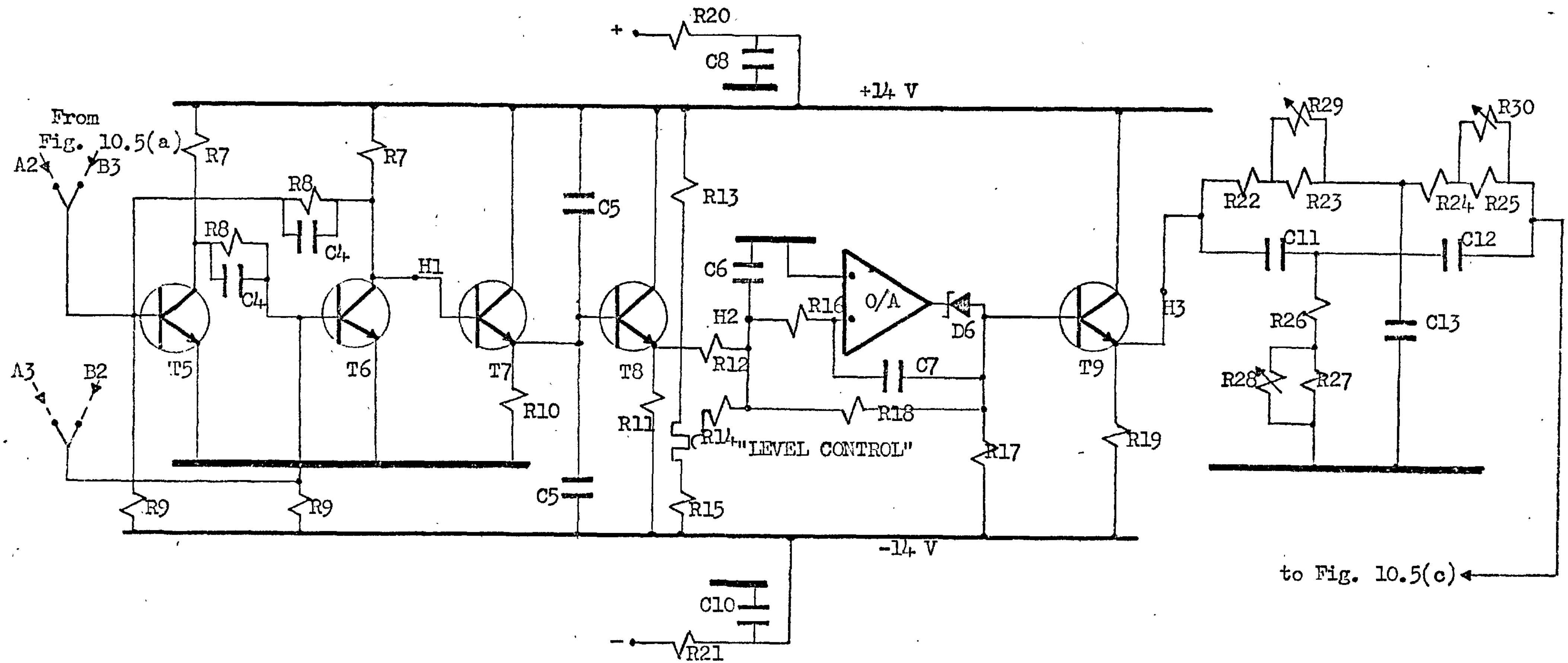

From
Fig. 10.5(a)
A2
B3
A3
B2
+
R20
C8
+14 V
R7
R7
R8
R8
C4
C4
H1
C5
C5
R13
C6
H2
R16
O/A
D6
C7
R12
R18
R14
"LEVEL CONTROL"
R17
T5
T6
T7
T8
T9
H3
R10
R11
R9
R9
R15
R19
-14 V
C10
-
R21
R29
R30
R22
R23
R24
R25
C11
C12
R26
C13
R28
R27
to Fig. 10.5(c)

Fig. 10.5 (b)

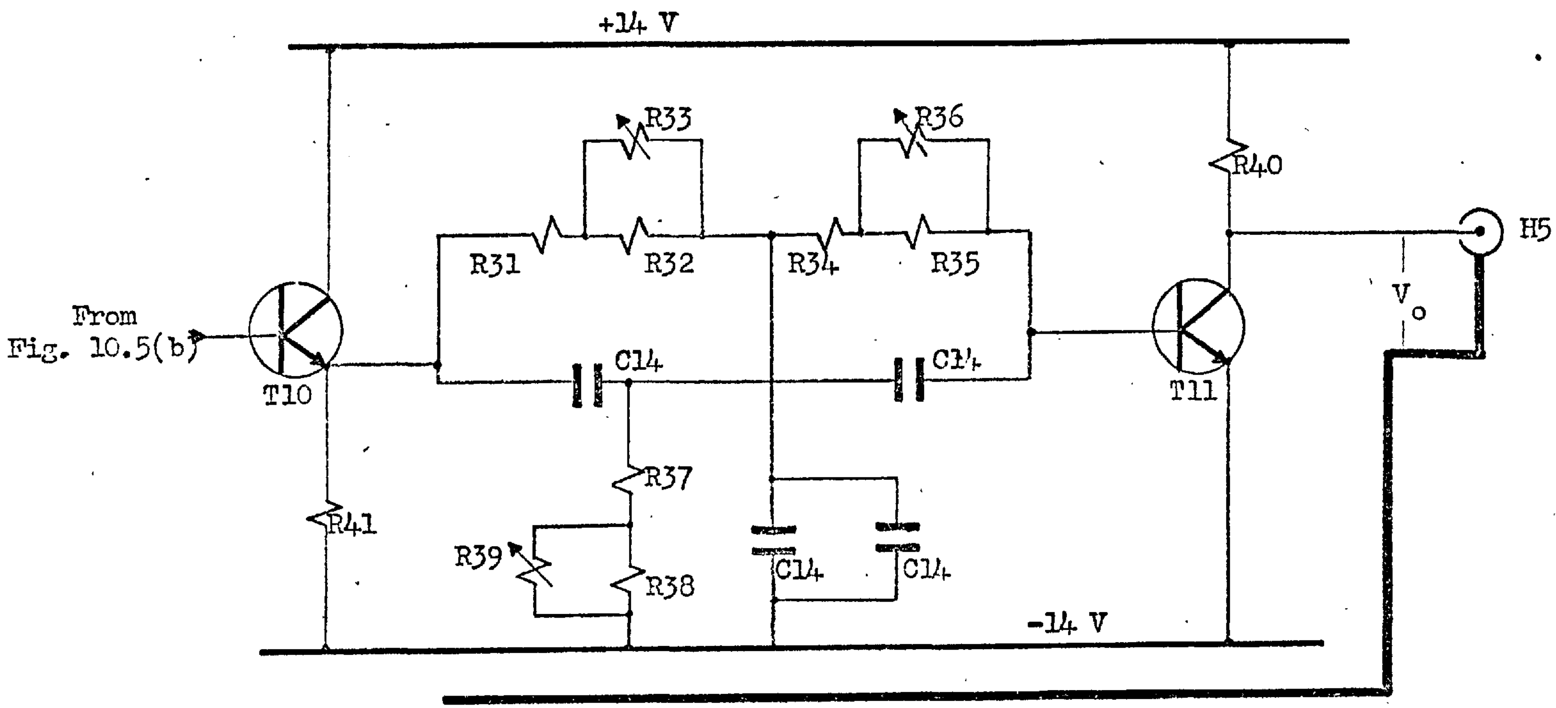

Fig. 10.5(c)

Fig. 10.5 The angle device.

Table 10. 4 List of components in Fig. 10.5

Resistances: $\frac{1}{4}$ watt

R1, R14 - 10 K ohm (K)
R2, R4 - 5.6 K
R3, - 120 K
R5, R10 - 4.7 K
R6, R23, R25 - 20 K
R7 - 2.7 K
R8 - 27 K
R9 - 100 K
R11, R16, R19, - 5.6 K
R12 - 47 K
R13, R15 - 82 K
R17 - 2.2 K
R18 - 33 K
R20, R21 - 12 ohm
R22 - 7.93 K

R24 - 7.5 K
R26 - 12 K
R27 - 180 ohm
R28, R29, R30 - 0 to 100 K pot.
R31, R34 - 1.5 K
R32, R35 - 20 K
R33. R36, R39 - 10 K
R27 - 2 K
R38 - 7.5 K
R40, R41 - 5.6 K

Capacitors

C1, C8, C10 - 25 micro farad(mf)
C2 - 2000 pf
C3 - 0.01 mf
C4 - 47 pf
C5 - 50 mf
C6, C7 - 0.25 mf
C9 - 1500 pf
C11, C12, C13, C14 - 0.1 mf

Diodes

D1 - 3.9V, 400 mW zener diode
D2, D3, D4, D5 - OA91 diode
D6 - OAZ202, 5.6V zener diode

Transinstors

T1, to T7 - 2N2926 (NPN)
T8, T9 - 2N2925 (NPN)
T10 - BFY51 (NPN)
T11 - 2N3702 (PNP)

O/A — Integrated circuit operational amplifier, PLESSEY TYPE SL702B.

T1 needed to change the state of T2. Transistors T1 and T2 form the pulse shaper and squarer stage. T3 and T4 are emitter follower buffer stages, and each supplies a differentiating stage. Capacitor C2 and resistance R6 form the differentiator while C3 blocks back any d.c. and the diodes D2, D3, D4 and D5 allow only one polarity of pulse to pass. The independent buffering of the pulses by T3 and T4 prevents any interaction between the two channels 'A' and 'B'.

Having prevented any interaction of the channels on one another, the pulses are then combined at the bistable vibrating stage, T5 and T6, and the frequency of vibration is doubled (see Fig. 10.6) because both the positive-going and negative-going zero-crossovers of each wave are used. Transistors T7 and T8 form a cascaded buffer to decouple the next filter section. Ballast capacitors C5 and the combination of R20 and C8 stabilize the rail voltage and eliminate high frequency oscillations.

The operational amplifier O/A is an integrated circuit. The zener diode D6 allows the output from O/A to swing both positive and negative while R12, R16, R18, C7 and C6 form a low-pass filter (see Sect. 10.3.1.2). An adjustable d.c. bias controls the level of the signal and provides the necessary small off-set required by the internal circuitry of the O/A. Since R18 = 33 K and R12 = 47 K, the d.c. gain of the O/A is 33/47 and the incoming siganl which swings between - 7V and + 7V is attenuated to values within the unsymmetrical + 6V and - 7V capability of the integrated circuit.

Transistor T9 forms a buffer to the 100 Hz Twin-T filter and T10 is a buffer to the 300 Hz Twin-T filter while T11 buffers the external load.

The relationship between the output voltage V_o(Fig. 10.5) and the rotor angle, appears as a saw- tooth wave in the calibration curve of Fig. 10.7. Good linearity isachieved over the range from -90° to $+ 90^{\circ}$ with a sensitivity of 4.22 mV/deg which can be increased by further amplification.

The circuit has been found reliable, robust and has the advantage of being linear. The bistable stage (Fig. 10.5) can be triggered by A2 and B2 only, to provide a linear output over a range from 0 to 360 degrees although the filtering becomes more difficult.

10.3.1.2 <u>The filter unit</u>

The filter unit accepts the superimposed square waves at H3(see Fig. 10.6) and gives out the d.c. component with a very much reduced a.c. component. It is designed in three stages.

(1) to allow the low frequency variations of the d.c. component to pass with minimum possible attenuation and delay. The theoretical transfer function of the practical angle device can however allow for the filter characteristics,

(2) to give a notched attenuation at 100 Hz because this harmonic and multiples of it are generated as a consequence of the bistable switching action.

(3) to give a notched attenuation at 300 Hz for the same reason.

The low-pass filter of stage (1), consisting of the operational amplifier and R12, R16, R18, C7 and C6, generates a transfer function with a second order polynomial[43] in the denominator.

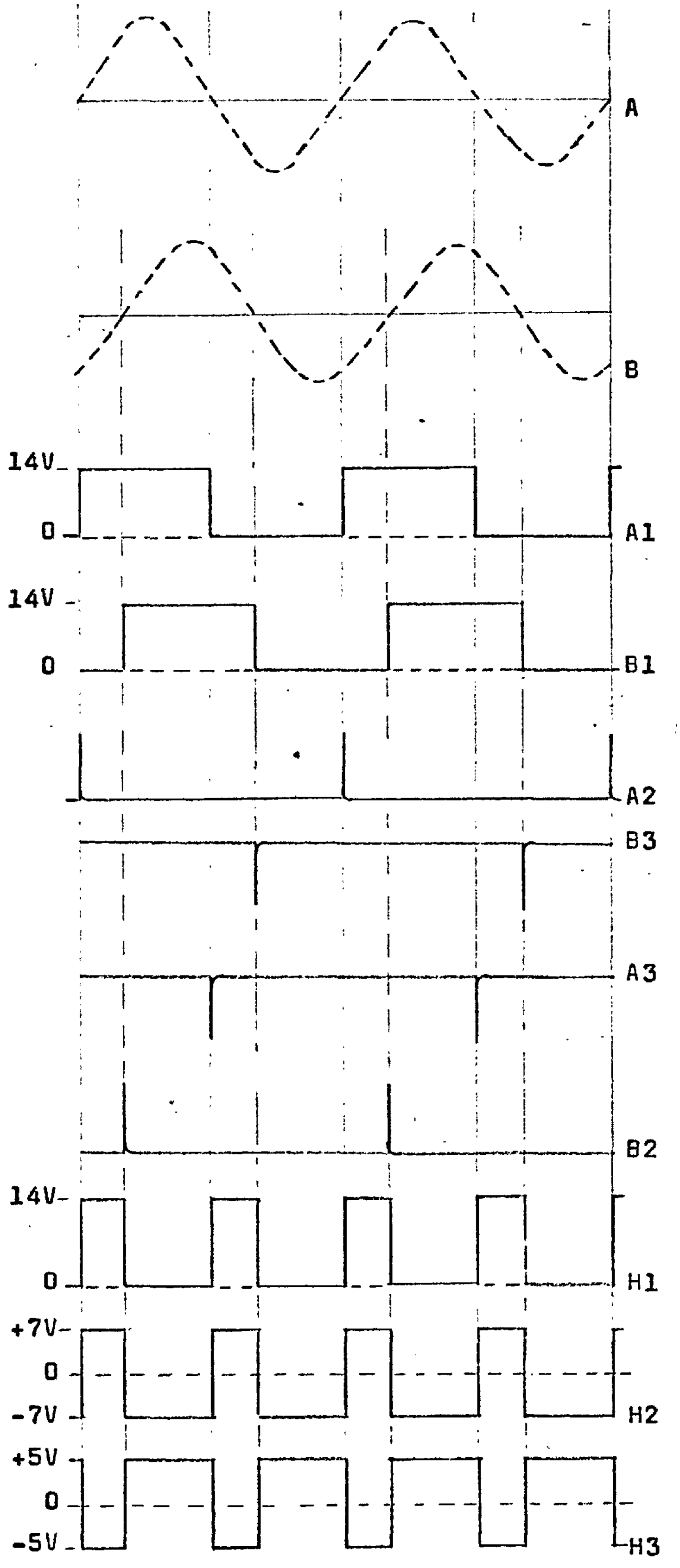

Fig. 10.6 Output voltages in Figs. 10.3 and 10.4 at different points with respect to earth for the case of 60 degrees phase angle.

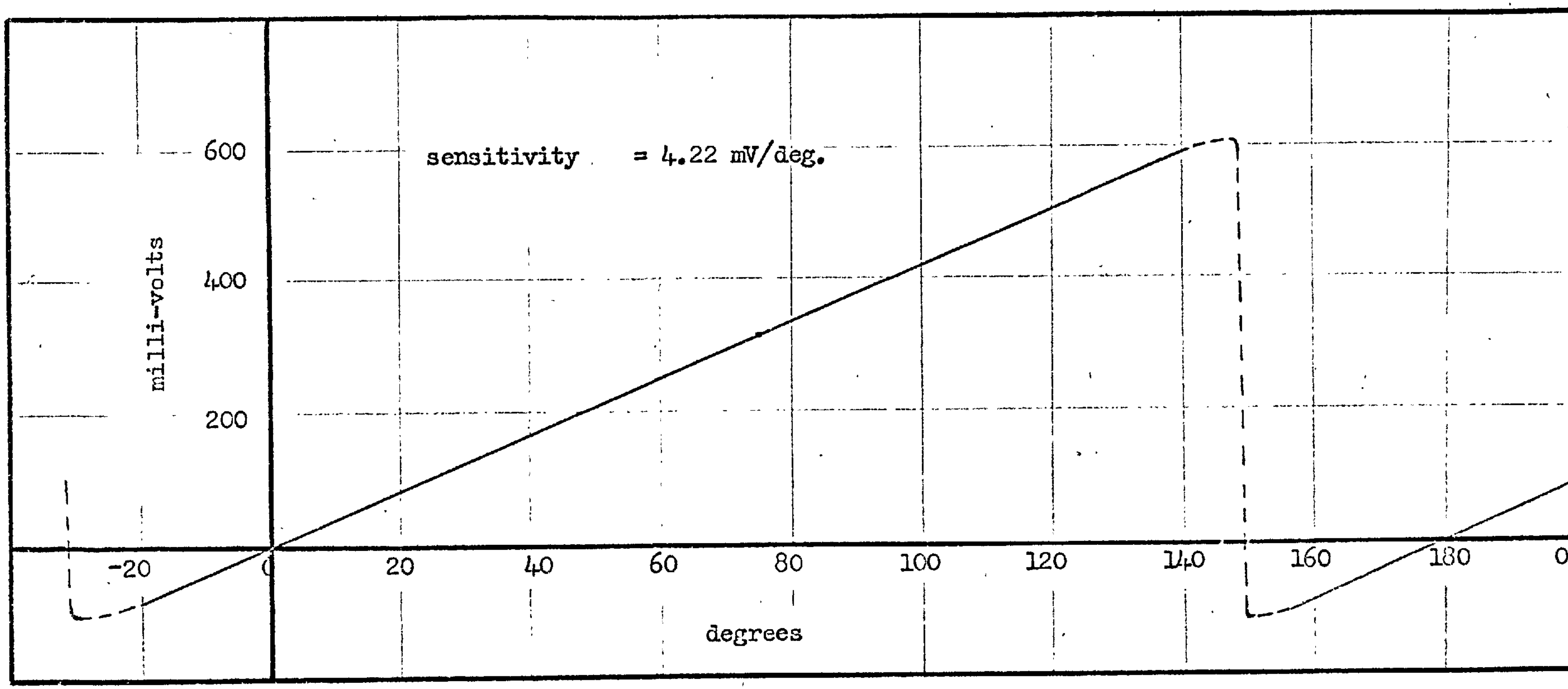

Fig. 10.7 Calibration of the angle device.

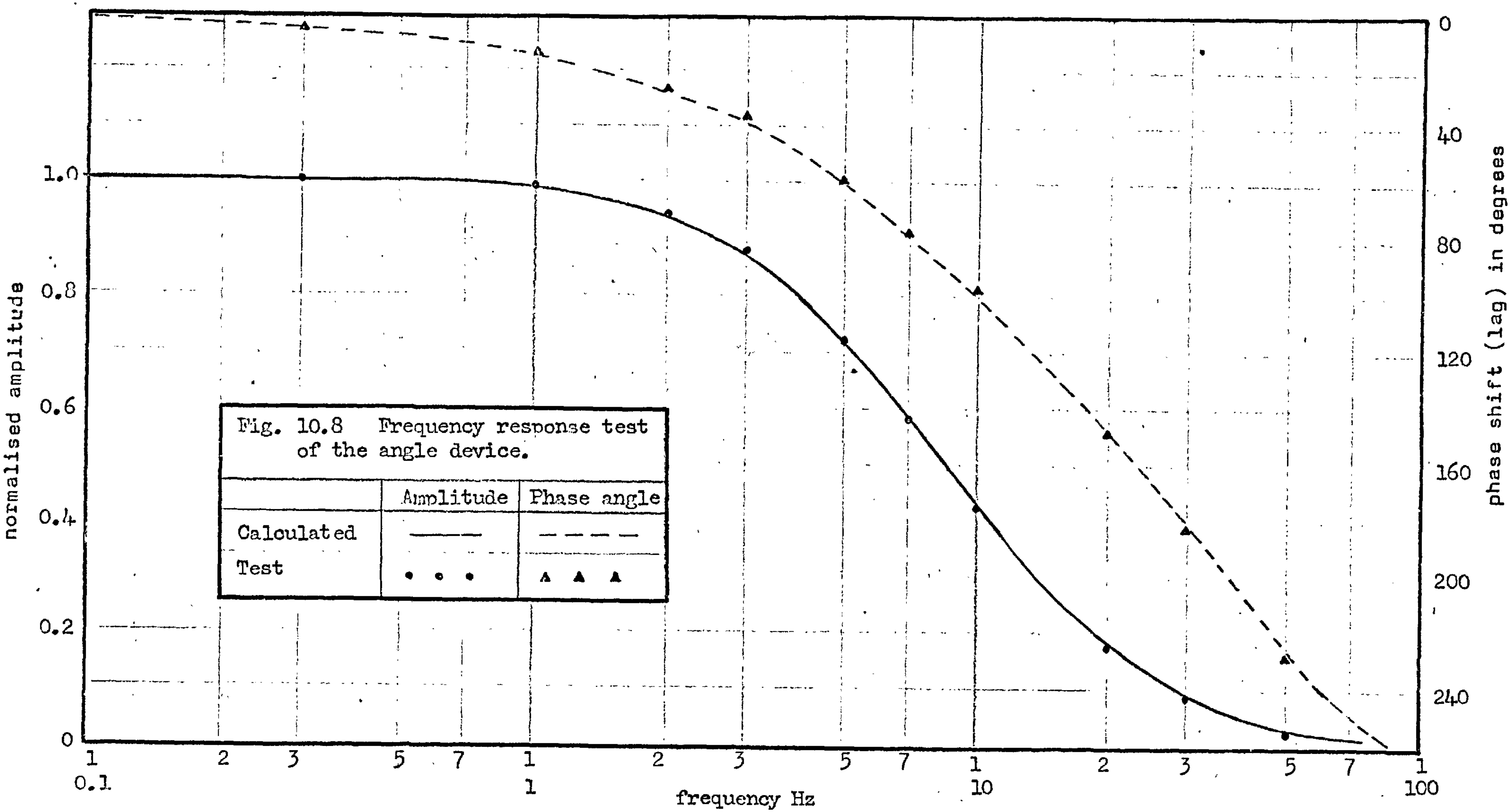

Fig. 10.8 Frequency response test of the angle device.

$$\frac{K}{Ap^2 + Bp + 1} \qquad (10.4)$$

where $K = - R18/R12$

$A = R16 \times R18 \times C6 \times C7$

$B = R16 \times R18 \left(\frac{1}{R12} + \frac{1}{R16} + \frac{1}{R18}\right) C7$

The numerical values of these coefficients were chosen to obtain an attenuation of 12 db per octave from about 12 Hz onwards.

The Twin-T filters[44] generate imaginary zeros to suppress 100Hz, 300 Hz with two transfer functions each of the form

$$\frac{1 + \tau^2 p^2}{\tau^2 p^2 + 4\tau p + 1} \qquad (10.5)$$

when the filter is balanced. The numerical values of all filter components appear in Table 10.4.

A transfer Function Analyser was used to determine the frequency response of the operational amplifier and filters. It was assumed that the transistor circuits before the O/A (see Fig. 10.5) produced negligibible time delay. The test results appear in Fig. 10.8 together with results calculated from Eqns. (10.4) and (10.5) for the three filter stages.

10.3.2 The voltage feedback signal

A d.c. signal proportional to the terminal voltage is obtained by using the same circuit as in Ref. 3. Six silicon diodes are used in a rectifier bridge circuit. Three single phase transformers with centre-tapped secondary windings isolate the bridge from the three phase terminal voltage and are connected in delta on the primary and six phase star on the secondary side. The dominant harmonic frequency because of the rectifier bridge circuit is 300 Hz, it is attenuated by a Twin-T filter section. Higher noise frequencies are attenuated by low-pass R-C filter sections in cascade. For low frequencies relevant to this study, it is fair to assume that the rectifier and filters do not introduce any appreciable phase shift .

10.4 The Regulators and Associated Circuitry

The simulation of the angle and voltage regulators was done on a small analogue conputer. In the following sections the regulators and associated circuitry are described.

10.4.1 The angle regulator

Two alternative types of torque winding regulators were used, namely, a proportionate angle regulator and a regulator with proportionate and derivative signals. The proportionate regulator can be treated as a special case when the derivatives are omitted. In Fig. 10.9 is shown the derivative regulator with the following transfer function.

$$\left(1 + \frac{.1p}{(1 + .01p)(1 + .01p)} + \frac{.02p^2}{(1 +.01p)(1 +.01p)(1 +.02p)(1 +.01p)}\right) \frac{K_t}{1 + \tau_t p} \qquad (10.6)$$

The frequency response curves in Fig. 10.10 are for different values of τ_t in expression (10.6). The value of τ_t can be made zero to represent a thyristor excitation system, or it can have a finite value to represent the short-circuit field time constant of the conventional d.c. exciter of a large alternator.

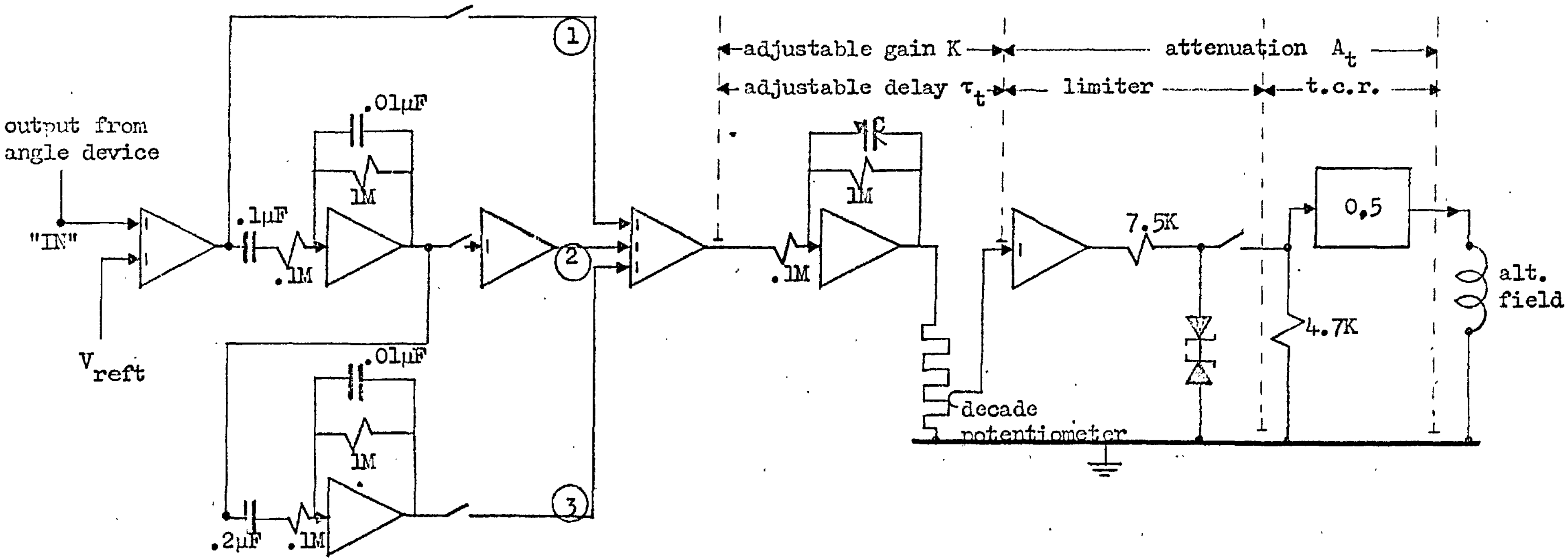

Fig. 10.9 The angle regulator.

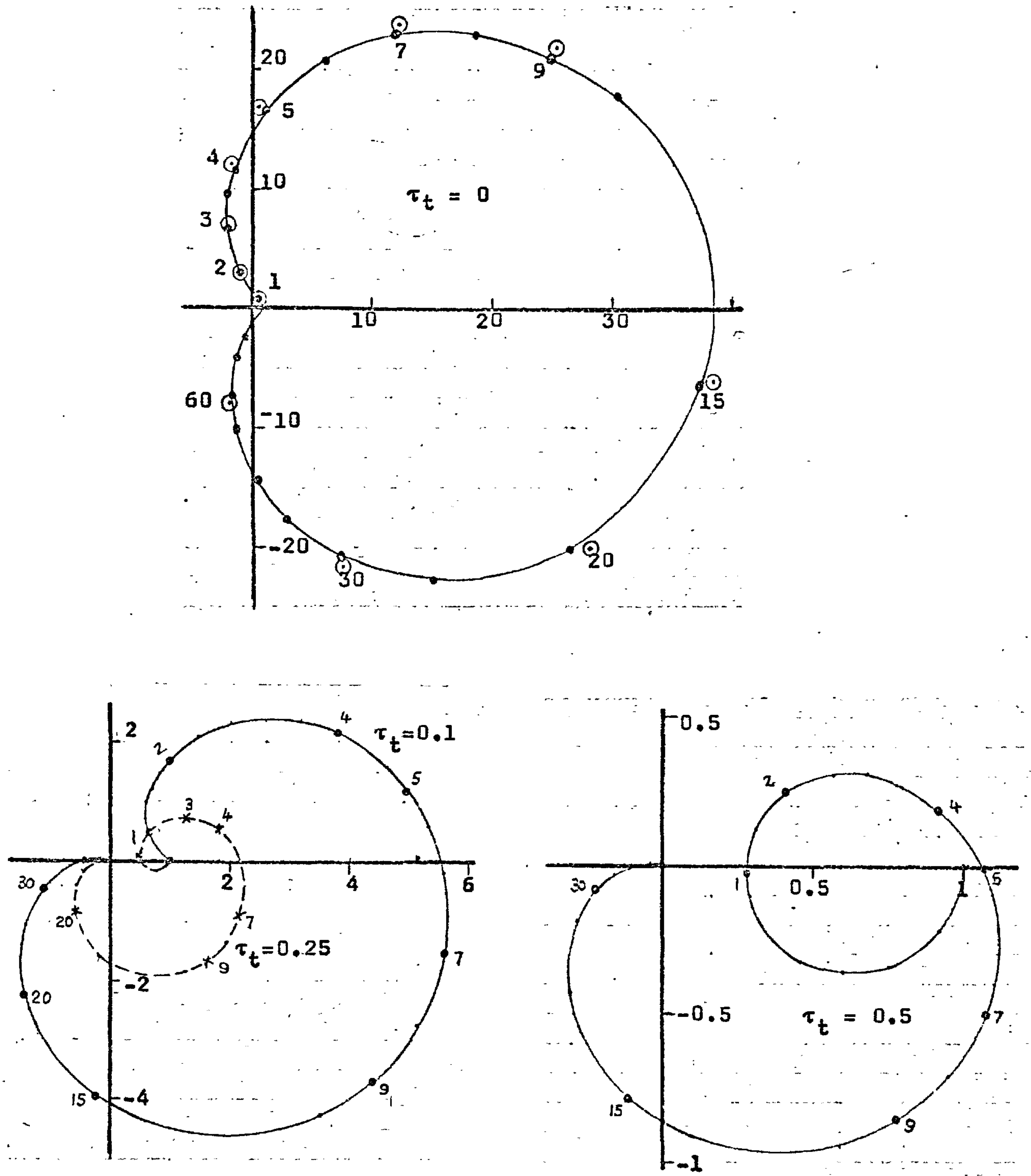

Fig. 10.10 Frequency response curves for the derivative angle angle regulator.

× × ∘ ∘ • calculated; ⊙ ⊙ measured

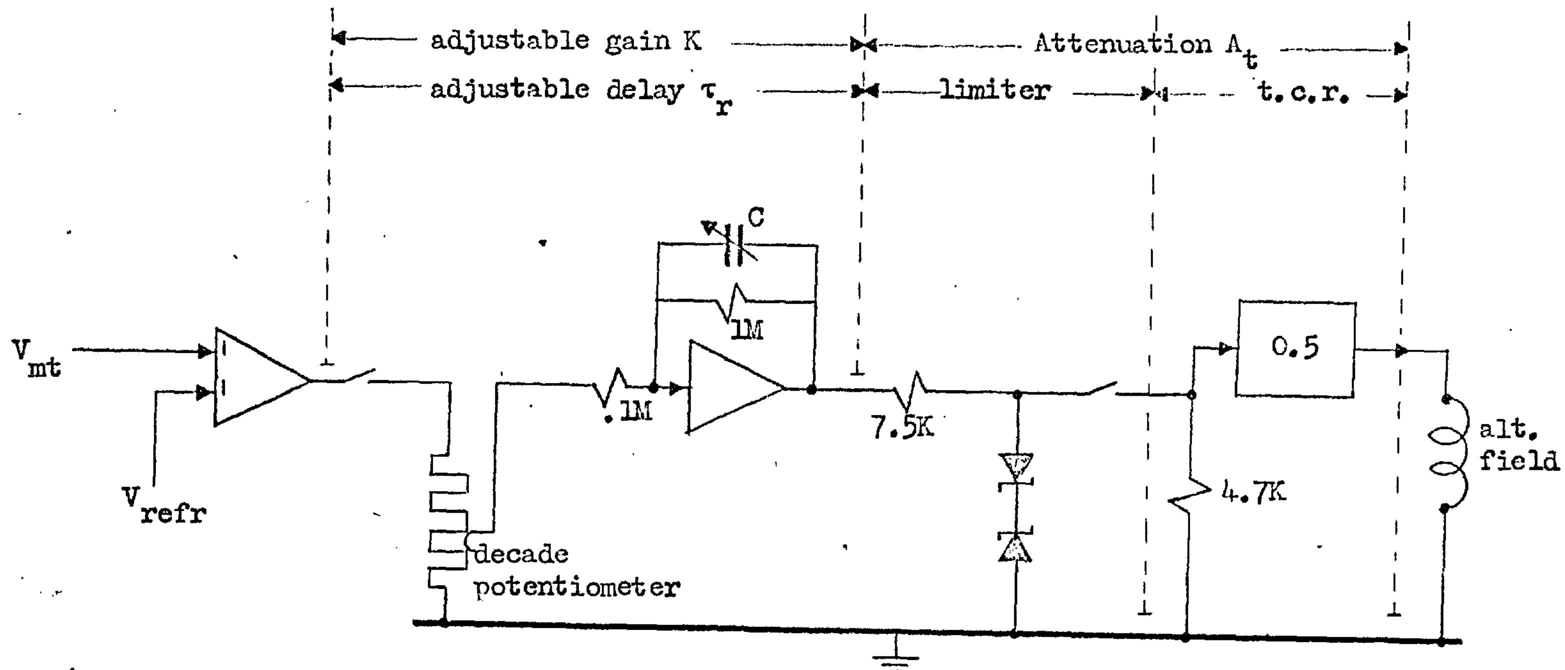

Fig. 10.11 The voltage regulator.

In the circuit of Fig. 10.9 conventional differentiating circuits[45] are used to differentiate at low frequencies but to cut off high frequencies or noise, since the frequency range in this study is 0 - 4 Hz. However, in theoretical computations the effect of delays is also considered, apart from the single main time delay τ_t.

The angle signal from the angle device in Fig. 10.5 is applied to the point marked 'IN' on Fig. 10.9. The circuit marked '1' carries the signal straight to the summing amplifier, the circuit marked '2' brings the first derivative and the circuit '3' the second derivative signal. The total signal passes through an amplifier with a time delay and the level is then adjusted by a precision decade potentiometer which controls the gain K_t. The signal is carried through a buffer amplifier and a limiter to the input of the time constant regulator. The limiter circuit consists of two back to back Zener diodes which conduct if the signal exceeds $\pm$ 16 volts and is used to protect the subsequent time constant regulator circuitry. This protection is of particular importance when the feedback signal contains a first or second derivative component which may increases rapidly to a large value during transient disturbances.

The circuit described above represents the proportionate angle regulator when the fist and second derivative feedback circuits marked '2' and '3' are omitted.

10.4.2 The voltage regulator

The analogue simulation of a single delay proportionate voltage regulator is shown in Fig. 10.11. An adder is used to sum up the feedback signal and the reference V_{refr} which is used to adjust the steady-state excitation of the system. A precision decade potentiometer is used to adjust the gain K_r while the next stage introduces the single time delay τ_r. The signal is finally passed through a limiter (see Sect. 10.4.1) before it reaches the time constant regulator input. The transfer function is

$$\frac{K_r}{1 + \tau_r p} \tag{10.7}$$

Equations (10.6) and (10.7) are used to calculate the results in Chapter 11.

---o0o---

CHAPTER 11

11. Comparison of Measurements and Computations

11.1 General

The micro-machine system shown in Fig. 10.1 was connected to the fixed sypply, referred to as an infinite bus. Stability limit studies were carried out to determine the reactive power Q_o at which stability was lost, for a given active power P_o and given gains for a voltage regulator and an angle regulator when used as follows:

1. a proportionate bus "angle regulator only" (see Sect. 9.1)
2. a proportionate terminal "angle regulator only"
3. a proportionate terminal angle regulator and a proportionate voltage regulator
4. a derivative terminal angle regulator which had proportionate-, first derivative and seond derivative terms, and a proportionate voltage regulator.

The angle regulator and voltage regulator each had a single time delay τ and tests were done for different values of τ_t and τ_r. Results were obtained for a reference angle of 33.75^o only.

In the present chapter the experimental results are presented together with computed values which neglect the effects of armature and line resistance as well as saturation.

11.2 The Stability Code

Instability was most clearly indicated by the rotor angle variation $\Delta\delta$, relative to the equilibrium condition and it was decided to consider the condition of equilibrium unstable if the rotor angle

1. drifted by 2° from equilibrium, and subsequently did not settle back within two minutes,
2. built up an oscillation of 2° about the mean, either as a limit cycle or as an increasing oscillation.

It was not easy to find a precise point at which this occurred, particularly because of erratic variations of the a.c. and d.c. supplies and the alternator field currents. To minimise the possibility of erratic judgement because of erratic variations in the supplies, the stability experiments were conducted during periods of steadier load conditions in the laboratory. The erratic variations in the alternator field currents were caused by alternator brush contact fluctuations in a low resistance circuit but this was improved by adding resistance into the field circuit (see Sect.10.1.2).

For bus angle feedback, the equilibrium is maintained at $\delta = 33.75^{\circ}$ for any power level, but with generator terminal angle feedback it is only true at zero power. At any power level, the rotor deviation is determined by the angle $(\delta - \delta_t)$ which increases with the increase in negative reactive absorption. Within the stability limit the rotor adjusts itself to the new condition. Hence for assessment of the stability limit the stability code was applied at each new equilibrium condition.

11.3 The Regulator Constants

11.3.1 The angle regulator gain K_t

The angle regulator (see Fig. 10.9) gain K_t depends on several factors, namely

A_t ; the fixed attenuation of the limiter and time constant regulator, numerically equal to 0.1925

K_δ : the angle device constant, numerically

$$= \text{angle device sensitivity } \left(\frac{\text{volts}}{\text{radian}}\right) \times \frac{1}{\text{base field voltage}}$$

$$= 0.422 \times 57.3 \times \frac{1}{683.4} \quad \text{(see Fig. 10.7 and Table 10.2)}$$

$$= 0.0353 \quad \frac{\text{p.u. voltage}}{\text{radian}}$$

K : the adjustable amplifier gain constant (see Fig. 10.9).

Thus $K_t = A_t \times K_\delta \times K$

$$= 0.1925 \times 0.0353 \times K$$

$$= 6.8 \times 10^{-3}\ K$$

11.3.2 The voltage regulator gain K_r

The voltage regulator (see Fig. 10.11) gain K_r depends on several factors, namely,

A_t : the fixed attenuation of the limiter and t.c.r. (see Sect. 11.3.1)

R_e : the rectifier constant; the rectified output is treated as the terminal voltage, (see Sect. 9.1), numerically

$$R_e = \text{rectifier conversion factor} \times \frac{\text{base armature}}{\text{base field voltage}}$$

$$= 0.1575 \left(\frac{\text{d.c. volts}}{\text{a.c. line volts r.m.s.}}\right) \times \frac{220 \text{ (a.c. line volts, r.m.s.)}}{683.4 \text{ (d.c. volts)}}$$

$$= 0.0507$$

K : the adjustable amplifier gain constant (see Fig. 10.11)

Thus $K_r = A_t \times R_e \times K$

$$= 0.1925 \times 0.0507 \times K$$

$$= 9.76 \times 10^{-3} K$$

11.4 Starting of the System

In the stability experiments including a voltage regulator the system shown in Fig. 10.1 was synchronized without any current in the torque winding. The prime mover control was adjusted to give zero active power P_o at the infinite bus. The reactive power Q_o at the infinite bus was brought to zero by adjusting V_{refr} (see Fig. 10.11). The t-winding was then energised and the d.c. off-set bias (see Sect. 10.1.2) used to adjust the steady torque winding current to zero. The input signals to the angle device (see Fig. 10.5) were switched on and the circuit to the angle regulator (see Fig. 10.9) closed. The output from the angle divice and regulator was adjusted to zero by means of the angle regulator reference voltage V_{reft} in Fig. 10.9. A precision decade potentiometer was used to adjust the regulator gain K_t below the limiting level and the torque winding feedback circuit was closed. Before any experiments were conducted the system was loaded to $P_o = 0.8$ p.u. and $Q_o = 0.6$ p.u. and was run for about half an hour to establish a reasonable steady temperature in all the windings.

The above procedure was followed for most of the stability tests except for the cases without a voltage regulator, when the reactive winding excitation was adjusted manually. When there were derivative components in the angle feedback, the various derivative circuits in the regulator (see Fig. 10.9) were the last to be closed after synchronization and the first to be opened before synchronism was lost.

11.5 Steady-state Stability Limit Curves for Proportionate Bus Angle Regulator

After starting and warming of the set (see Sect. 11.4) the active power at the infinite bus was adjusted to say 0.2 p.u. and the regulator gain K_t was adjusted by the potentiometer to a stable value (see Sect. 10.4.1). To make the micro-machine system deliver negative vars the positive excitation of the reactive winding was decreased in small steps to zero and then increased in the negative direction. After every small change in the excitation the rotor angle was observed with the aid of a stroboscope for about five minutes. The rotor was considered to be stable, if after the disturbance it settled down to equilibrium according to the stability code, otherwise it was unstable.

The regulator gain K_t was increased in steps and the above procedure was repeated to locate the steady-state stability limit. The active power P_o was adjusted to a new value and the entire process repeated to obtain a new set of steady-state stability limit points.

The experimental and computed results shown in Fig. 11.1 agree well in the low gain region AB but the agreement is less good at higher gains in the BC region. The discrepancy may be because the instability in the BC region is of the oscillating type and computed results are sensitive to small errors in the measured transient-and subtransient parameters. However, in general, Fig. 11.1 shows that the active power P_o does not significantly influence the results.

11.6 Steady-state Stability Limit Curves for Proportionate Terminal Angle Regulator

The experimental stead-state stability limits for the proportionate terminal angle regulator were obtained in a manner similar to that described in Sect. 11.5.

Fig. 11.2 shows fairly good agreement between experimental and theoretical results in the low gain region but, as in Fig. 11.1, the agreement in the high gain region is less good for the same reasons as stated in Sect. 11.5. However, an increase in the active load P_o has the same effect on both experimental and theoretical results.

11.7 Steady-state Stability Limit Curves for Proportionate Terminal Angle Regulator and Proportionate Voltage Regulator

The experimental steady-state stability limits for a system with an angle regulator and a voltage regulator (a.v.r.) were obtained by using a value of K_r within the stable region before testing for the stability limit in the same manner (see Sect. 11.5) as for an angle regulator only. The active power P_o was changed and the procedure repeated to obtain a curve for each value of P_o, and the results are shown in Fig. 11.3(a). The entire process was repeated for a different value of K_r and the results appear in Fig. 11.3(b).

Theorectically as well as experimentally, an increase in power increases the maximum reactive absorption Q_o in Fig. 11.3 at any value of K_t, irrespective of whether K_r is high or low. Although there is fair agreement between comuted and measured points in the low gain region AB, it is not at as good in the high gain BC region, for reasons discussed in Sect. 11.5. On the whole, the agreement in Fig. 11.3(b) is less favourable than in Fig. 11.3(a) possibly because of the higher voltage regulator gain.

The results in Fig. 11.3 also illustrate that a combination of two simple delay type regulator systems is capable of increasing the maximum negative reactive absorption to a useful value greater than 1 p.u. for all values of power if K_t is less than about 9×10^{-3}.

11.8 Steady-state Stability Limit Curves for Derivative Terminal Angle Regulator and Proportionate Voltage Regulator

The transfer function, including first and second derivative angle terms, (see Eqn. 10.6) was simulated on the analogue computer (see Fig. 10.9) and K_t was adjusted on the potentiometer as for the proportionate angle regulator. The stability limit tests were carried out for different values of angle regulator gain K_t, active power P_o, and voltage regulator gain K_r in the same way as described in Sect. 11.7

Fig. 11.4 shows some of the experimental computed limits for a time delay of 0.5 seconds in each regulator. The overall agreement between computed and measured values is fairly good except for the very high gain region CD. In this region, the natural frequency of oscillatory instability is relatively low and difficult to distinguish from a drift due to fluctuations in the supply.

Hence, there is greater uncertainty associated with measurements in this region. Compared with Fig. 11.3, Fig. 11.4 shows that the maximum value of Q_o is about the same (- 1.2 p.u.) at the same value of $K_t = 3 \times 10^{-3}$. However for a minimum $Q_{o\ max}$ of - 1 p.u., $K_{t\ max}$ is about twice the value without derivative compensation (also see Sect. 9.4.6).

The derivative angle terms give little increase in negative reactive absorption when $\tau_t = \tau_r = 0.5$ compared to $\tau_t = \tau_r = 0.0$. Large d.w.r generators with conventional d.c. excitation systems will therefore only have a marginal increase in $Q_{o\ max}$ and little gain in $K_{t\ max}$ when derivative compensation is added in the form suggested by Eqn. (10.6).

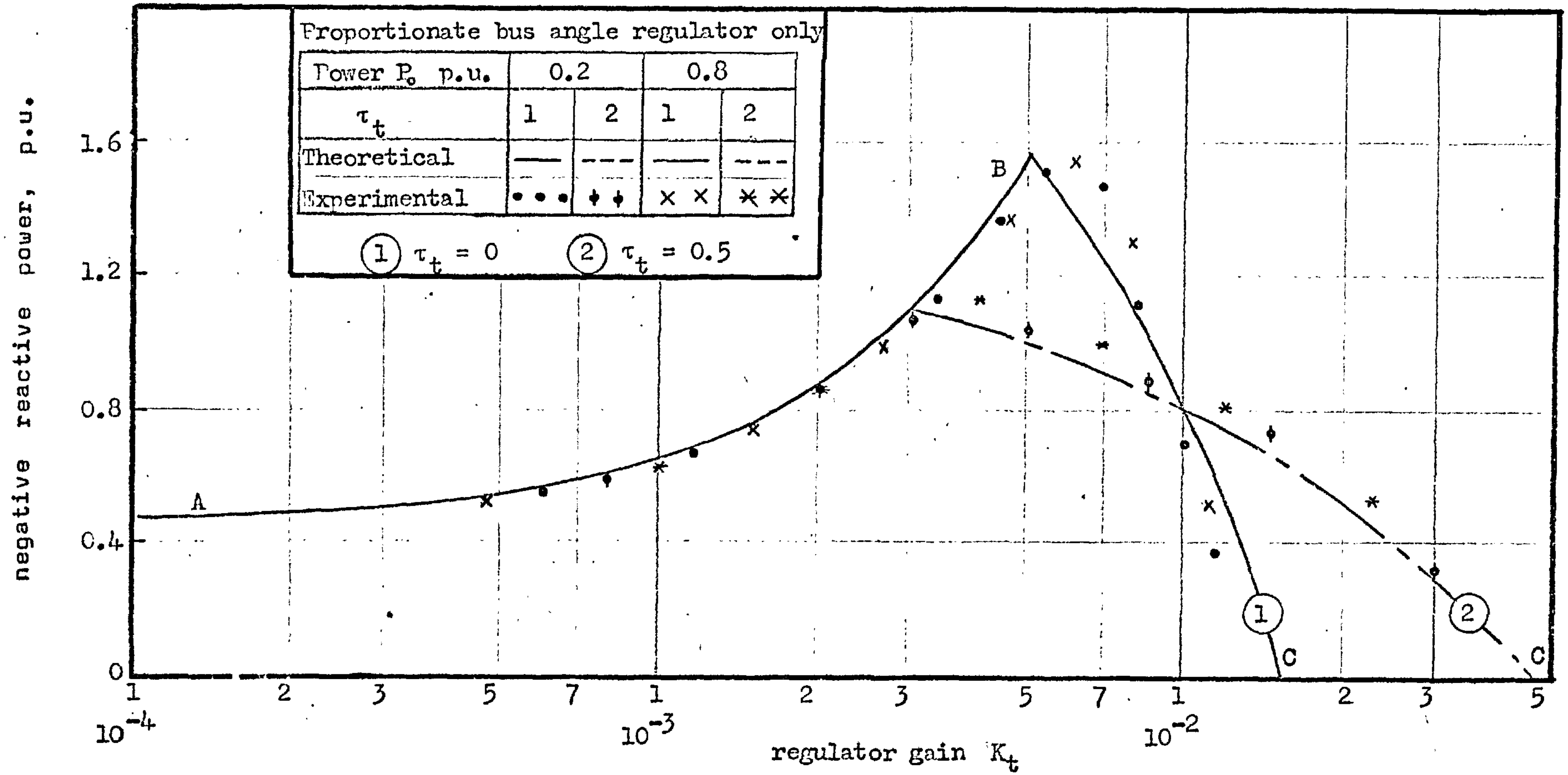

Fig. 11.1 Steady-state stability limit curves

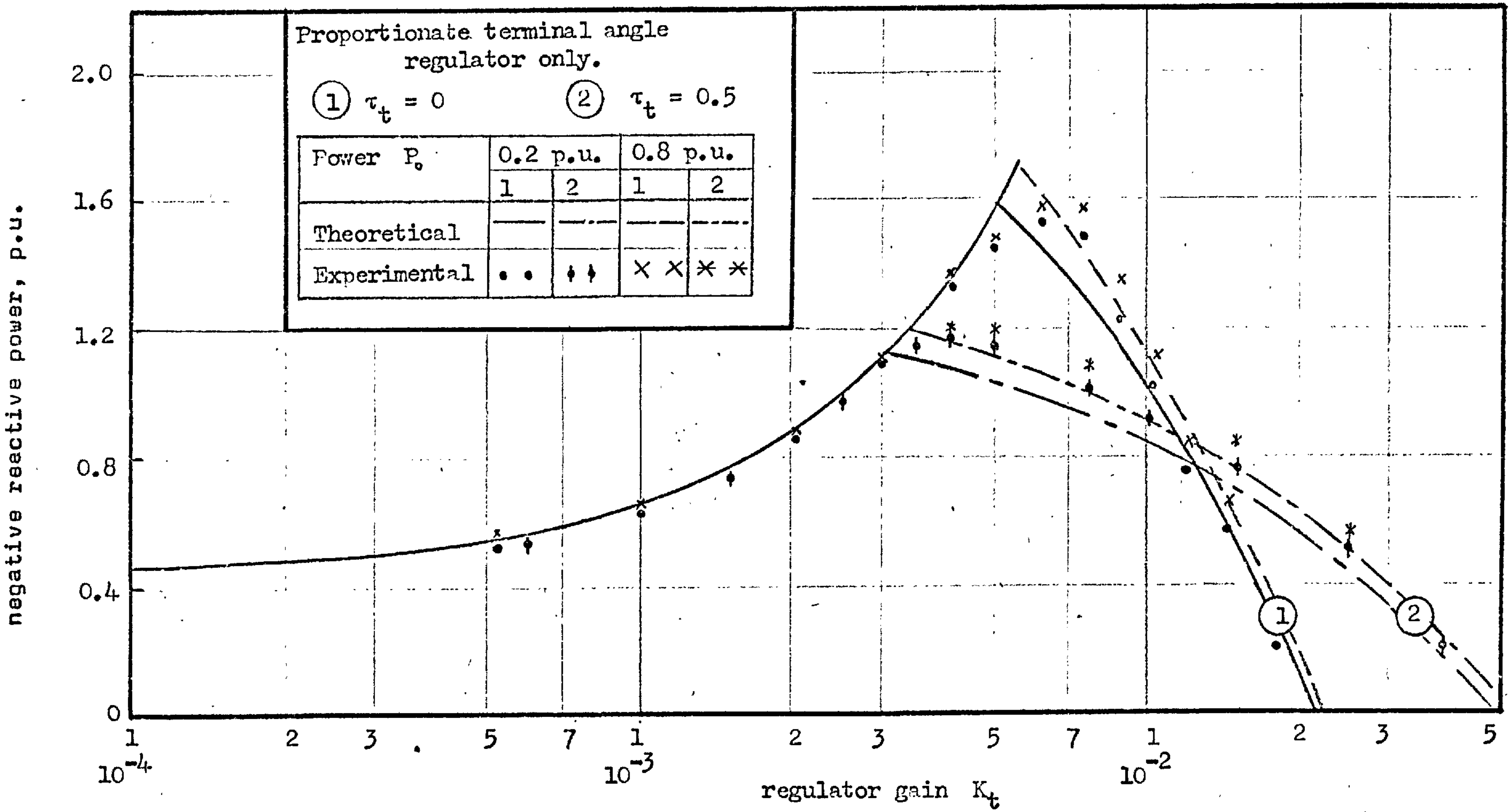

Fig. 11.2 Steady-state stability limit curves.

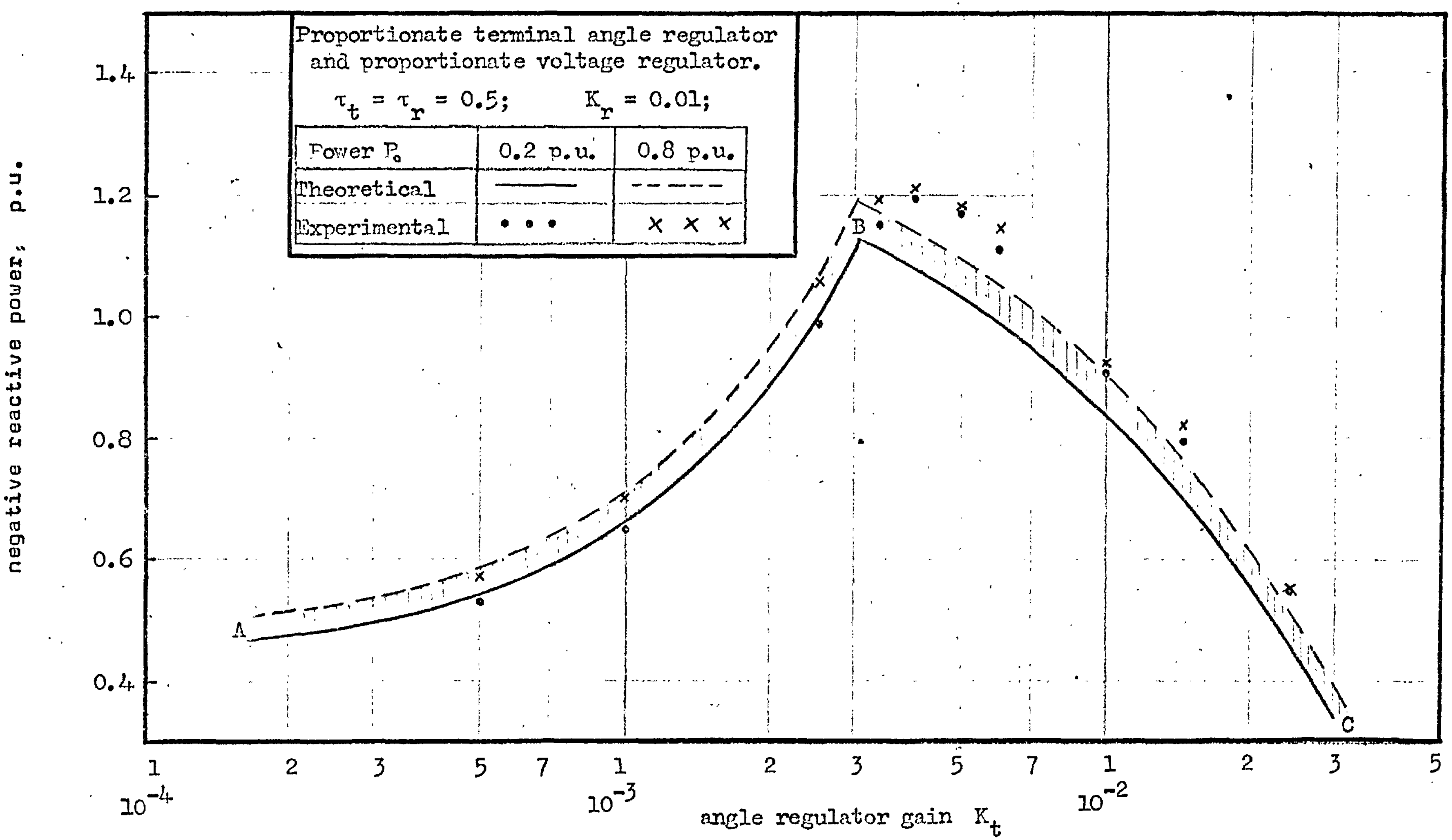

Fig. 11.3(a)   Steady-state stability limit curves.

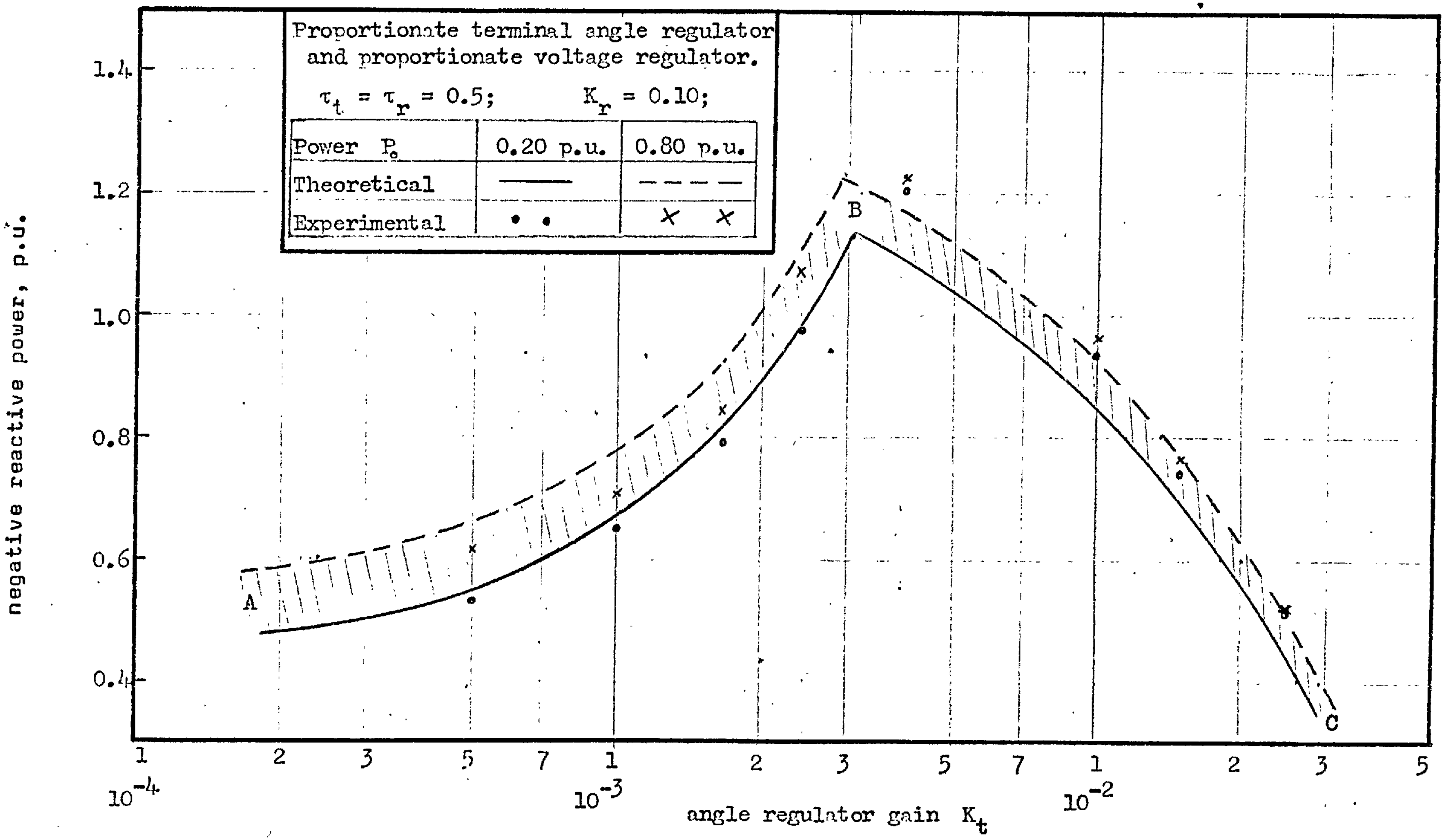

Fig. 11.3(b) Steady-state stabiltity limit curves.

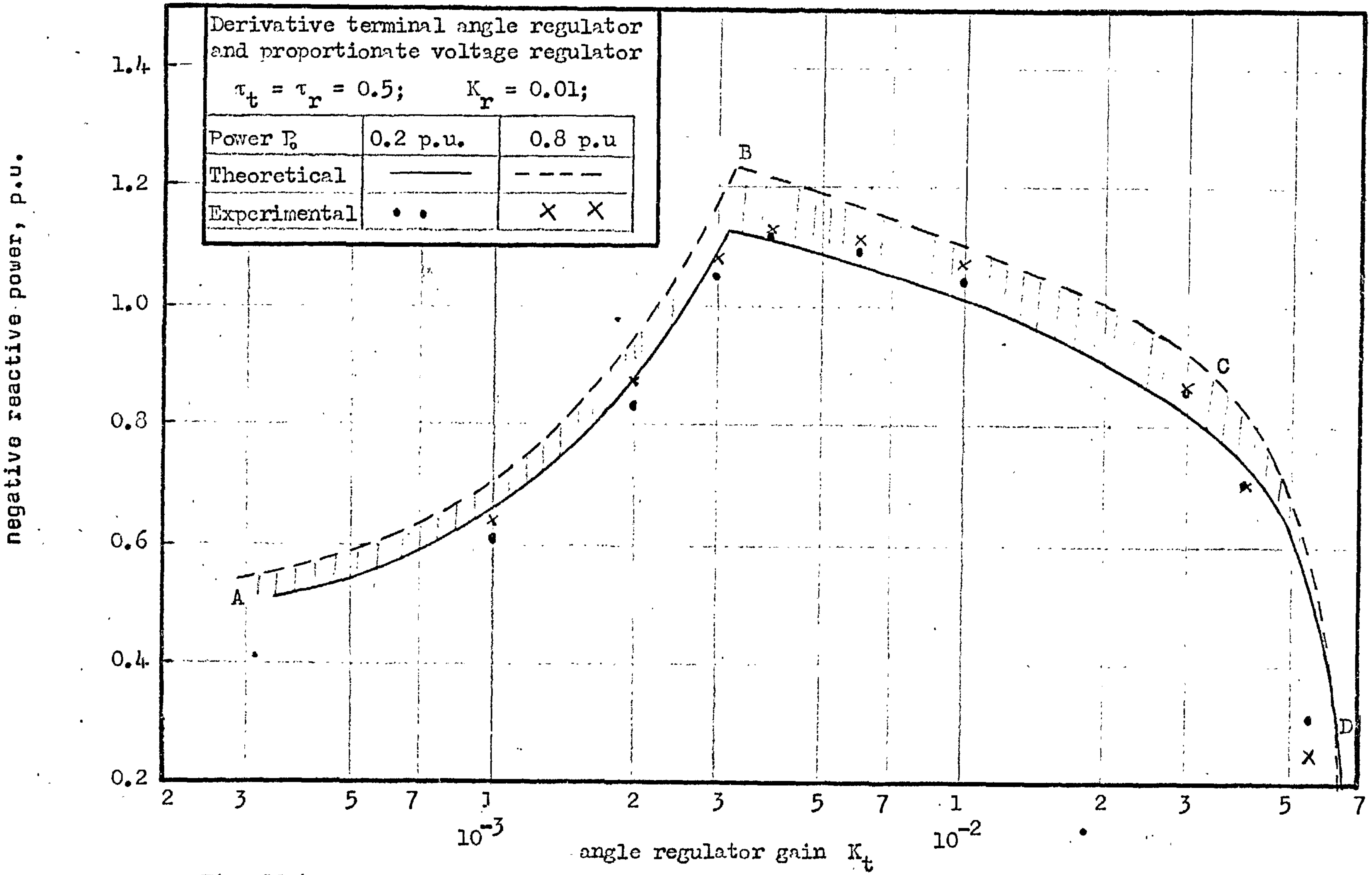

Fig. 11.4 Steady-state stability limit curves.

CHAPTER 12

12. CONCLUSIONS

The purpose of the work described in this thesis has been to investigate methods of representing machines in order to study the steady-state and transient stability of a synchronous generator connected through a transmission line to a fixed supply.

Two types of machines have been studied viz. a synchronous generator with a conventional single field winding on the rotor d-axis, referred to as a conventionally wound rotor (c.w.r.) machine; and a synchronous generator with two separate field windings on the rotor, referred to as a divided winding rotor (d.w.r.) machine. In the case of the c.w.r. machine, the emphasis has been on the transient behaviour after a symmetrical three-phase short-circuit. In the case of the d.w.r. machine the main investigation has been concerned with steady-state stability during small disturbances, although calculations were also made for the transient stability after a three-phase fault.

Different types of transient disturbances have been analysed and compared by using the equivalent two-axis circuits and the Laplace approach to find the different expressions for the electromagnetic torque of the c.w.r. machine. It was found that the transient torque after different disturbances consisted of an individual component for each disturbance in addition to three main common components. viz. the synchronizing- and saliency torque, the torque due to field flux decrement and the damping torque.

Different methods of analysing the synchronous machine transient response have been compared, including a new accurate method which does not neglect the rate of change of the armature flux linkages Ψ_d and Ψ_q. It has been shown that an angular "back swing" in the rotor can occur when a three-phase fault is applied. The back swing is caused by high transient losses which cause a unidirectional braking torque during the initial period of the fault. The braking torque can be calculatd when the $p\Psi_d$ and $p\Psi_q$ terms are not neglected in the expressions for the armature axis voltages. The accurate method also allows more fully for the action of the damper winding than simply by means of a constant damping coefficient. An approximate method which allows for damping but not for $p\Psi$ has also been used for calculations and comparisons have been drawn between the approximate and accurate results.

For the accurate method a new set of first order differential equations have been developed in a form particularly suitable for a step-by-step solution on a digital computer. The axis flux linkages and currents which change at about supply frequency, are solved simultaneously. The time interval for a step-by-step calculation must be short compared with the period of the a.c. cycle and hence requires a large amount of digital computer time. Efforts were made to reduce the time by using more powerful methods of integration and by rearranging the order in which equations were being solved. The best achievement permitted a 5 milli-second step length when the fifth order Kutta-Merson method was used.

Tests and calculations of the back swing phenomenon have been made for a c.w.r. micro-machine system while calculations have also been made for a 30 MW c.w.r. turbo-alternator.

A detailed study has revealed the effect of the short-circuit braking torque when

1. the machine is at a reduced load,
2. the tie-line reactance is increased,
3. the inertia constant is small.

The conclusion can be drawn that in countries where the load centres are not far apart and transmission lines are relatively short, as in England, a short-circuit anywhere along a transmission line may be close enough to the alternators to cause back swing. If the load is remote from the generating centre, as in the case of systems with hydro-stations, a back swing may occur alter a fault if the generator was relatively over-excited in order to maintain voltage stabiltity at the receiving end. For such conditions an accurate result is not obtained unless the $p\Psi$ terms are included. When generators have rectifier excitation, the accurate method must be used for any transient condition during which the field current falls to zero. Induction motor recovery studies are also affected by the $p\Psi$ terms since the short-circuit braking torque increases the deceleration.

It is well known that the stable operating range of a c.w.r. generator can be extended under leading current conditions, by means of an a.v.r. acting on the single direct axis field, but such a system has limitations at light load conditions. The use of a second field winding on the quadrature axis of the rotor, excited by a continuous feedback rotor angle signal, showed[4] a dramatic improvement in the stable operating range for all values of load. Another scheme[5] showed that a machine with two divided windings on the rotor (d.w.r.) could be controlled to operate stably beyond the normal c.w.r. range during steady-state conditions and that it also had an improved transient response. In the light of the c.w.r. machine stability limitations, and the promise held out by the d.w.r. machine, it was decided to investigate more closely the stability problems of the latter.

The non-linear equations have been developed, following the generalized machine theory, for a machine with a field winding on the d-axis as well as on the q-axis. As the field windings of a d.w.r. machine are not necessarily on the d- and q-axis, a new transformation matrix has been established to replace, mathematically, the two physical field windings by two fictitious field windings, one on each axis. The equations were then used to calculated the transient response after a three-pahse fault on a hypothetical[5] 30 MW d.w.r. turbo-alternator and also to study the steady-state stability of a micro-machine with a divided winding rotor.

The transient stability calculations have used the approximate method as well as the accurate method. A new set of first order differential equations have been developed in the same way as for the c.w.r. machine with the difference that the field winding on the q-axis introduces an additional equation. The results corroborate the earlier deductions about the back swing phenomenon, although the effect seems less severe perhaps because the rotor movement of the d.w.r. machine is more constrained by the feedback control signals.

Steady-state stability tests and calculations of the d.w.r. micro-machine have shown fairly good agreement and it can be concluded that:

1. The torque winding current of a d.w.r. machine controls the active power although it also affects the reactive power. The reactive winding current controls the reactive power only, and a suitable feedback can therefore regulate the reactive without affecting the active power. However, all this is based on the assumption of zero saliency and that, by means of a feedback signal to the torque winding, the rotor is held at a constant angle ϕ_r with reference to a fixed supply.

When the feedback signal is taken with reference to the terminal voltage, the above conclusions are only approximately true because the rotor is not held at a fixed angle.

2. The angle feedback to the torque winding acts as a stabilizing circuit for the terminal voltage feedback to the reactive winding. This means that the a.v.r. can have a gain so high that the system would be unstable if the stabilizing angle regulator were removed. Furthermore, a considerable change in the time delay of the a.v.r. has negligible effect on the steady-state stability although it may affect the transient response of the system. Conversely, the only effect from the a.v.r. seems to be a small improvement in the steady-state stability limit of a system with an angle regulator only. These conclusions lead to the following salient deductions:

(a) The a.v.r. design seems to be almost independent of the angle regulator and it is believed that the a.v.r. of a present large c.w.r. machine will most probably be equally suitable for a large d.w.r. machine in future.

(b) The stable operating range of a d.w.r. system with an angle regulator and a voltage regulator, is almost the same as a d.w.r. system with an angle regulator only.

Any improvement in the steady-state stability limit can probably only be achieved by an inherent improvement of the angle regulator stability.

3. It has been shown that the stability of the system with an angle- and a voltage regulator can e improved if the gain margin of the angle regulator is improved by including first- and second derivative compensating terms. Although the compensation provided a dramatic increase in negative reactive aborption when the regulators had negligible delay, it was less effective when both regulators had a delay of 0.5 seconds which corresponds to the short-circuit field time constant of a large d.c. exciter. However, the derivative angle regulator used, was by no means an optimum design and could be redesigned to give improved compensation at a given value of time delay.

---oOo---

APPENDIX I

THE ACCURATE METHOD OF ANALYSING A C.W.R. MACHINE

From Eqns. (4.12) and (4.13) the derivatives of the flux linkages Ψ_d and Ψ_q are found as

$$p\Psi_d = \frac{X''_d}{\omega} \cdot pi_d + (X''_d - X_a)\left[\frac{p\Psi_f}{X_{fd}} + \frac{p\Psi_{kd}}{X_{kd}}\right] \quad (A1.1)$$

$$p\Psi_q = \frac{X''_q}{\omega} \cdot pi_d + (X''_q - X_a)\,\frac{p\Psi_{kq}}{X_{kq}} \quad (A1.2)$$

Equating the right hand sides of Eqns. (4.1) and (4.24) yields

$$p\Psi_d + \nu\Psi_q + r_a i_d = \sqrt{2}\, V_{bd} - \frac{X}{\omega} \cdot pi_d - Ri_d - \frac{X}{\omega} \cdot \nu i_q \quad (A1.3)$$

The values of $p\Psi_d$ from Eqn. (A1.1) and of Ψ_q from Eqn.(4.13) are substituted into Eqn. (A1.3) which then contains the terms $p\Psi_{kd}$ and $p\Psi_f$. The expressions for these, given by Eqns. (4.14) and (4.16), are substituted into the modified Eqn. (A1.3).

After re-arranging the terms, an expression gor pi_d is found as

$$pi_d = a_1 i_d + a_2 \nu i_q + a_3\Psi_f + a_4\Psi_{kd} + a_5 \nu\Psi_{kq} + a_6 V_{bd} + a_7 v_f$$

and likewise for pi_q. The values of the constants a_1, a_2 etc.) see Eqn. (4.26)) are:-

$$a_1 = -\left(r_a + R + \frac{X_{md} g_1^2}{g_3 \omega X_{fd} T'_{do}} + \frac{g_1 g_3}{\omega\, X_{kd} T''_{do}}\right) \cdot \frac{\omega}{(X + X''_d)};$$

$$a_2 = -\frac{X + X''_q}{X + X''_d};$$

$$a_3 = \left(\frac{g_1}{X_{fd}T'_{do}} + \frac{g_1^2 X_{md}}{X_{fd}X_{fd}X_{kd}T'_{do}} - \frac{g_1 g_3}{X_{kd}X_{fd}T''_{do}} \right) \cdot \frac{\omega}{(X + X''_d)} ;$$

$$a_4 = \left(-\frac{g_1}{T''_{do}X_{kd}} - \frac{g_1^2 X_{md}}{g_3 X_{kd}X_{fd}T'_{do}} \right) \cdot \frac{\omega}{(X + X''_d)} ;$$

$$a_5 = -\frac{g_2 \omega}{X_{kq}(X + X''_d)} ; \qquad a_6 = \frac{\sqrt{2}\ \omega}{X + X''_d} ; \qquad a_7 = -\frac{g_1 \cdot \omega}{X_{fd}(X + X''_d)} ;$$

where $g_1 = X''_d - X_a$; $g_2 = X''_q - X_a$; $g_3 = X'_d - X_a$;

$$b_1 = (X + X''_d)/(X + X''_q) ;$$

$$b_2 = -\left(r_a + R \frac{g_2 X_{mq}}{\omega T_{kq} T''_{qo}} \right) \cdot \frac{\omega}{(X + X''_q)} ;$$

$$b_3 = \frac{\omega g_1}{X_{fd}(X + X''_q)} ;$$

$$b_4 = \frac{\omega g_1}{X_{kd}(X + X''_q)} ;$$

$$b_5 = \frac{\omega g_2}{X_{kq} T''_{qo} (X + X''_q)} ; \qquad B_6 = -\frac{\sqrt{2}\ \cdot\ \omega}{X + X''_q} ; \qquad b_7 = 0.0 ;$$

<u>From Eqn. (4.16) for $p\Psi_f$:-</u>

$$c_1 = \frac{g_1 X_{md}}{\omega g_3 T'_{do}} ; \qquad c_3 = -\left(1 + \frac{g_1 X_{md}}{X_{kd}X_{fd}}\right);$$

$$c_4 = \frac{g_1 X_{md}}{X_{kd}T'_{do}g_3} ; \qquad c_2 = c_5 = c_6 = 0.0 ; \qquad c_7 = 1.0 ;$$

From Eqn. (4.14) for $p\Psi_{kd}$;-

$$d_1 = \frac{g_3}{T''_{do}} \; ; \qquad d_3 = \frac{g_3}{X_{fd}T''_{do}} \; ; \qquad d_4 = -\frac{1}{T''_{do}} \; ;$$

$$d_5 = 0.0 \; ; \quad d_2 = d_6 = d_7 = 0.0 \; ;$$

From Eqn. (4.15) for $p\Psi_{kq}$:-

$$e_1 = e_3 = e_4 = e_6 = e_7 = 0.0 \qquad e_2 = \frac{X_{mq}}{\omega T''_{qo}}$$

$$e_5 = \frac{-1}{T''_{qo}} \; ;$$

---o0o---

APPENDIX II

THE APPROXIMATE METHOD OF ANALYSING A D.W.R. MACHINE

If i_{fd} and i_{kd} are eleminated from Eqns. (8.17),(8.19) and (8.21), the following expression is obtained for Ψ_d:

$$\Psi_d = (L_{dd} - \frac{L_{md}^2}{L_{ffd}})\, i_d + \Psi_{fd}\frac{L_{md}}{L_{ffd}} + \left[\frac{L_{md} - \frac{L_{md}^2}{L_{ffd}}}{L_{kkd} - \frac{L_{md}^2}{L_{ffd}}}\right]\left[\Psi_{kd} - \Psi_{fd}\frac{L_{md}}{L_{ffd}} - (L_{md} - \frac{L_{md}^2}{L_{ffd}})\, i_d\right] \qquad (A2.1)$$

If i_{fq} and i_{kq} are eliminated from Eqns. (8.18),(8.20) and (8.22) a similar expression is found for Ψ_q :

$$\Psi_q = (L_{qq} - \frac{L_{mq}^2}{L_{ffq}})\, i_q + \Psi_{fq}\frac{L_{mq}}{L_{ffq}} + \left[\frac{L_{mq} - \frac{L_{mq}^2}{L_{ffq}}}{L_{kkq} - \frac{L_{mq}^2}{L_{ffq}}}\right]\left[\Psi_{kq} - \Psi_{fq}\frac{L_{mq}}{L_{ffq}} - (L_{mq} - \frac{L_{mq}^2}{L_{ffq}})\, i_q\right] \qquad (A2.2)$$

The combinations of inductance terms in Eqns. (A2.1) and (A2.2) can be expressed in terms of the transient and subtransient reactances of the machine when the following identities are used:-

$$\omega\,(L_{dd} - \frac{L_{md}^2}{L_{ffd}}) = X_d' \;; \qquad \omega\,(L_{qq} - \frac{L_{mq}^2}{L_{ffq}}) = X_q' \;;$$

$$\omega\,(L_{md} - \frac{L_{md}^2}{L_{ffd}}) = (X_d' - X_a) \;; \qquad \omega\,(L_{mq} - \frac{L_{mq}^2}{L_{ffq}}) = X_q' - X_a) \;;$$

$$\omega\left(L_{kkd} - \frac{L_{md}^2}{L_{ffd}}\right) = \left[\frac{X_d' - X_a}{X_d'' - X_a}\right] X_{kd} \; ; \qquad \omega\left(L_{kkq} - \frac{L_{mq}^2}{L_{ffq}}\right) = \left[\frac{X_q' - X_a}{X_q'' - X_a}\right] X_{kq} \; ;$$

$$\frac{L_{md}}{L_{ffd}} = \frac{X_d' - X_a}{X_{fd}} \; ; \qquad \frac{L_{mq}}{L_{ffq}} = \frac{X_q' - X_a}{X_{fq}}$$

$$\frac{X_d' X_{kd}}{X_d' + X_{kd}} = X_d'' \; ; \qquad \frac{X_q' X_{kq}}{X_q' + X_{kq}} = X_q'' \; ;$$

where X_a, X_{fd}, X_{fq}, X_{kd} and X_{kq} are leakage reactances.

When the abovementioned idendities are used in the equations for Ψ_d and Ψ_q, it is found that:

<u>the coefficient of i_d is</u>

$$X_d' - \frac{(X_d'' - X_a)(X_d' - X_a)}{X_{kd}} = X_d'',$$

<u>the coefficient of Ψ_{fd} is</u>

$$\frac{X_d' - X_a}{X_{fd}} - \frac{(X_d' - X_a)(X_d'' - X_a)}{X_{fd} X_{kd}} = \frac{X_d'' - X_a}{X_{fd}}$$

<u>the coefficient of i_q is</u>

$$X_q' - \frac{(X_q'' - X_a)(X_q' - X_a)}{X_{kq}} = X_q'',$$

<u>the coefficient of Ψ_{fq} is</u>

$$\frac{X_q' - X_a}{X_{fq}} - \frac{(X_q' - X_a)(X_q'' - X_a)}{X_{fq} X_{kq}} = \frac{X_q'' - X_a}{X_{fq}}$$

and the expressions (A2.1) and (A2.2) are simplified to Eqns. (8.32) and (8.33).

The rates of change of secondary flux linkages are found by eliminating the secondary currents from the voltage Eqns. (8.13) to

(8.16).

From Eqns. (8.13) and (8.21)

$$p\Psi_{fd} = v_{fd} - r_{fd}i_{fd} \tag{A2.3}$$

An expression for i_{fd} is obtained by eliminating i_{kd} from Eqns. (8.19) and (8.21), as

$$i_{fd} = -\frac{(X_d'' - X_a)\,\omega}{(X_d' - X_a)X_{kd}X_{ffd}}\left[(\Psi_{kd}X_{md} - \Psi_{fd}X_{kkd}) - X_{md}\;L_{kd}i_d\right] \tag{A2.4}$$

while r_{fd} can be written as

$$r_{fd} = (X_{fd} + X_{md})/\omega T_{do}' \tag{A2.5}$$

The expressions in Eqns. (A2.4) and (A2.5) are substituted in Eqn. (A2.3) to yield Eqn. (8.34) as the final expression for $p\Psi_{fd}$. The expression for $p\Psi_{fq}$ in Eqn. (8.35) is found in a similar way.

The secondary current i_{fd} is eliminated from Eqns (8.19) and (8.20) to find

$$i_{kd} = \frac{(X_d'' - X_a)}{X_{kd}(X_d' - X_a)}\left[\omega\Psi_{kd} - \frac{(X_d' - X_a)}{X_{fd}}\,\omega\Psi_{fd} - (X_d' - X_a)i_d\right] \tag{A2.6}$$

r_{kd} can be written as

$$r_{kd} = (X_{kd} + X_d' - X_a)/\omega T_{do}'' \tag{A2.7}$$

The expressions in Eqns. (A2.6) and (A2.7) are substituted in the the following expression to find Eqn. (8.36): $p\Psi_{kd} = -r_{kd}i_{kd}$

The expression for $p\Psi_{kq}$ in Eqn. (8.37) is found in a similar way.

---oOo---

APPENDIX III

THE ACCURATE METHOD OF ANALYSING A D.W.R. MACHINE

From Eqns. (8.32) and (8.33), the derivatives of the flux linkages Ψ_d and Ψ_q are found as

$$p\Psi_d = \frac{X''_d}{\omega} \; pi_d + (X''_d - X_a)\left[\frac{p\Psi_{fd}}{X_{fd}} + \frac{p\Psi_{kd}}{X_{kd}}\right] \tag{A3.1}$$

$$p\Psi_q = \frac{X''_q}{\omega} pi_q + (X''_q - X_a)\left[\frac{p\Psi_{fq}}{X_{fq}} + \frac{p\Psi_{kq}}{X_{kq}}\right] \tag{A3.2}$$

Equating the right hand sides of Eqns. (8.11) and (4.24) yields

$$p\Psi_d + v\Psi_q + r_a i_d = \sqrt{2}\, V_{bd} - \frac{X}{\omega} pi_d - Ri_d - \frac{X}{\omega} vi_q \tag{A3.3}$$

The values of $p\Psi_d$ from Eqn. (A3.1) and Ψ_q from Eqn.(8.33) are substituted into Eqn. (A.3.3) which then contains the terms $p\Psi_{fd}$ and $p\Psi_{kd}$. The expressions for these, given by Eqns.(8.34) and (8.36), are substituted into the modified Eqn. (A3.3).

After rearranging the terms, an expression for pi_d is found as

$$pi_d = a_1 i_d + a_2 vi_q + a_3\Psi_{fd} + a_4 v\Psi_{fq} + a_5\Psi_{kd} + a_6 v\Psi_{kq} + a_7 V_{bd} + a_8 v_{fd}$$

where

$$a_1 = -\left[r_a + R + \frac{g_1^2 X_{md}}{g_3 T'_{do}\omega X_{fd}} + \frac{g_1 g_3}{T''_{do} X_{kd}\omega}\right]\frac{\omega}{(X''_d + X)};$$

$$a_2 = -\frac{X''_q + X}{X''_d + X};$$

$$a_3 = \left[\frac{g_1}{X_{fd}T'_{do}}\left(1 + \frac{g_1 X_{md}}{X_{kd}X_{fd}}\right) - \frac{g_1 g_3}{X_{kd}X_{fd}T''_{do}}\right]\frac{\omega}{(X''_d + X)};$$

$$a_4 = \frac{-g_2}{X_{fq}}\left[\frac{\omega}{X''_d + X}\right]; \quad a_5 = \left[\frac{g_1}{X_{kd}T''_{do}} - \frac{g_1^2 X_{md}}{g_3 T'_{do} X_{fd} X_{kd}}\right]\frac{\omega}{(X''_d + X)}$$

$$a_6 = -\frac{g_2\omega}{X_{kq}(X''_d + X)}; \quad a_7 = \frac{\sqrt{2}\omega}{(X''_d + X)}; \quad a_8 = -\frac{g_1\omega}{X_{fd}(X''_d + X)}$$

where $g_1 = X''_d - X_a$; $g_2 = X''_q - X_a$;

$g_3 = X'_d - X_q$; $g_4 = X'_q - X_a$;

Similarly

$$pi_q = b_1 \nu i_d + b_2 i_q + b_3 \nu \Psi_{fd} + b_4 \Psi_{fq} + \nu b_5 \Psi_{kd} + b_6 \Psi_{kq} + b_7 V_{bq} + b_9 v_{fq}$$

$$b_1 = \frac{X''_d + X}{X''_q + X};$$

$$b_2 = -\left[r_a + R + \frac{g_2^2 X_{mq}}{g_4 T'_{qo} X_{fq}\omega} + \frac{g_2 g_4}{X_{kq}T''_{qo}\omega}\right]\frac{\omega}{(X''_q + X)};$$

$$b_3 = \frac{g_1\omega}{X_{fd}(X''_q + X)};$$

$$b_4 = \left[\frac{g_2}{T'_{qo}X_{fq}}\left[1 + \frac{g_2 X_{mq}}{X_{kq}X_{fq}}\right] - \frac{g_2 g_4}{X_{kq}X_{fq}T''_{qo}}\right]\frac{\omega}{(X''_q + X)};$$

$$b_5 = \frac{g_1\omega}{X_{kd}(X''_q + X)}; \quad b_6 = -\left[\frac{g_2^2 X_{mq}}{g_4 T'_{qo} X_{fq} X_{kq}} - \frac{g_2}{X_{kq}T''_{qo}}\right]\frac{\omega}{(X''_q + X)};$$

$$b_9 = -\frac{g_2\omega}{X_{fq}(X''_q + X)}; \quad b_7 = \frac{-\sqrt{2}\,\omega}{(X''_q + X)}; \quad b_8 = 0.0 .$$

Also $p\Psi_{fd} = c_1 i_d + c_2 i_q + c_3 \Psi_{fd} + c_4 \Psi_{fq} + c_5 \Psi_{kd} + c_6 \Psi_{kq} + c_7 v_{fd}$

$$c_1 = \frac{g_1 X_{md}}{g_3 T'_{do}\omega}; \quad c_3 = -\left[1 + \frac{g_1 X_{md}}{X_{kd}X_{fd}}\right]\frac{1}{T'_{do}};$$

$$c_5 = \frac{g_1 X_{md}}{g_3 T'_{do} X_{kd}}; \quad c_2 = c_4 = c_6 = 0; \quad c_7 = 1;$$

and $p\Psi_{fq} = d_1 i_d + d_2 i_q + d_3\Psi_{fd} + d_4\Psi_{fq} + d_5\Psi_{kd} + d_6\Psi_{kq} + d_7 v_{fq}$

$$d_2 = \frac{g_2 X_{mq}}{g_4 T'_{qo}\omega} \; ; \quad d_4 = \frac{-1}{T'_{qo}} \left[1 + \frac{g_2 X_{mq}}{X_{kq} X_{fq}}\right] ;$$

$$d_6 = \frac{g_2 X_{mq}}{g_4 T'_{qo} X_{kq}} \; ; \quad d_1 = d_3 = d_5 = 0 \; ; \; d_7 = 1.0;$$

and $p\Psi_{kd} = e_1 i_d + e_3\Psi_{fd} + e_5\Psi_{kd}$

$$e_1 = \frac{g_3}{T''_{do}\omega} \; ; \quad e_3 = \frac{g_3}{T''_{do} X_{fd}} \; ; \quad e_5 = -\frac{1}{T''_{do}} \; ;$$

$$e_2 = e_4 = e_6 = e_7 = 0.0$$

and $p\Psi_{kq} = f_2 i_q + f_4\Psi_{fq} + f_6\Psi_{kq}$

$$f_2 = \frac{g_4}{T''_{qo}\omega} \; ; \quad f_4 = \frac{g_4}{T''_{qo} X_{fq}} \; ; \quad f_6 = -\frac{1}{T''_{qo}} \; ;$$

$$f_1 = f_3 = f_5 = f_7 = 0.0;$$

---oOo---

APPENDIX IV

LINEARISING THE EQUATIONS FOR SMALL PERTURBATIONS

When the external tie-line reactance is lumped with the alternator's armature leakage reactance, the axis components of terminal voltage as given by Eqns. (8.11) and (8.12) become the axis components of infinite bus voltage so that

$$v_{bd} = p\Psi_d + \nu\Psi_q + r_a i_d \qquad \text{(A4.1)}$$

$$v_{bq} = -\nu\Psi_d + p\Psi_q + r_a i_q \qquad \text{(A4.2)}$$

where Ψ_d , Ψ_q are modified flux linkages associated with the infinite bus voltage.

The above equations are simplified if it is assumed that the transient changes are slow in relation to the a.c. cycle. This implies that the frequency of small oscillations superimposed on the variables is much lower than the system frequency of 50 Hz. In fact, for steady-state stability studies the highest frequency of interest is about 2 Hz and hence the assumption is justified.

Neglecting the $p\Psi_d$ and $p\Psi_q$ terms and assuming that $\nu = \omega =$ constant, the above equations can be reduced to:

$$v_{bd} = \omega\Psi_q + r_a i_d \qquad \text{(A4.3)}$$

$$v_{bq} = -\omega\Psi_d = r_a i_q \qquad \text{(A4.4)}$$

and the expression for the electrical torque becomes

$$T_e = -\frac{1}{2}\left(v_{bq} i_q - r_a i_q^2 + v_{bd} i_d - r_a i_d^2\right) \qquad \text{(A4.5)}$$

If the machine position is $\theta = \omega t - \delta$ and ωt is the position of the synchronously rotating reference axis, then it can be shown[3,4,22] that

$$v_{bd} = v_b \sin\delta = X_q(p)i_q + r_a i_d + G_q(p)v_{fq} \tag{A4.6}$$

$$v_{bq} = v_b \cos\delta = X_d(p)i_d + r_a i_q - G_d(p)v_{fd} \tag{A4.7}$$

$$T_e = -\frac{1}{2}\left((v_b\cos\delta - r_a i_q)i_q + (v_b\sin\delta - r_a i_d)i_d\right) \tag{A4.8}$$

Eqns. (A4.6) to (A4.8) are linearized for small perturbations around a steady equilibrium point, denoted by a subscript o, to

$$v_b\cos\delta_o.\Delta\delta = X_q(p).\Delta i_q + r_a.\Delta i_d + G_q(p).\Delta v_{fq} \tag{A4.9}$$

$$-v_b\sin\delta_o.\Delta\delta = -X_d(p).\Delta i_d + r_a.\Delta i_q - G_d(p).\Delta v_{fd} \tag{A4.10}$$

$$\Delta T_e = -\frac{1}{2}\left((v_b\cos\delta_o - r_a i_{qo})\Delta i_q - (v_b\sin\delta_o.\Delta\delta + r_a.\Delta i_q)\, i_{qo}\right.$$
$$\left. + (v_b\sin\delta_o - r_a i_{do})\Delta i_d + (v_b\cos\delta_o.\Delta\delta - r_a.\Delta i_d)i_{do}\right) \tag{A4.11}$$

The expression for mechanical motion is

$$T_m - T_e = Jp^2(\omega t - \delta) = T_i$$

which can be reduced for small perturbations, to

$$\Delta T_i = -Jp^2.\Delta\delta$$
$$\text{and } \Delta T_m = \Delta T_i + \Delta T_e \tag{A4.12}$$

The "input transformation" equation (9.1) is obtained by combining Eqns. (A4.9) to (A4.12), and putting

$$v_{bdo} = v_{bd}\sin\delta_o$$

$$v_{bqo} = v_{bq}\cos\delta_o$$

---oOo---

APPENDIX V

VALUES OF $A_r(p)$ FOR GENERATOR ANGLE δ_t

A small change in i_d, δ, i_q causes a change $\Delta\delta_t$ in the terminal load angle, where

$$\Delta\delta_t = A_1'(p).\Delta i_d + A_2'(p).\Delta\delta + A_3'(p).\Delta i_q \tag{9.10}$$

The relationship between δ_t and quantities i_d, δ, i_q is found from the fact that

$$\tan\delta_t = V_{mtd}/V_{mtq}$$

$$= \frac{V_{bd} + I_q X_c}{V_{bq} - I_d X_c} \tag{A5.1}$$

Partial differentiation of δ_t (see Eqn.(A5.1)) with respect to i_d, δ and i_q gives

$$\Delta\delta_t = \frac{\partial(\delta_t)}{\partial i_d}.\Delta i_d + \frac{\partial(\delta_t)}{\partial\delta}.\Delta\delta + \frac{\partial(\delta_t)}{\partial i_q}.\Delta i_q \tag{A5.2}$$

If the right hand side of Eqn. (A5.1) is partially differentiated and compared with Eqns. (A5.2) and (9.10) it is found that

$$\left.\begin{aligned} A_1'(p) &= -X_c V_{mtdo}/\sqrt{2}V_{mto}^2 \\ A_2'(p) &= (V_b^2 + Q_o X_c)/V_{mto}^2 \\ A_3'(p) &= X_c V_{mtqo}/\sqrt{2}V_{mto}^2 \end{aligned}\right) \tag{A5.3}$$

REFERENCES

1. MEHTA, D.B. and ADKINS, B. :- 'Transient torque and load angle of a synchronous generator following several types of system disturbance', Proc. IEE, vol 107, part A, p. 61, 1960

2. MESSERLE, H.K. and BRUCK, R.W. :- 'Steady-state Stability of synchronous generators as affected by regulators and governors', Monograph no. 134, IEE. June 1955.

3. JACOVIDES, L.J. and ADKINS B.: 'Effect of Excitation Regulation on Synchronous Machine Stability', Proc. IEE, 1966, 113,(6), pp. 1021 - 1034.

4. KAPOOR, S.C., KALSI, S.S. and ADKINS, B.: 'Improvement of alternator stability by controlled quadrature excitation', Proc. IEE, 1969, 116, (5), pp. 771 - 780.

5. SOPER, J.A. and FAGG, A.R. : 'Divided-winding-rotor synchronous generator' Proc. IEE, 1969, 116 (1), pp. 113 - 126.

6. SHACKSHAFT, G.: 'General-purpose turbo-alternator model', ibid, vol 110, p. 703, 1963.

7. HARLEY, R.G. : 'Recording the Load Angle of a Synchronous Machine', Int. J. Elec. Engng. Educ., vol. 4,1966, pp.397 - 404.

8. HARLEY, R.G. : 'Kraghoek en Draaimoment Eienskappe van 'n Sinchrone Masjien', Trans. S.A.I.E.E., vol. 57, prt. 12, Dec. 1966, ,pp. 254 - 277.

9. HARLEY, R.G. : 'System Transient Stability' Elec. Times, vol. 154, Dec. 1968, No. 25, pp. 862 - 866, No. 26, pp. 892 - 894.

10. PARK, R.H. and BANKER, E.H. 'System stability as a design problem', Trans. AIEE, vol 48, p.170, 1929.

11. CRARY, S.B. and WARING, M.L. : 'Torque angle characteristics of synchronous machines following system disturbances', ibid, vol. 51, p. 764, no. 3, September, 1932.

12. CHING, Y.K. and ADKINS, B. : 'Transient theory of synchronous generators under unbalanced conditions', Proc. IEE, vol 101, p. 166, no. 4, 1954.

13. ALDRED, A.S. and SHACKSHAFT, G. : 'The effect of a voltage regulator on the steady-state and transient stability of a synchronous generator', ibid, 105A, p. 420, 1958.

14. EASTON, V., FITZPATRICK, J.A. and PARTON, K.C. : 'The performance of continuously acting voltage regulators with additional rotor angle control', CIGRE, no. 309. June, 1960.

15. SURANA, S.L. and HARIHARAN, M.V. :'Transient response and transient stability of power systems', Proc. IEE, 115, no 1 p. 114, January, 1968.

16. PRABHASHANKAR, K. and JANISCHEWSYJ, W. : 'Digital simulation of multi-machine power systems for stability studies', Trans IEEE, PAS-87, no. 1, p.73, January, 1968.

17. HUMPAGE, W.D. and SAHA, T.N. : 'Digital computer methods in dynamic-response analyses of turbogenerator units' Proc. IEE, vol 114, no. 8, p. 1115, August, 1967.

18. NICHOLSON, H. : 'Integrated control of a nonlinear turbo-alternator model under fault conditions', Proc. IEE, Vol. 114, no. 6, p. 834, June, 1967.

19. DHARMA RAO and RAMACHANDRA RAO : 'Solution of transient-stability problems through the number series approach', ibid, vol. 111, no. 4, p. 775, April, 1964.

20. YU H KU : 'Transient analysis of AC machinery', Trans. AIEE, vol. 48, p. 707, July, 1959.

21. LOKAY, H.E. and BOLGER, R.L. : 'Effect of tubine-generator representation in system stability studies', Trans. IEEE, PAS. 84, no. 10, p.933, October, 1965.

22. ADKINS, B. : 'The general theory of elctrical machines', Chapman and Hall, 1959.

23. WYLIE, C.R. (Jr.): 'Advanced Engineering Mathematics', McGraw Hill, 2nd ed. 1960.

24. CRARY, S.B. : 'Power system stability', vol II, 1947, Chapman and Hall, London.

25. EL-ABIAD, A.H. and NAGAPPAN, K. : 'Transient stability regions of multi-machine power systems', Trans. IEEE, PAS-85, no. 20, February, 1966.

26. FALLSIDE, F. and PATEL, M.R. : 'On the application of the Lyapunov method to synchronous machine stability', Internat. Journ. Control, vol. 4, p. 501, 1966.

27. CLESS, G.E. : 'Direct method of Lyapunov applied to transient power system stability', Trans. IEEE, vol. 58, 1966, pt 3, p 159.

28. CONCORDIA, C. : 'Steady-state Stability of Synchronous Machines as affected by Voltage Regulator Characteristics', Trans. AIEE., 1944, 63, pp. 215 - 220.

29. MILES, J.G. : 'Analysis of Overall Stability of Multi-machine Power Systems', Proc. IEE, 1962, 109A, pp. 203 - 211.

30. BUSEMANN, F. and CASSON, W. : 'Results of full scale stability tests on the British 132 kV grid system', Proc. IEE, vol. 105, prt. A, no. 22, p. 347, August, 1958.

31. RALSTON, A. and WILF, H.S. : 'Mathematical Methods for Digital Computers' New York: Wiley, 1962 .

32. LANCE, G.N. : 'Numerical Methods for High Speed Computers' Ilffe and Sons, London, 1960, p. 56.

33. ALFORD, R.J. : 'The stability of a synchronous generator associated with an induction motor load', Ph.D. Thesis, London University, 1964.

34. SHACKSHAFT, G. : Private communication.

35. ADKINS, B. : 'Micro-machine studies at Imperial College', Elect. Times, 7th July, 1960, 138 pp. 3 - 8.

36. IEC Technical Committee No.2: Recommendations on Methods for Determining Synchronous Machine Quantities from Tests, August, 1964.

37. GRAHAM, A. C. : 'Mirco-machine Turbine Simulation', DIC Dissertation, Imperial College, London 1968.

38. HUMPAGE, W.D. and Stott, B. : 'Predictor-corrector methods of numerical integration in digital-computer analyses of power-system transient stability', Proc. IEE., 1965, 112, (8) pp. 1557 - 1565.

39. HAMDI-SEPEN, C. : 'Process for increasing the transient stability power limits on a.c. transmission systems' CIGRE, Paper 305, 1962.

40. PARSONS A.J. and HAMMONS T.J. : 'The Design of a Micro-Alternator for Power System Stability Investigations', Proc. 2nd S.R.C. Power System Conf. pp. 624 - 658, Glasgow, Jan. 1967.

41. CLAYTON, A.E, and HANCOCK N.N. . 'The Performance and Design of Direct Current Machines' (3rd edition, Pitman, London)

42. C.E.G.B. : 'Modern Power Station Practice', Sect. D, Correspondence Tuition, Appendix.

43. BLACKMAN P.F. 'The Pole-Zero Approach to Systems Analysis', (Morgan Brothers Ltd) London.

44. SMITH, D.H. : 'The Characteristics of Parallel -T RC Networks', Electronic Engng., Feb. 1957, pp. 71 - 77.

45. KORN and KORN: 'Electronic Analogue and Hybrid Computers', (McGraw-Hill, N.Y., 1964).

46. FITZGERALD, A.E. and KINGSLEY, C. (Jr.) : 'Electric machinery', 2nd ed. McGraw Hill.

---oOo---